

**University of Alberta**

The application of the multisolute osmotic virial equation to  
cryobiology

by

Richelle Catherine Prickett

A thesis submitted to the Faculty of Graduate Studies and Research  
in partial fulfillment of the requirements for the degree of

Doctor of Philosophy

in

Chemical Engineering and Medical Sciences

Departments of Chemical and Materials Engineering  
and Medical Sciences - Laboratory Medicine and Pathology

©Richelle Catherine Prickett

Spring 2010

Edmonton, Alberta

Permission is hereby granted to the University of Alberta Libraries to reproduce single copies of this thesis and to lend or sell such copies for private, scholarly or scientific research purposes only.

Where the thesis is converted to, or otherwise made available in digital form, the University of Alberta will advise potential users of the thesis of these terms.

The author reserves all other publication and other rights in association with the copyright in the thesis and, except as herein before provided, neither the thesis nor any substantial portion thereof may be printed or otherwise reproduced in any material form whatsoever without the author's prior written permission.

## **Examining Committee**

Co- Supervisors:

Dr. Janet A. W. Elliott, Chemical and Materials Engineering

Dr. Locksley E. McGann, Laboratory Medicine and Pathology

Dr. Murray Gray, Chemical and Materials Engineering

Dr. Monika Keelan, Laboratory Medicine and Pathology

Dr. Subir Bhattacharjee, Mechanical Engineering

Dr. Boris Rubinsky, Hebrew University of Jerusalem and University of California at Berkeley

***This thesis is dedicated to my grandfather,  
Dr. Harold Silvester,  
for his valuable advice, unconditional love,  
and unwavering support.***

## **Abstract**

### **Application of the Osmotic Virial Equation to Cryobiology**

Mathematical modelling of cellular osmotic responses to low temperatures is being increasingly used to overcome obstacles in the successful cryopreservation of cells and tissues. Current cryobiological models often contain simplifying assumptions regarding the solution behaviour of the complicated, multisolute intra- and extra-cellular solutions. In order to obtain more accurate predictions of cryobiological outcomes, equations derived from thermodynamic principles that more accurately describe the biological solution behaviour could be used to greatly advance the design of novel cryopreservation protocols.

The general hypothesis of this thesis is that the application of the multisolute osmotic virial equation, with mixing rules derived from thermodynamic first principles, to solutions of interest in cryobiology will result in more accurate predictions of the multisolute solution behaviour, which will lead to improved cryobiological modelling and increased understanding of cellular responses to cryopreservation.

Specifically, this thesis demonstrates that the osmotic virial coefficients, obtained from single-solute solution data, can be used in the multisolute osmotic virial equation to accurately predict the multisolute solution behaviour, without the need to fit multisolute solution data. The form of the multisolute osmotic virial equation proposed in this thesis was

used to predict the solution behaviour of a range of multisolute solutions of interest in cryobiology.

The equation commonly used in cryobiology to describe cellular osmotic equilibrium is based on ideal, dilute solution assumptions. In this thesis, a non-ideal osmotic equilibrium equation was derived and, combined with the multisolute osmotic virial equation, used to more accurately predict the osmotic equilibrium of human erythrocytes.

The improved equations proposed in this thesis were combined with experimental measurements of the incidence of intracellular ice formation in order to further the understanding of the role of several important cryobiological parameters on the formation of intracellular ice.

This thesis work has significantly contributed to the field of cryobiology by substantially improving the accuracy of two key equations used in the modelling of cellular osmotic responses to cryopreservation. The combination of accurate mathematical modelling and results from experiments will allow increased understanding of cellular responses to cryopreservation, leading to the design of novel cryopreservation protocols.

## **Acknowledgements**

I wish to express my sincere gratitude to the following individuals for their contribution to this thesis.

To my supervisors, Drs. Janet Elliott and Locksley McGann. Most people are lucky to find one mentor who inspires and challenges them – I am incredibly blessed to have two. Thank you for your wisdom, encouragement, and dedication.

To my committee members, Drs. Monika Keelan and Murray Gray. Thank you for your time, advice, and support.

To Drs. Boris Rubinsky and Subir Bhattacharjee, my external examiners. Thank you for your insightful comments and suggestions.

To Dr. John Nychka, my examining committee chair. Thank you for the helpful advice.

To Dr. Jason Acker, Yuri Shardt, Kathy Porter, Shamina Hakda, and Kelly Murphy for their technical assistance.

To past and present members of the McGann/Elliott and Acker/Holovati Cryolabs, including Garson Law and Adele Hansen, for their support, friendship, coffee-breaks, and answers to all of my lab-related questions.

To my MANGO cohorts, Dr. Heidi Elmoazzen, Dr. Jelena Holovati, and Dr. Lisa Ross-Rodriguez. Words cannot express how much your friendship and encouragement mean to me. I have learned so much from each of you – about science and about the type of person I aspire to be.

To my parents, Pat and Susan, and my sister Megan. Thank you for believing in me, for loving me, and for encouraging me.

To my family. Thank you for your prayers, love, and support.

To all of my friends. Thank you for bringing balance to my life.

To my husband, Brent. Without your unconditional love, steadfast support, and infallible ability to make me laugh, I would not have been able to achieve this. Thank you for standing by me through it all.

<b>Table of Contents</b>	<b>Page:</b>
<b>Chapter 1. Introduction</b>	<b>1</b>
1.1. Cryobiology	1
1.1.1. Cryo-injury	4
1.1.2. Cryoprotective agents	7
1.2. Mathematical modelling in cryobiology	9
1.3. Thermodynamic relationships in cryobiology	14
1.3.1. Freezing point depression and osmolality	14
1.3.2. Osmotic coefficient and osmolality	16
1.3.3. Water activity and osmolality	17
1.4. Multisolute solution models in cryobiology	18
1.5. Osmotic equilibrium	26
1.6. Current understanding of IIF in cryobiology	27
1.7. Improvements proposed in this thesis	33
1.8. Objectives and hypothesis of this thesis	35
1.8.1. General hypothesis	35
1.8.2. General objectives	35
1.8.3. Specific research objectives	35
1.9. References	37

<b>Chapter 2. Single-solute osmotic virial equation</b>	<b>52</b>
2.1. Introduction	52
2.2. Governing equations	53
2.3. Materials and methods	59
2.3.1. Obtaining the single-solute phase diagrams	59
2.3.2. Fitting the single-solute osmotic virial equation to data	63
2.4. Results	69
2.5. Discussion	70
2.6. References	72
<b>Chapter 3. Multisolute osmotic virial equation</b>	<b>93</b>
3.1. Introduction	93
3.2. Governing equations	95
3.2.1. Multisolute osmotic virial equation - general form	95
3.2.2. Multisolute osmotic virial equation - glycerol + DMSO	99
3.2.3. Multisolute osmotic virial equation - hemoglobin + ideal solute	100
3.2.4. Multisolute osmotic virial equation - bovine serum albumin + ovalbumin	104
3.3. Materials and methods	106
3.3.1. Obtaining the multisolute phase diagrams	106

3.4. Results	107
3.5. Discussion	112
3.6. References	116
<b>Chapter 4. Multisolute osmotic virial equation for use with electrolytes</b>	<b>131</b>
4.1. Introduction	131
4.2. Overview of multisolute solute solution theories for aqueous CPA + electrolyte solutions	134
4.2.1. Combination of the OVE with the Pitzer-Debye-Huckel equation	136
4.3. Using the multisolute OVE to investigate electrolyte effects on macromolecule solution behaviour	139
4.4. Materials and methods	141
4.4.1. Fitting the OVE to data	141
4.5. Results	142
4.5.1. CPA + NaCl + water solutions	142
4.5.2. HES + NaCl + water solutions	144
4.6. Discussion	146
4.7. References	152
<b>Chapter 5. A non-ideal replacement for the Boyle -van't Hoff equation</b>	<b>172</b>
5.1. Introduction	172

5.2. Governing equations	177
5.2.1. Osmotic virial equation: Model for $\pi(m)$	182
5.2.2. Osmotic virial equation: Best fit to measurements of $\pi(m)$	184
5.3. Materials and methods	186
5.4. Results	189
5.4.1. Boyle-van't Hoff equation	190
5.4.2. Non-ideal osmotic equilibrium equation, with osmotic virial model prediction.	190
5.4.3. Non-ideal osmotic equilibrium equation, with ESR data osmotic virial equation best fit.	191
5.5. Discussion	191
5.6. References	194
<b>Chapter 6. Effect of supercooling and cell volume on intracellular ice formation</b>	<b>205</b>
6.1. Introduction	205
6.1.1. Current understanding of IIF in cryobiology	206
6.1.2. The role of intracellular supercooling in IIF	207
6.1.3. The role of cell volume and extracellular ice nucleation temperature in IIF	209
6.1.4. Limitations of current IIF models	211

6.1.5. Objective	212
6.2. Materials and methods - empirical and theoretical	214
6.2.1. HUVEC cell culture	214
6.2.2. Experimental solutions	215
6.2.3. Cryomicroscopy experiments	217
6.2.4. Cell volume measurements	222
6.2.5. Statistical Analysis	223
6.2.6. Mathematical model - equations and specifications	224
6.3. Results	230
6.3.1. Percentage of IIF and percentage of cells with damaged membrane post-thaw	230
6.3.2. Effect of cell volume on IIF	232
6.3.3. Mathematical modelling to investigate effect of cell volume	234
6.4. Discussion	236
6.4.1. Comparison between this study and previous studies	236
6.4.2. Effect of cell volume on incidence of IIF for population of cells in isotonic and hypertonic solutions	237

6.4.3. Effect of cell volume on incidence of IIF on a cell-specific basis for cells in isotonic and hypertonic solutions	238
6.4.4. Results from model and interpretation of experimental results	239
6.4.5. Assumption in the model of intracellular solution of HUVECs	239
6.4.6. Translation of results into cryopreservation applications	240
6.5. References	242
<b>Chapter 7. Overall Discussion and General Conclusions</b>	<b>264</b>
7.1. Summary of thesis	264
7.2. Limitations of this study	270
7.3. Implications of this thesis	273
7.4. General conclusions and recommendations	274
7.5. References	277
<b>Appendix A: Relationship between freezing point depression and osmolality</b>	<b>279</b>
<b>Appendix B: Concentration unit conversions</b>	<b>283</b>

<b>Appendix C: The van't Hoff relation</b>	<b>288</b>
<b>Appendix D: Comparison between protein + ideal model and measured solution properties of the HUVEC cytoplasm</b>	<b>290</b>

<b>List of Tables</b>	<b>Page:</b>
1.1 Values for constants in the freezing point to osmolality conversion.	51
2.1 Osmotic virial coefficients for use with solution molality.	78
2.2 Osmotic virial coefficients for use with solution mole fraction.	79
2.3 Pitzer-Debye-Huckel equation parameters.	80
2.4 Osmotic virial coefficients for NaCl fit to Robinson and Stokes data	81
2.5 Summary of the approach used for linear regression of different forms of the single-solute osmotic virial equation.	82
3.1 Percent error and sum of squared errors in using (i) ideal and dilute, (ii) adding osmolalities and (iii) multisolute OVE to predict each multisolute solution as compared to measured data.	124
4.1 Summary of matrices and vectors used for linear regression to obtain HES osmotic virial coefficients	159
4.2 Percent errors and SSE from the predictions from the multisolute solution theories that do not require fitting of multisolute data.	160
4.3 HES osmotic virial coefficients for varying mass ratios (R) of HES + NaCl + water solutions.	161

<b>4.4</b>	Calculated HES osmotic virial coefficients for mass ratios (R) = 1, 2, 5, 10, and 20 of HES + NaCl + water solutions.	162
<b>5.1</b>	Osmotic virial coefficients for the solutes of the cytoplasm of human erythrocytes treated as a grouped solute.	199
<b>5.2</b>	Isotonic values for each data set.	199
<b>5.3</b>	Values of osmotically-inactive fraction for erythrocytes obtained from the traditional Boyle van't Hoff equation and from the non-ideal osmotic equilibrium equation.	199
<b>6.1</b>	Parameters used in the mathematical modelling of HUVECs.	250
<b>6.2</b>	Percentage of cells with intact and damaged membranes for cells undergoing IIF and cells not undergoing IIF in isotonic solutions.	251
<b>6.3</b>	Percentage of cells with intact and damaged membranes for cells undergoing IIF and cells not undergoing IIF in hypertonic solutions.	251
<b>6.4</b>	Cell diameters (average $\pm$ standard deviation) for cells undergoing IIF and cells not undergoing IIF for isotonic and hypertonic experiments.	252

<b>List of Figures</b>	<b>Page:</b>
<b>2.1</b> Osmolality of single-solute aqueous electrolyte solutions as a function of (a) solute molality and (b) solute mole fraction.	83
<b>2.2</b> Osmolality of single-solute aqueous CPA solutions as a function of (a) solute molality and (b) solute mole fraction.	84
Osmolality of single-solute aqueous (c) DMSO and (d) glycerol solutions as a function of solute molality.	85
<b>2.3</b> Osmolality of single-solute aqueous alcohol solutions as a function of (a) solute molality and (b) solute mole fraction.	86
<b>2.4</b> Osmolality of single-solute aqueous sugar solutions as a function of (a) solute molality and (b) solute mole fraction.	87
<b>2.5</b> Osmolality of single-solute aqueous macromolecule solutions as a function of (a) solute molality and (b) solute mole fraction.	88
<b>2.6</b> A comparison between the dissociation constant ( $k_{diss}$ ) and the Pitzer-Debye-Huckel electrolyte effects function ( $2(f^{\phi} + 1)$ ) for NaCl.	89
<b>2.7</b> Osmolality of single-solute aqueous NaCl solutions as a function of solute molality.	90

<b>2.8</b>	Osmolality determined from the freezing point using either the linear conversion or the nonlinear conversion.	91
<b>2.9</b>	Typical temperature measurements for a freezing point depression experiment.	92
<b>3.1</b>	Osmolality of a glycerol + DMSO + water solution as a function of total solute molality for (a) $R = 0.5$ and (b) $R = 2.0$ ; where $R = \text{mass glycerol}/\text{mass DMSO}$ .	125
	Osmolality of a glycerol + DMSO + water solution as a function of total solute mole fraction for (c) $R = 0.5$ and (d) $R = 2.0$ ; where $R = \text{mass glycerol}/\text{mass DMSO}$ .	126
<b>3.2</b>	Osmolality as a function of relative intracellular concentration for human erythrocytes:	
	(a) multisolute OVE prediction for Hb + ideal solute model	127
	(b) single solute OVE prediction for Hb alone or ideal, dilute solution alone	128
	(c) relative contributions from each component of Hb + ideal OVE model.	129
<b>3.3</b>	Osmolality of a BSA + OVL + water solution as a function of (a) total solute molality and (b) total solute mole fraction for $R = 1.5$ , where $R = \text{mass BSA}/\text{mass OVL}$ .	130

<b>4.1</b>	Osmolality as function of total solute molality for DMSO + NaCl + water solutions (R ranging from 0.2 to 19.0).	163
<b>4.2</b>	Osmolality as function of total solute molality for glycerol + NaCl + water solutions (R ranging from 0.25 to 9.0).	166
<b>4.3</b>	Osmolality as function of total solute molality for HES + NaCl + water solutions (R ranging from 0.5 to 20).	169
<b>4.4</b>	The second and third osmotic virial coefficients, B and C, for HES in varying concentrations of aqueous salt solutions as a function of R-value.	170
<b>4.5</b>	Osmolality as function of total solute molality for HES + NaCl + water solutions (R ranging from 1 to 20).	171
<b>5.1</b>	Relative osmolality as a function of relative intracellular molality for human erythrocytes.	200
<b>5.2</b>	Boyle-van't Hoff plot for human erythrocytes in phosphate buffered saline solutions.	201
<b>5.3</b>	Non-ideal osmotic equilibrium plot for human erythrocytes in phosphate buffered saline solutions, using our osmotic virial equation model for hemoglobin and an ideal solute to determine $m(\pi)$ .	202
<b>5.4</b>	Non-ideal osmotic equilibrium plot for human erythrocytes in phosphate buffered saline solutions, fitting the ESR data to the osmotic virial equation for	203

one “grouped solute” to determine  $m(\pi)$ .

<b>5.5</b>	Osmotic equilibrium plot for human erythrocytes in phosphate buffered saline solutions (a) over the entire osmolality range and (b) over the initial osmolality range.	204
<b>6.1</b>	(a) Picture of entire cryomicroscope system and (b) close-up of crucible carrier and quartz crucible for samples.	253
<b>6.2</b>	Image of SYTO® 13 (green)/EB (red) fluorescence used for membrane integrity assay.	254
<b>6.3</b>	Image of cells flashing due to intracellular ice formation.	255
<b>6.4</b>	Percentage of cells with IIF (closed diamonds) and percent cells membrane damaged post-thaw (red circles) for isotonic experiments.	256
<b>6.5</b>	Percentage of cells with IIF (closed diamonds) and percent cells membrane damaged post-thaw (red circles) for hypertonic experiments.	257
<b>6.6</b>	Percentage of cells with IIF for isotonic (blue triangles) and hypertonic (yellow diamonds) experiments.	258
<b>6.7</b>	Calculated relative cell volume (volume / isotonic volume) as a function of time.	259
<b>6.8</b>	Histogram of number of cell undergoing IIF as a function of time following extracellular ice nucleation for	260

- (a) isotonic experiments and (b) hypertonic experiments.
- 6.9** Calculated cell water volumes for 2230  $\mu\text{m}^3$  cells and 1115  $\mu\text{m}^3$  cells in isotonic ( $\pi = 300$  mOsm/kg solvent) and hypertonic solutions ( $\pi = 750$  mOsm/kg solvent). 261
- 6.10** Calculated relative cell water volumes (cell water volume/isotonic cell water volume) for 2230  $\mu\text{m}^3$  cells and 1115  $\mu\text{m}^3$  cells in isotonic ( $\pi = 300$  mOsm/kg solvent) and hypertonic solutions ( $\pi = 750$  mOsm/kg solvent). 262
- 6.11** Calculated intracellular supercooling for 2230  $\mu\text{m}^3$  cells and 1115  $\mu\text{m}^3$  cells in isotonic ( $\pi = 300$  mOsm/kg solvent) and hypertonic solutions ( $\pi = 750$  mOsm/kg solvent). 263
- D.1** The calculated osmolality as a function of the relative intracellular solute concentration. 291

## List of Symbols and Abbreviations

### Symbols

$A$	cell surface area	$\mu\text{m}^2$
$\underline{\underline{A}}$	matrix of derivatives of regression equation (equivalent to the Jacobian matrix)	
$A^*$	conversion between osmole fraction and osmolality	total moles/kg solvent
$A^\Phi$	Debye-Huckel slope	
$a$	activity	
$B$	second osmotic virial coefficient	$(\text{mole solute/kg solvent})^{-1}$
$B^*$	second osmotic virial coefficient	$(\text{mole solute/total moles})^{-1}$
$B_{MX}^\Phi$	second osmotic virial coefficient in the PDH equation	$(\text{mole solute/kg solvent})^{-1}$
$b$	empirical parameters in the PDH equation	
$b$	osmotically-inactive fraction	
$b^*$	non-ideal osmotically-inactive fraction of the cell volume	
$C$	third osmotic virial coefficient	$(\text{mole solute/kg solvent})^{-2}$
$C^*$	third osmotic virial coefficient	$(\text{mole solute/total moles})^{-2}$
$C_{MX}^\Phi$	third osmotic virial coefficient in the PDH equation	$(\text{mole solute/kg solvent})^{-2}$
$E_a$	activation energy	J/mol
$f^\Phi$	'electrolyte effects' function (PDH equation)	

$f_i$	predicted value of data point	
$I$	ionic strength	
$k_{diss}$	dissociation constant	
$L_p$	hydraulic conductivity	$\mu\text{m}^3/\mu\text{m}^2/\text{min}/\text{atm}$
$M$	mass	kg
$m$	molal concentration of solute	moles/kg solvent
$\mathbf{m}$	number of data points	
$n$	number of moles	mole
$\mathbf{n}$	number of parameters	
$P_s$	solute permeability	$\mu\text{m}^3/\mu\text{m}^2/\text{min}$
$R$	universal gas constant	$\mu\text{m}^3 \text{ atm}/\text{mol}/\text{K}$ J/moleK
$R\text{-value}$	mass ratio of solute 1 to solute 2	
$R^2$	coefficient of determination	
$SC$	supercooling	
$\overline{s}_1^{0L}$	entropy per mole of pure liquid water	J/moleK
$\overline{s}_1^{0S}$	entropy per mole of pure solid water	J/moleK
$T$	absolute temperature	K
$T_{nucl}$	nucleation temperature	$^{\circ}\text{C}$
$T_{ref}$	reference temperature	$^{\circ}\text{C}$
$t$	time	min
$\Delta T_{FP}$	freezing point depression	K or $^{\circ}\text{C}$

$T_{FP}^o$	freezing point of pure solvent (water)	273.15 K
$T_{FP}$	freezing point of the solution	K or °C
$V$	cell volume	$\mu\text{m}^3$
$V_b$	osmotically-inactive volume of the cell	$\mu\text{m}^3$
$W_1$	molecular weight of water	kg/mole
$X$	mass fraction	g/100 g of solution
$x$	mole fraction	mole/total moles
$\vec{y}$	vector of all the measured data points	
$y_i$	measured value of data point	

### **Symbols in equations from literature cited**

$a$	fitting parameters (Pegg's eqns)	
$b$	fitting parameters (Pegg's eqns)	
$C_1, C_2, \text{ and } C_3$	fitting parameters (Kleinhans & Mazur eqns)	
$f$	empirical function (Fahy's eqn)	
$T_m$	melting point of the solution	K or °C
$\alpha$	empirical constant (Levin's eqns)	
$\beta$	empirical constant (Levin's eqns)	
$\alpha$	degree of dissociation (Heyrovska's eqns)	
$i$	van't Hoff factor (Heyrovska's eqns)	

## **Greek Symbols**

$\alpha$	level of significance	
$\alpha$	empirical parameter (PDH equation)	
$\vec{\beta}$	vector of the regression coefficients	
$\beta_{MX}^{(0)}, \beta_{MX}^{(1)}$	empirical parameters (PDH equation)	
$\Phi$	osmotic coefficient	osmoles/mole
$\Pi$	osmotic pressure	atm
$\pi$	osmolality	osmoles/kg solvent
$\rho$	density of water	$1.0 \times 10^{-15} \text{ kg}/\mu\text{m}^3$
$\mu$	chemical potential	J/mole
$v$	molar volume	$\text{m}^3/\text{mole}$

## **Abbreviations**

ANOVA	analysis of variance
BSA	bovine serum albumin
CI	confidence interval
CPA	cryoprotective agent
DMSO	dimethyl sulphoxide
EB	ethidium bromide
EG	ethylene glycol
ESR	electron spin resonance
Hb	hemoglobin
HES	hydroxyethyl starch

HUVEC	human umbilical vein endothelial cell
IIF	intracellular ice formation
KCl	potassium chloride
LN <sub>2</sub>	liquid nitrogen
NaCl	sodium chloride
OVE	osmotic virial equation
OVL	ovalbumin
PBS	phosphate buffered saline
PDH	Pitzer-Debye-Huckel
PG	propylene glycol
SSE	sum of squared errors

### **Superscripts**

e	extracellular
h	hydrated
i	intracellular
o	standard state

### **Subscripts**

1	solvent
2,3,...	solutes
<i>i,j</i>	solutes
B	BSA

D DMSO  
G glycerol  
GS grouped solute  
H hemoglobin  
I ideal  
N NaCl  
O OVL  
o isotonic  
P protein  
w water

## **Chapter 1 - Introduction**<sup>1</sup>

Increasingly complex obstacles are arising in the search for successful cryopreservation protocols for a range of cells, tissues and organs. In order to solve these complicated issues, mathematical modelling is increasingly being used to interpret and understand experimental results; ascertain relationships between various parameters; and design novel cryopreservation protocols. The current cryobiological models, which often contain simplifying assumptions regarding the solution behaviour, qualitatively correlate with experimental results and allow general relationships between variables to be determined. However, in order to obtain more accurate predictions of cryobiological outcomes, the models need to more accurately capture the complicated biological behaviour. The application of equations, derived from thermodynamic principles, which more accurately describe the biological solution behaviour could be used to greatly advance the design of novel cryopreservation protocols.

### *1.1. Cryobiology*

Cryobiology is the study of the effect of low temperatures, ranging from 4 °C to -196 °C, on biological systems. Cryopreservation has applications in many areas, including medical and life sciences research,

---

<sup>1</sup> A version of sections of this chapter has been accepted for publication. R.C. Prickett, J.A.W. Elliott, and L.E. McGann 2009. *Cryobiology*. (doi:10.1016/j.cryobiol.2009.07.011).

transplant medicine, conservation of biodiversity, reproductive medicine, agriculture, and food sciences, amongst others.

Increasing numbers of cellular therapies and transplantation of natural and engineered cells, tissues, and organs are being utilized to treat numerous medical conditions. For example, blood cells are used on a daily basis to save lives by increasing red blood cell mass in both trauma and leukemia patients. In addition, stem cells are currently being investigated as viable treatments for a diverse range of diseases and conditions [8; 32; 48], which has made preservation of these cells increasingly important. Tissues and organs are transplanted to improve the quality of patients' lives, in the case of cornea transplants to cure blindness or cartilage replacement to treat arthritis, and to save lives, in the case of heart, lung, and kidney transplants. However, in order to increase the efficacy and safety of cellular transfusions and tissue/organ transplantations, time is needed to process, screen, and transport the biological samples. Currently, cryopreservation is the only feasible method for long-term preservation of structure and function in natural and engineered cells, tissues, and organs. While some cells and tissues have been cryopreserved for decades and used clinically, there are many obstacles in the cryopreservation of other cells, tissues, and organs that need to be overcome before successful cryopreservation can be consistently achieved.

Among these issues is the use of cryoprotective agents (CPAs), which are used to achieve high cell recovery after freezing and thawing. These additives, however, can cause adverse side effects if transfused into patients [9; 11; 53; 65; 88], but their removal from the cells pre-transfusion requires additional time and labour [9; 88] and can result in a decrease in the number of viable cells [9; 102].

The successful cryopreservation of tissue and organs systems is complicated by the fact that extracellular ice formation damages the extracellular matrix (ECM) and disrupts the cell-ECM interactions. This results in structural and functional losses in the tissue and organs post-thaw. In order to achieve successful low-temperature preservation of tissue and organ systems without the formation of ice, vitrification is being increasingly investigated [13; 22; 42; 66; 70; 75; 76; 85]. In order to vitrify tissue, extremely high CPA concentrations are required. Much research is focusing on designing novel cryopreservation solutions which contain multiple CPAs in order to obtain vitrifiable concentrations [21; 75; 76].

The traditional approach to designing cryopreservation protocols has focused on empirical testing of constant cooling rates combined with various concentrations of different CPAs. However, in order to maximize the efficacy of cryopreservation protocols, a single constant cooling rate is often insufficient and more complicated protocols are required [59; 89; 93]. The conventional approach of trial-and-error testing of protocols is exceedingly time- and resource-consuming, and it is almost impossible to

find optimal nonlinear protocols in this manner. In order to develop novel cryopreservation protocols, including those that involve complicated CPA cocktails, the avoidance of CPA usage, or nonlinear cooling profiles, new approaches to cryopreservation research are needed. Improved understanding of the solution thermodynamics of the complicated intra- and extra-cellular solutions in cryobiology will provide further insight into the cellular responses to low-temperatures and will further the design of novel cryopreservation protocols.

#### *1.1.1. Cryo-injury*

When cells are exposed to sub-zero temperatures, ice forms first in the extracellular solution. The formation of ice removes water from the solution, thus concentrating the extracellular solution. This causes an increase in the chemical potential of the extracellular water, which is equivalent to an increase in the osmolality or vapour pressure of the solution. Depending on the temperature, the cell responds to the increased osmolality in one of two ways. At relatively high sub-zero temperatures, the cell increases the osmolality of the intracellular solution by osmotically dehydrating, resulting in a shrunken cell with a concentrated intracellular solution. At lower sub-zero temperatures, the transport of water across the membrane is restricted, so the cell does not

osmotically dehydrate. Thus, the intracellular water is supercooled<sup>2</sup> and the cell attains equilibrium with the extracellular solution by forming ice inside the cell. These responses to the extracellular ice formation were expressed as a cohesive two-factor hypothesis of cryo-injury by Mazur [57]. It was known that when cells were either cooled too slowly or too rapidly they were damaged after thawing. According to Mazur's two-factor hypothesis, the damage from slow-cooling was attributed to the cell's exposure to concentrated solutions (often referred to as solution effects injury) and the damage from fast-cooling was attributed to the formation of intracellular ice. It was demonstrated that the relative cooling rates which were too low or too high were cell type specific and were shown to be dependent on the permeability characteristics of the cell [55]. Specifically, the hydraulic conductivity of the membrane and the temperature dependence of that permeability will dictate the cooling rates at which each type of damage occurs for that specific cell-type.

The exact mechanisms of injury due to exposure to concentrated solutions or the formation of intracellular ice have not been completely elucidated. There have been many proposed mechanisms of injury for both solution effects injury and intracellular ice formation (IIF) injury. Many of the theories on solution effects injury involve damage to the cell membrane. Lovelock proposed that the high salt concentrations that cells are exposed to during cooling causes the cell membrane to become leaky,

---

<sup>2</sup> Supercooling is when a solution is below its thermodynamic freezing point without the formation of ice.

causing an increase in intracellular solute concentration and thus lysing upon warming [50]. Meryman proposed that membrane damage occurs when cells are excessively shrunken to a critical volume. This damage causes the membrane to become leaky, resulting in an increase in intracellular concentration and cells lysis upon warming [60]. Farrant and Morris proposed that the hypertonic solutions produced during cooling alter the cell membranes, but that the solutions themselves are not the damaging factors. The altered cell membrane is damaged when exposed to another stress, such as the reduction in temperature during cooling (thermal shock) or dilution upon warming (dilution shock) [23].

Many mechanisms of damage from IIF have also been proposed, including: mechanical forces acting on the cell membrane [7; 25; 58]; frictional forces from the water flux across the cell membrane [64]; increased intracellular solute concentration following the formation of ice which may alter intracellular membranes [23]; irreversible damage to the intracellular proteins caused by the formation of disulfide bridges which occurs due to intracellular ice crystals bringing proteins in close contact with each other [47]; and intracellular ice induced formation of intracellular gas bubbles during warming [61]. As with the solution effects injury, none of these mechanisms can explain the experimental observations of injury from intracellular ice for all cell types or under all conditions. However, even without understanding the exact mechanism, it is commonly believed that the membrane is the site of the IIF damage [4; 5; 15; 55; 56]. Acker

and McGann investigated the incidence of IIF and membrane damage on a cell-specific basis using a cryomicroscope system and found a direct correlation between the cells that experienced IIF and those with post-thaw membrane damage [2; 4]. Whether the IIF is the cause or result of membrane damage is still unknown.

### *1.1.2. Cryoprotective agents*

In order to mitigate the damage caused by freezing, compounds referred to as cryoprotective agents (CPAs) are often added to the cells before cooling. There are two types of CPAs: (i) permeating CPAs, which are typically low-molecular weight compounds that can cross the cell membrane; and (ii) non-permeating CPAs, which are larger molecules that are unable to cross the cell membrane. Common permeating CPAs are dimethyl sulphoxide (DMSO), glycerol (although at temperatures  $\leq 4$  °C, glycerol is a non-permeating CPA), propylene glycerol (PG), ethylene glycol (EG), to name a few. Sugars (trehalose, sucrose, glucose), starches (hydroxyethyl starch), and proteins (skim milk proteins, egg proteins) are commonly used non-permeating CPAs.

The CPAs work by increasing the osmolality of the solution, which depresses the solution's thermodynamic freezing point (this relationship is described in section (1.3.1)). By decreasing the temperature at which ice first forms, the CPAs also decrease the amount of ice formed. At a given temperature, the solute concentration is also reduced, since there is more

liquid water in the solution. Lovelock demonstrated that the addition of glycerol protects erythrocytes from damage during cooling by altering the phase diagram of the solution and reducing the high salt concentration during freezing [51]. Since permeating CPAs cross the cell membrane, there is an increase in the intracellular osmolality of the cell due to the increasing concentration of the intracellular solutes. With permeating CPAs the increase in osmolality occurs without a reduction in the cell volume. In other words, at equilibrium (extracellular osmolality = intracellular osmolality) the cell will have the same volume as in the isotonic solution, but the intra- and extra-cellular osmolalities are both increased. In the presence of permeating CPAs, cells can be cooled slowly without solution effects injury, since at any given temperature the intra- and extra-cellular salts and other biological solutes are less concentrated because there is less ice formed.

Conversely, non-permeating CPAs cause an increase in the extracellular osmolality, but they cannot cross the cell membrane to increase the intracellular osmolality. Instead, the cell osmotically dehydrates until osmotic equilibrium is attained (extracellular osmolality = intracellular osmolality). The reduction in cell water corresponds to a reduction in the probability of IIF. Non-permeating CPAs are used to avoid the injury associated with IIF, as the cells have been partially dehydrated before cooling begins.

However, the use of CPAs often causes another type of damage to cells, which is referred to as toxicity. Toxicity-related injury from the CPAs is dependent on the concentration, temperature, and time of exposure [19]. Much research has focused on designing cocktails which contain multiple types of CPAs in order to achieve an overall high CPA concentration, but with each component at a low enough concentration to avoid the toxicity-related injury associated with each component. This has led to the development of very complicated, multisolute CPA solutions, often with three or more CPAs being utilized [21; 75; 76].

In addition to being toxic to the cells which are being cryopreserved, CPAs often cause adverse effects in patients when the cells are transfused. In the case of hematopoietic stem cells cryopreserved in DMSO, complications ranging from nausea, headaches, or abdominal cramps to acute renal failure or transient global amnesia have been reported [9; 11; 53; 65; 88]. Thus, another area of current research is designing cryopreservation protocols that allow the reduction or elimination of CPAs, while still achieving high cell recovery post-thaw. This research area has proven very difficult, with only few examples of successful cryopreservation in the absence of CPAs [41; 82].

## 1.2. Mathematical modelling in cryobiology

In order to overcome some of the obstacles in cryopreservation, mathematical modelling has been increasingly utilized to assist in the

design of novel cryopreservation protocols [35; 49; 80; 81; 84; 89; 98]. The use of modelling to predict cellular responses to cryopreservation was pioneered by Mazur [55] and has since been adopted by many researchers [3; 17; 34; 49; 63; 64; 71; 72; 73; 80; 81; 90; 91; 94; 98]. Modelling has been used to interpret experimental results [3; 55; 63], investigate the impact of various parameters on cellular responses to freezing [55], determine the conditions which result in IIF [29; 30; 34; 55; 71; 90; 94], calculate the transport of water and CPAs in cellular and tissue systems [1; 18; 31; 37; 62; 83], predict the behaviour of cryobiological solutions [20; 40; 44; 45; 46; 67; 68; 69; 100; 101], and design novel cryopreservation protocols [35; 49; 80; 81; 84; 89; 98].

Mazur's landmark mathematical model of cellular osmotic response to freezing involved numerical solutions to an equation which coupled water transport across the cell membrane with an ideal, dilute solution assumption for the cytoplasm, an exponential equation for the temperature dependence of the membrane's water permeability, and a constant cooling rate [55]. The predicted cell volumes as a function of cooling rate were compared to the predicted cell volumes of cells cooled infinitely slowly (i.e. the equilibrium cell volume). At any temperature, the differences between the predicted volume of a cell cooled at a given rate and the equilibrium curve gave a prediction of how supercooled the cell was. Mazur assumed that cells which retained more than 10 % of their isotonic volume and were more than 2 degrees supercooled when the temperature reached a critical

value would experience IIF. This model allowed qualitative predictions of the conditions that could lead to IIF for different cell types.

This basic approach of predicting the cellular osmotic response to sub-zero temperatures and using calculated predictors of cryo-injury has been taken up by other researchers. The research group of McGann and Elliott [17; 80; 81] have developed a cellular osmotic simulation program which can be used to calculate cellular osmotic responses to (i) the addition/removal of CPAs at a constant temperature or as a function of temperature and (ii) any temperature profile (linear or nonlinear) in the presence or absence of CPAs. The simulations require various cell specific inputs, including permeability parameters, temperature dependencies of permeability parameters, isotonic cell volume, osmotically-inactive fraction, and isotonic intra- and extra-cellular solution compositions. The information obtained from this model includes the cell volume, intracellular solution composition, and degrees of intracellular supercooling as functions of time (or temperature). It has been shown that the calculated intracellular osmolality and the intracellular supercooling are accurate indicators of damage for both two-step and graded freezing protocols [79]. Those two calculated indicators are assumed to be related to the damage caused by solution effects and IIF, respectively. However, translating the calculated results of the model into predictions of cryo-injury requires knowledge (or an assumption) of the levels of intracellular osmolality which leads to solution effects injury and the degree of

intracellular supercooling which leads to IIF. The model does not predict the magnitude of damage (i.e. how many cells in a population will be damaged by either mechanism), but allows for determination of conditions which are likely to lead to solution effects injury or IIF.

Other researchers have focused on developing models to predict the probability of IIF [34; 71; 90; 94] using a water transport equation to determine the cellular osmotic response to extracellular ice coupled with either an assumed supercooling tolerance [55; 71] or an ice nucleation theory [34; 90; 94]. In all of the IIF models, the amount of intracellular supercooling is an important parameter in predicting the probability of IIF. These models have led to an increased understanding of the conditions which lead to IIF and facilitated the development of hypothesis for the mechanisms of IIF. However, the models base the calculated amount of supercooling on ideal, dilute solution assumptions, which may result in erroneous calculations of the amount of intracellular supercooling at the IIF nucleation temperature or incorrect interpretation of the relationship between supercooling and IIF.

In order to model cellular osmotic responses, there are several important equations and various cell type-specific parameters required. Equations for the (i) transport of water and solutes across the cell membrane, (ii) osmolality of the intra- and extra-cellular solutions as a function of solution composition (referred to herein as the solution behaviour), and (iii) cellular osmotic equilibrium are required. To extend the

model to predicting IIF, an equation to predict nucleation is also required. The equations used to model cellular osmotic responses typically contain cell-type specific parameters, such as the membrane hydraulic conductivity ( $L_p$ ), the solute permeabilities for each permeating solute ( $P_s$ ), the temperature dependences of  $L_p$  and  $P_s$  (described with activation energies  $E_a^{Lp}$  and  $E_a^{Ps}$ ), the isotonic cell volume ( $V_o$ ), and the osmotically-inactive fraction of the cell volume ( $b$ ).

One of the limitations of many of the equations that are commonly used in cryobiological modelling is that they contain ideal, dilute solution assumptions. Assuming that the intra- and extra-cellular solutions are ideal and dilute at isotonic conditions may be reasonable, but this assumption is definitely violated as the solutions are concentrated either by the addition of CPAs or by the increasing amount of ice as the temperature is reduced to  $-40\text{ }^\circ\text{C}$  and below.

The research group of McGann and Elliott has developed transport equations for water and solutes that are correct for non-ideal, non-dilute solutions [1; 18] and these equations should be incorporated into cryobiological models. Much cryobiology research has focused on predicting the solution behaviour of solutions of cryobiological interest, but the equations that have been developed contain several significant limitations which have prevented their applicability to a wide range of solutions. In addition, others have recognized that the ideal, dilute osmotic equilibrium equation (the Boyle-van't Hoff equation) results in predictions

of the osmotically-inactive fraction that are larger than expected. Modifications to the Boyle-van't Hoff equation or explanations for the high osmotically-inactive fraction of erythrocytes have been proposed, but the corrections don't eliminate the ideal, dilute solution assumption in the equation [10; 14; 24; 26; 28; 36; 54; 78; 86; 96; 99].

### 1.3. Thermodynamic relationships in cryobiology

In mathematically describing cellular responses to cryobiology, there are several thermodynamic relationships which are important. Osmolality is a key cryobiological parameter because it defines the thermodynamic freezing point of the solution and is also the driving force for water transport across the cell membrane. Osmolality is defined by its relationship to the chemical potential and is related to several other thermodynamic quantities, such as freezing point depression, osmotic coefficient, and water activity. These quantities are often used interchangeably in cryobiological equations (with suitable unit conversions).

#### 1.3.1. *Freezing point depression and osmolality*

Since osmolality and freezing point play such a large role in cryobiology, equations have been developed to predict both of these quantities for multisolute extra- and intra-cellular solutions. Osmolality and

freezing point depression are related to each other, so once one is known, the other can be determined.

From the Gibbs-Duhem equation [74], the relationship between freezing point depression,  $\Delta T_{FP}$ , of an aqueous solution and osmolality,  $\pi$  (osmoles/kg solvent), can be obtained [97] (see Appendix A).

$$\Delta T_{FP} = T_{FP}^o - T_{FP} = \left[ W_1 / \left( \overline{s}_1^{0L} - \overline{s}_1^{0S} \right) \right] RT_{FP} \pi \quad (1.1)$$

where  $T_{FP}^o$  is the freezing point of the pure solvent (water),  $T_{FP}$  is the freezing point of the solution,  $W_1$  is the molecular weight of water (kg/mole),  $\overline{s}_1^{0L}$  is the entropy per mole of pure liquid water (J/moleK),  $\overline{s}_1^{0S}$  is the entropy per mole of pure water in the solid phase (J/moleK), and  $R$  (J/moleK) is the universal gas constant. In the derivation of equation (1.1), the molar entropies of water,  $\overline{s}_1^{0L}$  and  $\overline{s}_1^{0S}$ , are assumed to be constant. The values for the constants in equation (1.1) can be found in Table 1.1. Equation (1.1) can be rearranged to yield osmolality as a function of the freezing point depression:

$$\pi = \frac{T_{FP}^o - T_{FP}}{\left[ W_1 / \left( \overline{s}_1^{0L} - \overline{s}_1^{0S} \right) \right] RT_{FP}} \quad (1.2)$$

The nonlinear conversion between osmotic pressure and freezing point depression has been previously published [97]. However in that study the density of water is missing in the conversion between osmotic

pressure and osmolality, which results in a slightly different conversion between osmolality and freezing point depression.

Equation (1.1) can also be used to convert osmolality to freezing point depression. Since the freezing point of the solution ( $T_{FP}$ ) appears on both sides of equation (1.1), equation (1.1) is usefully rearranged so that  $T_{FP}$  appears only on the left hand side of the equation.

$$T_{FP}^o - T_{FP} = \frac{\left[ W_1 / \left( \overline{s}_1^{0L} - \overline{s}_1^{0S} \right) \right] R T_{FP}^o \pi}{1 + \left[ W_1 / \left( \overline{s}_1^{0L} - \overline{s}_1^{0S} \right) \right] R \pi} \quad (1.3)$$

By neglecting the last term in the denominator, the conversion between freezing point depression and osmolality, equation (1.3), is linearized yielding the widely used equation [6; 38; 95; 97]:

$$T_{FP}^o - T_{FP} \approx 1.86\pi$$

or

$$\pi \approx \frac{T_{FP}^o - T_{FP}}{1.86} \quad (1.4)$$

### 1.3.2. Osmotic coefficient and osmolality

The osmotic coefficient,  $\Phi$ , is often used to express the osmolality of a solution. For a single-solute solution, the osmotic coefficient is defined as:

$$\Phi = \frac{\pi}{m} \quad (1.5)$$

where  $m$  is the molal concentration of the solute (mole solute/kg solvent).

For a multisolute solution, the osmotic coefficient is defined as the osmolality divided by the total solute molality.

$$\Phi = \frac{\pi}{\sum_i m_i} \quad (1.6)$$

### 1.3.3. Water activity and osmolality

In addition to the relationships between freezing point, osmolality, and osmotic coefficient, the relationship between water activity and osmolality is often needed. Many cryobiological solution theories provide predictions of the solution behaviour in water activity, which is then converted to osmolality or freezing point.

Water activity,  $a_1$ , is defined through its relationship to chemical potential,  $\mu_1$  [74; 95]:

$$\mu_1 - \mu_1^o = RT \ln a_1 \quad (1.7)$$

where  $\mu_1$  is the chemical potential of water (J/mole),  $R$  is the universal gas constant (J/moleK), and  $T$  is temperature (K). The subscript 1 refers to the solvent (water) and the superscript o refers to the standard state.

Using the approach of Landau and Lifshitz [43]<sup>3</sup>, osmolality,  $\pi$  (osmoles/kg water), is defined by the following relationship to chemical potential:

---

<sup>3</sup> While many solution theories are written from an *a priori* assumption of dependence on mole fraction, Landau and Lifshitz [43] had a different *a priori* assumption involving dependence on molality.

$$\mu_1 - \mu_1^o = -RTW_1\pi \quad (1.8)$$

Comparing equations (1.7) and (1.8) gives the following relationship between water activity and osmolality:

$$\pi = -\frac{\ln a_1}{W_1} \quad (1.9)$$

The relationship between osmotic pressure,  $\Pi$ , and osmolality is:

$$\Pi = RT\rho_1\pi \quad (1.10)$$

where  $\rho_1$  is the density of water ( $\text{kg}/\text{m}^3$ ). Thus the relationship between osmotic pressure and water activity is:

$$\Pi = -RT \frac{\ln a_1}{v_1} \quad (1.11)$$

where  $v_1$  is the molar volume of water ( $\text{m}^3/\text{mole}$ ).

These quantities are extensively used in the solution thermodynamic equations used to model cellular responses to cryopreservation.

#### 1.4. Multisolute solution models in cryobiology

Due to the complicated intra- and extra-cellular solutions in cryobiology which contain a wide range of solutes, from electrolytes to CPAs to macromolecules, measuring all possible multisolute solutions is prohibitively time- and resource-consuming. Thus, an accurate predictive multisolute model is required. This need has long been recognized in cryobiology and many models for cryobiological solutions have been

developed [20; 40; 44; 45; 46; 67; 68; 69; 100; 101]. Within cryobiology, there are several different types of solution theories. The first is ideal, dilute solution theory in which interactions between solute molecules are not taken into account. This approach is often valid at very low solute concentrations, where the solute molecules are not interacting with each other. Additionally, some molecules (such as methanol) can be approximated as ideal solutes in water over a larger concentration range, up to almost 20 molal (i.e. interactions between methanol molecules in water do not contribute significantly to the solution behaviour). However, the ideal, dilute approach does not work well for the majority of relevant solutes in water past very low concentrations, including most CPAs, electrolytes, alcohols, and macromolecules.

In order to account for the non-ideal behaviour of solutions, several solution theories have been developed. These include empirical fitting equations and solution theories developed from thermodynamic principles. The empirical solution theories require parameters that are obtained by fitting multisolute solution data in order to predict multisolute data. The fitting parameters capture the non-ideal behaviour of the solutes which arise from the interactions between the solute molecules. The parameters are unique for each particular solution and must be obtained from multisolute data for each new combination of solutes. These solution theories provide accurate results for the specific solutions for which the fitting parameters can be obtained; however, they can only be used to

make predictions of solution behaviour for which multisolute solution data are available, which greatly limits their applicability in cryobiological modelling. Examples of this type of solution theory are the equations developed by Pegg [67; 68], Pegg and Arnaud [69], Woods *et al.* [100; 101], and Fahy [20].

Some multisolute solution theories have been developed from thermodynamic principles and applied to cryobiological solutions. For example, the van Laar equations have been applied to predict the behaviour of red blood cell cytoplasm [44; 45; 46]. The van Laar equations use the van der Waal's mixing rules, which are not accurate for many liquids, including solutions containing macromolecules or electrolytes [74]. The van der Waal's mixing rules can be removed from the van Laar equations, but this requires the use of empirical constants, which restricts the usage of the van Laar equations to solutions for which multisolute solution data are available.

The following section outlines some of the solution theories that have been applied in cryobiology to capture the non-ideality of the multisolute solutions, including the assumptions used in the equations and the limitations to each approach.

(i) Empirical solution theories

Pegg [67; 68] and Pegg and Arnaud [69] fit equations to data for melting point as a function of concentration for specific ternary and quaternary solutions in order to obtain empirical parameters for specific

combinations of solutes. The empirical parameters are typically functions of the mass ratio of the first solute to the second solute, (i.e. the R-value). Fitted equations for mixtures of DMSO + sodium chloride (NaCl) + water, glycerol + NaCl + water, and PG + glycerol + NaCl + water [67; 68; 69] were generated. The equations are in terms of total solute mass fraction  $\left(\sum_i X_i\right)$  and are of the general form:

$$T_m = a\left(\sum_i X_i\right) + b\left(\sum_i X_i\right)^2 + \dots \quad (1.12)$$

where  $T_m$  is the melting point of the solution ( $^{\circ}\text{C}$ ),  $a$  and  $b$  are fitting parameters which are typically functions of the R-value,  $\sum_i X_i$  is the total solute mass fraction (g/100g of solution), where  $i$  refers to each solute, and  $X_i$  is the mass fraction of solute  $i$  (g/100 g of solution). The polynomial expansion in total solute mass fraction is truncated after sufficient parameters are included to describe the multisolute melting point data. The non-ideal solution behaviour is captured by the fitting parameters which account for the interactions between all of the solute molecules.

Woods *et al.* also used this approach to develop equations to predict the melting point of solutions containing ethylene glycol (EG) + NaCl + water [100; 101].

The constants in equation (1.12) are specific for each solution and cannot be applied to different combinations of solutes. When multisolute

solution data is available, this approach results in accurate predictions. However, it is limited to solutions for which multisolute solution data are available. In addition, data for each new combination of solutes must be fit to obtain new coefficients.

Fahy fit functions to data for freezing point as a function of concentration for the ternary systems of glycerol + NaCl + water and DMSO + NaCl + water [20], of the form:

$$T = \frac{-\left[0.7451 - \left(0.56865 - f\left(\sum_i x_i\right)\right)^{1/2}\right]}{6.405 \times 10^{-3}} \quad (1.13)$$

where  $T$  is the temperature ( $^{\circ}\text{C}$ ),  $f$  is an empirical function that is obtained from the fit,  $\sum_i x_i$  is the total solute mole fraction (moles solute/total moles) where  $i$  refers to each solute, and  $x_i$  is the mole fraction of solute  $i$  (moles solute  $i$ /total moles).

Fahy used equation (1.13), along with other relationships, to calculate the composition, water content, salt concentration, and unfrozen fraction as a function of temperature. As with Pegg's equations, this approach results in highly accurate predictions, but is limited to solutions for which multisolute solution data are available and each new multisolute solution must be fit with a new function,  $f$ .

(ii) Multisolute solution theories derived from thermodynamic principles

Levin *et al.* proposed several models for the cytoplasm of an erythrocyte [44; 45; 46]. In two of these models, they assumed that the cytoplasm is an ideal solution with a certain amount of water bound to each solute [44; 46]. The papers referred to the solutes with bound water as "hydrated solutes". In one study, Levin *et al.* modelled the cytoplasm of an erythrocyte as a non-ideal, non-dilute, hydrated, pseudo binary solution of water and a "fictitious solute" [45]. The fictitious solute represents all the solutes which are in the cytoplasm of a red blood cell. Levin *et al.* used van Laar type equations for the activity coefficients of the two solution species (solute and solvent). The van Laar equation uses van der Waal's mixing rules, which are not accurate for many solutions [74], but Levin *et al.* addressed this limitation by replacing the mixing rules with empirical constants. The resulting equations for the solvent and solute activities,  $a_w^h$  and  $a_m^h$  respectively, are:

$$\ln a_w^h = \frac{\alpha}{\left(1 + \frac{\alpha}{\beta} \left(\frac{x_w^h}{x_m^h}\right)\right)^2} \quad (1.14)$$

$$\ln a_m^h = \frac{\beta}{\left(1 + \frac{\beta}{\alpha} \left(\frac{x_m^h}{x_w^h}\right)\right)^2} - \beta \quad (1.15)$$

where  $a_w^h$  is the water activity on a hydrated basis,  $a_m^h$  is the solute activity on a hydrated basis,  $x_w^h$  is the water mole fraction on a hydrated basis,  $x_m^h$

is the solute mole fraction on a hydrated basis, and  $\alpha$  and  $\beta$  are empirical constants. To determine the van Laar coefficients,  $\alpha$  and  $\beta$ , the water activity of the cytoplasm as a function of concentration is required. This necessitates additional simplifying assumptions about the composition of the cytoplasm in order to determine the water activity. In addition, due to the use of empirical parameters, this approach is limited to the solutions for which multisolute solution data are available.

*(iii) Multisolute solution theories in the absence of multisolute data*

In order to predict multisolute solution behaviour, all of the previous solution theories describing non-ideal solutions require empirical parameters obtained by fitting the multisolute data of the solution of interest. Although these solution theories are accurate for the particular subset of solutions for which the empirical parameters can be determined, they cannot be applied to solutions for which there are no multisolute solution data. In order to address this disadvantage, many investigators have used the approach of adding single-solute solution osmolalities to predict multisolute solution osmolalities (or freezing point depressions) [39; 52]. Most recently, Kleinhans and Mazur used this approach to predict the freezing point depressions of four different mixtures of a CPA and NaCl in water [40]. They fit the data for freezing point as a function of concentration of single-solute solutions containing water plus either DMSO, glycerol, EG, or NaCl with cubic polynomials as functions of solute molality.

$$T_{FP} = C_1 m + C_2 m^2 + C_3 m^3 \quad (1.16)$$

where  $T_{FP}$  is the freezing point of the solution ( $^{\circ}\text{C}$ ),  $C_1$ ,  $C_2$ , and  $C_3$  are fitting parameters, and  $m$  is the solute molality.

These coefficients were then used to predict the freezing point depressions of solutions containing water with two solutes. For a two-solute solution, with a solute-A molality of  $m_A$  and a solute-B molality of  $m_B$ , the predicted freezing point is:

$$\begin{aligned} T_{FP}^S &= T_{FP}^A + T_{FP}^B \\ &= (C_{1A} m_A + C_{2A} m_A^2 + C_{3A} m_A^3) + (C_{1B} m_B + C_{2B} m_B^2 + C_{3B} m_B^3) \end{aligned} \quad (1.17)$$

where  $T_{FP}^S$  is the freezing point of the two-solute solution,  $T_{FP}^A$  is the freezing point of a single-solute solution of solute A, and  $T_{FP}^B$  is the freezing point of a single-solute solution of solute B.

The summation of the freezing point depressions (or osmolalities) approach does allow prediction of multisolute solutions using only single-solute data. The fitting parameters ( $C_2$  and  $C_3$ ) account for the interactions between solute molecules of the same type. However this approach does not take into account the interactions between the different types of solute molecules (i.e. interactions between solute A and solute B). Nonetheless, this approach has been shown to work well in practice for the particular set of multisolute solutions in the Kleinhans and Mazur study.

All of the solution theories previously developed in cryobiology either (i) contain simplifying assumptions regarding the interactions between solute molecules (e.g. ideal and dilute solutions, approach of adding osmolalities) or (ii) require fitting of multisolute data to make predictions of the multisolute solution. Thus, a multisolute model which has takes into account the interactions between solute molecules and requires only single-solute information is required. Due to the large range of solutions of interest, the multisolute model must be shown to be accurate for combinations of many different types of solutes.

### 1.5. Osmotic equilibrium

Currently cellular osmotic equilibrium is described with the Boyle-van't Hoff relation, which states that the product of osmolality and equilibrium volume of the osmotically-active portion of the cell is constant. This is equivalent to the ideal gas law and is thus only applicable to ideal, dilute solutions.

It has been noted in the past that in some cases the Boyle-van't Hoff relationship yields osmotically-inactive fractions higher than predicted from desiccation experiments [86] that measure the dry volume of the cell, which can be used as another estimate of the osmotically-inactive volume of the cell. The discrepancy between osmotically-inactive volume and dry volume has been discussed for human erythrocytes [86]. There have been many explanations for this difference, including bound water [10; 86; 96],

the movement of chloride ions between the extra- and intra-cellular solutions [10], the osmotic properties of intracellular solutes [24; 27; 54; 78], the large entropy of dilution characteristic of macromolecular solutes [14], and erythrocyte membrane characteristics [28; 54; 99]. Improvements in how the osmotic equilibrium data is fit to the Boyle-van't Hoff equation have also been proposed in order to obtain more accurate predictions for the osmotically-inactive fraction [36]. However, none of the proposed corrections to the Boyle-van't Hoff eliminate the ideal, dilute solution assumption inherent in the equation.

#### 1.6. Current understanding of IIF in cryobiology

As with the mechanism of injury from IIF, the conditions which lead to the nucleation of intracellular ice are not understood. Since there is evidence that the IIF behaviour of cells is greatly influenced by the presence of extracellular ice [56; 77], it is believed that the interaction between extracellular ice and the cell plays an important role in nucleating intracellular ice. There are three main theories of how extracellular ice nucleates intracellular ice: (i) the pore theory [3; 56]; (ii) the membrane failure hypothesis [7; 16; 64]; and (iii) the surface-catalyzed nucleation of intracellular ice [90].

The hypothesis of the pore theory is that external ice grows through pores in the intracellular membrane to nucleate the supercooled intracellular water. Mazur [56] proposed the pore theory and stated that

above a critical temperature, the radius of the thermodynamically stable ice crystals are too large to grow through the intracellular pores (which have a radius of 3-8 Å). Thus, above this critical temperature the membrane will act as a barrier to extracellular ice, but below the critical temperature ice will grow through the membrane pores. Acker, Elliott, and McGann [3] refined Mazur's pore theory by including the effect of solutes and not neglecting the volume change on freezing in the capillary freezing point depression equation. They correlated the predictions of the critical temperature for ice growth through pores to intracellular ice propagation through gap junctions in monolayers.

The membrane failure hypothesis presumes that extracellular ice initiates IIF when the supercooled cytoplasm is exposed to extracellular ice due to mechanical failure of the plasma membrane. Various causes of membrane failure during freezing have been proposed, including endocytotic vesiculation during osmotic shrinking, thermal perturbations of the membrane, and electrical transients at the advancing ice front [87]. Muldrew and McGann [64] proposed that the membrane damage is due to frictional forces acting on the membrane during water efflux from the cell. The damage occurs at a critical osmotic pressure gradient between the intra- and extra-cellular solutions.

Unlike the previous two theories which assume that the barrier function of the membrane has to fail in order for IIF to occur, the theory of surface-catalyzed nucleation (SCN) assumes that the interaction between

the extracellular ice and the membrane causes a change in the internal surface of the membrane, which catalyzes the nucleation of intracellular ice [90].

In an effort to further the understanding of the mechanism of IIF and predict its occurrence in various cell types, a range of mathematical models of IIF have been proposed. The first model of IIF was developed by Mazur [55]. He coupled a water transport model with a supercooling tolerance, a critical cell water volume percentage, and a critical IIF nucleation temperature. The critical cell water volume was set to 10% of the isotonic water content based on observations from yeast and *E. coli*. Mazur proposed that the critical nucleation temperature could be calculated from his pore theory [56], but due to lack of experimental measurements for some of the parameters the critical temperature was based on experimental observations from the cell type of interest. The supercooling tolerance was assumed to be 2 °C. This model provided qualitative predictions of IIF behaviour for a range of cell types [55]. However, it provides predictions of the probability of IIF of 0 (no incidence of IIF) or 1 (100% incidence of IIF) and can thus not predict experimental observations of intermediate amounts of IIF. Pitt and Steponkus [71] modified Mazur's model to be able to predict transition regions between 0 % IIF and 100 % IIF by assuming that the supercooling tolerance and IIF nucleation temperature were independent random variables that could be described using a Weibull distribution. Subsequent to their initial

modification of Mazur's model, various adjustments were made to the IIF model to enable predictions of a range of experimental observations of IIF in *D. melanogaster* embryos, rye protoplasts, bovine oocytes, and mouse oocytes [73]. In one study, Pitt *et al.* applied their model to predict the IIF behaviour of *D. melanogaster* embryos frozen in ethylene glycol [72]. The model predictions were less accurate in the presence of a CPA than without CPA present, but this represented the first attempt to make predictions of IIF behaviour in the presence of a CPA that could be compared to independent experimental data.

In order to predict the IIF behaviour of human erythrocytes, Toscano *et al.* [94] proposed the first mechanistic model of IIF. The model incorporates the Turnbull and Fisher nucleation theory and the water transport model utilized by Mazur. The prediction of the nucleation of IIF depends on a kinetic coefficient and a thermodynamic barrier, both of which are dependent on the composition of the intracellular solution.

Toner *et al.* [90] proposed a model of IIF in which intracellular ice nucleation was catalyzed by the internal surface of the membrane (surface-catalyzed nucleation) or small particles in the intracellular solution (volume-catalyzed nucleation). Similar to the model of Toscano *et al.*, the nucleation rates for both mechanisms are predicted using both a kinetic and thermodynamic coefficient, which are functions of the composition of the cytoplasm. The nucleation rate equations are strongly dependent on the degree of intracellular supercooling. The model was validated using

experimental measurements of IIF behaviour of mouse oocytes and gave accurate predictions for constant cooling rate experiments, but the predictions were less accurate for isothermal IIF experiments. In order to predict the occurrence of IIF in human hepatocytes, Toner *et al.* simplified the model [91], most notably by eliminating the volume-catalyzed nucleation mechanism. In the simplified model the two nucleation parameters could be obtained from a single constant cooling rate experiment for each cell type. The incidence of IIF for a wide range of cell types, from mouse oocytes, one-cell mouse embryos, hepatocytes, *D. melanogaster* embryos, beta-islet cells, and rye protoplasts (cold-acclimated and non-acclimated), was predicted using Toner's model and reasonable agreement attained for both constant cooling rate and isothermal experiments [33]. In addition, the model of Toner *et al.* was utilized to optimize a cooling protocol for mouse oocytes in the absence of permeating CPAs [35].

In order to extend the model's applicability to freezing protocols with permeating CPAs, Karlsson *et al.* [34] made some modifications to Toner *et al.*'s model. In addition to predicting IIF in the presence of CPAs, the model of Karlsson *et al.* included a crystal growth model to predict the extent of intracellular crystallization and the size distribution of the intracellular ice crystals. The model developed by Karlsson *et al.* [34] represented the first mechanistic model of IIF in the presence of CPAs and the first incorporation of a crystal growth model with a nucleation

model. The model demonstrated that the effect of CPAs on IIF was dependent on the initial CPA concentration and rate of cooling. This model could be applied to optimize both conventional slow-cooling cryopreservation protocols and also vitrification protocols involving high CPA concentrations and rapid cooling.

As experimental evidence has shown that cell-to-cell contacts alter both the incidence of and damage associated with IIF [2; 5], the mechanistic models of IIF have been applied by Irimia *et al.* to investigate the effect of cell-to-cell contact of attached cells on the incidence and propagation of IIF in multi-cell systems [29; 30]. The model accuracy was confirmed using experimental measurements of IIF in four-cell arrays and was then used to predict IIF propagation in tissues.

The mechanistic models of IIF require several cell-specific parameters, including a kinetic coefficient and a thermodynamic coefficient, which are obtained from both isothermal and constant cooling rate experiments. Lack of experimental measurements for these parameters limits the applicability of the mechanistic models to a few cell types [33].

Mathematical modelling has been extensively used in cryobiology to understand and predict the occurrence of IIF in cells and how parameters such as intracellular supercooling and cell volume influence the incidence of IIF [33; 34; 55; 71; 72; 73; 90; 91; 92; 94]. In addition to furthering the understanding of the cellular responses to freezing, the use of modelling

has contributed significantly to the optimization of cryopreservation protocols for several cell types [35; 49; 89]. Additional improvements to the models are needed, as many of the equations used to predict IIF and interpret the relationships between intracellular supercooling, cell volume, and IIF contain ideal, dilute solution assumptions [12; 16; 34; 35; 55; 71; 72; 73; 90; 91; 92; 94]. In addition, using improved calculations to accurately determine the degree of intracellular supercooling and the cellular osmotic responses, the role of intracellular supercooling, cell volume, and extracellular ice nucleation temperature on incidence of IIF requires additional experimental investigation.

### 1.7. Improvements proposed in this thesis

This thesis work addressed two of the key limitations in current mathematical modelling of cellular osmotic responses to cryopreservation and demonstrated how the improved mathematical model can be combined with experimental measurements in order to gain additional understanding of cellular responses to cryopreservation.

Firstly, an accurate, predictive multisolute solution theory that requires only single-solute information was shown to be applicable to a wide range of aqueous ternary solutions of cryobiological interest. The multisolute osmotic virial equation (OVE) with novel mixing rules that have been derived from thermodynamic first principles was used to predict the solution behaviour of aqueous solutions of (i) two low-molecular weight

CPAs, (ii) a protein and an ideal solute (which is used to model the cytoplasm of an erythrocyte); (iii) two proteins, (iv) a low-molecular weight CPA and an electrolyte, and (v) a macromolecule and an electrolyte. In addition, the use of the multisolute OVE to solutions containing electrolytes was shown to be as accurate as using a more complicated electrolyte solution theory.

Secondly, a non-ideal osmotic equilibrium equation was derived that is correct for both ideal and non-ideal solutions. Using a non-ideal equation of state (the multisolute OVE) to express the intracellular solution osmolality as a function of solute concentration, the new non-ideal osmotic equilibrium equation was applied to the same data as the Boyle-van't Hoff equation in order to obtain the predicted osmotically-inactive fraction.

Finally, experimental measurements of the incidence of IIF following extracellular ice nucleation as a function of intracellular supercooling were made on a cryomicroscope which allowed cell-specific correlation of IIF with cell volume and post-thaw membrane integrity. In order to further investigate the role of cell volume and intracellular supercooling on the cellular osmotic response to the extracellular ice nucleation, a mathematical model was developed which incorporated the improved multisolute solution theory, the multisolute OVE, and the non-ideal osmotic equilibrium equation. Thus, the mathematical model used in this work does not contain ideal, dilute solution assumptions.

## 1.8. Objectives and hypothesis of this thesis

### 1.8.1. *General hypothesis*

The application of the multisolute osmotic virial equation, with mixing rules derived from thermodynamic first principles, to solutions of interest in cryobiology will result in more accurate predictions of the multisolute solution behaviour, which will lead to improved cryobiological modelling and increased understanding of cellular responses to cryopreservation.

### 1.8.2. *General objectives*

- 1) To develop predictive models of biological solutions.
- 2) To further the understanding of the link between supercooling, cell volume, and intracellular ice formation.

### 1.8.3. *Specific research objectives*

- 1) Develop a mathematical model that accurately predicts multisolute solution osmolality for intra- and extracellular solutions of interest in cryobiology (Chapters 2 - 4).
- 2) Develop a non-ideal osmotic equilibrium equation (Chapter 5).
- 3) Use experimental measurements and improved cryobiological modelling to understand the relationship between the incidence of

IIF and several important parameters, specifically intracellular supercooling and cell volume (Chapter 6).

The improvements in the solution thermodynamics and osmotic equilibrium equations used in cryobiological modelling proposed in this thesis will lead to increased understanding of cellular responses to cryopreservation. The combination of improved modelling and cryobiological experimentation may lead to the design of novel CPA solutions and cryopreservation protocols.

## 1.9. References

- [1] A. Abazari, J.A.W. Elliott, G.K. Law, L.E. McGann, and N.M. Jomha, A Biomechanical Triphasic Approach to the Transport of Nondilute Solutions in Articular Cartilage. *Biophysical Journal* (Accepted) (2009).
- [2] J.P. Acker, and L.E. McGann, Cell-cell contact affects membrane integrity after intracellular freezing. *Cryobiology* 40 (2000) 54-63.
- [3] J.P. Acker, J.A.W. Elliott, and L.E. McGann, Intercellular ice propagation: Experimental evidence for ice growth through membrane pores. *Biophysical Journal* 81 (2001) 1389-1397.
- [4] J.P. Acker, and L.E. McGann, Membrane damage occurs during the formation of intracellular ice. *Cryo-Letters* 22 (2001) 241-254.
- [5] J.P. Acker, and L.E. McGann, Innocuous intracellular ice improves survival of frozen cells. *Cell Transplantation* 11 (2002) 563-571.
- [6] F.G. Arnaud, and D.E. Pegg, Permeation of Glycerol and Propane-1,2-Diol into Human Platelets. *Cryobiology* 27 (1990) 107-118.
- [7] E. Asahina, Frost Injury in Living Cells. *Nature* 196 (1962) 445-446.
- [8] C. Boucherie, and E. Hermans, Adult stem cell therapies for neurological disorders: Benefits beyond neuronal replacement? *Journal of Neuroscience Research* 87 (2009) 1509-1521.
- [9] B. Calmels, P. Houze, J.C. Hengesse, T. Ducrot, C. Malenfant, and C. Chabannon, Preclinical evaluation of an automated closed fluid management device: Cytomate<sup>TM</sup>, for washing out DMSO from

- hematopoietic stem cell grafts after thawing. *Bone Marrow Transplantation* 31 (2003) 823-828.
- [10] J.S. Cook, Nonsolvent Water in Human Erythrocytes. *Journal of General Physiology* 50 (1967) 1311-1325.
- [11] K. Darabi, J.R. Brown, and G.S. Kao, Paradoxical embolism after peripheral blood stem cell infusion. *Bone Marrow Transplantation* 36 (2005) 561-562.
- [12] R.C. de Freitas, and K.R. Diller, Intracellular ice formation in three-dimensional tissues: Pancreatic islets. *Cell Preservation Technology* 2 (2004) 19-28.
- [13] I.A.M. de Graaf, A.L. Draaisma, O. Schoeman, G.M. Fahy, G.M.M. Groothuis, and H.J. Koster, Cryopreservation of rat precision-cut liver and kidney slices by rapid freezing and vitrification. *Cryobiology* 54 (2007) 1-12.
- [14] D.A.T. Dick, and L.M. Lowenstein, Osmotic Equilibria in Human Erythrocytes Studied by Immersion Refractometry. *Proceedings of the Royal Society of London, Series B* 149 (1958) 241-256.
- [15] K.R. Diller, E.G. Cravalho, and C.E. Huggins, Intracellular Freezing in Biomaterials. *Cryobiology* 9 (1972) 429-440.
- [16] M.F. Dowgert, and P.L. Steponkus, Effect of Cold-Acclimation on Intracellular Ice Formation in Isolated Protoplasts. *Plant Physiology* 72 (1983) 978-988.

- [17] S.L. Ebertz, and L.E. McGann, Osmotic parameters of cells from a bioengineered human corneal equivalent and consequences for cryopreservation. *Cryobiology* 45 (2002) 109-117.
- [18] H.Y. Elmoazzen, PhD Thesis, Osmotic transport in cryobiology, Dept. of Laboratory Medicine and Pathology, University of Alberta, Edmonton, Alberta (2006), pp. 221
- [19] H.Y. Elmoazzen, A. Poovadan, G.K. Law, J.A.W. Elliott, L.E. McGann, and N.M. Jomha, Dimethyl sulfoxide toxicity kinetics in intact articular cartilage. *Cell and tissue banking* 8 (2007) 125-133.
- [20] G.M. Fahy, Analysis of Solution Effects Injury Equations for Calculating Phase-Diagram Information for the Ternary-Systems NaCl-Dimethylsulfoxide-Water and NaCl-Glycerol-Water. *Biophysical Journal* 32 (1980) 837-850.
- [21] G.M. Fahy, B. Wowk, J. Wu, and S. Paynter, Improved vitrification solutions based on the predictability of vitrification solution toxicity. *Cryobiology* 48 (2004) 22-35.
- [22] G.M. Fahy, B. Wowk, J. Wu, J. Phan, C. Rasch, A. Chang, and E. Zendejas, Cryopreservation of organs by vitrification: perspectives and recent advances. *Cryobiology* 48 (2004) 157-178.
- [23] J. Farrant, and G.J. Morris, Thermal Shock and Dilution Shock as Causes of Freezing Injury. *Cryobiology* 10 (1973) 134-140.

- [24] J.C. Freedman, and J.F. Hoffman, Ionic and osmotic equilibria of human red blood cells treated with nystatin. *J Gen Physiol* 74 (1979) 157-85.
- [25] S. Fujikawa, Freeze-fracture and etching studies on membrane damage on human-erythrocytes caused by formation of intracellular ice. *Cryobiology* 17 (1980) 351-362.
- [26] C.M. Gary-Bobo, Nonsolvent Water in Human Erythrocytes and Hemoglobin Solutions. *Journal of General Physiology* 50 (1967) 2547-64.
- [27] C.M. Gary-Bobo, and A.K. Solomon, Properties of hemoglobin solutions in red cells. *J Gen Physiol* 52 (1968) 825-53.
- [28] P. Heubusch, C.Y. Jung, and F.A. Green, The osmotic response of human erythrocytes and the membrane cytoskeleton. *J Cell Physiol* 122 (1985) 266-72.
- [29] D. Irimia, and J.O.M. Karlsson, Kinetics and mechanism of intercellular ice propagation in a micropatterned tissue construct. *Biophysical Journal* 82 (2002) 1858-1868.
- [30] D. Irimia, and J.O.M. Karlsson, Kinetics of intracellular ice formation in one-dimensional arrays of interacting biological cells. *Biophysical Journal* 88 (2005) 647-660.
- [31] M.H. Jacobs, and D.R. Stewart, A simple method for the quantitative measurement of cell permeability. *Journal of Cellular and Comparative Physiology* 1 (1932) 71-82.

- [32] K.B. Jones, T. Seshadri, R. Krantz, A. Keating, and P.C. Ferguson, Cell-Based Therapies for Osteonecrosis of the Femoral Head. *Biology of Blood and Marrow Transplantation* 14 (2008) 1081-1087.
- [33] J.O.M. Karlsson, E.G. Cravalho, and M. Toner, Intracellular Ice Formation - Causes and Consequences. *Cryo-Letters* 14 (1993) 323-336.
- [34] J.O.M. Karlsson, E.G. Cravalho, and M. Toner, A Model of Diffusion-Limited Ice Growth inside Biological Cells during Freezing. *Journal of Applied Physics* 75 (1994) 4442-4445.
- [35] J.O.M. Karlsson, A. Eroglu, T.L. Toth, E.G. Cravalho, and M. Toner, Fertilization and development of mouse oocytes cryopreserved using a theoretically optimized protocol. *Human Reproduction* 11 (1996) 1296-1305.
- [36] I.I. Katkov, Challenge from the simple: Some caveats in linearization of the Boyle-van't Hoff and Arrhenius plots. *Cryobiology* 57 (2008) 142-149.
- [37] O. Kedem, and A. Katchalsky, Thermodynamic Analysis of the Permeability of Biological Membranes to Non-Electrolytes. *Biochim. Biophys. Acta.* 27 (1958) 229-246.
- [38] K. Kiyosawa, Theoretical and experimental studies on freezing point depression and vapor pressure deficit as methods to measure osmotic pressure of aqueous polyethylene glycol and bovine serum albumin solutions. *Biophys Chem* 104 (2003) 171-188.

- [39] F.W. Kleinhans, Membrane permeability modeling: Kedem-Katchalsky vs a two-parameter formalism. *Cryobiology* 37 (1998) 271-289.
- [40] F.W. Kleinhans, and P. Mazur, Comparison of actual vs. synthesized ternary phase diagrams for solutes of cryobiological interest. *Cryobiology* 54 (2007) 212-222.
- [41] S.C. Knight, J. Farrant, and L.E. McGann, Storage of human lymphocytes by freezing in serum alone. *Cryobiology* 14 (1977) 112-115.
- [42] L.L. Kuleshova, S.S. Gouk, and D.W. Hutmacher, Vitrification as a prospect for cryopreservation of tissue-engineered constructs. *Biomaterials* 28 (2007) 1585-1596.
- [43] L.D. Landau, and E.M. Lifshitz, *Course of Theoretical Physics, Statistical Physics, Vol. 5, 3rd Edition*, Pergamon Press, Oxford, 1980.
- [44] R.L. Levin, E.G. Cravalho, and C.E. Huggins, Effect of Hydration on Water-Content of Human Erythrocytes. *Biophysical Journal* 16 (1976) 1411-1426.
- [45] R.L. Levin, E.G. Cravalho, and C.E. Huggins, Effect of Solution Non-Ideality on Erythrocyte Volume Regulation. *Biochimica Et Biophysica Acta* 465 (1977) 179-190.
- [46] R.L. Levin, E.G. Cravalho, and C.E. Huggins, Concentration Polarization Effect in a Multicomponent Electrolyte Solution -

- Human Erythrocyte. *Journal of Theoretical Biology* 71 (1978) 225-254.
- [47] J. Levitt, Sulfhydryl-disulphide hypothesis of frost injury and resistance in plants. *Journal of Theoretical Biology* 3 (1962) 355-&.
- [48] Y. Li, J. Chen, L. Wang, L. Zhang, M. Lu, and M. Chopp, Intracerebral transplantation of bone marrow stromal cells in a 1-methyl-4-phenyl-1,2,3,6-tetrahydropyridine mouse model of Parkinson's disease. *Neuroscience Letters* 316 (2001) 67-70.
- [49] J. Liu, E.J. Woods, Y. Agca, E.S. Critser, and J.K. Critser, Cryobiology of rat embryos II: A theoretical model for the development of interrupted slow freezing procedures. *Biology of Reproduction* 63 (2000) 1303-1312.
- [50] J.E. Lovelock, The haemolysis of human red blood-cells by freezing and thawing. *Biochim Biophys Acta* 10 (1953) 414-26.
- [51] J.E. Lovelock, The mechanism of the protective action of glycerol against haemolysis by freezing and thawing. *Biochim Biophys Acta* 11 (1953) 28-36.
- [52] P.W. Madden, and D.E. Pegg, Calculation of Corneal Endothelial-Cell Volume During the Addition and Removal of Cryoprotective Compounds. *Cryo-Letters* 13 (1992) 43-50.
- [53] G. Marcacci, G. Corazzelli, C. Becchimanzi, M. Arcamone, G. Capobianco, F. Russo, F. Frigeri, and A. Pinto, DMSO-associated encephalopathy during autologous peripheral stem cell infusion: a

- predisposing role of preconditioning exposure to CNS-penetrating agents[quest]. *Bone Marrow Transplantation* 44 (2009) 133-135.
- [54] H.A. Massaldi, G.V. Richieri, and H.C. Mel, Alternative interpretation for the osmotic response of human erythrocytes. *J Cell Physiol* 127 (1986) 448-50.
- [55] P. Mazur, Kinetics of Water Loss from Cells at Subzero Temperatures and the Likelihood of Intracellular Freezing. *J Gen Physiol* 47 (1963) 347-69.
- [56] P. Mazur, Role of Cell Membranes in Freezing of Yeast and Other Single Cells. *Annals of the New York Academy of Sciences* 125 (1965) 658-&.
- [57] P. Mazur, S.P. Leibo, and E.H. Chu, A two-factor hypothesis of freezing injury. Evidence from Chinese hamster tissue-culture cells. *Exp Cell Res* 71 (1972) 345-55.
- [58] P. Mazur, The role of intracellular freezing in the death of cells cooled at supraoptimal rates. *Cryobiology* 14 (1977) 251-72.
- [59] L.E. McGann, and J. Farrant, Survival of tissue culture cells frozen by a two-step procedure to -196 degrees C. I. Holding temperature and time. *Cryobiology* 13 (1976) 261-8.
- [60] H.T. Meryman, The Exceeding of a minimum tolerable cell volume in hypertonic suspension as a cause of freezing injury. in: G.E.W. Wolstenholme, and M. O'Connor, (Eds.), *The Frozen Cell*, J.&A. Churchill, London, UK, 1970, pp. 51-67.

- [61] G.J. Morris, and J.J. McGrath, Intracellular ice nucleation and gas bubble formation in spirogyra. *Cryo-Letters* 2 (1981) 341-&.
- [62] I.N. Mukherjee, Y. Li, Y.C. Song, R.C. Long, and A. Sambanis, Cryoprotectant transport through articular cartilage for long-term storage: experimental and modeling studies. *Osteoarthritis and Cartilage* 16 (2008) 1379-1386.
- [63] K. Muldrew, and L.E. McGann, Mechanisms of Intracellular Ice Formation. *Biophysical Journal* 57 (1990) 525-532.
- [64] K. Muldrew, and L.E. McGann, The Osmotic Rupture Hypothesis of Intracellular Freezing-Injury. *Biophysical Journal* 66 (1994) 532-541.
- [65] Z.K. Otrrock, A. Beydoun, W.M. Barada, R. Masroujeh, R. Hourani, and A. Bazarbachi, Transient global amnesia associated with the infusion of DMSO-cryopreserved autologous peripheral blood stem cells. *Haematologica* 93 (2008) e36-37.
- [66] J.J. Pancrazio, F. Wang, and C.A. Kelley, Enabling tools for tissue engineering. *Biosensors and Bioelectronics* 22 (2007) 2803-2811.
- [67] D.E. Pegg, Simple Equations for Obtaining Melting-Points and Eutectic Temperatures for the Ternary-System Glycerol Sodium-Chloride Water. *Cryo-Letters* 4 (1983) 259-268.
- [68] D.E. Pegg, Equations for Obtaining Melting-Points and Eutectic Temperatures for the Ternary-System Dimethylsulfoxide Sodium-Chloride Water. *Cryo-Letters* 7 (1986) 387-394.

- [69] D.E. Pegg, and F.G. Arnaud, Equations for Obtaining Melting-Points in the Quaternary System Propane-1,2-Diol Glycerol Sodium-Chloride Water. *Cryo-Letters* 9 (1988) 404-417.
- [70] Y. Pichugin, G.M. Fahy, and R. Morin, Cryopreservation of rat hippocampal slices by vitrification. *Cryobiology* 52 (2006) 228-240.
- [71] R.E. Pitt, and P.L. Steponkus, Quantitative analysis of the probability of intracellular ice formation during freezing of isolated protoplasts. *Cryobiology* 26 (1989) 44-63.
- [72] R.E. Pitt, S.P. Myers, T.-T. Lin, and P.L. Steponkus, Subfreezing volumetric behavior and stochastic modeling of intracellular ice formation in *Drosophila melanogaster* embryos. *Cryobiology* 28 (1991) 72-86.
- [73] R.E. Pitt, M. Chandrasekaran, and J.E. Parks, Performance of a kinetic model for intracellular ice formation based on the extent of supercooling. *Cryobiology* 29 (1992) 359-373.
- [74] J.M. Prausnitz, R.N. Lichtenthaler, and E.G.d. Azevedo, *Molecular thermodynamics of fluid-phase equilibria* Prentice-Hall, Eaglewood Cliffs, New Jersey, 1986.
- [75] W.F. Rall, and G.M. Fahy, Ice-free cryopreservation of mouse embryos at  $-196\text{ }^{\circ}\text{C}$  by vitrification. *Nature* 313 (1985) 573-575.
- [76] W.F. Rall, and G.M. Fahy, Vitrification: A new approach to embryo cryopreservation. *Theriogenology* 23 (1985) 220-220.

- [77] D.H. Rasmussen, M.N. Macaulay, and A.P. Mackenzie, Supercooling and nucleation of ice in single cells. *Cryobiology* 12 (1975) 328-339.
- [78] R.R. Roepke, and E.J. Baldes, A Study of the Osmotic Properties of Erythrocytes. *Journal of Cellular Physiology and Comparative Physiology* 20 (1942) 71-93.
- [79] L.U. Ross-Rodriguez, Cellular osmotic properties and cellular responses to cooling, Department of Laboratory Medicine and Pathology, University of Alberta, Edmonton, Alberta (2009), pp. 219
- [80] L.U. Ross-Rodriguez, J.A.W. Elliott, and L.E. McGann, Investigating cryoinjury using simulations and experiments: 1. TF-1 cells during the two-step freezing (rapid cooling interrupted with a hold time) procedure. *Cryobiology* (Submitted) (2009).
- [81] L.U. Ross-Rodriguez, J.A.W. Elliott, and L.E. McGann, Investigating cryoinjury using simulations and experiments: 2. TF-1 cells during the graded freezing (interrupted slow cooling without hold time) procedure. *Cryobiology* (Submitted) (2009).
- [82] L.U. Ross-Rodriguez, J.A.W. Elliott, and L.E. McGann, Characterization of cryobiological responses in TF-1 cells using interrupted freezing procedures. *Cryobiology* (Accepted) (2009).

- [83] B. Rubinsky, and D.E. Pegg, A Mathematical-Model for the Freezing Process in Biological Tissue. Proceedings of the Royal Society of London Series B-Biological Sciences 234 (1988) 343-&.
- [84] B. Rubinsky, P.A. Perez, and M.E. Carlson, The thermodynamic principles of isochoric cryopreservation. Cryobiology 50 (2005) 121-138.
- [85] A. Sakai, and F. Engelmann, Vitrification, encapsulation-vitrification and droplet-vitrification: A review. Cryoletters 28 (2007) 151-172.
- [86] D. Savitz, V.W. Sidel, and A.K. Solomon, Osmotic Properties of Human Red Cells. Journal of General Physiology 48 (1964) 79-94.
- [87] P.L. Steponkus, Role of the plasma-membrane in the freezing-injury and cold-acclimation. Annual Review of Plant Physiology and Plant Molecular Biology 35 (1984) 543-584.
- [88] R. Syme, M. Bewick, D. Stewart, K. Porter, T. Chadderton, and S. Glück, The role of depletion of dimethyl sulfoxide before autografting: on hematologic recovery, side effects, and toxicity. Biology of Blood and Marrow Transplantation 10 (2004) 135-141.
- [89] M.R. Tijssen, H. Woelders, A. de Vries-van Rossen, C.E. van der Schoot, C. Voermans, and J.M. Lagerberg, Improved postthaw viability and in vitro functionality of peripheral blood hematopoietic progenitor cells after cryopreservation with a theoretically optimized freezing curve. Transfusion 48 (2008) 893-901.

- [90] M. Toner, E.G. Cravalho, and M. Karel, Thermodynamics and kinetics of intracellular ice formation during freezing of biological cells. *Journal of Applied Physics* 67 (1990) 1582-1593.
- [91] M. Toner, R.G. Tompkins, E.G. Cravalho, and M.L. Yarmush, Transport phenomena during freezing of isolated hepatocytes. *AIChE Journal* 38 (1992) 1512-1522.
- [92] M. Toner, E.G. Cravalho, and M. Karel, Cellular-Response of Mouse Oocytes to Freezing Stress - Prediction of Intracellular Ice Formation. *Journal of Biomechanical Engineering-Transactions of the Asme* 115 (1993) 169-174.
- [93] M. Toner, E.G. Cravalho, J. Stachecki, T. Fitzgerald, R.G. Tompkins, M.L. Yarmush, and D.R. Armant, Nonequilibrium freezing of one-cell mouse embryos. Membrane integrity and developmental potential, 1993, pp. 1908-1921.
- [94] W.M. Toscano, E.G. Cravalho, O.M. Silveas, and C.E. Huggins, Thermodynamics of Intracellular Ice Nucleation in Freezing of Erythrocytes. *Journal of Heat Transfer-Transactions of the Asme* 97 (1975) 326-332.
- [95] R.C. Weast, (Ed.), *Concentrative Properties of Aqueous Solutions*, CRC Press, Boca Raton, FL, 1982-1983.
- [96] S.C. Wiest, and P.L. Steponkus, The osmometric behavior of human erythrocytes. *Cryobiology* 16 (1979) 101-4.

- [97] D.J. Winzor, Reappraisal of disparities between osmolality estimates by freezing point depression and vapor pressure deficit methods. *Biophysical Chemistry* 107 (2004) 317-323.
- [98] H. Woelders, and A. Chaveiro, Theoretical prediction of 'optimal' freezing programmes. *Cryobiology* 49 (2004) 258-271.
- [99] P. Wong, The behavior of the human erythrocyte as an imperfect osmometer: A hypothesis. *Journal of Theoretical Biology* 238 (2006) 167-171.
- [100] E.J. Woods, M.A.J. Zieger, D.Y. Gao, and J.K. Critser, Equations for obtaining melting points for the ternary system ethylene glycol/sodium chloride/water and their application to cryopreservation. *Cryobiology* 38 (1999) 403-407.
- [101] E.J. Woods, A. Bagchi, J.D. Benson, X. Han, and J.K. Critser, Melting point equations for the ternary system water/sodium chloride/ethylene glycol revisited. *Cryobiology* 57 (2008) 336-336.
- [102] H. Yang, H. Zhao, J.P. Acker, J.Z. Liu, J. Akabutu, and L.E. McGann, Effect of dimethyl sulfoxide on post-thaw viability assessment of CD45(+) and CD34(+) cells of umbilical cord blood and mobilized peripheral blood. *Cryobiology* 51 (2005) 165-175.

**Table 1.1.** Values for constants in the freezing point to osmolality conversion (equations 1.1 - 1.3).

<b>Constant</b>	<b>Value</b>
$T_{FP}^o$	273.15 K
$W_1$	$1.802 \times 10^{-2}$ kg/mole
$\overline{s}_1^{oL} - \overline{s}_1^{oS}$	22.00 J/moleK
$R$	8.314 J/moleK

## **Chapter 2 - Single-solute osmotic virial equation<sup>1</sup>**

### **2.1. Introduction**

There are many solutes of interest in cryobiology, including electrolytes, sugars, macromolecules, and others. The thermodynamic solution behaviour of these individual solutes is often of interest when choosing effective cryoprotective agents (CPAs). Solute with large freezing point depressions at low non-toxic concentrations are promising candidates as CPAs.

Solute of interest in many areas, including cryobiology, have been extensively studied and the single-solute solution data is readily available in the literature for a wide range of solutes [2; 4; 8; 14; 18; 19; 28; 29; 34; 35; 38].

Multisolute data is also available for a number of solutions in cryobiology [2; 3; 6; 10; 14; 20; 21; 22; 30; 36; 39]. However, due to the number of possible combinations of solutes of interest, data is not available for all solutions of interest. A multisolute solution theory will be presented in Chapters 3 and 4 which requires only information from single-solute solutions to make predictions of a wide range of multisolute solutions.

---

<sup>1</sup>A version of sections of this chapter has been published. J.A.W. Elliott, R.C. Prickett, H.Y. Elmoazzen, K.R. Porter and L.E. McGann 2007. *Journal of Physical Chemistry B*. 111: 1775-1785.

A version of sections of this chapter has been accepted for publication. R.C. Prickett, J.A.W. Elliott, and L.E. McGann 2009. *Cryobiology*. (doi:10.1016/j.cryobiol.2009.07.011).

The osmotic virial equation (OVE) is one of the most widely-used thermodynamic equations of state in biology, and the single-solute OVE is applicable to a variety of solutions containing water plus a single solute (see Figures 2.1 - 2.5). The objective of this chapter was to determine the single-solute osmotic virial coefficients for a wide range of solutes in water.

## 2.2. Governing equations

In the OVE, the osmolalities of single-solute solutions are represented as truncated polynomials in molality, where each solute has unique coefficients for terms of second or higher order in concentration.

$$\pi = m_i + B_i m_i^2 + C_i m_i^3 + \dots \quad (2.1)$$

where  $\pi$  is the osmolality of the solution (osmoles/kg solvent),  $m_i$  is the molal concentration of the solute (moles solute/kg solvent), and  $B_i$  [(moles solute/kg solvent)<sup>-1</sup>] and  $C_i$  [(moles solute/kg solvent)<sup>-2</sup>] are the second and third osmotic virial coefficients for use with molality, respectively. It is common to see osmotic virial equations written as an expansion in molarity rather than molality. Since molality, unlike molarity, is not a function of temperature, it is practical to use molality for cryobiological modelling. If the osmotic virial equation is written in terms of molarity care must be taken in converting osmotic virial coefficients between various units.

The single-solute OVE can also be written in terms of mole fraction:

$$\pi = A^* \left( x_i + B_i^* x_i^2 + C_i^* x_i^3 + \dots \right) \quad (2.2)$$

where  $x_i$  is the mole fraction of the solute (moles solute/total moles of solution), and  $B_i^*$  [(moles solute/total moles)<sup>-1</sup>] and  $C_i^*$  [(moles solute/total moles)<sup>-2</sup>] are the second and third osmotic virial coefficients for use with mole fraction, respectively. The quantity in the parenthesis in equation (2.2) is osmole fraction ( $\tilde{\pi}$ ) so an additional conversion factor,  $A^*$ , between osmole fraction and osmolality is needed. The conversion factor is  $A^* = 1/(W_1 x_1)$ , where  $W_1$  is the molecular weight of the solvent (kg/mole) and  $x_1$  is the mole fraction of the solvent (moles solvent/total moles).

The values for the osmotic virial coefficients for a range of solutes for use in (i) molality are listed in Table 2.1 and (ii) mole fraction are listed in Table 2.2.

Equations (2.1) and (2.2) are valid for non-electrolytes in solution. In order to extend the application of the OVE to electrolyte solutions, an additional fitting constant in the single-solute OVE, called the dissociation constant ( $k_{diss}$ ), is used to capture the complicated behaviour of single-solute electrolyte solutions.

$$\pi = k_{diss} m_i + B_i (k_{diss} m_i)^2 + C_i (k_{diss} m_i)^3 + \dots \quad (2.3)$$

This dissociation constant, also known as the van't Hoff factor [23], accounts for the additional non-ideality of the solution behaviour from several electrolyte effects. Thus, the “dissociation constant” may not be

exactly equal to two, even for electrolytes known to completely dissociate [13].

For electrolytes, the single-solute OVE is written in terms of mole fraction as:

$$\pi = A^* \left( k_{diss}^* x_i + B_i^* \left( k_{diss}^* x_i \right)^2 + C_i^* \left( k_{diss}^* x_i \right)^3 + \dots \right) \quad (2.4)$$

where  $k_{diss}^*$  is the dissociation constant for use with mole fraction. The values for the dissociation constant and osmotic virial coefficients for sodium chloride (NaCl) and potassium chloride (KCl) are listed in Tables 2.1 and 2.2 for use in molality and mole fraction, respectively.

It can be argued that the single-solute OVE approach should not be used to describe the solution behaviour of electrolytes since: (i) the dissociation constant cannot be less than two for strong 1:1 electrolytes such as NaCl or KCl, and (ii) a constant cannot capture the complicated electrolyte solution behaviour, and that therefore an actual electrolyte solution theory, such the Pitzer-Debye-Huckel equations [24; 25], should be used.

There has been much debate in the literature with respect to the question of complete or partial dissociation of NaCl [11]. Much of the work published on NaCl is based on the assumption of complete dissociation [1; 24; 26; 29]. However, Heyrovska demonstrated that by assuming partial dissociation, equations can be developed that quantitatively explain the behaviour of aqueous NaCl solutions [12; 13]. Large amounts of experimental data on the densities of aqueous NaCl solutions have been

shown to agree with the equations developed using the assumption of partial dissociation [13]. Furthermore, the dissociation constant has been shown to be dependent on electrolyte concentration, reaching complete dissociation only at infinite dilution [23]. Using osmotic coefficient data, Heyrovská calculated the van't Hoff factor using [12]:

$$m[(1-\alpha)+2\alpha]=im \quad (2.5)$$

where  $\alpha$  = the degree of dissociation,  $m$  is the molal concentration of the electrolyte, and  $i$  is the van't Hoff factor. The degree of dissociation ( $\alpha$ ) for aqueous NaCl solutions ranging from 0 to 6.144 mol/kg solvent has been shown to vary between 1 (completely dissociated) to less than 0.8 [13]. This resulted in a van't Hoff factor ranging from of 2 ( $\alpha = 1$ ) to less than 1.8 ( $\alpha < 0.8$ ).

Many electrolyte solution theories have been developed to describe the complex solution behaviour of electrolytes in water. Among the most well-known is the Pitzer-Debye-Huckel electrolyte solution theory [24; 25]. Pitzer and colleagues incorporated the Debye-Huckel equations into a solution theory to describe the behaviour of a wide range of electrolyte solutions. Unlike the OVE approach of using an additional fitting constant, the Pitzer-Debye-Huckel equations for solutions of electrolytes utilize an ionic-strength-dependent function to capture the electrolyte solution behaviour [24; 25]. Since this function depends on the ionic strength of the solution it has to be calculated for every electrolyte concentration. The

Pitzer-Debye-Huckel equation in osmotic coefficient,  $\Phi$ , for 1:1 electrolytes such as NaCl or KCl, is:

$$\Phi - 1 = f^\Phi + B_{MX}^\Phi m + C_{MX}^\Phi m^2 \quad (2.6)$$

where  $B_{MX}^\Phi$  is the second osmotic virial coefficient,  $C_{MX}^\Phi$  is the third osmotic virial coefficient,  $f^\Phi$  is the 'electrolyte effects' function based on Debye-Huckel parameters, and  $m$  is the molality of the electrolyte.

Converting osmotic coefficient to osmolality using equation (1.5), and noting for NaCl  $\nu = 2$ , gives:

$$\pi = 2(f^\Phi + 1)m + 2B_{MX}^\Phi m^2 + 2C_{MX}^\Phi m^3 \quad (2.7)$$

In addition to the electrolyte effects function, the second osmotic virial coefficient,  $B_{MX}^\Phi$ , is also dependent on the ionic strength of the solution and thus must be calculated at each electrolyte concentration.

The electrolyte effects function is calculated using the Debye-Huckel slope,  $A^\Phi$ , the ionic strength of the solution,  $I$ , and an empirical parameter,  $b$ :

$$f^\Phi = -A^\Phi \left( \frac{\sqrt{I}}{1 + b\sqrt{I}} \right) \quad (2.8)$$

The values for all of the empirical parameters in the Pitzer-Debye-Huckel equation are listed in Table 2.3 [5; 24; 25].

The second virial coefficient is calculated based on three empirical parameters,  $\beta_{MX}^{(0)}$ ,  $\beta_{MX}^{(1)}$ , and  $\alpha$ , and the ionic strength of the solution:

$$B_{MX}^{\Phi} = \beta_{MX}^{(0)} + \beta_{MX}^{(1)} e^{-\alpha\sqrt{I}} \quad (2.9)$$

The third virial coefficient,  $C_{MX}^{\Phi}$ , is a constant, which was obtained by fitting the Pitzer-Debye-Huckel equation to single-solute NaCl data.

$$C_{MX}^{\Phi} = 0.00127 \quad (2.10)$$

A comparison between the dissociation constant ( $k_{diss}$ ) and the Pitzer-Debye-Huckel electrolyte effects function ( $2(f^{\Phi} + 1)$ ) for NaCl (Figure 2.6), demonstrates that the value obtained by fitting for  $k_{diss}$  is within the range of values for the  $2(f^{\Phi} + 1)$  function calculated for a variety of NaCl concentrations. In addition, both the single-solute OVE and the Pitzer-Debye-Huckel equation adequately captured the solution behaviour of an aqueous NaCl solution (Figure 2.7). The OVE fit shown in Figure 2.7 was obtained by fitting the OVE to the same data that was used to obtain the parameters for the Pitzer-Debye-Huckel equation that is also shown on Figure 2.7. The NaCl data used for the OVE fit and the Pitzer-Debye-Huckel fit in Figure 2.7 was measured at 25 °C [29], versus the NaCl data used for the OVE fit shown in Figure 2.1, which was obtained at sub-zero temperatures. The osmotic virial coefficients for the fit shown in Figure 2.7 are listed in Table 2.4.

The single-solute OVE (equations (2.1) and (2.2)) and the Pitzer-Debye-Huckel solution theory presented above (equations (2.6)-(2.10))

are for solutions containing water plus one solute. The Pitzer-Debye-Huckel solution theory is for electrolyte solutes, whereas the single-solute OVE can be applied to a wide variety of solutes, from electrolytes to CPAs to macromolecules. The application of the OVE to electrolyte solutions is straightforward, requiring only two fitting parameters to describe the solution behaviour of NaCl (the dissociation constant,  $k_{diss}$ , and a second virial coefficient,  $B$ ). Alternatively, the Pitzer-Debye-Huckel equation, which endeavours to also capture the solution behaviour of mixtures of electrolytes, contains more complexity. The Pitzer-Debye-Huckel equation has six empirical parameters and multiple functions that are ionic strength dependent [24; 25].

### 2.3. Materials and methods

#### 2.3.1. *Obtaining the single-solute phase diagrams*

Phase diagrams were either (i) measured by freezing point depression or (ii) obtained from the literature for various single-solute solutions. The phase diagram data were given as freezing point depression as a function of solute concentration, osmotic coefficient as a function of solute concentration, or as osmolality as a function of solute concentration. The data were converted to osmolality using the nonlinear conversion from freezing point depression, equation (1.2) or the conversion from osmotic coefficient, equation (1.5). Figure 2.8 shows that common practice of using the linear conversion between freezing point depression and

osmolality (equation (1.4)), as opposed to the nonlinear conversion, introduces over 7% error when the freezing point depression is 20 °C and over 18% error when the freezing point depression is 50 °C.

The concentration units varied among the studies, but were all converted to molality. The concentration unit conversion equations can be found in Appendix B.

#### (i) Freezing point depression measurements

The freezing point depression data of glycerol (Sigma-Aldrich, Oakville, Ontario) in distilled, deionized water (CORNING Mega-Pure™ system ACS), dimethyl sulphoxide (DMSO) (Sigma-Aldrich, Oakville, Ontario) in distilled, deionized water, and whey protein isolate (Power Pro®) (Dr. Paul Jelen, University of Alberta, Edmonton) in distilled, deionized water were collected<sup>2</sup>. The solutions were made on a mass basis in order to avoid any volume variations due to temperature. The solute masses were measured on an electronic mass balance (Mettler Toledo AB204-S, Greifensee, Switzerland). For the DMSO-in-water solutions and the glycerol-in-water solutions, the solutions were mixed using a vortex mixer (Cole-Palmer Model 4721-40, Vernon Hills, Illinois) for 10-15 seconds on a speed setting of 9 (out of 10). For both the DMSO + water solutions and the glycerol + water solutions, the concentrations used ranged from 0 % to 44 % w/w. Above this concentration, the viscosity of the solutions limited the accuracy of the freezing point

---

<sup>2</sup>Undergraduate student K. Porter measured the glycerol-in-water and DMSO-in-water data points.

depression measurements. For the whey protein-in-water solutions, the solutions were mixed on an electronic stirrer (Fisher Scientific Electronic Stirrer 2009, Fisher Scientific Ltd, Nepean, Ontario). Small amounts of the whey protein isolate powder were added to 10 g of the distilled, deionized water. The solution was mixed on the electronic stirrer until the powder dissolved. More whey protein isolate powder was added and the solution mixed on the electronic stirrer. This was repeated until all of the powder had been added to the water. The solution was covered with parafilm to avoid evaporation of water, placed on the electronic stirrer and mixed at 500 rpm for 30 minutes. The solution was placed in a 37 °C water bath for 30 minutes and then placed back on the magnetic stirrer at 500 rpm for 30 minutes. This was repeated until the protein was completely dissolved. The concentration of whey proteins used ranged from 0 % to 35 % w/w. Above this concentration, it was difficult to dissolve the whey protein in water.

Five millilitres (5 mL) of solution was transferred to a 50 mL disposable centrifuge tube (Fisher Scientific Ltd, Nepean, Ontario) using a disposable Pasteur pipette. A rubber stopper with a hole in the center was inserted into the top of the tube and a 0.125" type T thermocouple (OMEGA CPIN-18G-12, Laval, Quebec) was placed through the hole in the rubber stopper and lowered into the solution. The tube was lowered into a methanol bath (FTS Systems MC880 A1, Stone Ridge, New York), ensuring that the solution was completely immersed in methanol. The bath

was set to approximately 5 °C below the expected freezing point of the solution. The temperature data was gathered using a USB data acquisition system (OMEGA OMB-DAQ-55, Laval, Quebec) and accompanying software (OMEGA DAQVIEW XL, Laval, Quebec). The thermocouple was calibrated each day using the freezing point of distilled, deionized water.

Each sample was allowed to reach thermal equilibrium with the methanol bath and then ice was nucleated in the sample using forceps cooled in liquid nitrogen (Praxair, Edmonton, Alberta). Ice was nucleated by briefly removing the sample from the methanol bath and touching the cold forceps to the side of the tube. For the glycerol + water and the DMSO + water solutions with solute concentration less than 15 % (w/w) and for the whey protein + water solutions, the samples were returned to the bath to complete the freezing process. For the glycerol + water solutions and the DMSO + water solutions with greater than 15 % (w/w) solute concentration, the samples were left at room temperature until the ice crystals reached the thermocouple (solutions >15% (w/w)). Upon ice nucleation in the sample, release of the latent heat causes a sharp increase to the freezing point of the solution and the sample remains at that temperature until the freezing process is complete. The freezing point was taken to be the average of the temperatures recorded for the entire plateau. Figure 2.9 is a typical temperature versus time graph for a freezing point depression measurement. The viscosity of the glycerol + water and the DMSO + water solutions of mass percentage greater than

15% (w/w) slowed the ice crystal growth and the release of latent heat. The glycerol and DMSO experimental values were compared to literature values [2; 14; 18; 28; 35] and were found to be consistent with the published results. (See Figures 2.2c and 2.2d).

#### (ii) Obtaining phase diagrams from the literature

Phase diagrams for many single-solute aqueous solutions were obtained from the literature [2; 4; 8; 10; 14; 19; 28; 34; 38]. Various experimental methods were used to measure the phase diagrams, including freezing point depression measurements [19], differential thermal analysis (DTA) or differential scanning calorimetry (DSC) [2; 4; 10; 14; 28], and membrane osmometry [8; 34; 38].

It should be noted that measuring the phase diagram of viscous solutions using freezing point depression measurements, DTA, or DSC can result in inaccurate results due to the viscosity of the solution slowing the ice crystal growth and the release of latent heat, particularly at high concentrations.

#### *2.3.2. Fitting the single-solute osmotic virial equation to data*

After the data were converted to osmolality as a function of solute molality, linear regression was performed on the single-solute osmotic virial equation to obtain the osmotic virial coefficients for each solute. The single-solute OVE using concentration units of molality (equation (2.1) or (2.3)) or mole fraction (equation (2.2) or (2.4)) was fit to the single-solute

osmolality as a function of concentration data by minimizing the sum of squared errors (SSE). The SSE is defined as:

$$SSE = \sum_{i=1}^{\mathbf{m}} (y_i - f_i)^2 \quad (2.11)$$

where  $y_i$  is the value of the  $i^{\text{th}}$  data point,  $f_i$  is the value calculated from the OVE at the  $i^{\text{th}}$  data point, and  $\mathbf{m}$  is the number of data points.

The SSE was minimized using the SOLVER function in Excel (Microsoft, Redmond, WA, USA). However, in some instances SOLVER may give results that are a local minimum in the data, not the absolute minimum. Thus, minimizing the SSE was be done using a matrix approach.

The linear regression equation was generalized as:

$$\vec{y} = \sum_{i=1}^{\mathbf{n}} \vec{\beta}_i f_i(\vec{x}) + \varepsilon \quad (2.12)$$

where  $\vec{\beta}_i$  is a vector that contained the regression coefficients,  $f_i(\vec{x})$  were the functions of the variable  $x$  that were multiplied by the regression coefficients,  $\varepsilon$  was a vector of the errors in the prediction, and  $\mathbf{n}$  was the number of regression coefficients. The vector,  $\vec{y}$ , contained the values of the dependent variable for each data point.

$$\vec{y} = \begin{pmatrix} y_1 \\ y_2 \\ \vdots \\ y_{\mathbf{m}} \end{pmatrix}$$

The individual functions,  $f_i$ , were known and  $\vec{\beta}$  were the unknown coefficients. The  $\underline{\underline{A}}$ -matrix was defined as follows<sup>3</sup>:

$$\underline{\underline{A}} = \begin{bmatrix} f_1(\bar{x}_1) & f_2(\bar{x}_1) & f_3(\bar{x}_1) & \cdots & f_n(\bar{x}_1) \\ f_1(\bar{x}_2) & f_2(\bar{x}_2) & f_3(\bar{x}_2) & \cdots & f_n(\bar{x}_2) \\ \vdots & & & \ddots & \\ f_1(\bar{x}_m) & f_2(\bar{x}_m) & f_3(\bar{x}_m) & \cdots & f_n(\bar{x}_m) \end{bmatrix}$$

To minimize the SSE, the following equation was used to determine the vector,  $\vec{\beta}$  [9]:

$$\vec{\beta} = (\underline{\underline{A}}^T \underline{\underline{A}})^{-1} \underline{\underline{A}}^T \vec{y} \quad (2.13)$$

where  $\underline{\underline{A}}^T$  is the transpose of the  $\underline{\underline{A}}$ -matrix and the superscript -1 indicates the inverse of the matrix. This gave a vector of the form:

$$\vec{\beta} = \begin{pmatrix} \beta_1 \\ \beta_2 \\ \vdots \\ \beta_n \end{pmatrix}$$

where  $\beta_1$  is the first regression coefficient,  $\beta_2$  is the second regression coefficient,  $\beta_3$  is the third regression coefficient, etc.

To determine the confidence intervals of the regression coefficients, the model standard deviation,  $\hat{\sigma}$ , was needed:

---

<sup>3</sup> For linear regression the  $\underline{\underline{A}}$ -matrix is equivalent to the Jacobian matrix, which is defined as the derivative of the regression equation with respect to each regression coefficient. For nonlinear regression the Jacobian matrix should be used in place of the  $\underline{\underline{A}}$ -matrix.

$$\hat{\sigma} = \sqrt{\frac{SSE}{\mathbf{m} - \mathbf{n}}} = \sqrt{\frac{\bar{\mathbf{y}}^T \bar{\mathbf{y}} - \bar{\beta} \mathbf{A}^T \bar{\mathbf{y}}}{\mathbf{m} - \mathbf{n}}} \quad (2.14)$$

The 95% confidence intervals were found using the following formula:

$$\beta_i \pm t_{\alpha/2, \mathbf{m} - \mathbf{n}} \hat{\sigma} \sqrt{(\underline{\underline{\mathbf{A}^T \mathbf{A}}})_{ii}^{-1}} \quad (2.15)$$

where  $\beta_i$  is the  $i$ th regression coefficient ( $i = 1$  to  $\mathbf{n}$ ) and  $t_{\alpha/2, \mathbf{m} - \mathbf{n}}$  is the Student's t-test value at a significance of  $\alpha/2$  and  $(\mathbf{m} - \mathbf{n})$  degrees of freedom. For the 95 % confidence intervals,  $\alpha = 0.05$ .

The single-solute OVE for non-electrolytes (equations (2.1) and (2.2)) does not have a linear coefficient, so the equation was re-arranged so that it was in the form:  $y = \beta_1 x + \beta_2 x^2 + \beta_3 x^3 + \dots$ . For example, rearranging equation (2.1) so that the linear term has a regression coefficient gives:

$$\frac{\pi}{m_i} - 1 = B_i m_i + C_i m_i^2 + \dots \quad (2.16)$$

For electrolytes, there is a linear term in the OVE ( $k_{diss}$ ), so to solve for the osmotic virial coefficients, the  $\bar{\mathbf{y}}$  vector contained the measured osmolality (not  $\pi/m_i - 1$ ). Table 2.5 contains a summary of the matrix approach for each type of solute.

In Excel, matrices were set up in order to determine the osmotic virial coefficients for each solute. To obtain the coefficients for use in molality for non-electrolyte solutes, matrices were set up in the following manner:

$$\bar{y} = \left\langle \begin{array}{l} \pi/m_i - 1 \quad (1) \\ \pi/m_i - 1 \quad (2) \\ \vdots \\ \pi/m_i - 1 \quad (\mathbf{m}) \end{array} \right\rangle$$

where the number in parentheses indicates the rank order of the data point (i.e. (1) indicates that this is the first data point, (2) is the second data point, etc).

$$\underline{\underline{A}} = \begin{vmatrix} m_i(1); m_i^2(1); m_i^3(1); \dots; m_i^n(1) \\ m_i(2); m_i^2(2); m_i^3(2); \dots; m_i^n(2) \\ \vdots \quad \quad \quad \ddots \quad \quad \quad \vdots \\ m_i(\mathbf{m}); m_i^2(\mathbf{m}); m_i^3(\mathbf{m}); \dots; m_i^n(\mathbf{m}) \end{vmatrix}$$

where  $m_i$  is the molality of the solute. To solve for the osmotic virial coefficients in mole fraction, the  $\underline{\underline{A}}$ -matrix contained mole fraction ( $x_i$ ) instead of molality. The number of columns in the  $\underline{\underline{A}}$ -matrix was determined by the number of regression coefficients that were being fit to the data (i.e. number of columns =  $\mathbf{n}$ ) and the number of rows in the  $\underline{\underline{A}}$ -matrix was determined by the number of data points (number of rows =  $\mathbf{m}$ ).

Using the matrix approach, the coefficients for increasing orders of the osmotic virial equation were quickly determined by simply adding additional columns to the  $\underline{\underline{A}}$ -matrix (containing increasing orders of the solute concentration) and using equation (2.13) to obtain the values for  $\bar{\beta}$ .

It was found that using the SOLVER function in Excel to minimize the sum of squared errors typically gave the same values as the matrix method for the osmotic virial coefficients.

The coefficients in the single-solute OVE can be derived directly from knowledge of the interactions between solute molecules [27]. The second virial coefficient comes from interactions between two solute molecules; the third virial coefficient comes from interactions between three solute molecules, and so on. Because of this physical basis, only a small number of terms may be required in the single-solute OVE to accurately capture the solution behaviour of a wide range of solutes. To determine which order of polynomial adequately fits the single-solute data, increasing orders of the single-solute OVE (starting with linear) were used for each solute and the adjusted  $R^2$  parameter was calculated for each order of polynomial. The adjusted  $R^2$  is a measure of the goodness of fit of an equation to a data set, and it also takes into account the number of parameters in the fitted equation. The standard  $R^2$ , often used to determine goodness of fit, does not take into account the number of parameters in the model and may erroneously increase with increasing number of parameters in the equation. The adjusted  $R^2$  was used to assess the necessity of adding additional parameters to the model [9].

$$\text{adjusted } R^2 = 1 - \frac{VAR_E}{VAR_T} \quad (2.17)$$

where estimates of the variances of the errors,  $VAR_E$ , and the observations,  $VAR_T$ , are defined as:

$$\begin{aligned}
 VAR_E &= \frac{SSE}{\mathbf{m} - \mathbf{n}} = \frac{\sum_{i=1}^{\mathbf{m}} (y_i - f_i)^2}{\mathbf{m} - \mathbf{n}} \\
 VAR_T &= \frac{TSS}{\mathbf{m} - 1} = \frac{\sum_{i=1}^{\mathbf{m}} (y_i - \bar{y})^2}{\mathbf{m} - 1}
 \end{aligned}
 \tag{2.18}$$

where  $\bar{y}$  is the average of all of the data points. SSE is the sum of squared errors, also called the residual sum of squares, and TSS is the total sum of squares.

Increasing orders of polynomial were used until the adjusted  $R^2$  parameter either decreased or remained constant to the third significant figure (i.e. less than a 1% improvement was achieved by adding another parameter).

#### 2.4. Results

Single-solute phase diagrams for many solutes were obtained from the literature. For non-electrolyte solutions, the data were fit to the single-solute OVE in concentration units of molality (equation (2.1)) and mole fraction (equation (2.2)). The data for electrolytes were fit to equations (2.3) and (2.4). The single-solute OVE fits are shown on Figures 2.1 to 2.5. The solutes were grouped by type of molecules (i.e. electrolytes, common CPAs, sugars, alcohols, and macromolecules). The osmotic virial coefficients for use with solute molality are listed in Table 2.1 and for use with solute mole fraction in Table 2.2. Tables 2.1 and 2.2 also contain the

concentration ranges that were used to fit for the coefficients of each solute and the solubility limits for the electrolytes and sugars [19; 35].

The fits shown in Figures 2.1 to 2.5 demonstrate that the OVE adequately fit all of the single-solute solution osmolalities as a function of concentration data. The adjusted  $R^2$  for each fit was  $> 0.95$  for the fits in molality and  $> 0.91$  for the fits in mole fraction.

The whey protein + water freezing point depression measurements had a large standard deviation (see Figure 2.5). The ice growth through the samples was slow, resulting in inaccuracies in the measurement. The slow ice growth may be due to the concentration of the whey protein in the water. In order to avoid the issues with ice growth through concentrated solutions, other studies have utilized membrane osmometry to measure the phase diagram of protein solutions [8; 34; 38].

## 2.5. *Discussion*

The single solute osmotic virial coefficients were determined for a wide range of solutes in water, including electrolytes, common CPAs, and macromolecules. The common CPAs, such as DMSO, glycerol, and ethylene glycol, exhibit non-ideal solution behaviour. Thus, those solutes have a significant effect on the osmolality (or freezing point depression) at a relatively low concentration, as opposed to a solute which is more ideal, such as methanol. However, many sugars are often used as CPAs, such as trehalose or sucrose, and these solutes have a smaller effect on the

osmolality of the solution at a given concentration. The protective effect of the sugar molecules during freezing or drying may not be due solely to freezing point depression. It has been suggested that the protective effects of sugars may be due to membrane and protein stabilization [7].

It can be seen from Figure 2.5 and Tables 2.1 to 2.2 that the macromolecules are very non-ideal and have a marked effect on the osmolality at very low molal concentrations. Many macromolecules, such as hydroxyethyl starch [32; 33], skim milk powder (which contains whey proteins) [16; 37], and egg yolk (which contains a high protein content) [31] are used as part of cryopreservation protocols for many different cell types. These molecules are non-permeating CPAs, as they are too large to cross the cell membrane. Since the driving force for water transport is the osmolality difference between the intra- and extracellular solutions [15; 17], the very non-ideal, non-permeating molecules increase the water transport at low concentrations. Thus, they act by dehydrating the cell at above zero temperatures, allowing for rapid cooling without the likelihood of intracellular freezing.

In subsequent chapters, the single-solute osmotic virial coefficients will be used to make predictions of multisolite solution behaviour.

## 2.6. References

- [1] D.G. Archer, Thermodynamic properties of the NaCl+H<sub>2</sub>O system. 2. Thermodynamic properties of NaCl (aq), NaCl.2H<sub>2</sub>O (cr), and phase equilibria. *Journal of Physical and Chemical Reference Data* 21 (1992) 793-829.
- [2] P. Boutron, and A. Kaufmann, Stability of Amorphous State in System Water-Glycerol-Dimethylsulfoxide. *Cryobiology* 15 (1978) 93-108.
- [3] P. Boutron, and A. Kaufmann, Stability of the Amorphous State in the System Water-Glycerol-Ethylene Glycol. *Cryobiology* 16 (1979) 83-89.
- [4] P. Boutron, and A. Kaufmann, Stability of the Amorphous State in the System Water 1,2-Propanediol. *Cryobiology* 16 (1979) 557-568.
- [5] D.J. Bradley, and K.S. Pitzer, Thermodynamics of electrolytes. 12. Dielectric properties of water and Debye-Huckel parameters to 350-degrees-C and 1-Kbar. *Journal of Physical Chemistry* 83 (1979) 1599-1603.
- [6] F.H. Cocks, and W.E. Brower, Phase diagram relationships in cryobiology. *Cryobiology* 11 (1974) 340-58.
- [7] J.H. Crowe, L.M. Crowe, J.F. Carpenter, and C.A. Wistrom, Stabilization of dry phospholipid-bilayers and proteins by sugars. *Biochemical Journal* 242 (1987) 1-10.
- [8] D.A.T. Dick, An Approach to the Molecular Structure of the Living Cell by Water Flux Studies. in: E.B. Reeve, and A.C. Guyton, (Eds.),

Physical Bases of Circulatory Transport: Regulation and Exchange,  
W.B. Saunders Company, Philadelphia, 1967, pp. 217-234.

- [9] N.R. Draper, Applied Regression Analysis, John Wiley & Sons, Inc.,  
New York, 1998.
- [10] F.W. Gayle, F.H. Cocks, and M.L. Shepard, H<sub>2</sub>O-NaCl-Sucrose  
Phase-Diagram and Applications in Cryobiology. Journal of Applied  
Chemistry and Biotechnology 27 (1977) 599-607.
- [11] R. Heyrovska, A Reappraisal of Arrhenius' Theory of Partial  
Dissociation of Electrolytes. in: J.T. Stock, and M.V. Orna, (Eds.),  
Electrochemistry, past and present, ACS symposium series.,  
American Chemical Society, Washington, DC, 1989, pp. 75-91.
- [12] R. Heyrovska, Physical electrochemistry of strong electrolytes based  
on partial dissociation and hydration - Quantitative interpretation of  
the thermodynamic properties of NaCl(aq) from "zero to saturation".  
Journal of the Electrochemical Society 143 (1996) 1789-1793.
- [13] R. Heyrovska, Equations for Densities and Dissociation Constant of  
NaCl(aq) at 25[degree]C from "Zero to Saturation" Based on  
Partial Dissociation. Journal of the Electrochemical Society 144  
(1997) 2380-2384.
- [14] W.H. Hildebrandt, Low temperature quantitative phase equilibria and  
glass formation in the H<sub>2</sub>O-NaCl-DMSO system, Duke University,  
1975., 1975, pp. vi, 180 leaves.

- [15] M.H. Jacobs, The exchange of material between the erythrocyte and its surroundings. *Harvey Lectures* 22 (1927) 146-164.
- [16] T. Kaneko, A. Yamamura, Y. Ide, M. Ogi, T. Yanagita, and N. Nakagata, Long-term cryopreservation of mouse sperm. *Theriogenology* 66 (2006) 1098-1101.
- [17] B. Lucke, and M. McCutcheon, The Living Cell as an Osmotic System and its Permeability to Water. *Physiological Reviews* 12 (1932) 68-139.
- [18] A. Melinder, Thermophysical Properties of Aqueous Solutions Used as Secondary Working Fluids, Division of Applied Thermodynamics and Refrigeration, Department of Energy Technology, School of Industrial Engineering and Management, Royal Institute of Technology, Stockholm, 2007, pp. 129.
- [19] D.P. Miller, J.J. dePablo, and H. Corti, Thermophysical properties of trehalose and its concentrated aqueous solutions. *Pharmaceutical Research* 14 (1997) 578-590.
- [20] D.E. Pegg, Simple Equations for Obtaining Melting-Points and Eutectic Temperatures for the Ternary-System Glycerol Sodium-Chloride Water. *Cryo-Letters* 4 (1983) 259-268.
- [21] D.E. Pegg, Equations for Obtaining Melting-Points and Eutectic Temperatures for the Ternary-System Dimethylsulfoxide Sodium-Chloride Water. *Cryo-Letters* 7 (1986) 387-394.

- [22] D.E. Pegg, and F.G. Arnaud, Equations for Obtaining Melting-Points in the Quaternary System Propane-1,2-Diol Glycerol Sodium-Chloride Water. *Cryo-Letters* 9 (1988) 404-417.
- [23] R.H. Petrucci, and W.S. Harwood, *General Chemistry: Principles and Modern Applications*, Prentice-Hall, Inc., Upper Saddle River, NJ, 1997.
- [24] K.S. Pitzer, Thermodynamics of Electrolytes .1. Theoretical Basis and General Equations. *Journal of Physical Chemistry* 77 (1973) 268-277.
- [25] K.S. Pitzer, and G. Mayorga, Thermodynamics of Electrolytes .2. Activity and Osmotic Coefficients for Strong Electrolytes with One or Both Ions Univalent. *Journal of Physical Chemistry* 77 (1973) 2300-2308.
- [26] K.S. Pitzer, J.C. Peiper, and R.H. Busey, Thermodynamic Properties of Aqueous Sodium-Chloride Solutions. *Journal of Physical and Chemical Reference Data* 13 (1984) 1-102.
- [27] J.M. Prausnitz, R.N. Lichtenthaler, and E.G.d. Azevedo, *Molecular thermodynamics of fluid-phase equilibria* Prentice-Hall, Eaglewood Cliffs, New Jersey, 1986.
- [28] D.H. Rasmussen, and A.P. MacKenzie, Phase Diagram for System Water-Dimethylsulphoxide. *Nature* 220 (1968) 1315-1317.
- [29] R.A. Robinson, and R.H. Stokes, *Electrolyte solutions : the measurement and interpretation of conductance, chemical potential*

and diffusion in solutions of simple electrolytes, Butterworths Scientific Publications, London, England, 1959.

- [30] M.L. Shepard, C.S. Goldston, and F.H. Cocks, H<sub>2</sub>O-NaCl-Glycerol Phase-Diagram and Its Application in Cryobiology. *Cryobiology* 13 (1976) 9-23.
- [31] N. Songsasen, K.J. Betteridge, and S.P. Leibo, Birth of live mice resulting from oocytes fertilized in vitro with cryopreserved spermatozoa. *Biology of Reproduction* 56 (1997) 143-152.
- [32] A. Sputtek, P. Kuhn, and A.W. Rowe, Cryopreservation of erythrocytes, thrombocytes, and lymphocytes. *Transfusion Medicine and Hemotherapy* 34 (2007) 262-267.
- [33] A. Sputtek, G. Singbartl, R. Langer, W. Schleinzner, H.A. Henrich, and P. Kuhn, Cryopreservation of red-blood-cells with the nonpenetrating cryoprotectant hydroxyethyl starch. *Cryo-Letters* 16 (1995) 283-288.
- [34] V.L. Vilker, C.K. Colton, and K.A. Smith, The Osmotic-Pressure of Concentrated Protein Solutions - Effect of Concentration and Ph in Saline Solutions of Bovine Serum-Albumin. *J Colloid Interface Sci* 79 (1981) 548-566.
- [35] R.C. Weast, Ed., *CRC Handbook of Chemistry and Physics*, CRC Press, Boca Raton, FL, 1982-1983.
- [36] E.J. Woods, M.A.J. Zieger, D.Y. Gao, and J.K. Critser, Equations for obtaining melting points for the ternary system ethylene

glycol/sodium chloride/water and their application to cryopreservation. *Cryobiology* 38 (1999) 403-407.

- [37] C. Yildiz, P. Ottaviani, N. Law, R. Ayearst, L. Liu, and C. McKerlie, Effects of cryopreservation on sperm quality, nuclear DNA integrity, in vitro fertilization, and in vitro embryo development in the mouse. *Reproduction* 133 (2007) 585-595.
- [38] M.A. Yousef, R. Datta, and V.G.J. Rodgers, Confirmation of free solvent model assumptions in predicting the osmotic pressure of concentrated globular proteins. *J Colloid Interface Sci* 243 (2001) 321-325.
- [39] M.A. Yousef, R. Datta, and V.G.J. Rodgers, Model of osmotic pressure for high concentrated binary protein solutions. *AIChE Journal* 48 (2002) 913-917.

**Table 2.1.** Osmotic virial coefficients for use with solution molality.

<b>Solute</b> † [Reference]	<b>k<sub>diss</sub></b> [±95% CI <sup>‡</sup> ]	<b>B</b> <b>molal<sup>-1</sup></b> [±95% CI <sup>‡</sup> ]	<b>C</b> <b>molal<sup>-2</sup></b> [±95% CI <sup>‡</sup> ]	<b>Adj.</b> <b>R<sup>2</sup></b>	<b>Max</b> <b>Molality</b>	<b>Solubility</b> <b>limit</b> § <b>(molal)</b> [Temp]
NaCl [35]	1.678 [±0.02]	0.044 [±0.002]	0*	1.000	5.111	6.100 [0 °C]
KCl [35]	1.772 [±0.003]	0	0	1.000	2.005	3.726 [0 °C]
DMSO ** [2; 14; 28]	1 <sup>††</sup>	0.108 [±0.005]	0	0.990	14.975	
Glycerol ** [2; 18; 35]	1	0.023 [±0.001]	0	0.996	10.859	
PG [4; 18; 35]	1	0.039 [±0.001]	0	0.997	19.713	
EG [35]	1	0.037 [±0.001]	-0.001 [0.0001]	1.000	24.166	
Methanol [35]	1	0.004 [±0.0003]	0	0.998	66.345	
Mannitol [35]	1	0	0	1.000	0.999	1.181 [25 °C]
Sucrose [35]	1	0.125 [±0.002]	0	1.000	2.115	5.958 [20 °C]
Dextrose [35]	1	0.044 [±0.001]	0	1.000	2.379	4.542 [15 °C]
Trehalose [19]	1	-0.394 [±0.2]	0.388 [±0.2]	0.998	1.108	1.325 [-1.2 °C]
Hemoglobin [8]	1	49.252 [±18.6]	3.07x10 <sup>4</sup> [±1.83x10 <sup>3</sup> ]	0.999	1.23x10 <sup>-2</sup>	
BSA [34]	1	3.70x10 <sup>2</sup> [±3.62x10 <sup>2</sup> ]	1.60x10 <sup>5</sup> [±4.25x10 <sup>4</sup> ]	0.994	9.72x10 <sup>-3</sup>	
OVL [38]	1	3.78x10 <sup>2</sup> [±14.9]	0	0.990	1.95x10 <sup>-2</sup>	
Whey proteins [this study]	1	3.99 x10 <sup>2</sup> [±61.5]	0	0.954	3.03x10 <sup>-2</sup>	

†In addition to the solutes shown in the table, some very non-ideal solutes can be described using the osmotic virial equation. For example, ethanol is a very non-ideal solute and requires three parameters to adequately fit the solution behaviour for use with molality. (B = 0.0376, C = -0.002, D = 0.000023, adj R<sup>2</sup> = 0.999) (see Figure 2.3a).

‡95% confidence intervals were calculated using equation (2.15).

§ A blank indicates that there is either no solubility limit or the solubility limit is unknown.

\*Where 0 appears in table, it indicates that the coefficient was not included in the fit (i.e. C = 0, indicates a quadratic fit was adequate).

\*\* Phase diagram also measured in this study.

†† Where 1 appears in the dissociation constant column, it indicates that there is no dissociation into ions of this solute.

**Table 2.2.** Osmotic virial coefficients for use with solution mole fraction.

<b>Solute</b> [Reference]	<b>k<sub>diss</sub></b> [±95% CI <sup>‡</sup> ]	<b>B</b> $\left(\frac{\text{mole solute}}{\text{mole total}}\right)^{-1}$ [±95% CI <sup>‡</sup> ]	<b>C</b> $\left(\frac{\text{mole solute}}{\text{mole total}}\right)^{-2}$ [±95% CI <sup>‡</sup> ]	<b>Adj. R<sup>2</sup></b>	<b>Max Mole Frac</b>	<b>Solubility limit <sup>§</sup></b> $\left(\frac{\text{mole solute}}{\text{mole total}}\right)$ [Temp]
NaCl [35]	1.663 [±0.02]	2.749 [±0.1]	0*	1.000	0.084	0.099 [0 °C]
KCl [35]	1.772 [±0.003]	0	0	1.000	0.035	0.063 [0 °C]
DMSO ** [2; 14; 28]	1 <sup>††</sup>	2.423 [±1.4]	27.231 [±8.0]	0.995	0.213	
Glycerol ** [2; 18; 35]	1	1.950 [±0.1]	0	0.998	0.164	
PG [4; 18; 35]	1	2.831 [±0.08]	0	0.999	0.262	
EG [35]	1	1.501 [±0.07]	0	0.999	0.303	
Methanol [35]	1	0.395 [±0.02]	0	0.999	0.545	
Ethanol [35]	1	1.9949	-5.9843	0.999		
Mannitol [35]	1	0	0	0.999	0.017	0.021 [25 °C]
Sucrose [35]	1	7.182 [±0.1]	0	1.000	0.037	0.097 [20 °C]
Dextrose [35]	1	2.513 [±0.05]	0	1.000	0.041	0.076 [15 °C]
Trehalose [19]	1	-22.418 [±9.3]	1.250x10 <sup>3</sup> [±5.2x10 <sup>2</sup> ]	0.998	0.020	0.023 [-1.2 °C]
Hemoglobin [8]	1	1.978x10 <sup>4</sup> [±1.3x10 <sup>3</sup> ]	0	0.960	2.21x10 <sup>-4</sup>	
BSA [34]	1	9.535x10 <sup>4</sup> [±8.4x10 <sup>3</sup> ]	0	0.961	1.75x10 <sup>-4</sup>	
OVL [38]	1	2.310x10 <sup>4</sup> [±8.8x10 <sup>2</sup> ]	0	0.990	3.51x10 <sup>-4</sup>	
Whey proteins [this study]	1	2.20x10 <sup>4</sup> [±4.6x10 <sup>3</sup> ]	0	0.911	5.46x10 <sup>-4</sup>	

<sup>‡</sup>95% confidence intervals were calculated using equation (2.15).

<sup>§</sup> A blank indicates that there is either no solubility limit or the solubility limit is unknown.

\*Where 0 appears in table, it indicates that the coefficient was not included in the fit (i.e. C = 0, indicates a quadratic fit was adequate).

\*\* Phase diagram also measured in this study.

<sup>††</sup> Where 1 appears in the dissociation constant column, it indicates that there is no dissociation into ions of this solute.

**Table 2.3.** Pitzer-Debye-Huckel equation parameters [5; 25]

Parameter	Description	Value
$f^\Phi$	Pitzer-Debye-Huckel electrolyte effects function	$f^\Phi = -A^\Phi \left( \frac{\sqrt{I}}{1+b\sqrt{I}} \right)$
$A^\Phi$	Debye-Huckel slope	0.377*
$I$	Solution ionic strength	$I = \frac{1}{2} (z_m^2 m + z_x^2 m)$ <p>where <math>z_m</math> is the charge of the positive ion, <math>z_x</math> is the charge of the negative ion, and <math>m</math> is the molality of the solute. For a 1:1 electrolyte</p> $I = m$
$b$	Empirical parameter	1.2
$B_{MX}^\Phi$	2 <sup>nd</sup> virial coefficient	$B_{MX}^\Phi = \beta_{MX}^{(0)} + \beta_{MX}^{(1)} e^{-\alpha\sqrt{I}}$
$\beta_{MX}^{(0)}$		0.0765
$\beta_{MX}^{(1)}$		0.2664
$\alpha$	Empirical parameter	2.0
$C_{MX}^\Phi$	3 <sup>rd</sup> virial coefficient	0.00127

\*Value for  $A^\Phi$  is for water at 0 °C and saturated pressure [5].

All other values can be found in [25].

**Table 2.4.** Osmotic virial coefficients for NaCl fit to Robinson and Stokes data [29].

<b>Solute<sup>†</sup></b> [Reference]	<b>k<sub>diss</sub></b> [±95% CI <sup>†</sup> ]	<b>B*</b> <b>molal<sup>-1</sup></b> [±95% CI <sup>†</sup> ]	<b>Adj. R<sup>2</sup></b>
NaCl [29]	1.673 [±0.02]	0.0508 [±0.002]	1.000

<sup>†</sup>95% confidence intervals were calculated using equation (2.15)

**Table 2.5.** Summary of the approach used for linear regression of different forms of the single-solute osmotic virial equation.

Type of solute [concentration units]	$\bar{y}$ vector	Conversion of coefficients in $\bar{\beta}$ to osmotic virial coefficients
Non-electrolytes [molality]	$\pi/m_i - 1$	$\beta_1 = B$ $\beta_2 = C$ ...
Electrolytes [molality]	$\pi$	$\beta_1 = k_{\text{diss}}$ $\beta_2 = B(k_{\text{diss}})^2$ $\beta_3 = C(k_{\text{diss}})^3$ ...
Non-electrolytes [mole fraction]	$\pi/A^*x_i - 1$	$\beta_1 = B^*$ $\beta_2 = C^*$ ...
Electrolytes [mole fraction]	$\pi/A^*$	$\beta_1 = k_{\text{diss}}^*$ $\beta_2 = B^*(k_{\text{diss}}^*)^2$ $\beta_3 = C^*(k_{\text{diss}}^*)^3$ ...

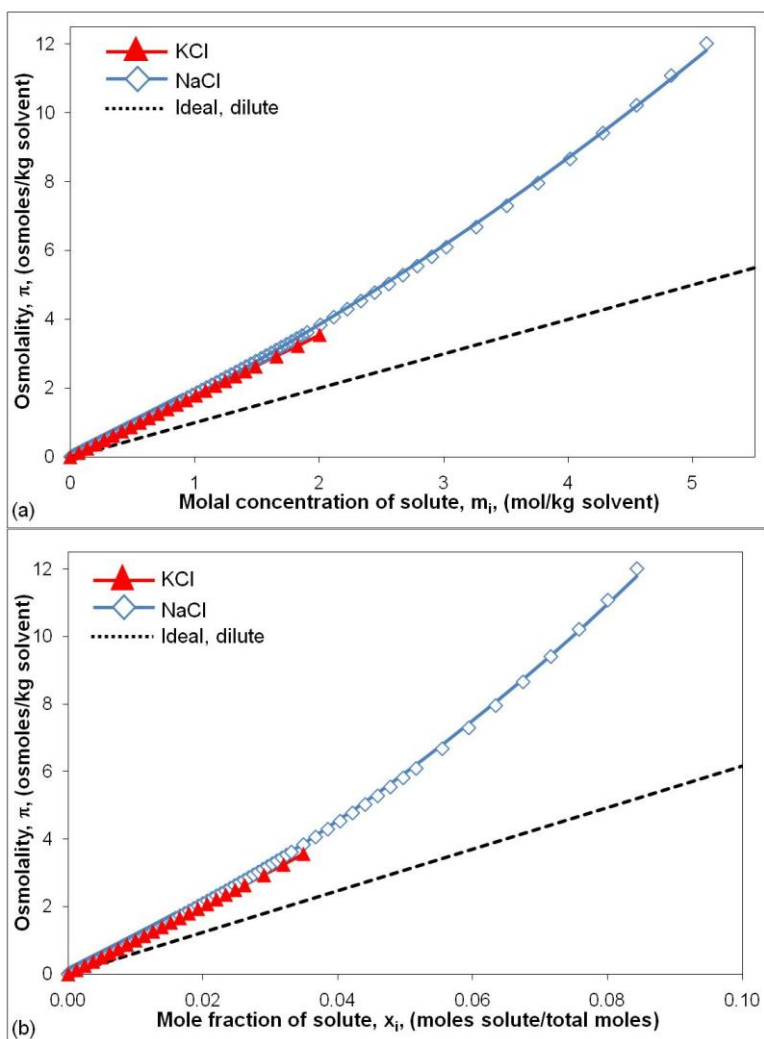


**Figure 2.1.** Osmolality of single-solute aqueous electrolyte solutions as a function of (a) solute molality and (b) solute mole fraction. The NaCl and KCl data are from the CRC tables [35]. Equation (2.3) was fit to the data in molality and equation (2.4) was fit to the data in mole fraction in order to obtain the dissociation constant and the osmotic virial coefficients for each solute. The dashed line is for an ideal, dilute solute ( $\pi = m$ ). The ideal, dilute line is not linear in the mole fraction graphs due to the nonlinear conversion between mole fraction and molality.

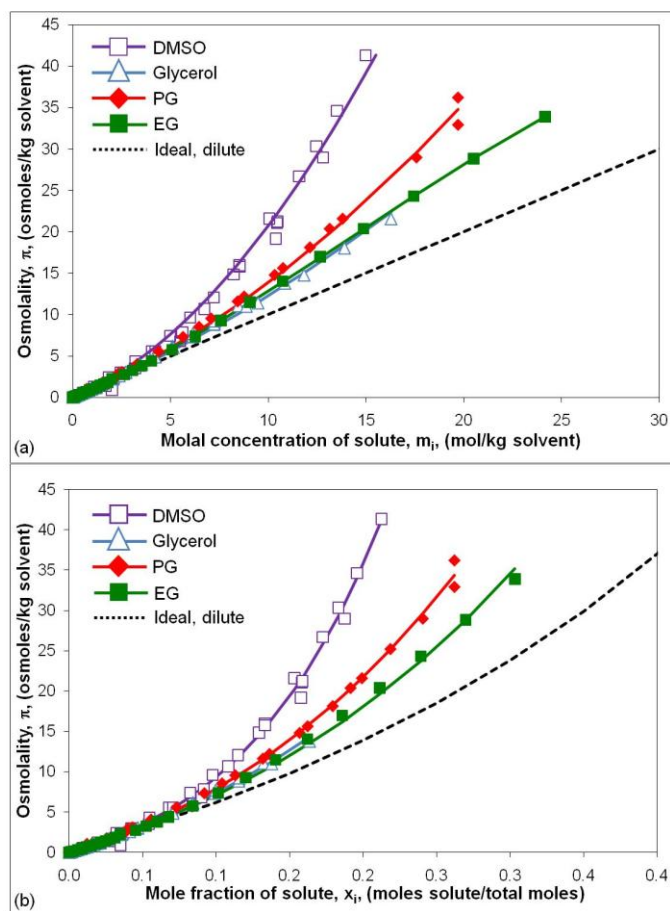


**Figure 2.2.** Osmolality of single-solute aqueous CPA solutions as a function of (a) solute molality and (b) solute mole fraction. The DMSO data are from various literature sources [2; 14; 28] and our measurements. The glycerol data are from various literature sources [2; 18; 35] and our measurements. The propylene glycol (PG) data are from various literature sources [4; 18; 35]. The ethylene glycol (EG) data are from the CRC tables [35]. Equation (2.1) was fit to the data in molality and equation (2.2) was fit to the data in mole fraction in order to obtain the osmotic virial coefficients for each solute. The dashed line is for an ideal, dilute solute ( $\pi = m$ ). The ideal, dilute line is not linear in the mole fraction graphs due to the nonlinear conversion between mole fraction and molality.

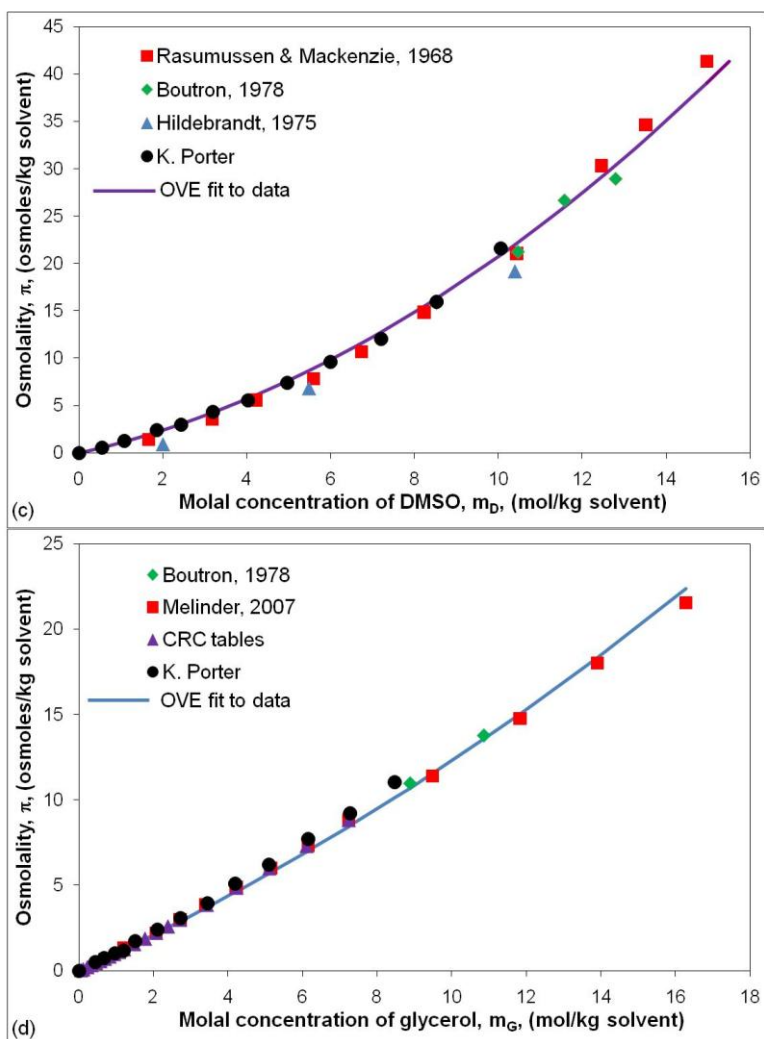


**Figure 2.2** (cont'd). Osmolality of single-solute aqueous (c) DMSO and (d) glycerol solutions as a function of solute molality. The closed circles are data points measured in our lab. The other symbols are from various literature sources. The DMSO data are from [2; 14; 28]. The glycerol data are from [2; 18; 35]. The solid line is the osmotic virial equation in molality (equation (2.1)) fit to all of the data in order to obtain the osmotic virial coefficients for each solute.

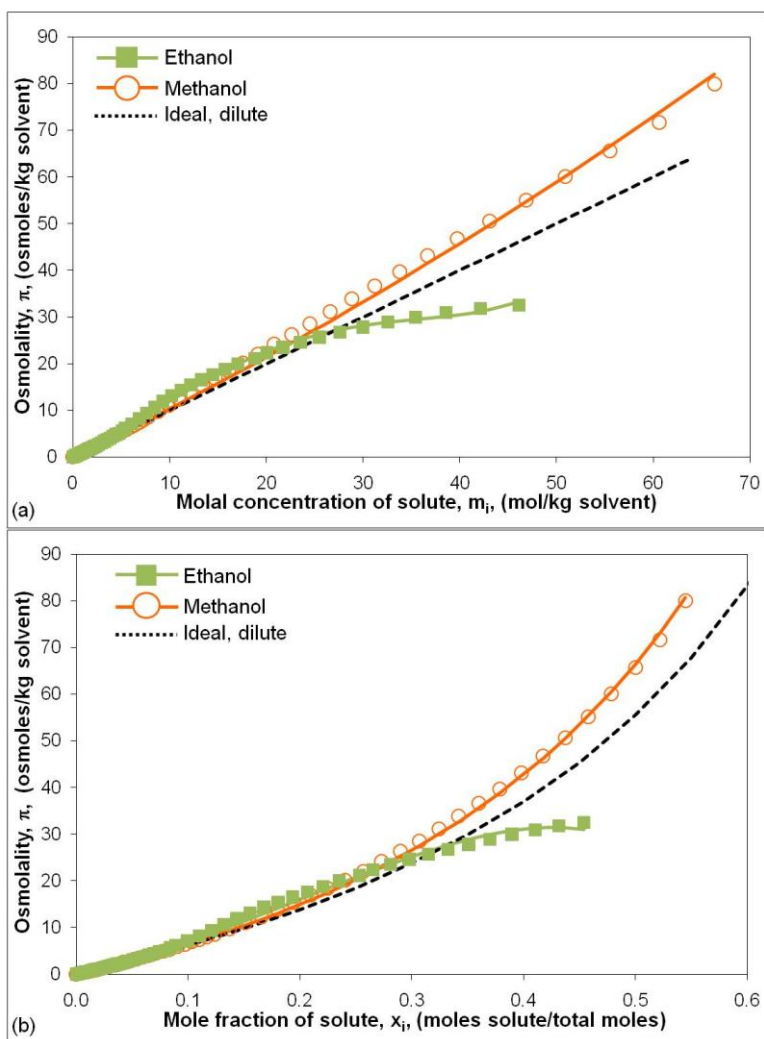


**Figure 2.3.** Osmolality of single-solute aqueous alcohol solutions as a function of (a) solute molality and (b) solute mole fraction. The methanol and ethanol data are from the CRC tables [35]. Equation (2.1) was fit to the data in molality and equation (2.2) was fit to the data in mole fraction in order to obtain the osmotic virial coefficients for each solute. The dashed line is for an ideal, dilute solute ( $\pi = m$ ). The ideal, dilute line is not linear in the mole fraction graphs due to the nonlinear conversion between mole fraction and molality.

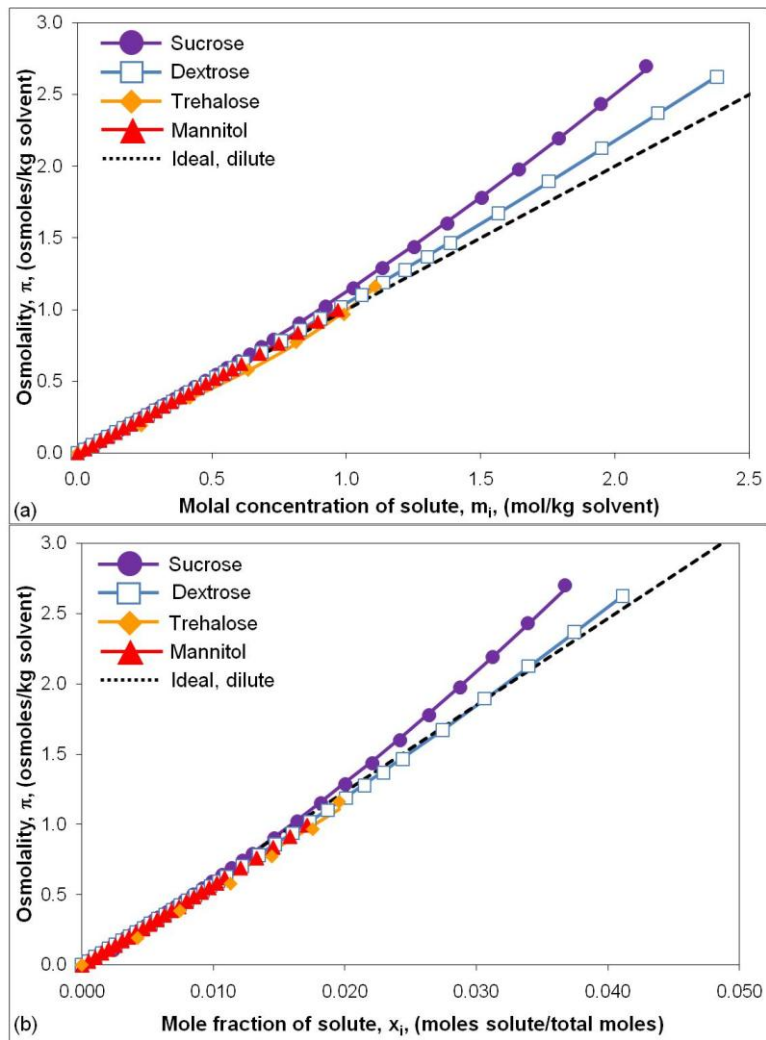


**Figure 2.4.** Osmolality of single-solute aqueous sugar solutions as a function of (a) solute molality and (b) solute mole fraction. The sucrose, dextrose, and mannitol data are from the CRC tables [35]. The data for trehalose is from Miller et al. [19]. Equation (2.1) was fit to the data in molality and equation (2.2) was fit to the data in mole fraction in order to obtain the osmotic virial coefficients for each solute. The dashed line is for an ideal, dilute solute ( $\pi = m$ ). The ideal, dilute line is not linear in the mole fraction graphs due to the nonlinear conversion between mole fraction and molality.

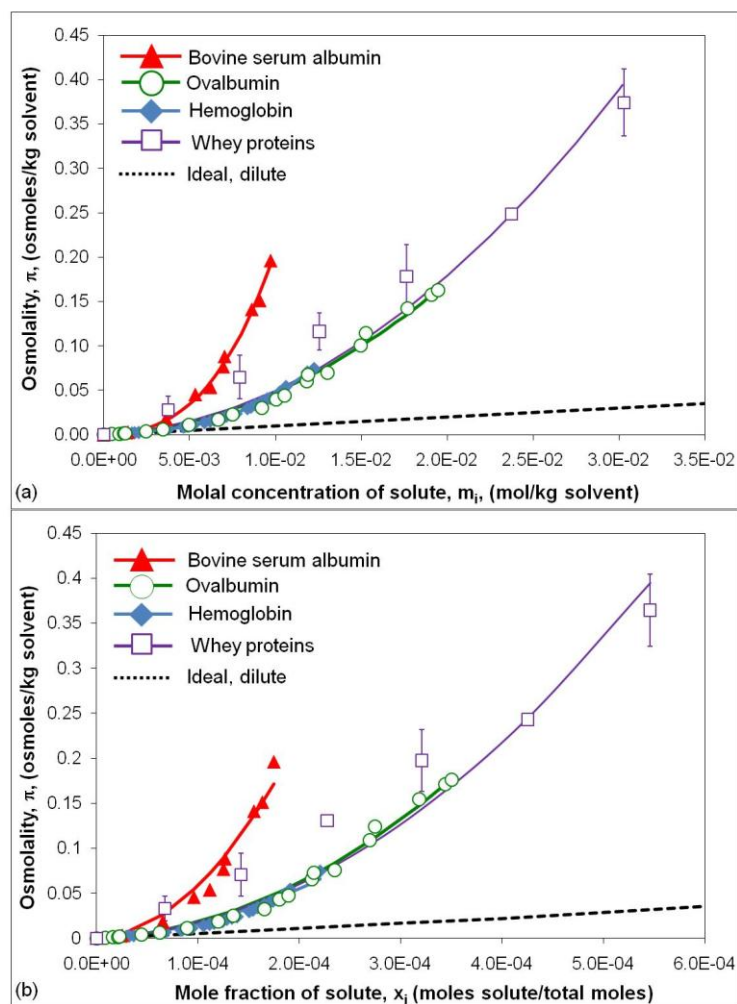


**Figure 2.5.** Osmolality of single-solute aqueous macromolecule solutions as a function of (a) solute molality and (b) solute mole fraction. The hemoglobin data are Adair's data published by Dick [8]. The bovine serum albumin data are from Vilker et al. [34]. The ovalbumin data are from Yousef et al. [38]. The whey protein data was measured in this study. Equation (2.1) was fit to the data in molality and equation (2.2) was fit to the data in mole fraction in order to obtain the osmotic virial coefficients for each solute. The dashed line is for an ideal, dilute solute ( $\pi = m$ ). The ideal, dilute line is not linear in the mole fraction graphs due to the nonlinear conversion between mole fraction and molality.

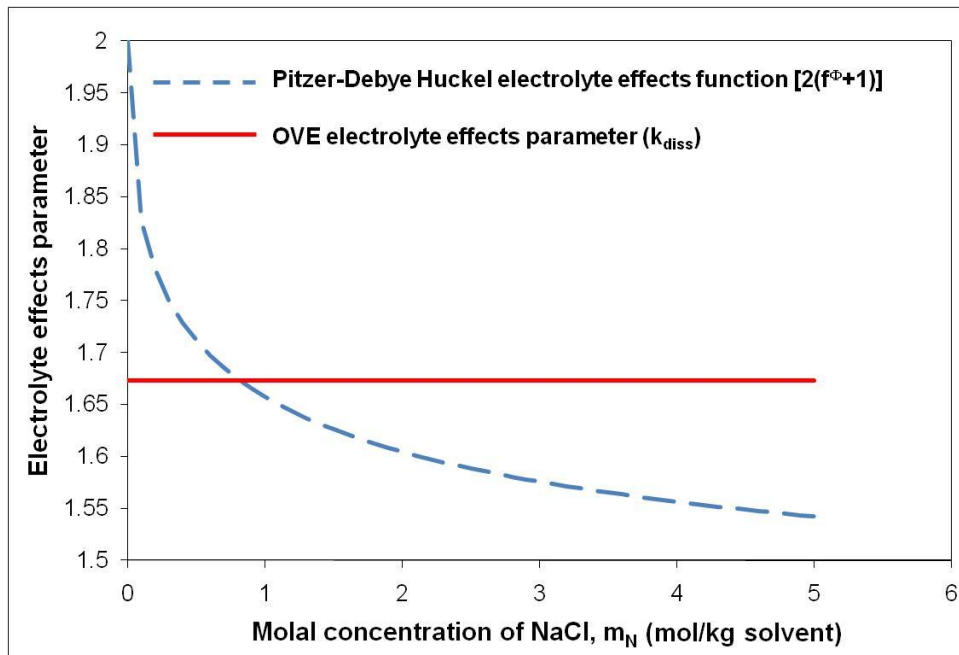


**Figure 2.6.** A comparison between the dissociation constant ( $k_{diss}$ ) and the Pitzer-Debye-Huckel electrolyte effects function ( $2(f^\phi + 1)$ ) for NaCl.

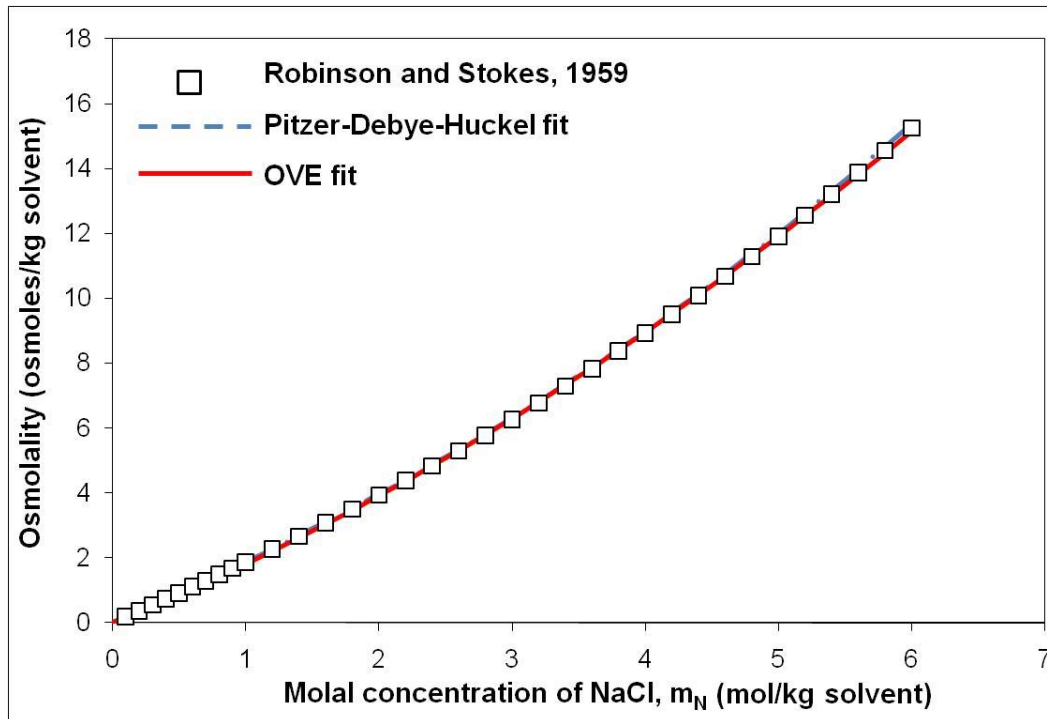


**Figure 2.7.** Osmolality of single-solute aqueous NaCl solutions as a function of solute molality. The open circles are data measured at 25 °C, obtained from from Robinson and Stokes [29] which were used by Pitzer and Mayorga [25] to determine the Pitzer-Debye-Huckel coefficients (Table 2.3). This data was used to obtain the single-solute NaCl osmotic virial coefficients at 25 °C (Table 2.4). The solid line is the single-solute osmotic virial equation in molality (equation (2.3)) fit to the data and the dashed line is the Pitzer-Debye-Huckel (equation (2.7)) fit to the data. Except at the highest NaCl concentrations, the dashed line is lying directly under the solid line and cannot be seen.

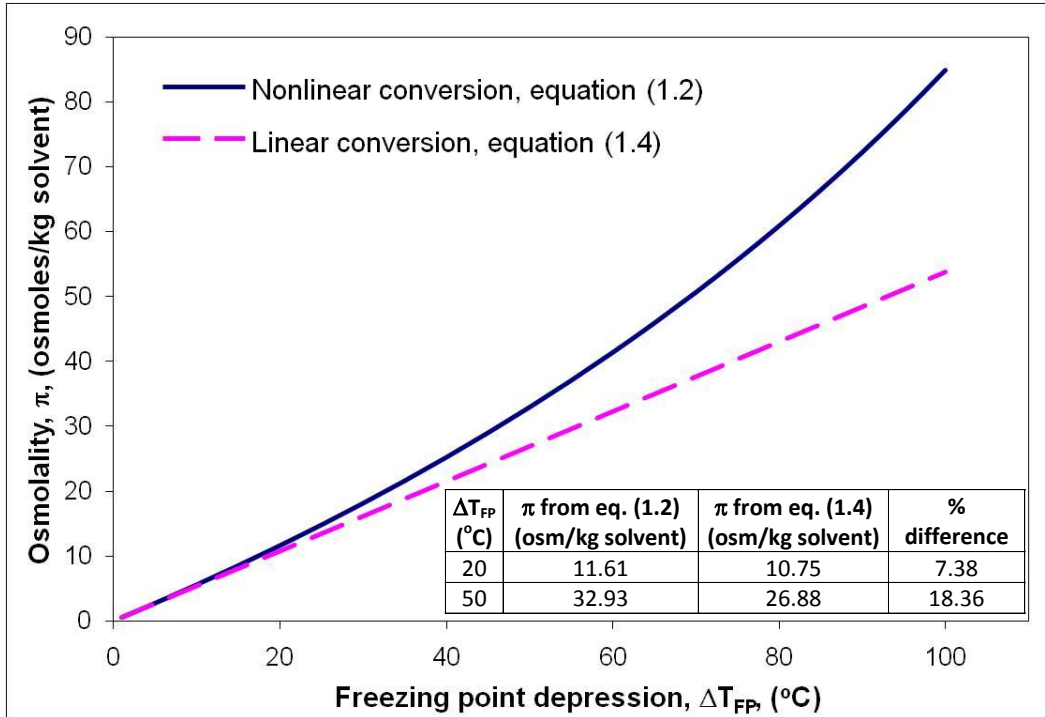


**Figure 2.8.** Osmolality determined from the freezing point using either the linear conversion (equation (1.4)) or the nonlinear conversion (equation (1.2)).

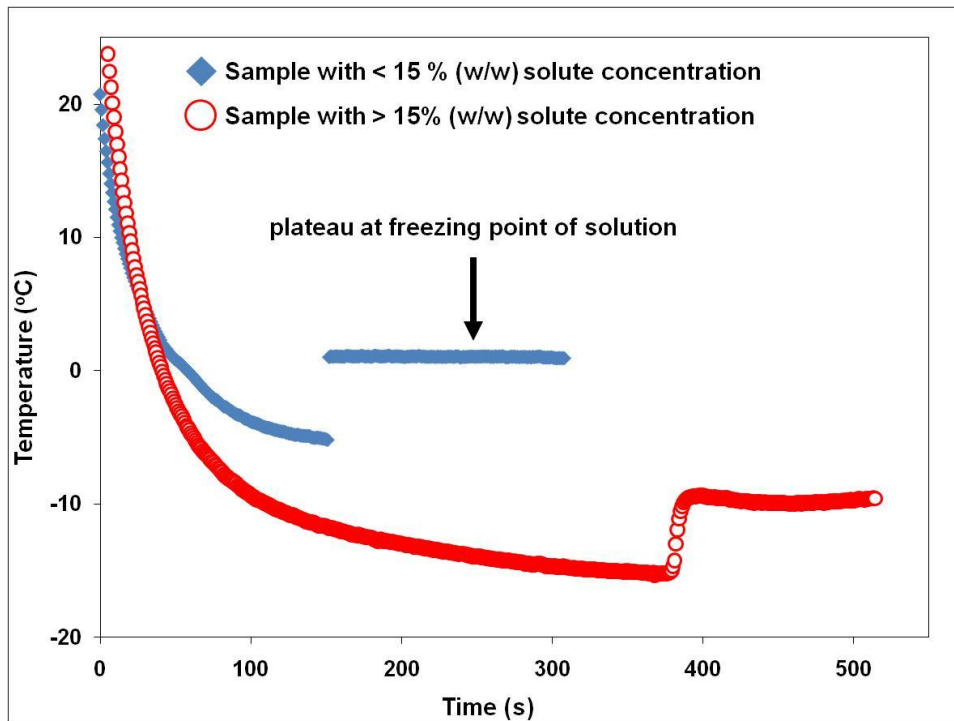


**Figure 2.9.** Typical temperature measurements for a freezing point depression experiment. The closed diamonds are from a typical sample with less than 15 % (w/w) solute concentration. The open circles are from a typical sample with greater than 15 % (w/w) solute concentration. The freezing point is determined by the average temperature during the plateau.

## **Chapter 3 - Multisolute osmotic virial equation<sup>1</sup>**

### **3.1. Introduction**

In many areas of biology, including cryobiology, the solution behaviour of both the extracellular and intracellular solutions plays an important role. The osmolality difference between the extra- and intra-cellular solutions drives the water flux across the cell membrane [20; 30]. A non-ideal replacement for the osmotic equilibrium equation is presented in Chapter 5 which demonstrates that the osmolality as a function of concentration for the intracellular solution is needed in order to accurately calculate the cellular osmotic response.

In cryobiology, the freezing point depression of solutions is also important. The freezing point determines the temperature at which ice can first form in the extracellular solution, how much ice will form at equilibrium at a given temperature, and the amount of supercooling in the intracellular solution. For these reasons, cryobiologists are interested in predicting both the osmolality and the freezing point depressions of multisolute extra- and intra-cellular solutions.

There are many solutes of interest in cryobiology, from electrolytes to cryoprotective agents (CPAs) to macromolecules, and there are many combinations of these solutes. Since measuring the solution properties of

---

<sup>1</sup>A version of sections of this chapter has been published. J.A.W. Elliott, R.C. Prickett, H.Y. Elmoazzen, K.R. Porter and L.E. McGann 2007. *Journal of Physical Chemistry B*. 111: 1775-1785.

A version of sections of this chapter has been accepted for publication. R.C. Prickett, J.A.W. Elliott, and L.E. McGann 2009. *Cryobiology*. (doi:10.1016/j.cryobiol.2009.07.011).

all possible combinations is prohibitively time- and resource-consuming, much work has been done to predict the solution behaviour of these complicated multisolute solutions using a range of solution theories [13; 24; 26; 27; 28; 36; 37; 38; 48]. Solution theories have been developed for cryobiological solutions which are accurate for a certain subset of solutions, but these equations either require fitting of multisolute data, thus restricting them to solutions for which multisolute data is available [13; 27; 36; 37; 38; 48], or they do not take into account all of the solute interactions [24; 26; 28]. The challenge is to develop a solution theory that (i) takes into account all of the solute interactions, (ii) is accurate for many solutions, and (iii) does not require fitting of multisolute data.

The osmotic virial equation (OVE) has been widely utilized for predicting solution behaviour of complicated multisolute solutions [9; 16; 17; 18; 22; 29; 32; 47; 50; 51; 52]. The osmolalities of single- or multi-solute solutions are represented as truncated polynomials in concentration, where each solute has unique coefficients for terms of second or higher order in concentration. The word “virial” is derived from the Latin word for force or energy, “*vis*” [19]. The coefficients in the virial equation can be obtained from knowledge of the forces between molecules [39]. As opposed to previous work done with the osmotic virial equation for multisolute solutions, the approach taken by this study differs in the treatment of the interaction term. Typically the determination of the cross coefficient, which is a measure of the interaction between two

different solutes in a multisolute solution, requires measurements of the multisolute system [16; 17; 18; 22; 29; 32; 50; 51; 52] in addition to the measurements of the single-solute systems used to determine the second virial coefficients of the pure species. However, in this study, mixing rules, which have been derived from thermodynamic first principles [11; 12], are used to predict the cross coefficient from measurements of single-solute solutions alone.

The objective of this chapter was to demonstrate the applicability of this form of the multisolute OVE to a wide range of multisolute solutions, containing a broad selection of solutes including CPAs, small molecules, and macromolecules. The applicability of the multisolute OVE to solutions containing electrolytes will be demonstrated in Chapter 4.

### 3.2. Governing equations

#### 3.2.1. *Multisolute osmotic virial equation - general form*

For simplicity, first consider a form of the multisolute OVE (truncated to second order) for a ternary solution with non-electrolyte solutes,  $i$  and  $j$ :

$$\pi = m_i + m_j + B_i m_i^2 + B_j m_j^2 + 2B_{ij} m_i m_j \quad (3.1)$$

where  $m_i$  is the molal concentration of solute  $i$  (mole/kg solvent),  $B_i$  is the second virial coefficient of solute  $i$  ((mole/kg solvent)<sup>-1</sup>), and  $B_{ij}$  is the second virial cross coefficient for the two solutes,  $i$  and  $j$  ((mole/kg solvent)<sup>-1</sup>).

Equation (3.1) describes the contribution of each solute to the overall osmolality. The parameter  $B_i$  accounts for the interactions between two identical solute molecules of type  $i$ . This parameter is unique to each type of solute. The cross coefficient,  $B_{ij}$ , accounts for interactions between solutes  $i$  and  $j$ .

When determining the osmolality of a multisolute solution, it is often assumed that the contribution of each solute to the overall osmolality of the solution is additive [23; 24; 31], which is equivalent to setting  $B_{ij} = 0$ . When the osmolalities of single-solute solutions are summed to predict osmolalities of multisolute solutions, the interactions between the different types of solutes are not accounted for, often leading to incorrect predictions of the solution osmolality. However, Kleinhans and Mazur demonstrated for certain combinations of CPAs + NaCl in water, that the adding osmolalities approach was adequate [24]. In Chapter 4, the predictions from Kleinhans and Mazur's adding-osmolalities approach will be compared to the predictions from the multi-solute OVE which has been adapted for solutions containing electrolytes.

In order to determine the cross coefficient,  $B_{ij}$ , most approaches require measurements of the ternary solution and the coefficient is found by regressing ternary data [16; 17; 18; 22; 29; 32; 50; 51; 52], similar to the methods outlined in Chapter 2 to determine the pure-species second virial coefficient from measurements of single-solute solutions. Alternatively, the cross coefficient can be predicted from detailed

molecular knowledge of solute-solute interactions [39]. For applications in biology it is desirable to be able to predict the cross coefficients from measurements of single-solute solutions alone. Mixing rules for the multisolute OVE have been derived from thermodynamic first principles, assuming a semi-dilute regular solution, which allow for the prediction of the osmotic virial cross coefficient using only the single-solute osmotic virial coefficients. The quadratic mixing rule is [12]:

$$B_{ij} = \frac{B_i + B_j}{2} \quad (3.2)$$

For multisolute solutions which contain mixtures of highly non-ideal solutes such as proteins, a cubic mixing term is required. The cubic mixing term can also be derived from regular solution theory [11]:

$$C_{ijk} = (C_i C_j C_k)^{1/3} \quad (3.3)$$

where  $C_{ijk}$  is the third virial cross coefficient for solutes  $i, j$ , and  $k$ .

Using the mixing rules in equations (3.2) and (3.3), the OVE can be written for any number of solutes:

$$\pi = \sum_i m_i + \sum_i \sum_j \frac{(B_i + B_j)}{2} m_i m_j + \sum_i \sum_j \sum_k (C_i C_j C_k)^{1/3} m_i m_j m_k \quad (3.4)$$

It should be noted that for electrolytes, the molality of the electrolyte should be multiplied by its dissociation constant ( $k_{diss}$ ) (see Chapter 2).

The multisolute OVE can also be written in terms of the solute mole fraction:

$$\pi = A^* \left( \sum_i x_i + \sum_i \sum_j \frac{(B_i^* + B_j^*)}{2} x_i x_j + \sum_i \sum_j \sum_k (C_i^* C_j^* C_k^*)^{1/3} x_i x_j x_k \right) \quad (3.5)$$

where  $x_i$  is the mole fraction of the solute (moles solute/total moles of solution), and  $B_i^*$  [(moles solute/total moles)<sup>-1</sup>] and  $C_i^*$  [(moles solute/total moles)<sup>-2</sup>] are the second and third osmotic virial coefficients for use with mole fraction, respectively. The quantity in the parenthesis in equation (3.5) is osmole fraction ( $\tilde{\pi}$ ) so the conversion factor,  $A^*$ , between osmole fraction and osmolality is needed.

For two solutes in solution, the multisolute OVE written in terms of solute concentration in molality is:

$$\begin{aligned} \pi = m_2 + m_3 + B_2 m_2^2 + B_3 m_3^2 + (B_2 + B_3) m_2 m_3 + C_2 m_2^3 + C_3 m_3^3 \\ + 3(C_2^2 C_3)^{1/3} m_2^2 m_3 + 3(C_2 C_3^2)^{1/3} m_2 m_3^2 \end{aligned} \quad (3.6)$$

where the subscript 2 refers to the first solute and subscript 3 refers to the second solute (subscript 1 is typically reserved for the solvent).

Expressed in terms of solute mole fraction, the multisolute OVE is:

$$\pi = A^* \left( x_2 + x_3 + B_2^* x_2^2 + B_3^* x_3^2 + (B_2^* + B_3^*) x_2 x_3 + C_2^* x_2^3 + C_3^* x_3^3 \right. \\ \left. + 3(C_2^{*2} C_3^*)^{1/3} x_2^2 x_3 + 3(C_2^* C_3^{*2})^{1/3} x_2 x_3^2 \right) \quad (3.7)$$

These forms of the multisolute OVE (equations (3.6) and (3.7)) were used to predict the solution behaviour of a range of combinations of

solutes in water, including (i) glycerol + dimethyl sulphoxide (DMSO), (ii) hemoglobin + an ideal solute, and (iii) bovine serum albumin (BSA) + ovalbumin (OVL). The number of terms in the multisolute OVE depends on the number of single-solute osmotic virial coefficients required to describe each solute's solution behaviour.

### 3.2.2. Multisolute osmotic virial equation - glycerol + DMSO

When the solute concentration was expressed in molality, glycerol and DMSO both required only a second virial coefficient to describe their single-solute solution behaviour (see Table 2.1). Thus, the multisolute OVE for glycerol + DMSO expressed in molality is:

$$\pi = m_G + m_D + B_G m_G^2 + B_D m_D^2 + (B_G + B_D) m_G m_D \quad (3.8)$$

where  $m_G$  is the molality of glycerol (mole/kg solvent),  $m_D$  is the molality of DMSO (mole/kg solvent),  $B_G$  is the pure species second virial coefficient for glycerol for use in molality ( $[\text{mole/kg solvent}]^{-1}$ ), and  $B_D$  is the pure species second virial coefficient for DMSO for use in molality ( $[\text{mole/kg solvent}]^{-1}$ ).

When the solute concentration was written in mole fraction, glycerol required only a second virial coefficient and DMSO required a second and third virial coefficient to describe their single-solute solution behaviour (see Table 2.2). The multisolute OVE for use with mole fraction is:

$$\pi = A^* \left( x_G + x_D + B_G^* x_G^2 + B_D^* x_D^2 + (B_G^* + B_D^*) x_G x_D + C_D^* x_D^3 \right) \quad (3.9)$$

where  $x_G$  is the mole fraction of glycerol (moles glycerol/moles total),  $x_D$  is the mole fraction of DMSO (moles DMSO/moles total),  $B_G^*$  is the pure species second virial coefficient for glycerol for use in mole fraction ([moles/moles total]<sup>-1</sup>),  $B_D^*$  is the pure species second virial coefficient for DMSO for use in mole fraction ([moles/moles total]<sup>-1</sup>) and  $C_D^*$  is the pure species third virial coefficient for DMSO for use in mole fraction ([moles/moles total]<sup>-2</sup>).

### 3.2.3. Multisolute osmotic virial equation - hemoglobin + ideal solute

The cytoplasm of a human erythrocyte is made up of predominately hemoglobin and other small molecules, such as potassium chloride (KCl). In this study, the proposed osmotic model of the cytoplasm is the known amount of hemoglobin and a calculated amount of ideal solute, where the amount of the ideal solute was taken to be the concentration required to bring the osmolality of the intracellular solution to its isotonic value once the contribution of the isotonic molality of hemoglobin was taken into account. The value for the isotonic osmolality of erythrocytes cited in the literature ranges from 275 mOsm/kg solvent to 315 mOsm/kg solvent [2; 4]. The isotonic concentration of hemoglobin taken from the literature was 35.1 gram / 100 mL cells [43]. This value was determined

spectrophotometrically and when converted to molality, gave a value of 7.3 millimole/kg solvent [15; 44].

Hemoglobin required a second and third virial coefficient to describe its single-solute solution behaviour in molality (see Table 2.1) and the virial coefficients for an ideal solute are all zero. Thus, the multisolute OVE, written in terms of solute molality, for hemoglobin and an ideal solute is:

$$\pi = m_I + m_H + B_H m_H^2 + B_H m_I m_H + C_H m_H^3 \quad (3.10)$$

where  $m_I$  is the molality of the ideal solute (mole/kg solvent),  $m_H$  is the molality of hemoglobin (mole/kg solvent),  $B_H$  is the pure species second virial coefficient for hemoglobin for use in molality ([mole/kg solvent]<sup>-1</sup>), and  $C_H$  is the pure species third virial coefficient for hemoglobin for use in molality ([mole/kg solvent]<sup>-2</sup>). Even though the ideal solute has all zero virial coefficients, the quadratic mixing term still appears in the multisolute OVE.

In order to determine the accuracy of the model, measurements of the cytoplasm were required. Electron spin resonance (ESR) has been used to measure the cell water volume as a function of extracellular solution osmolality. Two studies involving human erythrocytes [6; 33] measured the relative cell water volume (cell water volume / cell water volume at isotonic) as a function of the inverse relative osmolality (isotonic osmolality / osmolality) using ESR. The relative cell water volume is equivalent to the inverse relative intracellular concentration (isotonic concentration /

concentration) of all of the intracellular solutes combined into one “grouped solute”:

$$\frac{V_w}{V_{w,o}} = \frac{m_o}{m} \quad (3.11)$$

where  $V_w$  is the cell water volume,  $m$  is the molal concentration of all intracellular solutes combined into one “grouped solute” and the subscript  $o$  refers to the isotonic condition. Equation (3.11) comes from the fact that the molal concentration of the intracellular solutes is equal to the number of moles of solute ( $n$ ) divided by the water mass ( $m = n/V_w \rho_w$  where  $\rho_w$  is the mass density of water). Assuming that the number of moles of solute remains the same as water leaves the cell, the ratio of the concentration at isotonic ( $m_o$ ) to the concentration at any anisotonic condition is equal to the ratio of cell water volume at the anisotonic condition to the cell water volume at isotonic.

By taking the experimental measurements from Du [6] and Moronne et al. [33] and inverting both  $\pi_o/\pi$  and  $V_{w,o}/V_w$  and multiplying the relative osmolality by the isotonic osmolality, the osmolality as a function of the relative intracellular grouped solute concentration was determined. The data were plotted as osmolality versus relative concentration since the isotonic concentration of the grouped solute was the least well known parameter.

At equilibrium, the osmolality of the cytoplasm is equal to the osmolality of the extracellular solution. In the absence of permeating solutes, the osmotic equilibrium is maintained by water transport across the cell membrane. As the cell dehydrates in hypertonic solutions, the contents of the cell concentrate at the same rate. The osmolalities of aqueous hemoglobin solutions were measured up to 12.3 millimole/kg solvent with no solute precipitation [5]. Applying the osmotic virial model of the cytoplasm to the most hypertonic data point measured by ESR, extrapolation to a hemoglobin molality of approximately 30 millimole/kg solvent was required. Incorporating the no-precipitation assumption, the relative concentration of hemoglobin is the same as the relative concentration of the ideal, dilute solute:

$$m_H / m_{H,o} = m_I / m_{I,o} \quad (3.12)$$

where the subscript o refers to the isotonic condition.

Equation (3.12) was used in equation (3.10) to express the ideal, dilute solute concentration as a function of the hemoglobin concentration and the isotonic concentrations of the ideal, dilute solutes and hemoglobin.

$$\pi = \left( \frac{m_{I,o}}{m_{H,o}} \right) m_H + m_H + B_H m_H^2 + B_H m_H \left( \frac{m_{I,o}}{m_{H,o}} \right) m_H + C_H m_H^3 \quad (3.13)$$

Substituting the normal hemoglobin concentration of 7.3 millimole/kg solvent [15; 43; 44] in equation (3.10) and using a value of 289 mOsm/kg solvent as the isotonic osmolality (average value from Du [6] and Moronne et al. [33]), the isotonic concentration for the additional solutes in human erythrocytes was calculated to be 197 millimole/kg solvent. This value does not represent the amount of ideal, dilute solutes actually present in the cytoplasm of an erythrocyte, but rather the "effective concentration" of ideal, dilute solute needed to create a solution with an osmolality of 289 mOsm/kg solvent, after the effect of the hemoglobin had been taken into account. The 197 millimole/kg solvent concentration of ideal, dilute solute accounted for the osmotic behaviour of all the solutes, including the dissociated ions, other than hemoglobin in the cytoplasm.

#### 3.2.4. Multisolute osmotic virial equation - bovine serum albumin + ovalbumin

When the solute concentration was in molality, BSA required a second and third osmotic virial coefficient to describe its single-solute solution behaviour. In molality, OVL required only a second virial coefficient to describe its single-solute solution behaviour (see Table 2.1). Thus, the multisolute OVE for BSA + OVL is:

$$\pi = m_B + m_O + B_B m_B^2 + B_O m_O^2 + (B_B + B_O) m_B m_O + C_B m_B^3 \quad (3.14)$$

where  $m_B$  is the molality of BSA (mole/kg solvent),  $m_O$  is the molality of OVL (mole/kg solvent),  $B_B$  is the pure species second virial coefficient for BSA for use in molality ( $[\text{mole/kg solvent}]^{-1}$ ),  $B_O$  is the pure species second virial coefficient for OVL for use in molality ( $[\text{mole/kg solvent}]^{-1}$ ), and  $C_B$  is the pure species third virial coefficient for BSA for use in molality ( $[\text{mole/kg solvent}]^{-2}$ ).

For solute concentration in mole fraction, BSA and OVL required only a second virial coefficient to describe the single-solute solution behaviour. The multisolute OVE in mole fraction for BSA and OVL is:

$$\pi = A^* \left( x_B + x_O + B_B^* x_B^2 + B_O^* x_O^2 + (B_B^* + B_O^*) x_B x_O \right) \quad (3.15)$$

where  $x_B$  is the mole fraction of BSA (moles BSA/total moles),  $x_O$  is the mole fraction of OVL (moles OVL/total moles),  $B_B^*$  is the pure species second virial coefficient for BSA for use in mole fraction ( $[\text{mole/total moles}]^{-1}$ ), and  $B_O^*$  is the pure species second virial coefficient for OVL for use in mole fraction ( $[\text{mole/total moles}]^{-1}$ ).

Equations (3.8), (3.13), and (3.14) were used to predict the multisolute osmolality of ternary aqueous solutions of DMSO + glycerol, hemoglobin + an ideal solute, and BSA + OVL, respectively, for solute concentration in molality. Equations (3.9) and (3.15) were used to predict the multisolute osmolality of the DMSO + glycerol and BSA + OVL aqueous solutions, respectively, for solute concentration in mole fraction. The predictions for the cytoplasm were not done in mole fraction, as the number of moles of

intracellular solute was not known, just the relative grouped solute molality.

### 3.3. *Materials and methods*

#### 3.3.1. *Obtaining the multisolute phase diagrams*

Phase diagrams were (i) measured by freezing point depression or (ii) obtained from the literature for various multisolute solutions. The phase diagrams have been converted to osmolality as a function of total solute molal concentration.

##### (i) Freezing point depression measurements<sup>2</sup>

Ternary glycerol (Sigma-Aldrich, Oakville, Ontario) + DMSO (Sigma-Aldrich, Oakville, Ontario) + distilled, deionized water (CORNING Mega-Pure™ system ACS) solutions were prepared for two different values of the mass ratio (R) of glycerol to DMSO: 0.5 and 2.0. For R = 0.5, solutions with total solute mass percentages of 4%, 9%, 15%, 21%, 27% and 33% were studied. For R = 2.0, the total solute mass percentages chosen were 3%, 6%, 9%, 12%, 15%, 21%, 27% and 33%. The mass of water was chosen to ensure that at least 10 mL of solution was made and that the masses of glycerol and DMSO were easy to work with (at least 1g of each).

---

<sup>2</sup> Undergraduate student, K. Porter measured each data point once and I measured each data point twice (or for the R = 0.5: 15%, 21%, 27% and 33% w/w solutions, three times).

The samples were thoroughly mixed using an electronic stirrer (Fisher Scientific Electronic Stirrer 2009, Fisher Scientific Ltd, Nepean, Ontario) for at least 30 minutes at 500 rpm. Three millilitres (3 mL) of the solutions were transferred to a 12 x 75 mm KIMAX® test tube (Fisher Scientific Ltd, Nepean, Ontario) using a pipette. The same freezing process was followed for the ternary mixtures as for the binary mixtures (described in Chapter 2), except that a 0.04" diameter type T thermocouple (OMEGA TMTSS-040G-6, Laval, Quebec) was used. Freezing point depression measurements were converted to osmolality using equation (1.2).

Measuring the phase diagram of viscous solutions using the freezing point depression method can result in inaccurate results due to the viscosity of the solution slowing the ice crystal growth and the release of latent heat, particularly at high concentrations.

#### (ii) Obtaining phase diagrams from the literature

Phase diagrams for the human erythrocyte cytoplasm [6; 33] and aqueous solutions of bovine serum albumin (BSA) + ovalbumin (OVL) [49], were obtained from the literature. The phase diagrams were measured by membrane osmometry [49] or electron spin resonance [6; 33].

### 3.4. Results

The multisolute OVE, with mixing rules derived from thermodynamic first principles (equations (3.4) and (3.5)), requires only single-solute

information to make predictions of multisolute solution behaviour. In addition to the multisolute OVE, other solution theories that allow predictions of multisolute solution behaviour using single-solute solution data are (i) ideal, dilute solution theory and (ii) adding osmolalities (or freezing point depressions). The predictions from these three solution theories are shown in Figures 3.1 to 3.3. For the predictions from the adding-osmolalities approach and the multisolute OVE, the single-solute osmotic virial coefficients determined in Chapter 2 were utilized.

In order to assess which solution theory provided the most accurate predictions of solution osmolality, the errors in the predictions from all three solution theories were quantified. The percent error was calculated using:

$$\% \text{ error} = \frac{|Prediction - Measured|}{Measured} \times 100 \quad (3.16)$$

For the predictions of solution osmolality done with the solute concentration in molality, the errors for each solution theory for each of the solutions studied are listed in Table 3.1 (the errors were calculated at the maximum measured total solute molality). In addition to determining the percent error at the maximum molality, the sum of squared errors (SSE) was calculated using equation (2.11) to assess how accurately each solution theory predicted the measured data points over the entire range of the solute concentration.

$$SSE = \sum_{i=1}^m (y_i - f_i)^2 \quad (2.11)$$

Since the SSE is a summation over all of the data points, the value obtained depends on the number of data points. Since each multisolute solution has a different number of data points, the values of the SSE should only be used to compare between solution theories for a specific solution. The SSE for each solution theory are also listed in Table 3.1.

The results shown Table 3.1 demonstrate that the predictions of the multisolute solution osmolality from the multisolute OVE result in smaller errors than the practice of adding osmolalities or assuming ideal, dilute solution for the solutions studied. The multisolute OVE was shown to accurately predict the solution behaviour of ternary aqueous solutions of (i) two small molecular weight compounds (glycerol + DMSO); (ii) the cytoplasm of a human erythrocyte modelled as a mixture of hemoglobin and an ideal solute; and (iii) two macromolecules (BSA + OVL).

For the aqueous glycerol + DMSO system, it can be seen in Figures 3.1 (a - d) that the agreement between the experimental measurements and the predictions using the multisolute OVE for the R = 2.0 solutions was not as good as for the R = 0.5 solutions. This may be due to the increased amount of glycerol in the R = 2.0 solutions. The high viscosity of glycerol made accurate freezing point depression measurements progressively more difficult as the glycerol concentration increased. Also, the predictions in solute molality were more accurate than those in solute

mole fraction. When writing the equation for the excess Gibbs energy from which the multisolute OVE is derived [12], an *a priori* assumption was required regarding whether to express the concentration in molality or mole fraction. Landau and Lifshitz [25] chose to express the excess Gibbs energy in molality, whereas regular solution theory is written in terms of mole fraction [39]. For the multisolute solutions that were investigated in this thesis, the assumption of Landau and Lifshitz to use molality resulted in more accurate predictions of the solution behaviour.

Figure 3.2 shows that modeling the cytoplasm of erythrocytes as a solution of hemoglobin and an ideal, dilute solute in water agreed remarkably well with ESR data for human erythrocytes [6; 33]. Note that the line in Figure 3.2 (a) is a prediction from equation (3.13) with no adjustable parameters. The dotted line is an extrapolation of the predictions beyond the range of hemoglobin data that was regressed to determine the osmotic virial coefficients for hemoglobin. It is important to distinguish the range where the hemoglobin coefficients were known to be accurate from the range in which the osmotic virial equation was extrapolated because the third osmotic virial coefficient is simply an empirical coefficient and its physical meaning is not clear. However, Figure 3.2 (a) shows that if the coefficients were assumed to be valid over the entire concentration range, the proposed osmotic virial equation (equation (3.13)) gave an accurate prediction of the osmolality of the cytoplasm.

In Figures 3.2 (b - c), the concentrations over which the parameters were fit was not differentiated from the concentrations over which the parameters were extrapolated. The predictions in Figure 3.2 (b) show that including both the hemoglobin and the ideal, dilute solute was important since assuming the cytoplasm was all hemoglobin or all ideal, dilute solute did not accurately predict the data as well as the proposed osmotic virial equation. Furthermore, Figure 3.2 (c) shows that the hemoglobin, the ideal, dilute solute and the interaction between the two types of solutes all contributed significantly to the total solution osmolality. At the maximum predicted osmolality, the hemoglobin contributed 13.1% of the total solution osmolality, the ideal, dilute solute contributed 53.4% of the total solution osmolality and the hemoglobin – ideal solute interactions contributed 33.5% of the total solution osmolality. The osmotic virial equation, with the proposed mixing rules for only two solutes (a protein and an ideal, dilute solute) captured the thermodynamic behaviour of the complicated biological solution in human erythrocytes within experimental error.

For the aqueous BSA + OVL system, Figure 3.3 (a) shows that the agreement between the experimental measurements and the predictions using the proposed osmotic virial equation (equation (3.14)) was better than the predictions from the free solvent model. The free solvent model is a predictive solution theory that was used for the BSA + OVL solution by Yousef *et al.* [49]. Similarly to the multisolute OVE, the free solvent does

not require fitting of the multisolute data. However, when solute molality is used, the predictions from the free solvent model were less accurate for the BSA + OVL solution than those from the multisolute OVE. In Figure 3.3 (b), it can be seen that the predictions from the multisolute OVE (equation (3.15)) were not as accurate in mole fraction. In mole fraction, the predictions from adding osmolalities are the most accurate, with both the free solvent model and the multisolute OVE over-predicting the osmolality. Again, the *a priori* assumption of Landau and Lifshitz [25] to express the concentration in terms of molality instead of mole fraction resulted in more accurate predictions of the solution behaviour of BSA and OVL in water.

### 3.5. Discussion

The single-solute osmotic virial coefficients provided in Chapter 2 were used in the multisolute osmotic virial equation (OVE) to predict the aqueous solution behaviour of a variety of combination of solutes, including two CPAs, a protein and an ideal solute, and two proteins. The predictions were more accurate when the *a priori* assumption of Landau and Lifshitz [25] was used and the solute concentration was expressed in molality, as compared to the predictions when the regular solution theory convention of expressing the solute concentration in mole fraction [39] was used.

In the absence of multisolute solution data, the multisolute OVE should be used to predict multisolute solution behaviour. In addition to only requiring single-solute information to make predictions of multisolute solution behaviour, the mixing rules for the multisolute osmotic virial equation were derived from thermodynamic first principles [11; 12]. The multisolute OVE was shown in this thesis and other studies [47] to be accurate for a wide range of multisolute solutions. Depending on the type of solute and the units of concentration, a form of the single-solute OVE, equations (2.1) through (2.4), should be fit to the single-solute data to obtain the osmotic virial coefficients (Tables 2.1 and 2.2). Using those coefficients, the multisolute OVE can be used to predict the solution behaviour for a variety of combination of solutes. As with the single-solute OVE, the multisolute OVE can be written in other concentration units, but the single-solute osmotic virial coefficients used to make the predictions must be in the same concentration units as the predictions.

When compared to other solution theories which only require single-solute information, such as assuming an ideal and dilute solution or the practice of adding osmolalities, the multisolute OVE provided more accurate predictions for all of the solutions studied when the solute concentration is expressed in molality (see Table 3.1). The approach of adding osmolalities, recently utilized by Kleinhans and Mazur [24], has been shown to be accurate for three CPA + NaCl + water solutions, but did not work well for other multisolute solutions, such as aqueous mixtures

of two CPAs, a protein and an ideal solute, or two proteins (Figures 3.1.(a-b), 3.2, 3.3 (a)). In addition to being less accurate for most non-ideal solutions, the ideal and dilute solution theory and the practice of adding osmolalities contain simplifying assumptions regarding the interactions between the solute molecules which are not thermodynamically correct for non-ideal solutions. The multisolute osmotic virial equation was more accurate for the more non-ideal mixtures, because the solute-solute interactions were taken into account.

Many other solution theories have been proposed for multisolute solutions of interest in cryobiology [13; 24; 26; 27; 28; 36; 37; 38; 48]. These solution theories have resulted in accurate predictions of multisolute solution behaviour, but for a limited number of combinations of solutes.

Predictions of multisolute solution behaviour are needed in cryobiology, since both osmolality and freezing point depression play such crucial roles in the cryopreservation process. In addition, since there is such a wide range of solutes present in cryobiological solutions, from proteins to electrolytes to CPAs, the solution behaviour of all of the different solutions of interest cannot be measured. The multisolute OVE with the proposed mixing rules is an accurate solution theory based on thermodynamic principles that allows predictions of multisolute solution behaviour using only single-solute information. More accurate predictions of the solution behaviour will lead to increased accuracy in modelling the

cellular response to cryopreservation protocols. It is believed that more accurate modelling will lead to the development of novel cryopreservation protocols for cells such as human hepatocytes, human corneal cells, human islets, and mouse oocytes [3; 8; 21; 46]. In addition, improvements to already established cryopreservation protocols, such as the reduction or elimination of CPAs, could be achieved using accurate cryopreservation modelling [40; 45].

Since this thesis work was performed and published, the form of the multisolute OVE that has been shown to be accurate in this thesis has already been incorporated by other cryopreservation researchers for a variety of applications [1; 12; 35; 41; 42]. It has been used in (i) the development of non-ideal, non-dilute transport equations for cellular systems [12], (ii) modelling CPA and water transport in articular cartilage [1; 35], (iii) investigating cryo-injury and developing optimal protocols for a hematopoietic stem cell line (TF-1 cells) [41; 42], and (iv) developing a non-ideal, non-dilute osmotic equilibrium equation (Chapter 5). In addition to these applications, other researchers have agreed that the multisolute OVE should be used to model cryopreservation solutions [14] and have proposed to use it in future studies of anhydrous preservation of cellular systems [10].

### 3.6. References

- [1] A. Abazari, J.A.W. Elliott, G.K. Law, L.E. McGann, and N.M. Jomha, A Biomechanical Triphasic Approach to the Transport of Nondilute Solutions in Articular Cartilage. *Biophysical Journal* (Accepted) (2009).
- [2] J.S. Cook, Nonsolvent Water in Human Erythrocytes. *Journal of General Physiology* 50 (1967) 1311-1325.
- [3] R.C. de Freitas, K.R. Diller, J.R.T. Lakey, and R.V. Rajotte, Osmotic Behavior and Transport Properties of Human Islets in a Dimethyl Sulfoxide Solution. *Cryobiology* 35 (1997) 230-239.
- [4] D.A.T. Dick, *Cell water*, Butterworths, Washington, 1966.
- [5] D.A.T. Dick, An Approach to the Molecular Structure of the Living Cell by Water Flux Studies. in: E.B. Reeve, and A.C. Guyton, (Eds.), *Physical Bases of Circulatory Transport: Regulation and Exchange*, W.B. Saunders Company, Philadelphia, 1967, pp. 217-234.
- [6] J. Du, *Biophysical Study of Mammalian Sperm Utilizing Electron Paramagnetic Resonance*, Purdue University, 1995, pp. 122.
- [7] J. Du, *Biophysical Study of Mammalian Sperm Utilizing Electron Paramagnetic Resonance*, Purdue University, 1995, pp. 122.
- [8] S.L. Ebertz, and L.E. McGann, Osmotic parameters of cells from a bioengineered human corneal equivalent and consequences for cryopreservation. *Cryobiology* 45 (2002) 109-117.

- [9] E. Edmond, and A.G. Ogston, An approach to the study of phase separation in ternary aqueous systems. *Biochem J* 109 (1968) 569-576.
- [10] G.D. Elliott, N. Chakraborty, and D. Biswas, Anhydrous Preservation of Mammalian Cells: Cumulative Osmotic Stress Analysis. *Biopreservation and Biobanking* 6 (2008) 7.
- [11] J.A.W. Elliott, Derivation of cubic mixing rule for osmotic virial coefficient from regular solution theory (Personal Communication), (April 20, 2006).
- [12] H.Y. Elmoazzen, Osmotic transport in cryobiology, Dept. of Laboratory Medicine and Pathology., University of Alberta, Edmonton, Alberta, 2006, pp. 221.
- [13] G.M. Fahy, Analysis of Solution Effects Injury Equations for Calculating Phase-Diagram Information for the Ternary-Systems NaCl-Dimethylsulfoxide-Water and NaCl-Glycerol-Water. *Biophysical Journal* 32 (1980) 837-850.
- [14] G.M. Fahy, Theoretical considerations for oocyte cryopreservation by freezing. *Reproductive Biomedicine Online* 14 (2007) 709-714.
- [15] J.C. Freedman, and J.F. Hoffman, Ionic and osmotic equilibria of human red blood cells treated with nystatin. *J Gen Physiol* 74 (1979) 157-85.
- [16] J. Gaube, A. Pfennig, and M. Stumpf, Thermodynamics of Aqueous Poly(Ethylene Glycol)-Dextran 2-Phase Systems Using the

- Consistent Osmotic Virial Equation. *Fluid Phase Equilibria* 83 (1993) 365-373.
- [17] J. Gaube, A. Pfennig, and M. Stumpf, Vapor-Liquid-Equilibrium in Binary and Ternary Aqueous-Solutions of Poly(Ethylene Glycol) and Dextran. *Journal of Chemical and Engineering Data* 38 (1993) 163-166.
- [18] C.A. Haynes, H.W. Blanch, and J.M. Prausnitz, Separation of Protein Mixtures by Extraction - Thermodynamic Properties of Aqueous 2-Phase Polymer Systems Containing Salts and Proteins. *Fluid Phase Equilibria* 53 (1989) 463-474.
- [19] Virial theorem. (December 21, 2008 version) Wikipedia, the free encyclopedia [http://en.wikipedia.org/wiki/Virial\\_theorem](http://en.wikipedia.org/wiki/Virial_theorem).(accessed on March 10, 2009)
- [20] M.H. Jacobs, The exchange of material between the erythrocyte and its surroundings. *Harvey Lectures* 22 (1927) 146-164.
- [21] J.O.M. Karlsson, A. Eroglu, T.L. Toth, E.G. Cravalho, and M. Toner, Fertilization and development of mouse oocytes cryopreserved using a theoretically optimized protocol. *Human Reproduction* 11 (1996) 1296-1305.
- [22] R.S. King, H.W. Blanch, and J.M. Prausnitz, Molecular Thermodynamics of Aqueous 2-Phase Systems for Bioseparations. *AIChE Journal* 34 (1988) 1585-1594.

- [23] F.W. Kleinhans, Membrane permeability modeling: Kedem-Katchalsky vs a two-parameter formalism. *Cryobiology* 37 (1998) 271-289.
- [24] F.W. Kleinhans, and P. Mazur, Comparison of actual vs. synthesized ternary phase diagrams for solutes of cryobiological interest. *Cryobiology* 54 (2007) 212-222.
- [25] L.D. Landau, and E.M. Lifshitz, *Course of Theoretical Physics, Statistical Physics, Vol. 5, 3rd Edition*, Pergamon Press, Oxford, 1980.
- [26] R.L. Levin, E.G. Cravalho, and C.E. Huggins, Effect of Hydration on Water-Content of Human Erythrocytes. *Biophysical Journal* 16 (1976) 1411-1426.
- [27] R.L. Levin, E.G. Cravalho, and C.E. Huggins, Effect of Solution Non-Ideality on Erythrocyte Volume Regulation. *Biochimica Et Biophysica Acta* 465 (1977) 179-190.
- [28] R.L. Levin, E.G. Cravalho, and C.E. Huggins, Concentration Polarization Effect in a Multicomponent Electrolyte Solution - Human Erythrocyte. *Journal of Theoretical Biology* 71 (1978) 225-254.
- [29] M. Li, Z.Q. Zhu, Y.T. Wu, and D.Q. Lin, Measurement of phase diagrams for new aqueous two-phase systems and prediction by a generalized multicomponent osmotic virial equation. *Chemical Engineering Science* 53 (1998) 2755-2767.

- [30] B. Lucke, and M. McCutcheon, The Living Cell as an Osmotic System and its Permeability to Water. *Physiological Reviews* 12 (1932) 68-139.
- [31] P.W. Madden, and D.E. Pegg, Calculation of Corneal Endothelial-Cell Volume During the Addition and Removal of Cryoprotective Compounds. *Cryo-Letters* 13 (1992) 43-50.
- [32] K. Mishima, K. Nakatani, T. Nomiya, K. Matsuyama, M. Nagatani, and H. Nishikawa, Liquid-Liquid Equilibria of Aqueous 2-Phase Systems Containing Polyethylene-Glycol and Dipotassium Hydrogenphosphate. *Fluid Phase Equilibria* 107 (1995) 269-276.
- [33] M.M. Moronne, R.J. Mehlhorn, M.P. Miller, L.C. Ackerson, and R.I. Macey, ESR measurement of time-dependent and equilibrium volumes in red cells. *J Membr Biol* 115 (1990) 31-40.
- [34] M.M. Moronne, R.J. Mehlhorn, M.P. Miller, L.C. Ackerson, and R.I. Macey, ESR measurement of time-dependent and equilibrium volumes in red cells. *J. Membr. Biol.* 115 (1990) 31-40.
- [35] I.N. Mukherjee, Y. Li, Y.C. Song, R.C. Long, and A. Sambanis, Cryoprotectant transport through articular cartilage for long-term storage: experimental and modeling studies. *Osteoarthritis and Cartilage* 16 (2008) 1379-1386.
- [36] D.E. Pegg, Simple Equations for Obtaining Melting-Points and Eutectic Temperatures for the Ternary-System Glycerol Sodium-Chloride Water. *Cryo-Letters* 4 (1983) 259-268.

- [37] D.E. Pegg, Equations for Obtaining Melting-Points and Eutectic Temperatures for the Ternary-System Dimethylsulfoxide Sodium-Chloride Water. *Cryo-Letters* 7 (1986) 387-394.
- [38] D.E. Pegg, and F.G. Arnaud, Equations for Obtaining Melting-Points in the Quaternary System Propane-1,2-Diol Glycerol Sodium-Chloride Water. *Cryo-Letters* 9 (1988) 404-417.
- [39] J.M. Prausnitz, R.N. Lichtenthaler, and E.G.d. Azevedo, *Molecular thermodynamics of fluid-phase equilibria* Prentice-Hall, Eaglewood Cliffs, New Jersey, 1986.
- [40] L.U. Ross-Rodriguez, J.A.W. Elliott, and L.E. McGann, Characterization of cryobiological responses in TF-1 cells using interrupted freezing procedures. *Cryobiology* (Accepted) (2009).
- [41] L.U. Ross-Rodriguez, J.A.W. Elliott, and L.E. McGann, Investigating cryoinjury using simulations and experiments: 1. TF-1 cells during the two-step freezing (rapid cooling interrupted with a hold time) procedure. *Cryobiology* (Submitted) (2009).
- [42] L.U. Ross-Rodriguez, J.A.W. Elliott, and L.E. McGann, Investigating cryoinjury using simulations and experiments: 2. TF-1 cells during the graded freezing (interrupted slow cooling without hold time) procedure. *Cryobiology* (Submitted) (2009).
- [43] D. Savitz, V.W. Sidel, and A.K. Solomon, Osmotic Properties of Human Red Cells. *Journal of General Physiology* 48 (1964) 79-94.

- [44] A.K. Solomon, M.R. Toon, and J.A. Dix, Osmotic properties of human red cells. *J Membr Biol* 91 (1986) 259-73.
- [45] M.R. Tijssen, H. Woelders, A. de Vries-van Rossen, C.E. van der Schoot, C. Voermans, and J.M. Lagerberg, Improved postthaw viability and in vitro functionality of peripheral blood hematopoietic progenitor cells after cryopreservation with a theoretically optimized freezing curve. *Transfusion* 48 (2008) 893-901.
- [46] M. Toner, R.G. Tompkins, E.G. Cravalho, and M.L. Yarmush, Transport phenomena during freezing of isolated hepatocytes. *AIChE Journal* 38 (1992) 1512-1522.
- [47] E.J. Woods, A. Bagchi, J.D. Benson, X. Han, and J.K. Critser, Melting point equations for the ternary system water/sodium chloride/ethylene glycol revisited. *Cryobiology* 57 (2008) 336-336.
- [48] E.J. Woods, M.A.J. Zieger, D.Y. Gao, and J.K. Critser, Equations for obtaining melting points for the ternary system ethylene glycol/sodium chloride/water and their application to cryopreservation. *Cryobiology* 38 (1999) 403-407.
- [49] M.A. Yousef, R. Datta, and V.G.J. Rodgers, Model of osmotic pressure for high concentrated binary protein solutions. *AIChE Journal* 48 (2002) 913-917.
- [50] M.T. Zafarani-Moattar, and J. Gasemi, Liquid-liquid equilibria of aqueous two-phase systems containing polyethylene glycol and ammonium dihydrogen phosphate or diammonium hydrogen

phosphate. Experiment and correlation. Fluid Phase Equilibria 198 (2002) 281-291.

[51] M.T. Zafarani-Moattar, and R. Sadeghi, Liquid-liquid equilibria of aqueous two-phase systems containing polyethylene glycol and sodium dihydrogen phosphate or disodium hydrogen phosphate - Experiment and correlation. Fluid Phase Equilibria 181 (2001) 95-112.

[52] M.T. Zafarani-Moattar, R. Sadeghi, and A.A. Hamidi, Liquid-liquid equilibria of an aqueous two-phase system containing polyethylene glycol and sodium citrate: experiment and correlation. Fluid Phase Equilibria 219 (2004) 149-155.

**Table 3.1.** Percent error and sum of squared errors in using (i) ideal and dilute, (ii) adding osmolalities and (iii) multisolute OVE to predict each multisolute solution as compared to measured data.

Solute (R-value) <sup>†</sup>	Max total solute molality	Ideal, dilute		Adding Osmolalities		Multisolute OVE	
		% error at max molality <sup>‡</sup>	SSE <sup>§</sup>	% error at max molality <sup>‡</sup>	SSE <sup>§</sup>	% error at max molality <sup>‡</sup>	SSE <sup>§</sup>
Glycerol + DMSO (R = 0.5)	6.0	33.8%	13.63	12.0%	1.76	1.1%	0.02
Glycerol + DMSO (R = 2.0)	5.7	30.2%	9.30	20.6%	4.52	8.5%	0.92
Hb + ideal* [6; 33]	m/m <sub>o</sub> = 2.8	46.5%	0.59	30.2%	0.24	6.4%	0.013
BSA + OVL (R=1.5) [49]	0.01	87.4%	0.0089	36.9%	0.0014	12.7%	0.00015

<sup>†</sup>R values are the mass ratios:  $R = \frac{\text{Mass of solute 1}}{\text{Mass of solute 2}}$

<sup>‡</sup>Percent error calculated using eq. (3.16) at the maximum total solute molality at which osmolality was measured for each solution.

<sup>§</sup>SSE calculated using eq. (2.11). The values of the SSE should only be compared for the different predictions for each specific solution, not between solutions.

\*Predictions of the RBC cytoplasm using the Hb + ideal osmotic virial equation model were done in relative concentration (m/m<sub>o</sub>) (see Figure 3.2).

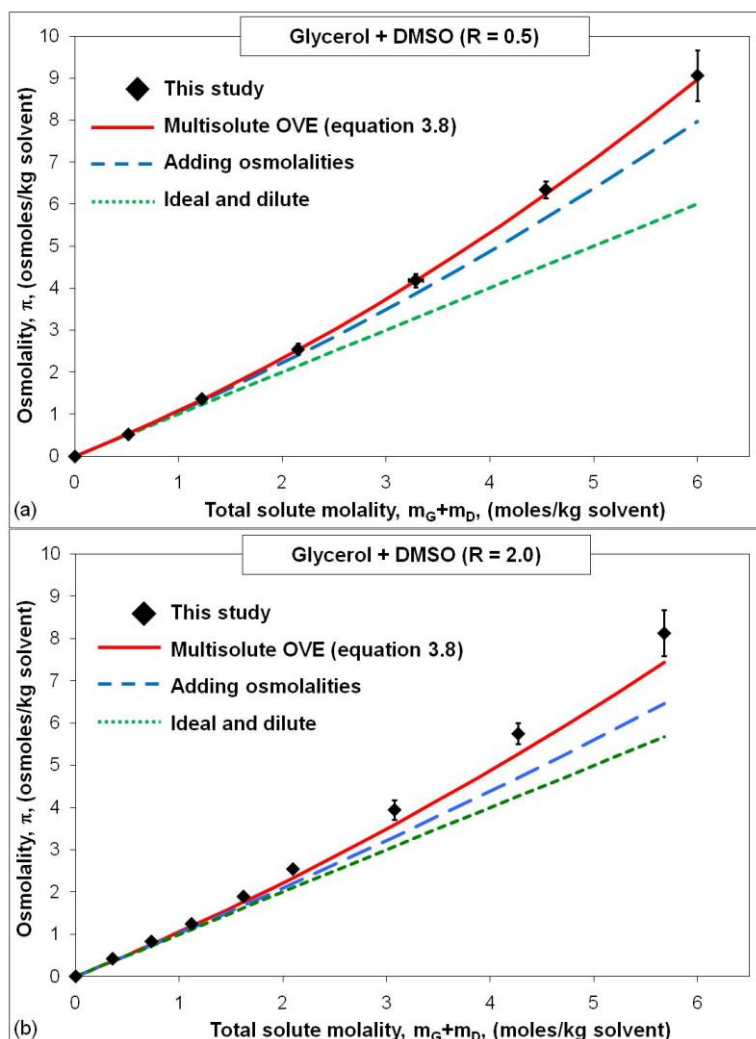


**Figure 3.1.** Osmolality of a glycerol + DMSO + water solution as a function of total solute molality for (a)  $R = 0.5$  and (b)  $R = 2.0$ ; where  $R = \text{mass glycerol}/\text{mass DMSO}$ . The diamonds are our experimental measurements, which have been converted from freezing point depression to osmolality using the nonlinear conversion, equation (1.2). The solid line is the prediction from the multisolute OVE, equation (3.8). The long-dashed line is the prediction from adding osmolalities and the short-dashed line is the prediction from assuming an ideal, dilute solution ( $\pi = m_G + m_D$ ).

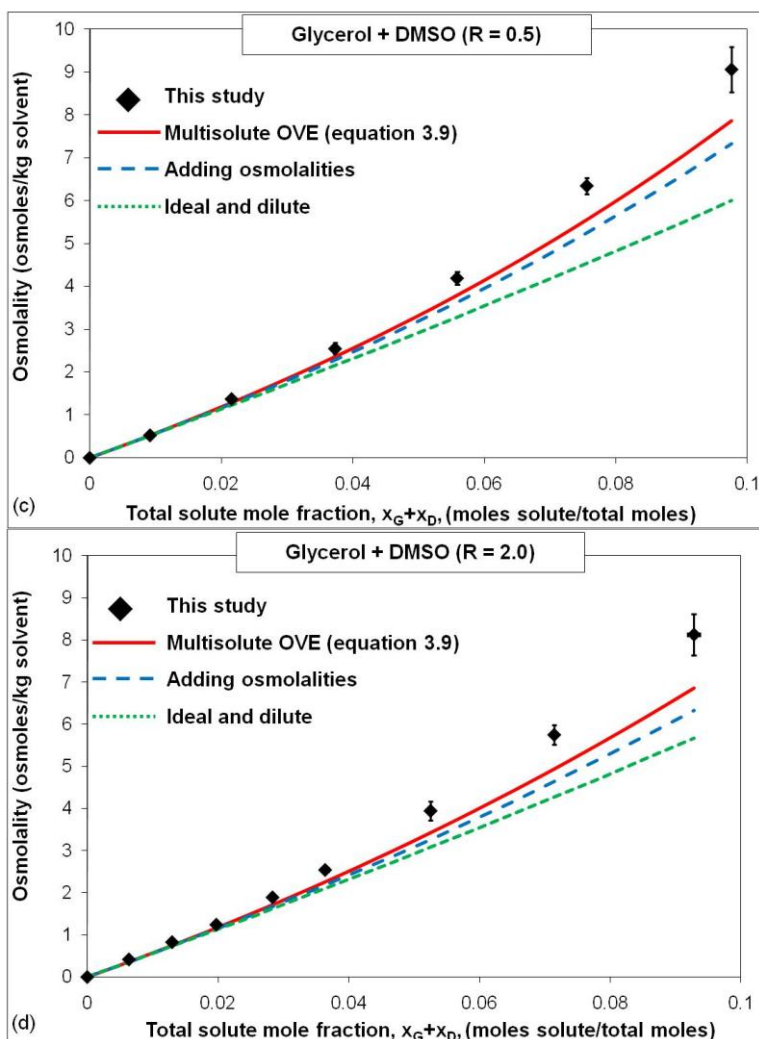


**Figure 3.1** (cont'd). Osmolality of a glycerol + DMSO + water solution as a function of total solute mole fraction for (c)  $R = 0.5$  and (d)  $R = 2.0$ ; where  $R = \text{mass glycerol}/\text{mass DMSO}$ . The diamonds are our experimental measurements, which have been converted from freezing point depression to osmolality using the nonlinear conversion, equation (1.2). The solid line is the prediction from the multisolute OVE, equation (3.9). The long-dashed line is the prediction from adding osmolalities and the short-dashed line is the prediction from assuming an ideal, dilute solution

$$\left( \pi = \frac{1}{w_1 x_1} (x_G + x_D) \right)$$

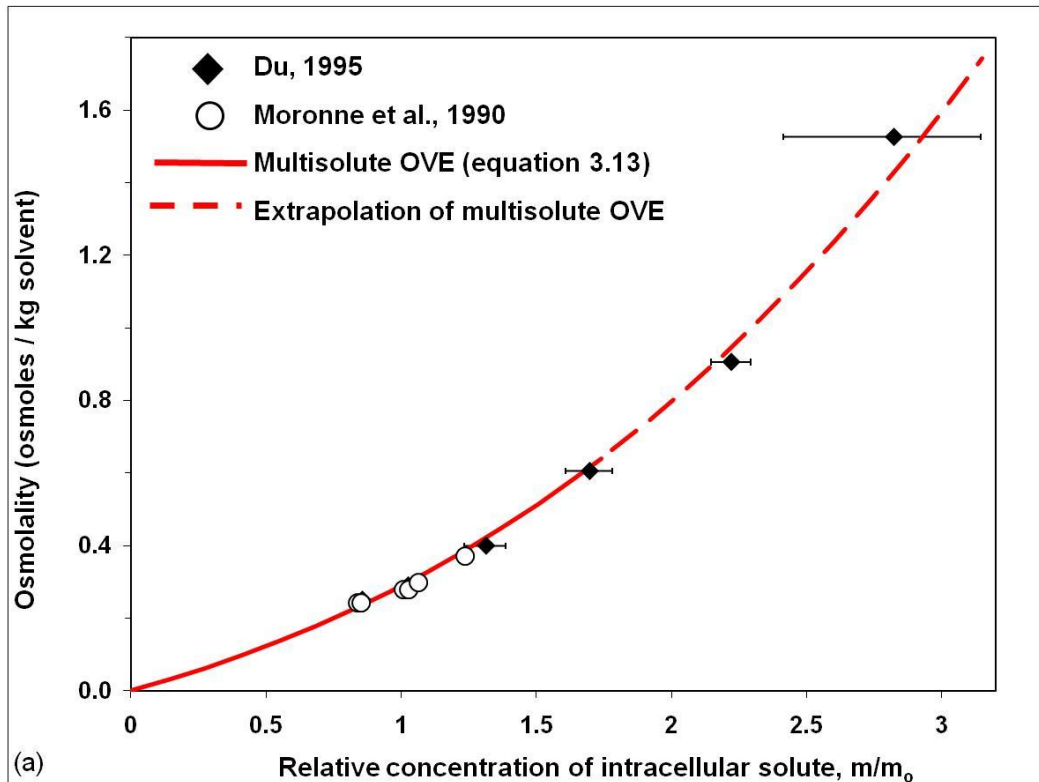


**Figure 3.2 (a).** Osmolality as a function of relative intracellular concentration for human erythrocytes. The closed diamonds are the ESR data from Du [7] and the open circles are the ESR data from Moronne et al [34]. The solid line is predicted using the multisolute OVE (equation (3.13)) with hemoglobin and an ideal, dilute solute with no adjustable parameters. The dashed line is the extrapolation of equation (3.13) past the concentration range for which the hemoglobin parameters were determined.

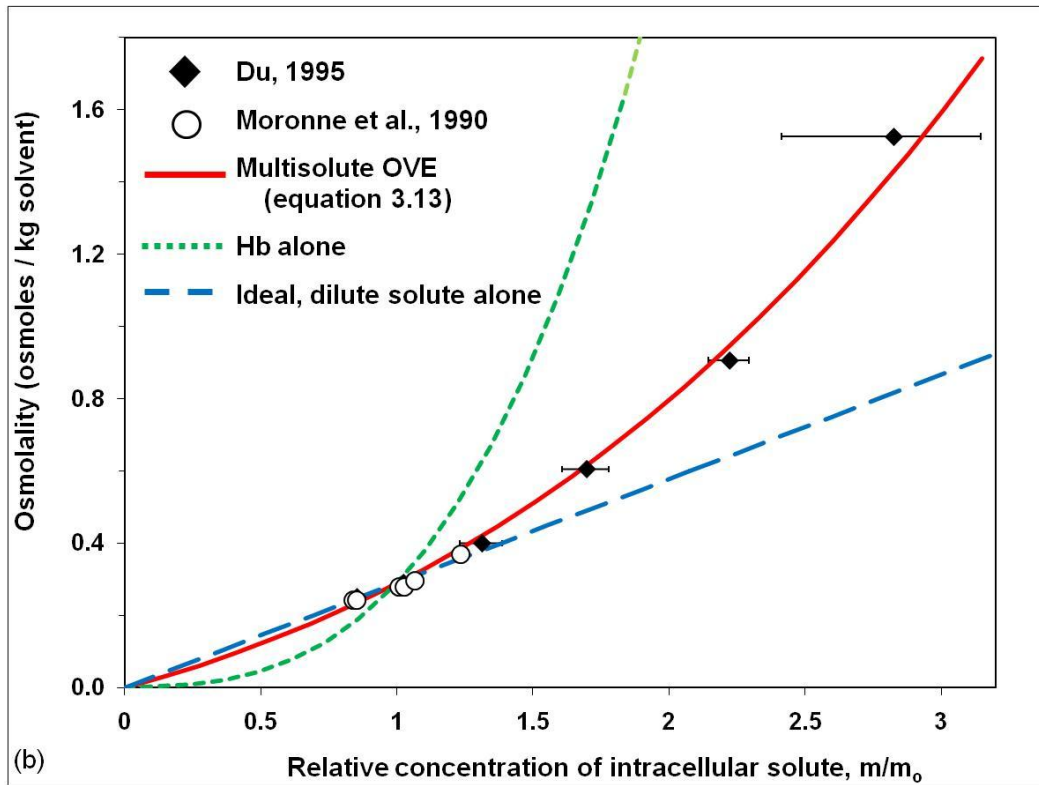


**Figure 3.2 (b).** Osmolality as a function of relative intracellular concentration for human erythrocytes. The closed diamonds are the ESR data from Du [7] and the open circles are the ESR data from Moronne et al [34]. The solid line is predicted using the multisolute OVE (equation (3.13)) with hemoglobin and an ideal, dilute solute. The short dashed line is predicted using the single-solute osmotic virial equation (equation (2.1)) with hemoglobin alone. The long dashed line is predicted using the single-solute osmotic virial equation (equation (2.1)) with an ideal, dilute solute alone.

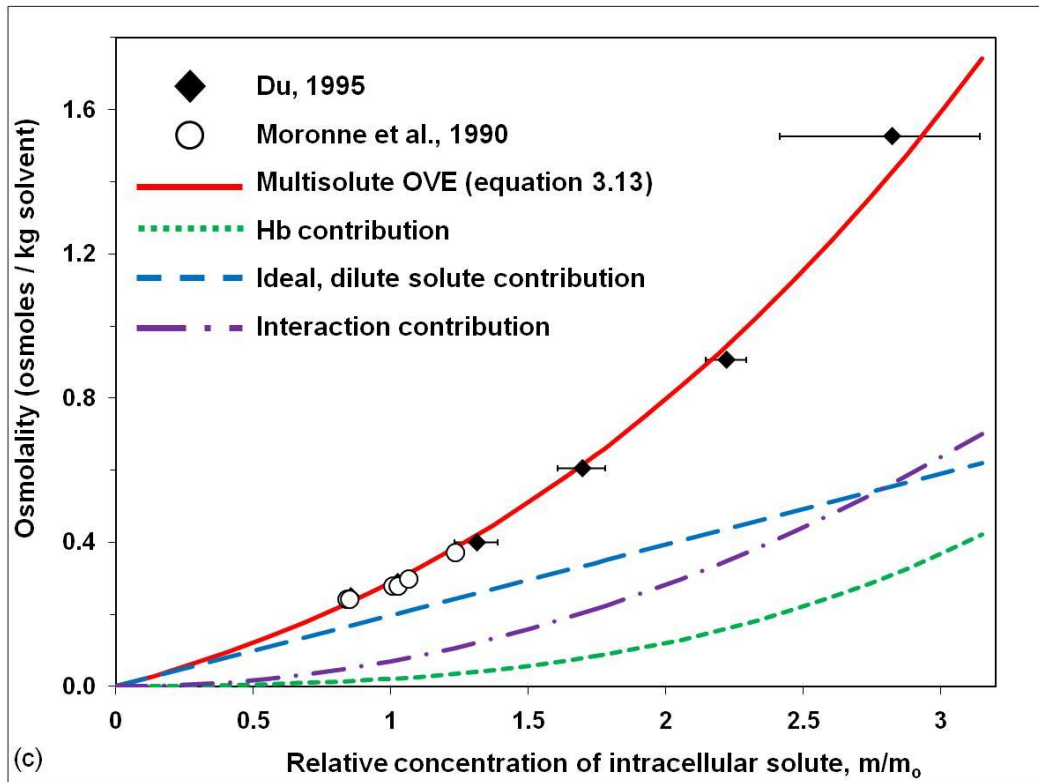


**Figure 3.2 (c).** Relative contributions to osmolality as a function of relative intracellular concentration for human erythrocytes. The closed diamonds are the ESR data from Du [7] and the open circles are the ESR data from Moronne et al [34]. The short dashed line is the calculated contribution of the hemoglobin to the total solution osmolality. The long dashed line is the calculated contribution of the ideal, dilute solute to the total solution osmolality. The cross-hatched line is the calculated contribution of the interactions between the solutes to the total solution osmolality. The solid line is the sum of the three contributions; the predicted total solution osmolality using the multisolute OVE (equation (3.13)) with hemoglobin and an ideal, dilute solute.

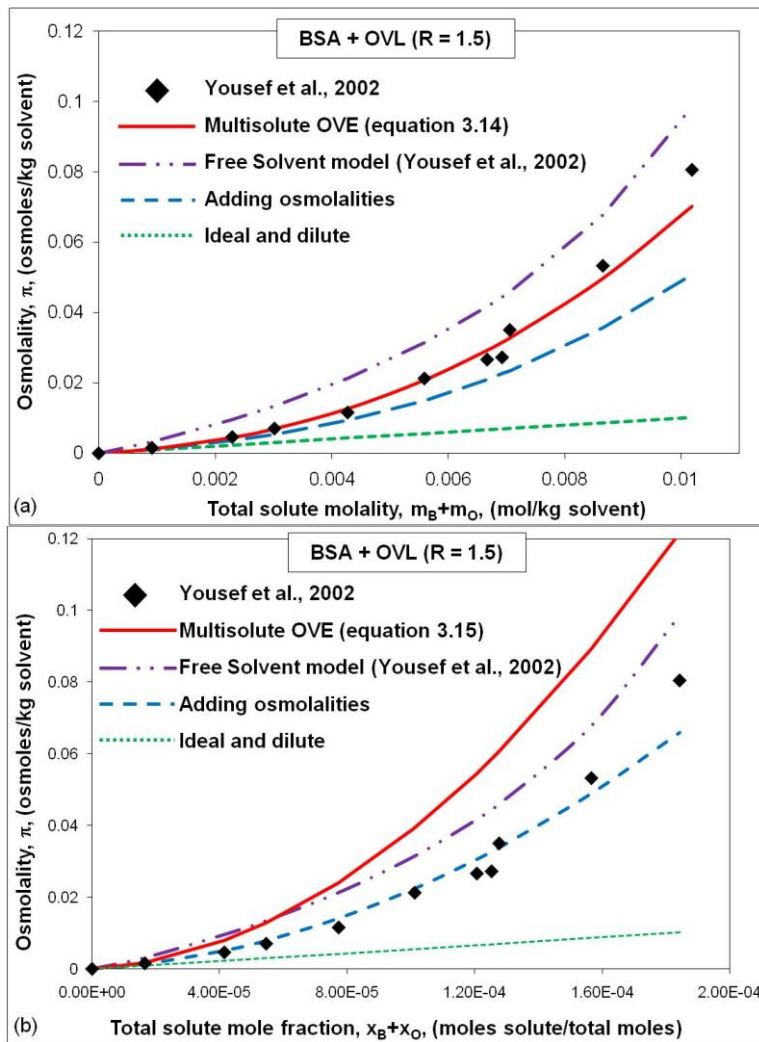


**Figure 3.3.** Osmolality of a BSA + OVL + water solution as a function of (a) total solute molality and (b) total solute mole fraction for  $R = 1.5$ , where  $R = \text{mass BSA}/\text{mass OVL}$ . The diamonds are experimental measurements from Yousef et al. [49]. The solid line is the prediction from the multisolute osmotic virial equation (equation (3.14) or equation (3.15)). The long-dashed line is the prediction from adding osmolalities and the short-dashed line is the prediction from assuming an ideal, dilute solution. The long-and-short-dashed line is a model from the literature [49].

## **Chapter 4 - Multisolute osmotic virial equation**

### **for use with electrolytes**

#### **4.1. Introduction**

The osmolality as a function of concentration of multisolute solutions containing electrolytes is of great importance in many areas of biology, including cryopreservation. Electrolytes are ubiquitous in biological solutions and are often in solution with other solutes, such as macromolecules or CPAs. One of the predominant intracellular solutes is potassium chloride (KCl) and sodium chloride (NaCl) is found in many extracellular solutions, both *in vivo* (plasma) and *ex vivo* (phosphate buffered saline solutions). The solution behaviour of these complicated multisolute solutions plays a role in the cellular response to the extracellular environment.

In order to extend the application of the osmotic virial equation (OVE) to electrolyte solutions, an additional fitting constant in the single-solute OVE, called the dissociation constant, is used to capture the complicated behaviour of single-solute electrolyte solutions. It can be argued that the single-solute OVE approach should not be used to describe the solution behaviour of electrolytes since: (i) the dissociation constant should not be less than two for strong 1:1 electrolytes such as NaCl or KCl, and (ii) a constant cannot capture the complicated electrolyte solution behaviour and an actual electrolyte solution theory, such the Pitzer-Debye-Huckel equations [25; 26], should be used.

There has been much debate in the literature with respect to the question of complete or partial dissociation of NaCl [12]. Much of the work published on NaCl is based on the assumption of complete dissociation [2; 25; 27; 28]. However, others have shown that by assuming partial dissociation, equations can be developed that quantitatively explain the behaviour of aqueous NaCl solutions [13; 14]. Large amounts of experimental data on the densities of aqueous NaCl solutions have been shown to agree with the equations developed using the assumption of partial dissociation [14]. The dissociation constant has also been shown to be dependent on electrolyte concentration, reaching complete dissociation only at infinite dilution [24]. Using osmotic coefficient data, the degree of dissociation for aqueous NaCl solutions ranging from 0 to 6.144 mol/kg solvent was determined to vary between 1 (completely dissociated) to less than 0.8 [14].

One of the most well-known electrolyte solution theories, the Pitzer-Debye-Huckel equation for solutions of electrolytes [25; 26], utilizes an ionic-strength-dependent function to capture the electrolyte solution behaviour, as opposed to the OVE approach of using an additional fitting constant. The accuracy of the single-solute OVE and the Pitzer-Debye-Huckel equation for aqueous solutions of NaCl is shown in Figure 2.7. It was demonstrated that both of these approaches accurately capture the behaviour of single-solute aqueous NaCl solutions over a wide concentration range. In Chapter 2 it was shown that the application of the

OVE to electrolyte solutions is straightforward, requiring only two fitting parameters to describe the solution behaviour of NaCl (the dissociation constant,  $k_{diss}$ , and a second virial coefficient,  $B$ ). Alternatively, the Pitzer-Debye-Huckel equations, which endeavour to also capture the solution behaviour of mixtures of electrolytes, contain more complexity. The Pitzer-Debye-Huckel equation has six empirical parameters and multiple functions that are ionic strength dependent [25; 26].

Thus, the objective of this chapter was to demonstrate that, for multisolute solutions containing NaCl and a small non-electrolyte molecule, using the single-solute OVE to capture the electrolyte solution behaviour resulted in predictions that were as accurate as using an electrolyte solution theory to capture the electrolyte solution behaviour. In order to compare predictions of the multisolute solution behaviour, both the single-solute OVE for electrolytes and the Pitzer-Debye-Huckel equation for electrolytes were inserted into the multisolute OVE proposed in Chapter 3. The osmotic virial coefficients used in this chapter for the CPAs (glycerol and DMSO) are listed in Table 2.1. The osmotic virial coefficients used in this chapter for NaCl are listed in Table 2.4<sup>1</sup>.

In addition, this study also investigated the use of the multisolute OVE approach for aqueous solutions of macromolecules and electrolytes. There are many reports of varying ionic strength solutions affecting

---

<sup>1</sup> The values for the NaCl osmotic virial coefficients used in this chapter are the values obtained from fitting the data from Robinson and Stokes data, as this was the data used in the Pitzer *et al.* [26] study to obtain the parameters in the Pitzer-Debye-Huckel equation.

macromolecules in solution [6; 11; 37; 40], which has been attributed to changes in protein folding [41] and changes in the interactions between macromolecules [4; 5; 18; 29; 32; 36]. The system of hydroxyethyl starch (HES) and NaCl in water was used as a model to show how the multisolute OVE proposed in Chapter 3 can be utilized to capture the changing macromolecular solution behaviour in salt solutions. HES was chosen as the model macromolecule because it is an important solute in many biological applications, present in plasma expanders [3; 19] and cryopreservation solutions [3; 34; 35], among others.

#### 4.2. Overview of multisolute solute solution theories for aqueous CPA + electrolyte solutions:

Various methods have been proposed to predict solution behaviour of aqueous solutions containing CPAs and electrolytes. As outlined in Chapter 3, many of these approaches require either (i) fitting of multisolute data to obtain empirical parameters [9; 10; 21; 22; 23; 38; 39] or (ii) simplifying assumptions regarding the interactions between solute molecules [17]. Recently, Kleinhans and Mazur investigated the use of the adding-osmolalities approach for several aqueous solutions containing a CPA and NaCl. The predictions from this approach were accurate for the specific concentration ranges and solutions they studied. However, this approach is not accurate for increasingly non-ideal solutions (see Figures 3.1 - 3.3).

The form of the multisolute OVE proposed in Chapter 3 addresses the limitations of the previous multisolute solution theories that have been applied in cryobiology. This form of the multisolute osmotic virial equation, with mixing rules that were derived from first principles, is a solution theory derived from thermodynamic principles that takes into account solute-solute interactions and allows predictions of multisolute solutions without the need to fit multisolute data.

The form of the multisolute osmotic virial equation proposed in Chapter 3 is:

$$\pi = \sum_i m_i + \sum_i \sum_j \frac{(B_i + B_j)}{2} m_i m_j + \sum_i \sum_j \sum_k (C_i C_j C_k)^{1/3} m_i m_j m_k \quad (3.4)$$

where the subscripts  $i, j, k$  refer to the individual solutes.

For electrolytes, the molality of the electrolyte is multiplied by the dissociation constant throughout equation (3.4). Equation (3.4) can be used to predict multisolute solution behaviour based only on the single-solute osmotic virial coefficients ( $B_i, C_i$ ).

Written for an aqueous solution containing one electrolyte solute (subscript 2) and one non-electrolyte solute (subscript 3), equation (3.4) is:

$$\begin{aligned} \pi = & k_{diss} m_2 + m_3 + B_2 (k_{diss} m_2)^2 + B_3 m_3^2 + (B_2 + B_3) k_{diss} m_2 m_3 \\ & + C_2 (k_{diss} m_2)^3 + C_3 m_3^3 + (C_2^2 C_3)^{1/3} (k_{diss} m_2)^2 m_3 + (C_2 C_3^2)^{1/3} k_{diss} m_2 m_3^2 \end{aligned} \quad (4.1)$$

(The subscript 1 is usually reserved for the solvent, water).

For small molecules, such as many CPAs and electrolytes, a third virial coefficient is not typically required to describe the single-solute

solution behaviour, so the cubic terms in equation (4.1) may be set to zero, giving:

$$\pi = k_{diss} m_2 + m_3 + B_2 (k_{diss} m_2)^2 + B_3 m_3^2 + (B_2 + B_3) k_{diss} m_2 m_3 \quad (4.2)$$

However, macromolecules often require a third virial coefficient to describe the non-ideality of their solution behaviour. Thus, solutions containing a macromolecule and electrolyte will contain the  $C_3 c_3^3$  term, but the cubic mixing terms will still be equal to zero (provided the electrolyte does not have a third virial coefficient):

$$\pi = k_{diss} m_2 + m_3 + B_2 (k_{diss} m_2)^2 + B_3 m_3^2 + (B_2 + B_3) k_{diss} m_2 m_3 + C_3 m_3^3 \quad (4.3)$$

The multisolute OVE can be used to make predictions of a wide range of combinations of solutes using only single-solute information. Equation (4.2) was used to predict the solution behaviour of a multisolute aqueous solution containing an electrolyte and a small molecule. Equation (4.3) was used for aqueous solutions containing an electrolyte and a macromolecule.

#### 4.2.1. *Combination of the OVE with the Pitzer-Debye-Huckel equation:*

In equations (4.1) to (4.3), the contribution of the electrolyte to the multisolute solution osmolality is predicted using the osmotic virial coefficients determined from fitting single-solute electrolyte solution data. However it can be argued that the predictions from the multisolute OVE for

the solution behaviour of an aqueous solution containing an electrolyte and a non-electrolyte could be improved by replacing the single-solute OVE approach with an electrolyte solution theory, such as the Pitzer-Debye-Huckel equation, to capture the electrolyte solution behaviour. The purpose of this study was to compare the predictions from the multisolute OVE of the osmolality of aqueous multisolute solutions containing NaCl with a CPA, using either the OVE or the Pitzer-Debye-Huckel solution theory to capture the electrolyte solution behaviour.

To make predictions of aqueous multisolute solutions containing an electrolyte and a CPA, the Pitzer-Debye-Huckel electrolyte solution theory was used to calculate the contribution to the total solution osmolality from the electrolyte and the multisolute OVE was used to calculate the contribution from the non-electrolyte solute and also the contribution from the interactions between the two different solutes. In order to accomplish this, the virial coefficients from the Pitzer-Debye-Huckel equation were made equivalent to the osmotic virial coefficients in the multisolute OVE so that they could be used in the multisolute OVE mixing rule.

In the single-solute OVE for electrolytes, equation (2.3), it can be seen that the molality of the electrolyte is always multiplied by the electrolyte effects parameter ( $k_{diss}$ ). In the Pitzer-Debye-Huckel equation for a single electrolyte in solution, equation (2.7), it can be seen that the electrolyte effects function,  $2(f^\Phi + 1)$ , only appears in the linear term. Comparing the

quadratic terms of the Pitzer-Debye-Huckel equation (2.7) and the OVE (2.3) for a single electrolyte solute shows:

$$2B_{MX}^{\Phi} = B_i k_{diss}^2 \quad (4.4)$$

Looking at the linear terms:

$$k_{diss} = 2(f^{\Phi} + 1) \quad (4.5)$$

Combining equations (4.4) and (4.5) gives

$$B_i = \frac{2B_{MX}^{\Phi}}{[2(f^{\Phi} + 1)]^2} \quad (4.6)$$

Thus, the mixing rule for the osmotic virial equation becomes:

$$B_{23} = \frac{\left( B_2 + \frac{2B_{MX}^{\Phi}}{[2(f^{\Phi} + 1)]^2} \right)}{2} \quad (4.7)$$

Using equation (4.7) with the multisolute OVE, equation (4.3), and using the Pitzer-Debye-Huckel equation for the electrolyte contribution to the osmolality gives:

$$\begin{aligned} \pi = & [2(f^{\Phi} + 1)]m_2 + m_3 + 2B_{MX}^{\Phi}m_2^2 + B_3m_3^2 \\ & + \left( B_2 + \frac{2B_{MX}^{\Phi}}{[2(f^{\Phi} + 1)]^2} \right) [2(f^{\Phi} + 1)]m_2m_3 + C_3m_3^3 \end{aligned} \quad (4.8)$$

Equation (4.8) was compared to equation (4.3) (or equation (4.2) if  $C_3 = 0$ ) to determine if using an electrolyte solution theory (the Pitzer-Debye-Huckel equation) to determine the electrolyte contribution to the osmolality of a multisolute solution was more accurate than using the OVE to determine the electrolyte contribution to the total solution osmolality. In both equations the multisolute OVE was used to determine the contribution from the non-electrolyte solute and the mixing rule for the multisolute OVE shown in Chapter 3 was used to determine the contribution from the interactions between the electrolyte and non-electrolyte solute. Equation (4.8) will be referred to herein as the PDH-OVE approach and equation (4.2) is referred to as the multisolute OVE approach.

#### 4.3. Using the multisolute OVE to investigate electrolyte effects on macromolecule solution behaviour

All of the work presented previously on this form of the multisolute OVE, equation (3.4), has been using information from single solutes to make predictions of multisolute solution behaviour (Chapter 3 and [1; 8; 20; 30; 31; 38]). However, in some cases only multisolute solution data is available. For example, most macromolecule solution behaviour is measured in varying ionic strength solutions [6; 16; 37; 40]. The ionic strength of a solution may have a marked effect on macromolecule solution behaviour [11; 37; 41]. In order to study the effect of salt

concentration on the solution behaviour of a macromolecule, the osmotic virial approach was adapted to use the multisolute OVE, equation (4.3) to determine single-solute osmotic virial coefficients in a range of different salt solutions. The osmotic virial coefficients of a macromolecule in varying salt concentrations were determined and assessed as a function of salt concentration. To determine the single-solute osmotic virial coefficients, the multisolute OVE was rearranged such that the quantities that were known were on the left hand side of the equation and the unknown quantities on the right hand side of the equation. Rearranging equation (4.3) for an aqueous solution of a macromolecule and electrolyte (where the molality of both solutes and the osmotic virial coefficients of the electrolyte are known) gives:

$$\pi - k_{diss}m_2 - m_3 - B_2(k_{diss}m_2)^2 - B_2k_{diss}m_2m_3 = B_3[m_3^2 + k_{diss}m_2m_3] + C_3m_3^3 \quad (4.9)$$

The osmotic virial coefficients of the macromolecule,  $B_3$  and  $C_3$ , were determined by fitting equation (4.9) to multisolute osmolality as a function of concentration data using linear regression. This was done in a range of salt concentrations to determine  $B_3$  and  $C_3$  as a function of salt concentration.

#### 4.4. Materials and methods

##### 4.4.1. *Fitting the OVE to data*

The osmotic virial coefficients for use with solute concentration in molality were determined for each CPA or electrolyte by fitting the single-solute OVE, equation (2.3), to the single-solute data. The details of the fitting procedure are outlined in Chapter 2.

The multisolute solution data for aqueous solutions of HES and NaCl was obtained from the literature [16]. The freezing point as a function of total solute concentration was measured for various R-values of HES in NaCl using differential scanning calorimetry (DSC), where R is the mass ratio of HES to NaCl ( $R = \text{mass HES} / \text{mass NaCl}$ ). For cryobiological applications, mass ratios (or R-values) are often chosen to express the solution composition since as the solution freezes, pure water is removed as ice, so the solutes become concentrated, but the mass ratio of the two solutes remains constant. Jochem and Korber measured the phase diagrams for HES and NaCl in water for R-values ranging from 0.5 to 20 [16].

In order to determine the osmotic virial coefficients for HES in the different salt solutions, linear regression was performed using Excel (Microsoft, Redmond, WA, USA) using the matrix method for linear regression [7]. The confidence intervals were also calculated at various levels of significance. A detailed description of the linear regression procedure utilized to obtain the osmotic virial coefficients and the

statistical analysis done on the coefficients is described in Chapter 2. Table 4.1 shows the matrices that were used for the linear regression.

#### 4.5. Results

##### 4.5.1. CPA + NaCl + water solutions

The multisolute OVE for an electrolyte and small molecule, equation (4.2), and the PDH-OVE approach, equation (4.8), were both used to predict the solution behaviour of a CPA and NaCl in water. Two different CPAs were chosen, DMSO and glycerol, and a range of R-values for each multisolute solution studied. The results for DMSO + NaCl + water can be found in Figure 4.1 (a-h), for R values ranging from 0.2 to 19.0. The results for glycerol + NaCl + water can be found in Figure 4.2 (a-g) for R-values ranging from 0.25 to 9.0. In addition to the OVE approach and the PDH-OVE approach, two other predictions are also shown in the figures. The solution behaviour of the CPA + NaCl in water solutions was also predicted by adding the osmolalities of the single-solute solutions, which requires the same amount of information as the multisolute OVE, equation (4.2), but neglects the mixing term.

$$\pi = k_{diss}m_2 + m_3 + B_2(k_{diss}m_2)^2 + B_3m_3^2 \quad (4.10)$$

This approach is equivalent to the Kleinhans and Mazur approach of adding freezing point depressions [17]. In Figures 4.1 and 4.2, single-solute osmotic virial coefficients from Chapter 2 were utilized in the

adding-osmolalities predictions, not the Kleinhans and Mazur coefficients. Thus, the predictions from the adding-osmolalities approach and the multisolute OVE approach utilize the same coefficients.

The fourth prediction shown in Figures 4.1 and 4.2 was obtained by assuming that the mixtures of CPA and NaCl are ideal, dilute solutions. This approach assumes that none of the solute molecules are interacting with each other (i.e. all of the virial coefficients are equal to zero) and thus the osmolality is equal to the sum of the solute molalities. The dissociation constant for the electrolyte is still taken into account. Thus, the ideal, dilute solution osmolality is given by:

$$\pi = k_{diss}m_2 + m_3 \quad (4.11)$$

The error in the predictions was quantified by calculating the percent error at the maximum solute molality and the sum of squared errors (SSE) over the entire concentration range. The percent error was calculated using equation (3.16) and the sum of squared errors (SSE) was calculated using equation (2.11). As mentioned in Chapter 3, the SSE depends on the number of data points and each multisolute solution has a different number of data points, the SSE values should only be compared for the different predictions of each multisolute solution and not amongst the various multisolute solutions.

The percent errors at the maximum solute molality and the SSE for the four predictive multisolute solution theories are listed in Table 4.2.

The results in Table 4.2 demonstrate that the multisolute OVE and the PDH-OVE methods typically resulted in more accurate predictions than the practice of adding osmolalities or assuming an ideal, dilute solution. The only exception was that the practice of adding osmolalities was the most accurate for the glycerol + NaCl + water solutions containing high concentrations of glycerol. However, the discrepancy between the measured values and the predictions from the multisolute OVE for solutions containing high concentrations of glycerol could be due to difficulties in accurately measuring the freezing point of highly viscous solutions.

#### *4.5.2. HES + NaCl + water solutions*

The HES + NaCl + water phase diagrams from the literature [16] are shown in Figure 4.3. The lines on the graph show the fit to each phase diagram to obtain the HES osmotic virial coefficients for each R-value. The HES coefficients obtained by fitting the phase diagrams are listed in Table 4.3. The values for the HES second and third osmotic virial coefficients, B and C respectively, were graphed as a function of the R-value (Figure 4.4).

The confidence intervals at varying levels of confidence were determined for each osmotic virial coefficient using the methods outlined in Chapter 3. The levels of confidence ( $1-\alpha$ ) were set at  $\alpha = 0.05$ ,  $0.0275$ , and  $0.01$ . For all of the R-values except for the  $R = 0.5$  solution, the

confidence interval bands at all levels of confidence followed the same trend as the actual data points. The 95 % confidence intervals (i.e.  $\alpha = 0.05$ ) are shown on Figure 4.4 and listed in Table 4.3. As they were very close to the data points, the confidence interval bands for the  $C_{\text{HES}}$ -values cannot always be clearly seen on the graph.

For the  $R = 0.5$  solution, the confidence interval bands for the osmotic virial coefficients did not follow the same trend as the actual data points at the different levels of confidence. For example, the  $B_{\text{HES}}$  coefficient for the  $R = 0.5$  solution is less than the  $B_{\text{HES}}$  coefficient for the  $R = 1.0$  solution. However, for the 95 % confidence intervals, the upper confidence limit of the  $B_{\text{HES}}$ -value for  $R = 0.5$  was essentially equal to the upper confidence limit of the  $B_{\text{HES}}$ -value for  $R = 1.0$ . For the 97.5 % and 99 % confidence intervals, the upper confidence limit of the  $B_{\text{HES}}$ -value for  $R = 0.5$  was greater than the upper confidence limit for the  $R = 1.0$ . Also, at the 99% confidence level, the lower confidence limit for the  $C_{\text{HES}}$ -value at  $R = 0.5$  was less than the lower confidence limit for the  $C_{\text{HES}}$ -value at  $R = 1.0$ , even though the  $C_{\text{HES}}$  at  $R = 0.5$  solution was greater than the  $C_{\text{HES}}$  for the  $R = 1.0$  solution. The difference between the trends in the data points and in the confidence intervals made it difficult to determine an optimal function to fit to the data when the  $R = 0.5$  coefficient was included.

In addition, the  $R = 0.5$  solution contained twice as much NaCl as HES on a mass basis (or  $1.54 \times 10^4$  times as much on a mole basis). Thus, this solution was most likely dominated by the NaCl solution behaviour,

making it difficult to obtain accurate HES parameters. For these reasons, the  $R = 0.5$  osmotic virial coefficients were not included in the subsequent analysis to determine a relationship between the osmotic virial coefficients and the R-value.

To provide an empirical equation for each of the HES osmotic virial coefficients as a function of R-value, functions of the following forms were fit to the data:

$$B_{HES} \left( molal^{-1} \right) = \frac{1}{aR} \exp \left[ -b(\ln(R) - c)^2 \right] + d \quad (4.12)$$

$$C_{HES} \left( molal^{-2} \right) = fR^g + h \quad (4.13)$$

where  $a = 0.460$ ,  $b = 0.946$ ,  $c = 1.575$ ,  $d = -0.537$ ,  $f = 1.078 \times 10^3$ ,  $g = -3.334$ , and  $h = 2.957 \times 10^2$ .

For aqueous solutions of HES in NaCl, the HES osmotic virial coefficients can be calculated at any R-value using equations (4.12) and (4.13). These equations were used to calculate the osmotic virial coefficients for  $R = 1, 2, 5, 10,$  and  $20$  (see Table 4.4). The calculated coefficients were then used to predict the measured phase diagrams (Figure 4.5).

#### 4.6. Discussion

Predictions of the solution behaviour for aqueous multisolite solutions containing an electrolyte and a small non-electrolyte were made using four different predictive multisolite solution theories that do not require fitting of multisolite solution data. The multisolite solution theories utilized were: (i)

ideal, dilute solution theory, (ii) the practice of adding osmolalities, (iii) the multisolute OVE using the single-solute osmotic virial coefficients to capture the electrolyte solution behaviour, and (iv) the multisolute OVE using the Pitzer-Debye-Huckel equation [25; 26] to capture the electrolyte solution behaviour (PDH-OVE). In both of the multisolute OVE approaches, the solution behaviour of the non-electrolyte was captured using the single-solute osmotic virial coefficients and the interactions between the two different solutes were captured using a mixing rule for the multisolute OVE proposed in Chapter 3.

For aqueous solutions containing a commonly used CPA (DMSO or glycerol) plus NaCl, the predictions from the multisolute OVE using the coefficients from the single-solute OVE to capture the electrolyte solution behaviour worked as well as using the Pitzer-Debye-Huckel equation to capture the electrolyte solution behaviour (Figures 4.1 and 4.2, Table 4.2). However, the OVE approach was much simpler to use, having only one additional fitting constant ( $k_{diss}$ ) versus the Pitzer-Debye-Huckel function ( $2(f^\Phi + 1)$ ), which contains the Debye-Huckel slope ( $A^\Phi$ ), an empirical parameter ( $b$ ), and the ionic strength of the solution ( $I$ ). In addition, the osmotic virial coefficients for the electrolyte are constants, whereas in the Pitzer-Debye-Huckel equation, the second virial coefficient ( $B_{MX}^\Phi$ ) is also a function of ionic strength and is calculated using three additional empirical constants ( $\beta_{MX}^{(0)}$ ,  $\beta_{MX}^{(1)}$ , and  $\alpha$ ). The multisolute OVE was shown to be an accurate predictive solution theory for multisolute solutions containing

one electrolyte, except in the glycerol + NaCl system at high glycerol concentrations. However, due to the increased complexity of solutions containing more than one electrolyte, it is not known if the multisolute OVE would accurately predict the solution behaviour of those complicated solutions. The Pitzer-Debye-Huckel equation has been shown to be accurate for mixtures of electrolytes [25].

In addition, in Chapter 3 it was shown that the multisolute OVE approach is typically more accurate than adding osmolalities or assuming the solutions are ideal and dilute. The adding-osmolalities approach did provide accurate predictions for some solutions [17], but should not be used once the solutions become increasingly non-ideal (Figures 3.1 - 3.3). This is due to the fact that the adding-osmolalities approach does not take into account the interactions between the different types of solute molecules (i.e. between the electrolyte and the CPA) and these interactions become increasingly important as the concentration increases. The multisolute OVE predictions for the glycerol + NaCl + water solutions were not as accurate as the predictions from the adding-osmolalities approach, but this may be due to difficulties in measuring the freezing point of increasingly viscous glycerol solutions.

Additionally, the use of the multisolute OVE approach was investigated for aqueous solutions of a macromolecule (HES) plus an electrolyte (NaCl) to determine if the multisolute OVE could be used to capture the changing macromolecular solution behaviour in varying

concentrations of electrolytes. The aqueous HES + NaCl system was chosen as a model since it plays an important role in biology [3; 19; 34; 35]. The multisolute OVE was rearranged so that the single-solute HES osmotic virial coefficients could be obtained from multisolute solution data. Phase diagrams for different mass ratios of HES to NaCl in water ( $R = 0.5, 1, 2, 5, 10$  and  $20$ ) were obtained from the literature [16] and the coefficients for HES obtained for all of the  $R$ -values (Figure 4.3 and Table 4.3). From the phase diagrams with different compositions of HES and NaCl, it can be seen that the varying salt concentration plays a role in the HES solution behaviour. The dependence of the HES osmotic virial coefficients on the salt concentration was determined by plotting the HES osmotic virial coefficients as a function of  $R$ -value and fitting a function to the data (Figure 4.4 and Table 4.4). Empirical equations obtained by fitting the HES osmotic virial coefficient values, equations (4.12) and (4.13), can be used to calculate the osmotic virial coefficients for HES in other concentrations of salt solutions. The calculated coefficients were used to predict the HES + NaCl + water solution behaviour (Figure 4.5). This study demonstrated that the multisolute OVE approach is a simple method to capture the changing macromolecular solution behaviour in different concentrations of aqueous salt solutions.

Similar work using the virial coefficients to investigate how the solution behaviour of a macromolecule is affected by electrolytes has been done on aqueous solutions of lysozyme + NaCl [18]. In that study the virial

coefficients were calculated from predictions of the potential mean force between two lysozyme proteins in solutions with varying ionic strength and pH, and the predictions compared with experimental measurements. A dependence of the second virial coefficient on NaCl concentration was observed. As the NaCl concentration increased from approximately 0.2 molar to 1.75 molar, the second virial coefficient of lysozyme decreased from approximately  $3 \times 10^4$  mL/mol/g<sup>2</sup> to  $-8 \times 10^4$  mL/mol/g<sup>2</sup>. Although the dependence on salt concentration does not follow the same trend as was observed with HES in this study, there is still a marked dependence of the lysozyme solution behaviour on the salt concentration. The differences in the behaviour of the macromolecules with changes in salt concentration may be due to differences in the structure and composition of the macromolecules: HES is a starch and lysozyme is a globular protein. As the experimental data for the lysozyme + NaCl solutions consisted of only one data point for each NaCl concentration, the multisolute OVE could not be fit to the data to obtain the lysozyme osmotic virial coefficients.

There is other evidence of salts affecting macromolecule solution behaviour [6; 11; 37; 40]. Unfortunately, in each of these studies it was either not entirely clear how the osmolality and final solution composition were measured or the osmolality of the solutions were only measured for one concentration of electrolyte. Thus, the same type of analysis as was done with HES + NaCl + water data in this study could not be done on those data sets.

The form of the multisolute OVE proposed in Chapter 3, utilizing mixing rules derived from thermodynamic principles, requires only single-solute information to make predictions of multisolute solution behaviour. The application of the OVE to biological solutions is extremely attractive due to the wide range of solutes of interest and the seemingly limitless combinations of these solutes. It has been shown to be accurate for a wide range of multisolute solutions, from two small molecules, a protein and an ideal solute, two proteins, and now for solutions containing electrolytes.

#### 4.7. References

- [1] A. Abazari, J.A.W. Elliott, G.K. Law, L.E. McGann, and N.M. Jomha, A Biomechanical Triphasic Approach to the Transport of Nondilute Solutions in Articular Cartilage. *Biophysical Journal* (Accepted) (2009).
- [2] D.G. Archer, Thermodynamic properties of the NaCl+H<sub>2</sub>O system. 2. Thermodynamic properties of NaCl (aq), NaCl.2H<sub>2</sub>O (cr), and phase equilibria. *Journal of Physical and Chemical Reference Data* 21 (1992) 793-829.
- [3] W. Banks, C.T. Greenwood, and D.D. Muir, Studies on hydroxyethyl starch. 1. Review of chemistry of hydroxyethyl starch, with reference to its use as a blood-plasma volume expander. *Starke* 24 (1972) 181-187.
- [4] F. Bonnete, S. Finet, and A. Tardieu, Second virial coefficient: variations with lysozyme crystallization conditions. *Journal of Crystal Growth* 196 (1999) 403-414.
- [5] R.A. Curtis, J. Ulrich, A. Montaser, J.M. Prausnitz, and H.W. Blanch, Protein-protein interactions in concentrated electrolyte solutions - Hofmeister-series effects. *Biotechnology and Bioengineering* 79 (2002) 367-380.
- [6] D.A.T. Dick, An Approach to the Molecular Structure of the Living Cell by Water Flux Studies. in: E.B. Reeve, and A.C. Guyton, (Eds.),

Physical Bases of Circulatory Transport: Regulation and Exchange,  
W.B. Saunders Company, Philadelphia, 1967, pp. 217-234.

- [7] N.R. Draper, Applied Regression Analysis, John Wiley & Sons, Inc.,  
New York, 1998.
- [8] H.Y. Elmoazzen, J.A.W. Elliott, and L.E. McGann, Osmotic Transport  
across Cell Membranes in Nondilute Solutions: A New Nondilute  
Solute Transport Equation. *Biophysical Journal* 96 (2009) 2559-  
2571.
- [9] G.M. Fahy, Analysis of Solution Effects Injury Equations for Calculating  
Phase-Diagram Information for the Ternary-Systems NaCl-  
Dimethylsulfoxide-Water and NaCl-Glycerol-Water. *Biophysical  
Journal* 32 (1980) 837-850.
- [10] G.M. Fahy, Simplified Calculation of Cell Water-Content During  
Freezing and Thawing in Nonideal Solutions of Cryoprotective  
Agents and Its Possible Application to the Study of Solution Effects  
Injury. *Cryobiology* 18 (1981) 473-482.
- [11] G.D. Fullerton, K.M. Kanal, and I.L. Cameron, Osmotically  
unresponsive water fraction on proteins: Non-ideal osmotic  
pressure of bovine serum albumin as a function of pH and salt  
concentration. *Cell Biology International* 30 (2006) 86-92.
- [12] R. Heyrovska, A Reappraisal of Arrhenius' Theory of Partial  
Dissociation of Electrolytes. in: J.T. Stock, and M.V. Orna, (Eds.),

Electrochemistry, past and present, ACS symposium series.,  
American Chemical Society, Washington, DC, 1989, pp. 75-91.

- [13] R. Heyrovská, Physical electrochemistry of strong electrolytes based on partial dissociation and hydration - Quantitative interpretation of the thermodynamic properties of NaCl(aq) from "zero to saturation". Journal of the Electrochemical Society 143 (1996) 1789-1793.
- [14] R. Heyrovská, Equations for Densities and Dissociation Constant of NaCl(aq) at 25[degree]C from "Zero to Saturation" Based on Partial Dissociation. Journal of the Electrochemical Society 144 (1997) 2380-2384.
- [15] W.H. Hildebrandt, Low temperature quantitative phase equilibria and glass formation in the H<sub>2</sub>O-NaCl-DMSO system, Duke University, 1975., 1975, pp. vi, 180 leaves.
- [16] M. Jochem, and C. Körber, Extended phase diagrams for the ternary solutions H<sub>2</sub>O-NaCl-glycerol and H<sub>2</sub>O-NaCl-hydroxyethylstarch (HES) determined by DSC. Cryobiology 24 (1987) 548-548.
- [17] F.W. Kleinhans, and P. Mazur, Comparison of actual vs. synthesized ternary phase diagrams for solutes of cryobiological interest. Cryobiology 54 (2007) 212-222.
- [18] E.R.A. Lima, E.C. Biscaia, M. Bostrom, F.W. Tavares, and J.M. Prausnitz, Osmotic second virial coefficients and phase diagrams for aqueous proteins from a much-improved Poisson-Boltzmann

- equation. *Journal of Physical Chemistry C* 111 (2007) 16055-16059.
- [19] N.M. Matharu, L.M. Butler, G.E. Rainger, P. Gosling, R.K. Vohra, and G.B. Nash, Mechanisms of the anti-inflammatory effects of hydroxyethyl starch demonstrated in a flow-based model of neutrophil recruitment by endothelial cells. *Critical Care Medicine* 36 (2008) 1536-1542.
- [20] I.N. Mukherjee, Y. Li, Y.C. Song, R.C. Long, and A. Sambanis, Cryoprotectant transport through articular cartilage for long-term storage: experimental and modeling studies. *Osteoarthritis and Cartilage* 16 (2008) 1379-1386.
- [21] D.E. Pegg, Simple Equations for Obtaining Melting-Points and Eutectic Temperatures for the Ternary-System Glycerol Sodium-Chloride Water. *Cryo-Letters* 4 (1983) 259-268.
- [22] D.E. Pegg, Equations for Obtaining Melting-Points and Eutectic Temperatures for the Ternary-System Dimethylsulfoxide Sodium-Chloride Water. *Cryo-Letters* 7 (1986) 387-394.
- [23] D.E. Pegg, and F.G. Arnaud, Equations for Obtaining Melting-Points in the Quaternary System Propane-1,2-Diol Glycerol Sodium-Chloride Water. *Cryo-Letters* 9 (1988) 404-417.
- [24] R.H. Petrucci, and W.S. Harwood, *General Chemistry: Principles and Modern Applications*, Prentice-Hall, Inc., Upper Saddle River, NJ, 1997.

- [25] K.S. Pitzer, Thermodynamics of Electrolytes .1. Theoretical Basis and General Equations. *Journal of Physical Chemistry* 77 (1973) 268-277.
- [26] K.S. Pitzer, and G. Mayorga, Thermodynamics of Electrolytes .2. Activity and Osmotic Coefficients for Strong Electrolytes with One or Both Ions Univalent. *Journal of Physical Chemistry* 77 (1973) 2300-2308.
- [27] K.S. Pitzer, J.C. Peiper, and R.H. Busey, Thermodynamic Properties of Aqueous Sodium-Chloride Solutions. *Journal of Physical and Chemical Reference Data* 13 (1984) 1-102.
- [28] R.A. Robinson, and R.H. Stokes, *Electrolyte solutions : the measurement and interpretation of conductance, chemical potential and diffusion in solutions of simple electrolytes*, Butterworths Scientific Publications, London, England, 1959.
- [29] D.F. Rosenbaum, and C.F. Zukoski, Protein interactions and crystallization. *Journal of Crystal Growth* 169 (1996) 752-758.
- [30] L.U. Ross-Rodriguez, J.A.W. Elliott, and L.E. McGann, Investigating cryoinjury using simulations and experiments: 1. TF-1 cells during the two-step freezing (rapid cooling interrupted with a hold time) procedure. *Cryobiology* (Submitted) (2009).
- [31] L.U. Ross-Rodriguez, J.A.W. Elliott, and L.E. McGann, Investigating cryoinjury using simulations and experiments: 2. TF-1 cells during

the graded freezing (interrupted slow cooling without hold time) procedure. *Cryobiology* (Submitted) (2009).

- [32] A. Salabat, Prediction of liquid-liquid phase diagrams of aqueous salt+PEG systems using a thermodynamic model. *Calphad* 30 (2006) 296-300.
- [33] M.L. Shepard, C.S. Goldston, and F.H. Cocks, H<sub>2</sub>O-NaCl-Glycerol Phase-Diagram and Its Application in Cryobiology. *Cryobiology* 13 (1976) 9-23.
- [34] A. Sputtek, P. Kuhn, and A.W. Rowe, Cryopreservation of erythrocytes, thrombocytes, and lymphocytes. *Transfusion Medicine and Hemotherapy* 34 (2007) 262-267.
- [35] A. Sputtek, G. Singbartl, R. Langer, W. Schleinzner, H.A. Henrich, and P. Kuhn, Cryopreservation of red-blood-cells with the nonpenetrating cryoprotectant hydroxyethyl starch. *Cryo-Letters* 16 (1995) 283-288.
- [36] P.M. Tessier, A.M. Lenhoff, and S.I. Sandler, Rapid measurement of protein osmotic second virial coefficients by self-interaction chromatography. *Biophysical Journal* 82 (2002) 1620-1631.
- [37] V.L. Vilker, C.K. Colton, and K.A. Smith, The Osmotic-Pressure of Concentrated Protein Solutions - Effect of Concentration and Ph in Saline Solutions of Bovine Serum-Albumin. *J Colloid Interface Sci* 79 (1981) 548-566.

- [38] E.J. Woods, A. Bagchi, J.D. Benson, X. Han, and J.K. Critser, Melting point equations for the ternary system water/sodium chloride/ethylene glycol revisited. *Cryobiology* 57 (2008) 336-336.
- [39] E.J. Woods, M.A.J. Zieger, D.Y. Gao, and J.K. Critser, Equations for obtaining melting points for the ternary system ethylene glycol/sodium chloride/water and their application to cryopreservation. *Cryobiology* 38 (1999) 403-407.
- [40] M.A. Yousef, R. Datta, and V.G.J. Rodgers, Confirmation of free solvent model assumptions in predicting the osmotic pressure of concentrated globular proteins. *J Colloid Interface Sci* 243 (2001) 321-325.
- [41] R.J. Zimmerman, K.M. Kanal, J. Sanders, I.L. Cameron, and G.D. Fullerton, Osmotic pressure method to measure salt induced folding/unfolding of bovine serum albumin. *Journal of Biochemical and Biophysical Methods* 30 (1995) 113-131.

**Table 4.1.** Summary of matrices and vectors used for linear regression to obtain HES osmotic virial coefficients.

$\bar{y}$ vector	$\pi - k_{diss}m_2 - m_3 - B_2(k_{diss}m_2)^2 - B_2k_{diss}m_2m_3$
<u>A</u> matrix	First column = $m_3 + k_{diss}m_2$ Second column = $m_3^2$
Conversion of coefficients in $\bar{\beta}$ to osmotic virial coefficients	$\beta_1 = B_3$ $\beta_2 = C_3$ ...

**Table 4.2.** Percent errors and SSE from the predictions from the multisolute solution theories that do not require fitting of multisolute data.

Solutes [R-value]*	Max total solute molality	Ideal, dilute		Adding Osmolalities		Multisolute OVE		PDH-OVE	
		% error at max. molality <sup>†</sup>	SSE <sup>‡</sup>	% error at max. molality <sup>†</sup>	SSE <sup>‡</sup>	% error at max. molality <sup>†</sup>	SSE <sup>‡</sup>	% error at max. molality <sup>†</sup>	SSE <sup>‡</sup>
DMSO + NaCl [R=0.2] [15]	5.1	30.9%	1.3x10 <sup>2</sup>	6.4%	1.3	0.3%	1.2	0.1%	1.2
DMSO + NaCl [R=19.0] [15]	16.1	62.6%	2.1x10 <sup>3</sup>	7.9%	28.8	1.5%	6.2	3.3%	13.6
Glycerol + NaCl [R=0.67] [33]	6.3	28.5%	14.4	6.5%	0.7	1.3%	0.2	2.1%	0.3
Glycerol + NaCl [R=9.0] [33]	17.2	16.1%	23.5	9.9%	5.5	30.5%	52.0	34.4%	68.4

\*R values are the mass ratios:  $R = \frac{\text{Mass of solute 1}}{\text{Mass of solute 2}}$

<sup>†</sup>Percent error calculated using equation (3.16) at the maximum total solute molality at which osmolality was measured for each solution.

<sup>‡</sup>SSE calculated using equation (2.11). The values of the SSE should only be compared for the different predictions for each specific solution, not between solutions.

**Table 4.3.** HES osmotic virial coefficients for varying mass ratios (R) of HES + NaCl + water solutions.

$R = \frac{\text{Mass of HES}}{\text{Mass of NaCl}}$	<b>B</b> molal <sup>-1</sup> [±95% CI†]	<b>C</b> molal <sup>-2</sup> [±95% CI†]
0.5	-0.833 ± 0.638	7.85x10 <sup>4</sup> ± 5.68x10 <sup>4</sup>
1.0	-0.318 ± 0.132	1.11x10 <sup>4</sup> ± 2.42x10 <sup>3</sup>
2.0	-0.027 ± 0.074	1.36x10 <sup>3</sup> ± 3.71x10 <sup>2</sup>
5.0	-0.089 ± 0.079	3.98x10 <sup>2</sup> ± 86.8
10.0	-0.425 ± 0.205	3.54x10 <sup>2</sup> ± 83.8
20.0	-0.515 ± 0.256	1.96x10 <sup>2</sup> ± 45.0

**Table 4.4.** Calculated HES osmotic virial coefficients for mass ratios (R) = 1, 2, 5, 10, and 20 of HES + NaCl + water solutions.

$R = \frac{\text{Mass of HES}}{\text{Mass of NaCl}}$	<b>B</b> molal <sup>-1</sup>	<b>C</b> molal <sup>-2</sup>
1.0	-0.329	1.11x10 <sup>4</sup>
2.0	-0.016	1.36x10 <sup>3</sup>
5.0	-0.103	3.46x10 <sup>2</sup>
10.0	-0.405	3.01x10 <sup>2</sup>
20.0	-0.521	2.96x10 <sup>2</sup>

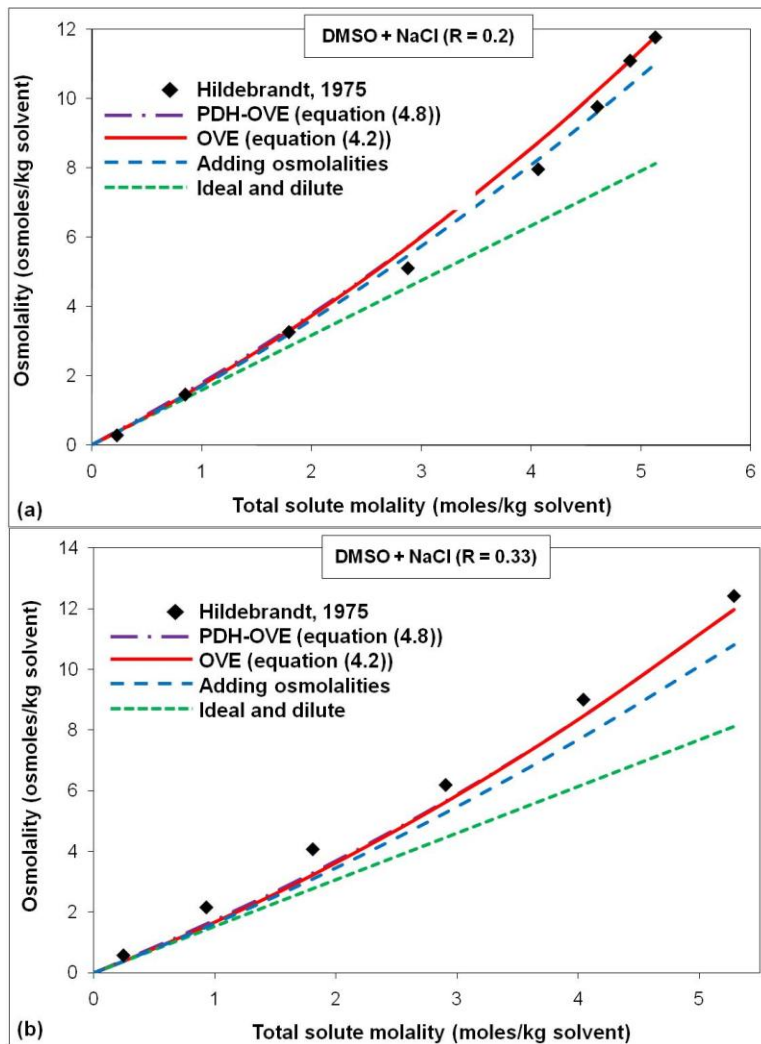


**Figure 4.1 (a-h).** Osmolality as function of total solute molality for DMSO + NaCl + water solutions (R ranging from 0.2 to 19.0). The closed diamonds are data from Hildebrandt [15]. The red solid line is the prediction from the multisolute OVE equation, equation (4.2). The purple long-and-short-dashed line is the prediction from the PDH-OVE equation, equation (4.8), which is lying directly under the red OVE line and cannot be seen. The blue long-dashed line is the prediction from the adding-osmolalities approach, equation (4.10). The green short-dashed line is the prediction from assuming an ideal, dilute solution, equation (4.11).

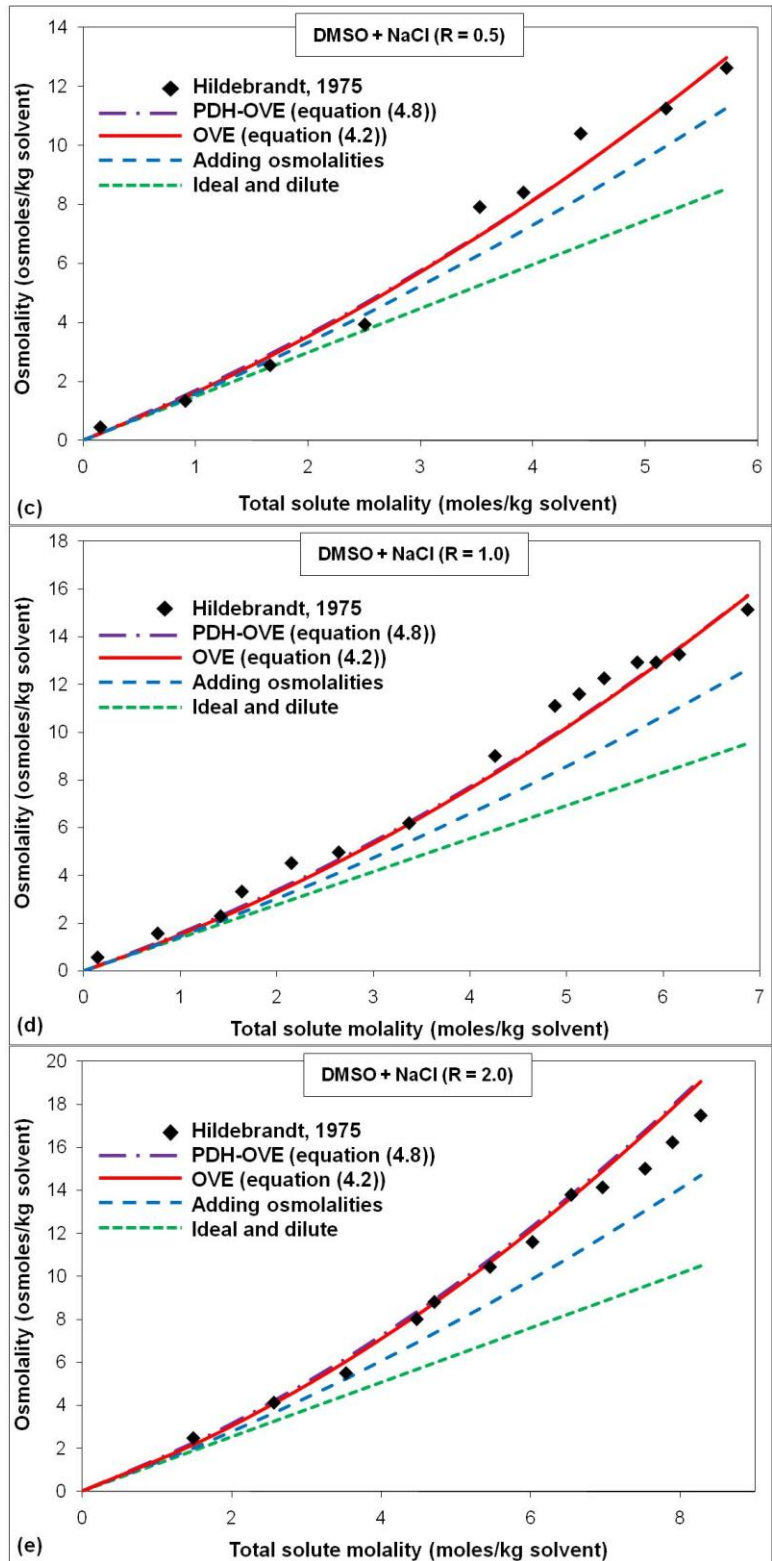


**Figure 4.1** (cont'd). Osmolality as function of total solute molality for DMSO + NaCl + water solutions ( $R$  ranging from 0.2 to 19.0).

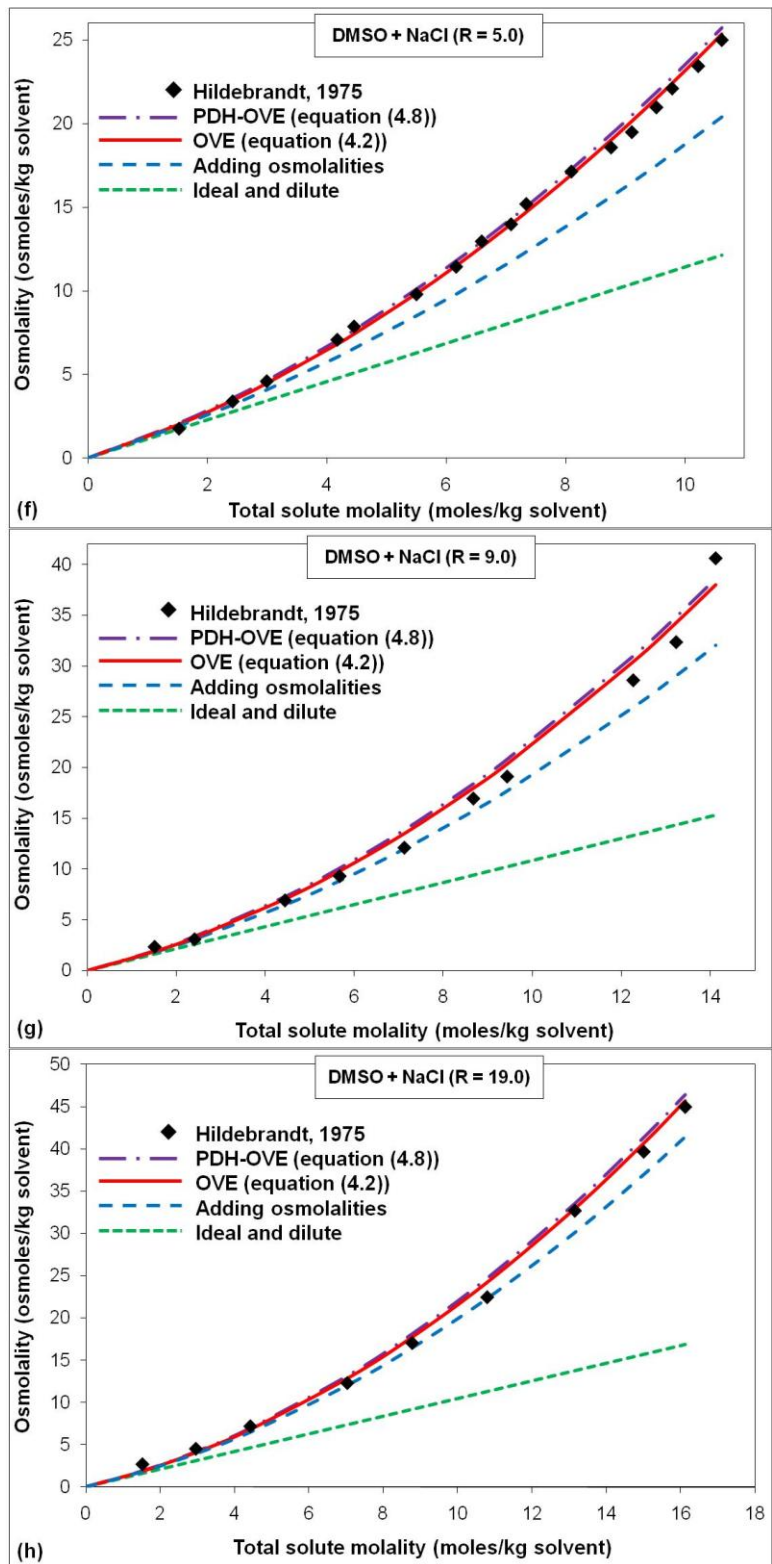


**Figure 4.1 (cont'd).** Osmolality as function of total solute molality for DMSO + NaCl + water solutions (R ranging from 0.2 to 19.0).

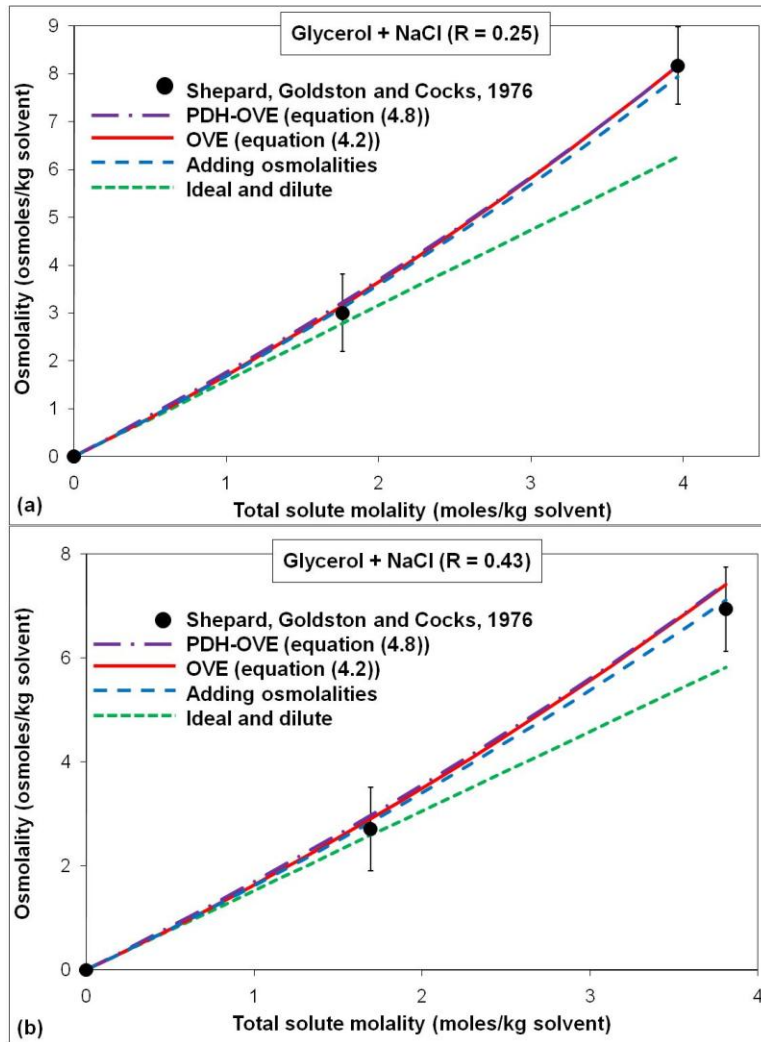


**Figure 4.2 (a-g).** Osmolality as function of total solute molality for glycerol + NaCl + water solutions ( $R$  ranging from 0.25 to 9.0). The closed circles are data from Shepard *et al.* [33]. The red solid line is the prediction from the multisolute OVE equation, equation (4.2). The purple long-and-short-dashed line is the prediction from the PDH-OVE equation, equation (4.8). The blue long-dashed line is the prediction from the adding-osmolalities approach, equation (4.10). The green short-dashed line is the prediction from assuming an ideal, dilute solution, equation (4.11).

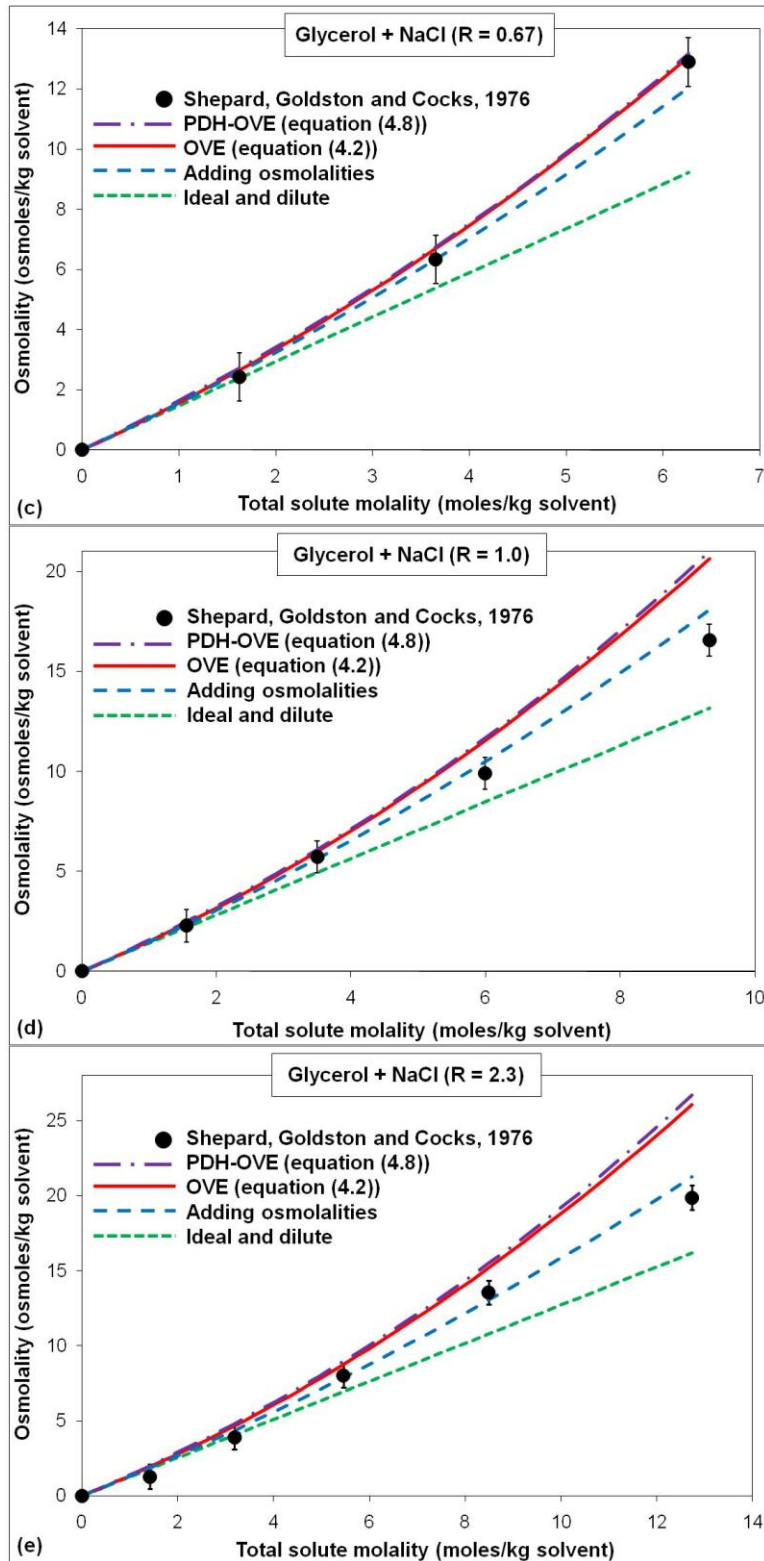


**Figure 4.2 (cont'd).** Osmolality as function of total solute molality for glycerol + NaCl + water solutions (R ranging from 0.25 to 9.0).

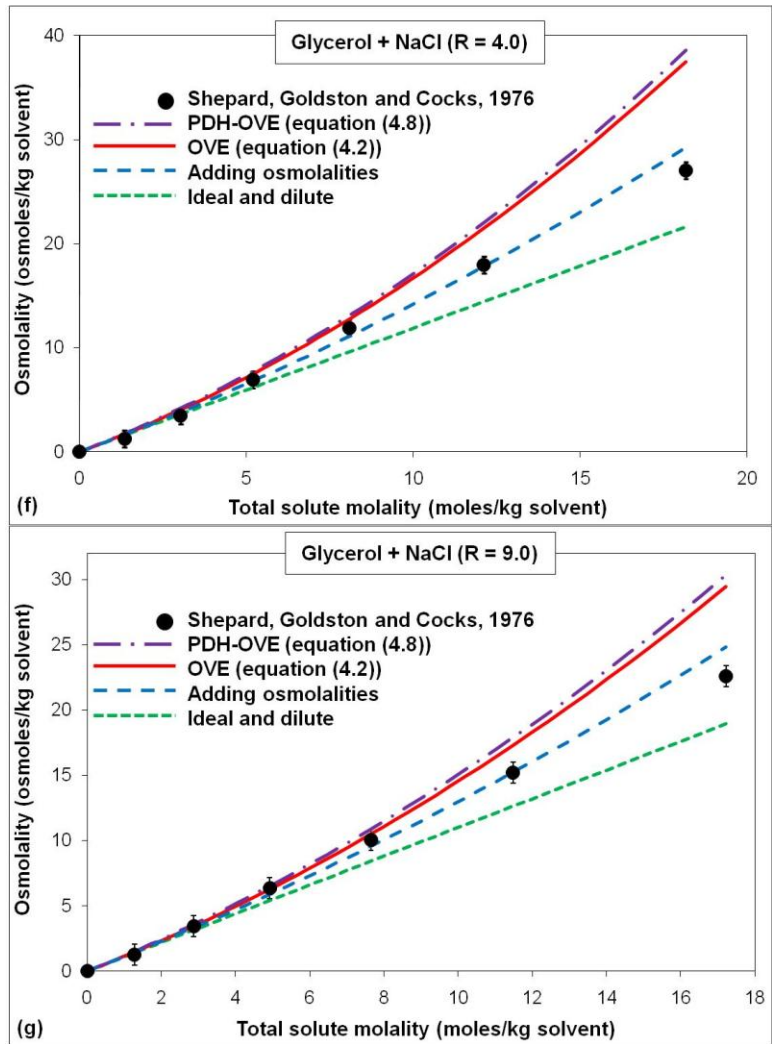


**Figure 4.2 (cont'd).** Osmolality as function of total solute molality for glycerol + NaCl + water solutions (R ranging from 0.25 to 9.0).

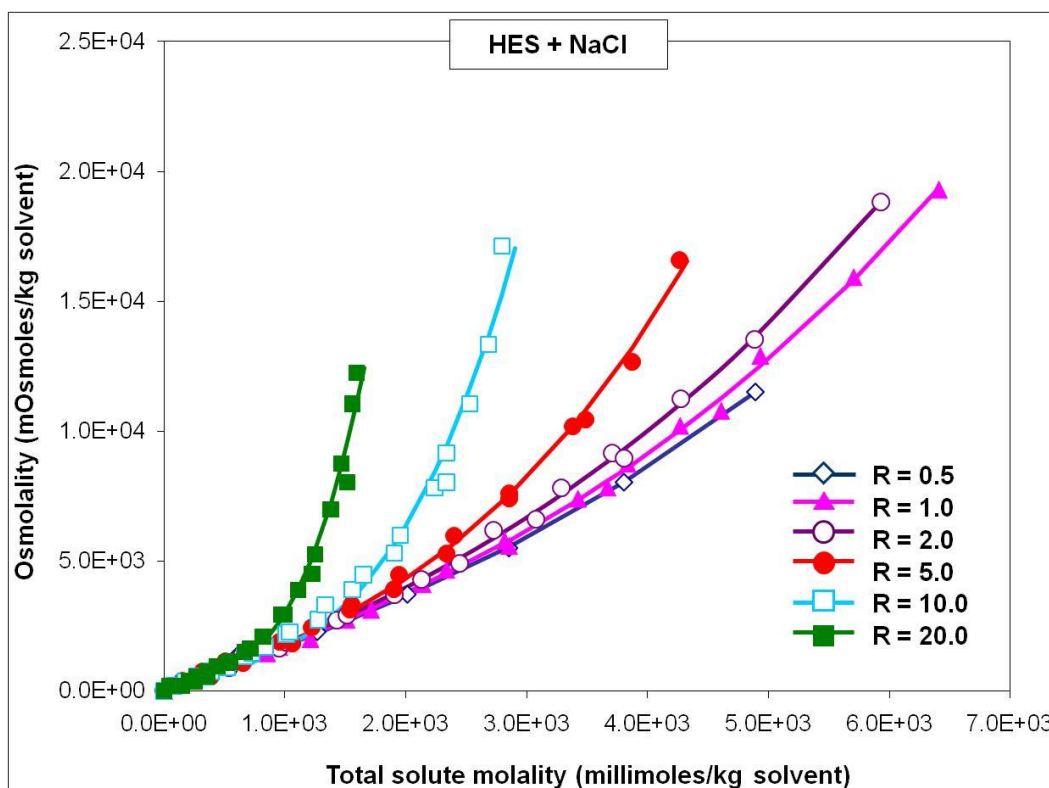


**Figure 4.3.** Osmolality as function of total solute molality for HES + NaCl + water solutions (R ranging from 0.5 to 20). The symbols are data from Jochem and Korber [16]. The solid lines are the rearranged multisolute OVE, equation (4.9), fit to the data.

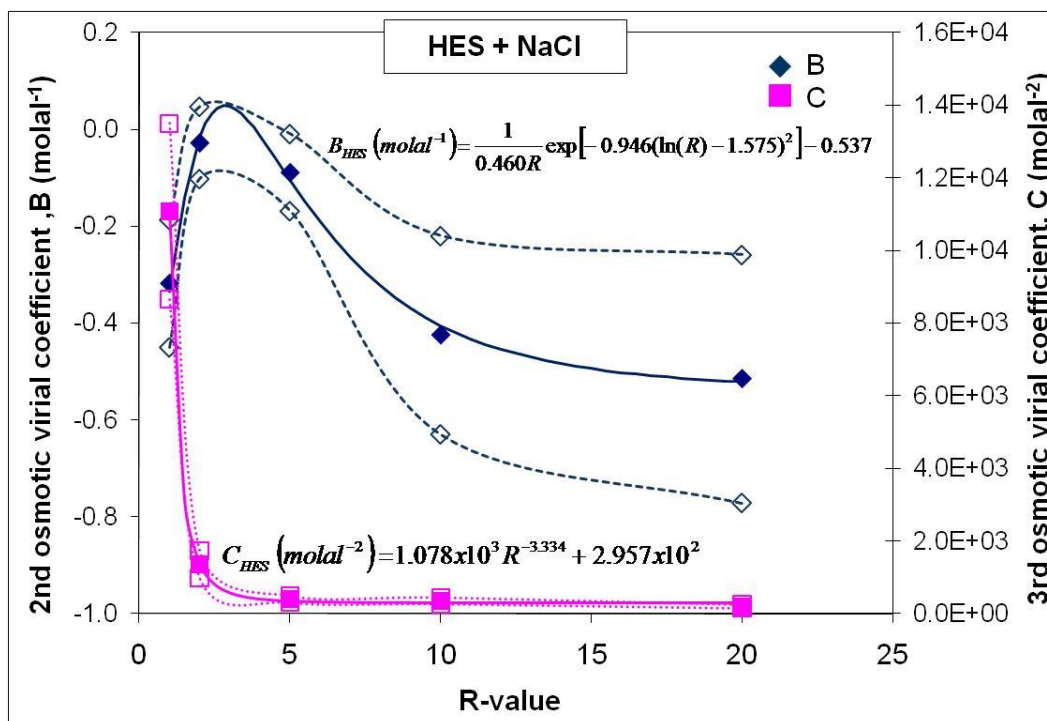


**Figure 4.4.** The second and third osmotic virial coefficients, B and C, for HES in varying concentrations of aqueous salt solutions as a function of R-value. The closed symbols are the values determined for the virial coefficients at each R-value. The solid lines are equation (4.12) fit to the second virial coefficient (B) values as a function of R-value and equation (4.13) fit to the third virial coefficient (C) values as a function of R-value, respectively. The open symbols are the values of the 95 % confidence intervals for the osmotic virial coefficients at each R-value. The dashed lines are the upper and lower 95 % confidence bands (generated by connecting the values of the upper and lower values of the 95 % confidence interval at each R-value with a smoothed line).

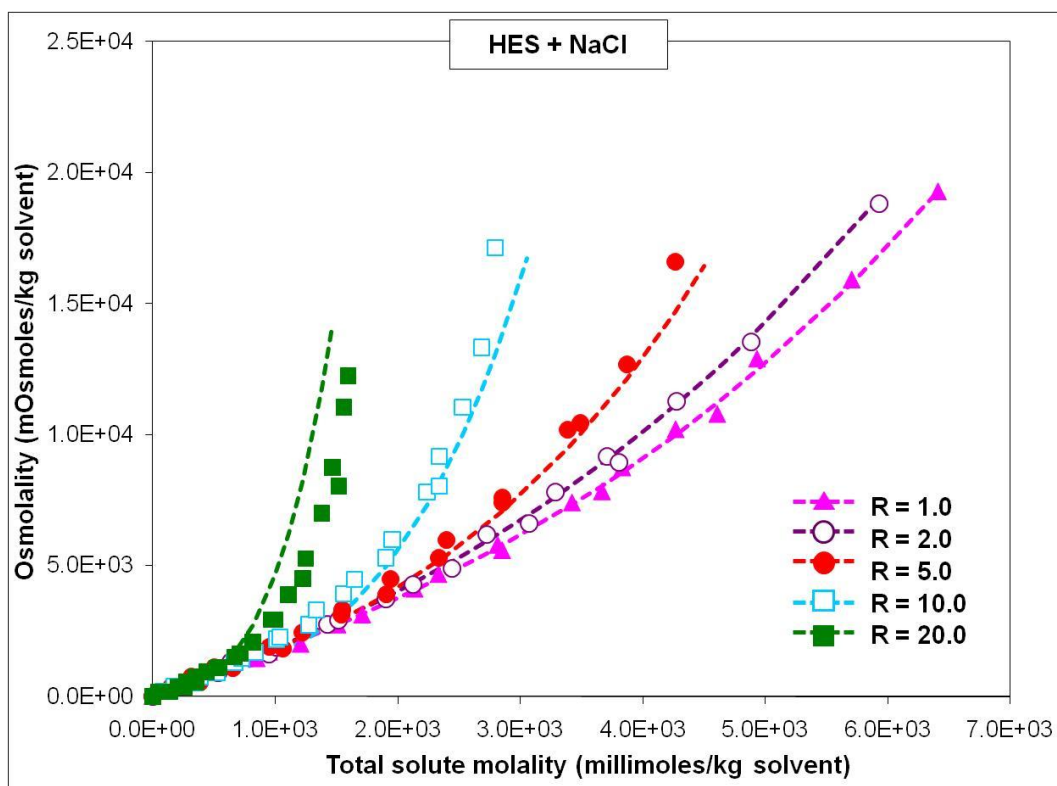


**Figure 4.5.** Osmolality as function of total solute molality for HES + NaCl + water solutions (R ranging from 1 to 20). The symbols are data from Jochem and Korber [16]. The dashed lines are the predictions from the multisolute OVE, equation 4.3, using the calculated coefficients from equations (4.12) and (4.13), which are listed in Table 4.4.

## Chapter 5 - A non-ideal replacement for the

### Boyle-van't Hoff equation<sup>1</sup>

#### 5.1. Introduction

Using the multisolute OVE model developed in Chapters 3 and 4 to express the intracellular solute concentration as a function of osmolality, a non-ideal osmotic equilibrium equation was developed to replace the ideal, dilute Boyle-van't Hoff equation.

For many endeavors in which biological samples are manipulated *ex vivo*, including biopreservation, a description of the osmotic equilibrium (or equilibrium cell volume as a function of osmolality) is required. Currently cellular osmotic equilibrium is described with the Boyle-van't Hoff relation which states that the product of osmolality and equilibrium volume of the osmotically-active portion of the cell is constant. The equation arose when van't Hoff applied Boyle's law for gases (which states the product of pressure and volume is constant for ideal gases) to solutions, showing that for ideal, dilute aqueous solutions the product of osmotic pressure and volume is constant [30; 31]. Written in its usual form, the Boyle-van't Hoff equation is

$$\frac{V}{V_o} = \left( \frac{V_{w,o}}{V_o} \right) \frac{\pi_o}{\pi} + \frac{V_b}{V_o} = (1-b) \frac{\pi_o}{\pi} + b \quad (5.1)$$

---

<sup>1</sup>A version of this chapter has been published. R.C. Prickett, J.A.W. Elliott, S. Hakda, and L.E. McGann 2008. *Cryobiology*. 57: 130-136.

where  $V$  is the cell volume ( $\mu\text{m}^3$ ),  $V_o$  is the isotonic volume ( $\mu\text{m}^3$ ),  $V_{w,o}$  is the isotonic volume of water in the cell ( $\mu\text{m}^3$ ),  $\pi$  is the osmolality (osmoles/kg solvent),  $\pi_o$  is the isotonic osmolality (osmoles/kg solvent),  $V_b$  is the osmotically-inactive volume of the cell (i.e. the volume of the cell that does not participate in the osmotic response) ( $\mu\text{m}^3$ ) and  $b = V_b/V_o$  is the osmotically-inactive fraction of the cell volume.

To determine the osmotically-inactive fraction, equilibrium cell volumes are measured after the cells are exposed to solutions of known osmolality. These measurements have been performed using several techniques, including the use of electronic particle counters [10; 13; 19; 33; 37], optical measurements under a microscope [35; 36], assessing packing volume following centrifugation [2; 25; 27], and light scattering [29], among others. The Boyle-van't Hoff equation is then used to determine the osmotically-inactive fraction of cells by extrapolating osmotic equilibrium measurements to infinite osmolality. This is commonly done using a Boyle-van't Hoff plot, which is the equilibrium relative cell volume  $\left(\frac{V}{V_o}\right)$  plotted as a function of inverse relative osmolality  $\left(\frac{\pi_o}{\pi}\right)$ .

From equation (5.1), the value of the y-intercept of a linear fit of the data is the osmotically-inactive fraction,  $b$ . It can be noted from equation (5.1), that the osmotically-inactive fraction can also be determined from one minus the slope. Comparing the values obtained from the intercept and

one minus the slope is a method to check the self-consistency of the osmotic equilibrium data.

It has been noted in the past that in some cases the Boyle van't Hoff relationship yields osmotically-inactive fractions higher than predicted from desiccation experiments [27] that measure the dry volume of the cell, which can be used as another estimate of the osmotically-inactive volume of the cell. The discrepancy between osmotically-inactive volume and dry volume has been discussed for human erythrocytes [27]. The osmotically-inactive fraction for human erythrocytes determined using the Boyle-van't Hoff equation ranges from 0.41 to 0.48 [2; 18; 28]. This is at the higher end of the values found for other mammalian cell types (0.18 to 0.41 [7; 10; 12; 19]). The dry volume fraction for erythrocytes measured by desiccation is 0.27 to 0.30 [2; 27]. There have been many explanations for this difference, including bound water [2; 27; 32], the movement of chloride ions between the extracellular and intracellular solutions [2], the osmotic properties of intracellular solutes [9; 11; 22; 26], the large entropy of dilution characteristic of macromolecular solutes [4], and erythrocyte membrane characteristics [15; 22; 34]. However, none of these hypotheses have been explicitly proven and much debate still surrounds the osmotically-inactive fraction of the erythrocyte.

As stated when these equations first appeared [20; 24; 30; 31], the Boyle-van't Hoff and the van't Hoff equations are only thermodynamically correct for ideal, dilute solutions (even though osmolality appears in the

equations). Thus, contrary to what is commonly believed [6; 10; 16; 35], the product of osmolality and osmotically-active cell volume is not constant in solutions that are not ideal and dilute. It has been recognized that intracellular solutions are not always ideal and dilute [17; 21] and thus should not always adhere to the Boyle-van't Hoff relation. This was pointed out by Lucke and McCutcheon in 1932 [20], who stated "To be an ideal osmometer both cell and medium would have to behave as ideal solutions and the membrane must be perfectly semipermeable". The osmolality of erythrocyte cytoplasm is not equal to the intracellular solute molality, thus it is not an ideal, dilute solution, which can be seen in Figure 5.1. Furthermore, since the osmotically-inactive fraction is found by extrapolating osmotic equilibrium measurements to infinite osmolality, the ideal, dilute solution constraint is obviously violated. Many have argued that most cell types, including erythrocytes, are 'ideal osmometers' because when the osmotic equilibrium data is plotted on a Boyle-van't Hoff plot ( $V/V_o$  versus  $\pi_o/\pi$ ) it appears to be well fit using a straight line (i.e. the Boyle-van't Hoff equation). However, most of the osmotic equilibrium data do not contain extremely hypertonic data points (i.e. data points close to zero on the x-axis) where the solutions have definitely diverged from an ideal, dilute solution. The problem in applying the Boyle-van't Hoff equation arises in the extrapolation to infinite osmolality to determine the osmotically-inactive fraction. It is at these extremely hypertonic conditions where the osmotic equilibrium data would show definite non-linear

behaviour and diverge from the Boyle-van't Hoff equation. Thus, when applying the Boyle-van't Hoff equation to the osmotic equilibrium data that is available, it may appear to fit, but the osmotically-inactive fraction that is obtained from extrapolating to the y-intercept may be erroneously large.

Recognizing that the cytoplasm of the erythrocyte is not an ideal, dilute solution, others have made adjustments to the equations for the kinetics of water movement [8; 17; 21]. The water transport equations are derived from a chemical potential driving force, thus the non-ideality of the cytoplasm can be taken into account by using osmolality where concentration (or molality) had been used. While extracellular and intracellular osmolalities are equal at osmotic equilibrium, the equation to describe osmotic equilibrium (i.e. the Boyle-van't Hoff equation) results from applying conservation of mass to the intracellular solutes. Therefore, simply using a non-ideal osmolality in the Boyle-van't Hoff equation is not the correction that should be made to account the non-ideality of the cytoplasm. In the osmotic equilibrium equation, molality, not osmolality, should be used, even for non-ideal, non-dilute solutions. This will be shown in the derivation below.

The objective of this chapter was to derive a non-ideal osmotic equilibrium equation to replace the Boyle-van't Hoff equation. Additionally, it was demonstrated that the anomalous osmotic behaviour of human erythrocytes can be corrected by using the non-ideal equation instead of the Boyle-van't Hoff equation. Others have experimentally shown that the

observed anomalies in the osmotic equilibrium of erythrocytes disappear when the cytoplasmic solutes are removed from the cytoplasm and the cells become red cell ghosts [1; 18]. This supports the hypothesis of this work that the non-ideality of the cytoplasm (due in large part to the hemoglobin and its interactions with the other intracellular solutes) contributes to the observed difference between inferred osmotically-inactive volume from the Boyle-van't Hoff equation and the measured dry volume.

## 5.2. Governing equations

In order to explain why the Boyle-van't Hoff equation is not applicable to solutions that are not ideal and dilute, the derivation of the osmotic equilibrium equation is required. Osmotic equilibrium equations result from assuming that the number of intracellular solute molecules remains constant and only cell water crosses the cell membrane in response to the changes in extracellular osmolality. This is the same as assuming ideal semipermeability of the membrane and applying conservation of mass to the intracellular solutes.

$$N_s = N_{s_o} \quad (5.2a)$$

or,

$$m\rho_w V_w = m_o\rho_w V_{w,o} \quad (5.2b)$$

where  $N_s$  is the number of intracellular solute molecules,  $m$  is the molality of intracellular solute molecules (mole/kg solvent),  $\rho_w$  is the density of

water ( $\text{kg}/\mu\text{m}^3$ ),  $V_w$  is the volume of osmotically active intracellular water ( $\mu\text{m}^3$ ) and the subscript  $o$  refers to the isotonic condition. The water density,  $\rho_w$ , cancels out of equation (5.2b).

The osmotically-*active* water volume of the cell is, by definition, the total cell volume minus the osmotically-inactive volume ( $V_b$ ).

$$V_w = V - V_b = V - bV_o \quad (5.3)$$

Combining equations (5.2b) and (5.3) gives

$$m_o(V_o - bV_o) = m(V - bV_o). \quad (5.4)$$

Equation (5.4) can be rearranged to give

$$\frac{V}{V_o} = (1 - b) \frac{m_o}{m} + b. \quad (5.5)$$

Equation (5.5) is the general osmotic equilibrium equation arising directly from conservation of mass and does not contain dilute solution assumptions. This equation is correct for ideal and non-ideal solutions. Equation (5.5), not equation (5.1), should be used to determine the osmotically-inactive fraction, but a problem arises in applying the equation since the molality of intracellular solutes is not known. Thus, the *van't Hoff* relation has been used to relate intracellular solute molality to osmolality. The van't Hoff relation, which is only thermodynamically correct for ideal, dilute solutions [30; 31], implies (see Appendix C)

$$\pi = m \quad (5.6)$$

where  $\pi$  is the osmolality. Under equilibrium conditions, the intracellular osmolality ( $\pi^i$ ) is equal to the extracellular solution osmolality ( $\pi^e$ ), but given the different compositions of the intracellular and extracellular solutions, the solute molalities of the intracellular and extracellular solutions are not the same. Combining equation (5.6) with (5.5) yields the well-known Boyle-van't Hoff equation (equation (5.1)). The fact that the van't Hoff relation (equation (5.6)) is applicable only to ideal, dilute solutions is well established. The analogy between ideal gases (product of pressure and volume is constant) and aqueous solutions (product of osmotic pressure and volume is constant) only holds for ideal solutions, or according to van't Hoff 'for solutions which are diluted to such an extent that they are comparable to ideal gases' [30; 31]. Furthermore, in the Textbook of Physical Chemistry by Glasstone, it is clearly stated that the Boyle-van't Hoff equation (equation (50), page 663) and the analogous Morse equation (equation (68), page 671) are only applicable to dilute solutions [14]. By using equation (5.6) to relate osmolality to molality, the Boyle-van't Hoff equation includes an ideal, dilute solution assumption. Although this assumption may be valid at isotonic conditions, intracellular osmolality diverges increasingly from ideal at higher equilibrium osmolalities. Even though a straight line can often fit the data points on a Boyle-van't Hoff plot ( $V/V_o$  vs.  $\pi_o/\pi$ ), the Boyle-van't Hoff equation is not thermodynamically correct when extrapolated to infinite osmolality in order

to obtain the osmotically-inactive fraction. This may result in osmotically-inactive fractions which are incorrect.

In deriving a replacement osmotic equilibrium equation for the Boyle-van't Hoff relation, it is important to note that if the cytoplasm is not an ideal, dilute solution, solute molality in equation (5.5) cannot be replaced with osmolality. At osmotic equilibrium, the intracellular and extracellular osmolalities are equal ( $\pi^i = \pi^e$ ) and the equilibrium osmolality is usually known during the osmotic equilibrium experiments. The equilibrium osmolality must be used to determine the intracellular solute molality in order to correctly determine the osmotically-inactive fraction from equation (5.5). However, the extracellular solute molality does not equal the intracellular solute molality, since the two solutions have different solute compositions. Thus, an accurate description of the *intracellular* solute molality as a function of the equilibrium osmolality is required. Herein, a non-ideal equation of state for the relationship between osmolality and intracellular solution molality (the multisolute osmotic virial equation (OVE) from Chapter 3) was combined with the assumption that the number of intracellular solute molecules remains constant, to derive a non-ideal replacement for the Boyle-van't Hoff equation that is applicable for ideal, dilute solutions as well as many non-ideal, non-dilute solutions.

When the osmolality begins to diverge from ideal, an expression for the intracellular osmolality as a function of molality,  $\pi(m)$ , is required. For multisolute solutions, such as cytoplasm, the osmolality can be written as

a function of the individual solute molalities (shown in equation (3.13)) or the individual solutes can be grouped together to create an effective concentration of one "grouped solute" and the osmolality written as a function of that grouped solute molality (shown in equation (5.9)). This function can be inverted to give:

$$m = m(\pi) \quad (5.7a)$$

and its value at isotonic conditions

$$m_o = m(\pi_o) \quad (5.7b)$$

where  $m$  is either the molality of one of the intracellular solutes or is the molality of the grouped solute.

Equation (5.5) can then be written:

$$\frac{V}{V_o} = (1 - b^*) \frac{m(\pi_o)}{m(\pi)} + b^* \quad (5.8)$$

where  $b^*$  is a new osmotically-inactive fraction of the cell obtained without any ideal, dilute solution assumptions.

The intracellular molality of solutes is generally not known, and for non-ideal solutions, the molality is related to the osmolality in a non-linear manner. As previously stated, the relationship,  $m(\pi)$ , can be determined using a non-ideal equation of state and in this study the multisolute OVE is used. The parameters in the OVE can be predicted by creating a model of the cytoplasm (as was demonstrated in Chapter 3 using hemoglobin and an ideal solute in the multisolute OVE) or found by fitting the single-solute OVE to experimental measurements of the cytoplasm.

### 5.2.1. Osmotic virial equation: Model for $\pi(m)$

In Chapter 3, the cytoplasm of a human erythrocyte was modelled as a solution of hemoglobin (Hb) and other solutes, where all other solutes were assumed to behave osmotically as ideal, dilute solutes. The hemoglobin, which is highly non-ideal, and the interactions between the hemoglobin and ideal solute contribute a significant portion to the cytoplasm osmolality and thus the cytoplasm is a very non-ideal solution. The form of the osmotic virial equation used to predict the osmolality of the erythrocyte cytoplasm was:

$$\pi = \left( \frac{m_{I,o}}{m_{H,o}} \right) m_H + m_H + B_H m_H^2 + B_H m_H \left( \frac{m_{I,o}}{m_{H,o}} \right) m_H + C_H m_H^3 \quad (3.13)$$

where  $\pi$  is the osmolality of the cytoplasm,  $m_H$  is the molality of hemoglobin,  $m_I$  is the molality of the ideal solutes,  $B_H$  is the second osmotic virial coefficient for hemoglobin ((mole Hb / kg water)<sup>-1</sup>), and  $C_H$  is the third osmotic virial coefficient for hemoglobin ((mole Hb / kg water)<sup>-2</sup>). Note that  $B_I$  and  $C_I$  are equal to zero and thus do not appear in equation (3.13). The osmotic virial coefficients for hemoglobin were determined by fitting osmolality as a function of molality data from aqueous solutions of hemoglobin (see Chapter 2) and are listed in Table 2.1. The virial coefficients take into account the interactions between the solute molecules in the solution. At the isotonic condition, the only unknown in equation (3.13) is the molality of the ideal solutes. For this study, the isotonic osmolality of the cytoplasm, which includes contributions from the

hemoglobin, the ideal solute, and their interactions, was taken to be 305 mOsm/kg solvent. The isotonic concentration of hemoglobin taken from the literature is 35.1 gram / 100 mL cells [27]. This value was determined spectrophotometrically and when converted to molality, gives a value of 7.3 millimolal [9; 28]. Using the above values and the values of the osmotic virial coefficients for hemoglobin listed in Table 2.1 in equation (3.13) and solving this equation for  $m_{i_o}$  yields an isotonic concentration of the ideal solute of 208 millimole/kg solvent. This concentration is slightly different than the value in Chapter 3, which is because the isotonic osmolality used in the experiments in this chapter was slightly different than the isotonic osmolalities in the literature data [5; 23] utilized in Chapter 3. In Chapter 3, the isotonic osmolality utilized was 289 mOsm/kg solvent, which is the average of the isotonic osmolality of Du [5] and Morrone *et al.* [23]. The ESR measurements of Du and Morrone *et al.* were used to determine the accuracy of the model in Chapter 3. In this study, the isotonic osmolality is the measured osmolality (305 mOsm/kg solvent) of the isotonic phosphate buffered saline solution that was made for the osmotic equilibrium experiments. Both values are within the range of isotonic osmolalities reported in the literature [2; 3].

This proposed model is not the actual composition of the cytoplasm of the erythrocyte, but rather this is the effective concentration of an ideal solute needed to model the osmotic behaviour of the cytoplasm once the effects of the known amount of hemoglobin were taken into account (i.e.

the ideal solute is used to model the contribution from the rest of the molecules and the dissociated ions in the cytoplasm). This model worked extremely well for predicting the osmotic behaviour of the erythrocyte cytoplasm (see Figure 5.1).

For each osmolality of interest, equation (3.13) was inverted to give the intracellular molality of hemoglobin at that osmolality,  $m_H(\pi)$ . The hemoglobin molalities were then used in equations (3.13) and (5.8) to determine the osmotically-inactive fraction.

#### *5.2.2. Osmotic virial equation: Best fit to measurements of $\pi(m)$*

Since creating a model for the cytoplasm involves making an assumption about the composition of the intracellular solutes, an alternative is to fit experimental measurements of cell water volume using a form of the single-solute OVE. Electron spin resonance (ESR) has been used to measure the relative cell water volume (cell water volume / cell water volume at isotonic) of human erythrocytes as a function of inverse relative equilibrium osmolality (isotonic osmolality / osmolality) in two studies [5; 23]. To fit the ESR data, all of the intracellular solutes (including hemoglobin) were treated as one grouped solute to determine  $\pi(m)$ . This grouped solute represented the effects of all the solutes in the cytoplasm and their interactions were taken into account with the virial coefficients of the grouped solute. The ESR data was presented as the relative cell water volume (which was converted to relative intracellular

solute molality, see equation (3.11)) as a function of inverse relative osmolality, so the data was fit as  $\frac{\pi}{\pi_o}$  as a function of  $\frac{m_{GS}}{m_{GS,o}}$ . The single grouped solute osmotic virial equation used is

$$\frac{\pi}{\pi_o} = A_{GS} \left( \frac{m_{GS}}{m_{GS,o}} \right) + B_{GS} \left( \frac{m_{GS}}{m_{GS,o}} \right)^2 + C_{GS} \left( \frac{m_{GS}}{m_{GS,o}} \right)^3 \quad (5.9)$$

where  $m_{GS}$  is the molality of all of the intracellular solute molecules grouped together,  $A_{GS}$  is the grouped solute linear coefficient,  $B_{GS}$  is the second virial coefficient for the grouped solute,  $C_{GS}$  is the third virial coefficient for the grouped solute (see Table 5.1) and the subscript  $o$  refers to the isotonic condition. This fit, along with the osmotic virial model (equation (3.13)) expressed as  $\pi/\pi_o$  versus  $m/m_o$  (or  $\frac{m_{GS}}{m_{GS,o}}$ ) is shown in Figure 5.1.

For each osmolality of interest, equation (5.9) was inverted to give the relative grouped solute molality  $\left( \frac{m_{GS}}{m_{GS,o}} \right)$  as a function of the relative osmolality  $\left( \frac{\pi}{\pi_o} \right)$ . The relative grouped solute molalities were used in equation (5.8) to determine the osmotically-inactive fraction.

This made it possible to re-analyze osmotic equilibrium data with equation (5.8) and either the hemoglobin and ideal solute model (equation (3.13)) or the best fit of the grouped solute data (equation (5.9)).

### 5.3. Materials and methods

Equilibrium volume measurements were performed by suspending human erythrocytes in hypertonic solutions of Dulbecco's phosphate buffered saline (PBS) (Invitrogen, Burlington, ON, Canada)<sup>2</sup>. A 10X isotonic solution of PBS was diluted with an appropriate amount of distilled, deionized water (CORNING Mega-Pure™ system ACS) to obtain 1X, 2X, 3X, 4X and 5X isotonic PBS solutions. The osmolalities of the PBS solutions were measured using a calibrated freezing point depression osmometer ( $\pi$ OSMETTE™, Model 5004 Automatic Osmometer, Precision System Inc.™, Natick, MA, USA) before the addition of the cells.

The erythrocytes used in this study were obtained from a normal human blood donor who consented to donating blood for research purposes at Canadian Blood Services. Ten (10) mL of blood was aliquoted into each of four 50 mL sterile plastic centrifuge tubes (Fisherbrand, Fisher Scientific Ltd., Nepean, ON, Canada), washed three times by centrifugation at 1500 g for 10 minutes and re-suspended in 1X isotonic PBS to a final volume of 45 mL. The isotonic (1X) PBS solution had an osmolality of 305 mOsm/kg solvent. After the third wash, the cells were diluted to a final concentration of  $1.0 - 1.7 \times 10^6$  cells/mL. One hundred (100)  $\mu$ L of this cell suspension was added to 10 mL of the hypertonic solution of interest. The cells were added to the hypertonic solution at

---

<sup>2</sup> The equilibrium volume measurements done in our lab were performed by undergraduate student S. Hakda

room temperature and were exposed to the solution for 30 seconds before being analyzed on the particle counter.

A particle counter (Coulter® Z<sub>2</sub><sup>TM</sup> series, Beckman Coulter, Mississauga, ON, Canada) and cell size analyzer (The Great Canadian Computer Company, Spruce Grove, AB, Canada) were used to determine the cell volumes in the various hypertonic solutions. Cells suspended in each hypertonic solution were run three times on the Coulter counter, except for the 5X PBS which was done twice. Between each hypertonic solution run, a calibration, consisting of three drops of the 10 µm beads (Beckman Coulter, Mississauga, ON, Canada) in 10 mL of the hypertonic solution, was run yielding a calibration factor that was used to calculate the equilibrium volume of the cells in that hypertonic solution.

The standard deviation in the five equilibrium cell volume measurements was determined for each hypertonic solution. The standard deviations are shown on the figures as the error bars.

Osmotic equilibrium data were also obtained from two literature sources [27; 37]. Savitz *et al.* measured the equilibrium volume of erythrocytes using both the hematocrit and isotope dilution method in anistonic solutions ranging from 192 to 480 mOsm/kg solvent [27]. Since both methods gave the same equilibrium volume results, the hematocrit data is used in this thesis. The Savitz *et al.* 1964 study [27] did not indicate the isotonic osmolality, but in a later paper [28], the authors used 290 mOsm/kg solvent as the isotonic osmolality. However, the hematocrit

at 290 mOsm/kg solvent was not measured. Thus, for this thesis, the isotonic hematocrit was calculated from a second order polynomial fit to the reported Savitz *et al.* data. This resulted in a calculated isotonic hematocrit of 0.4413.

Zhao *et al.* utilized an electronic particle counter to measure the equilibrium volume of human erythrocytes in anisotonic solutions ranging from 118 to 3186 mOsm/kg solvent [37]. The data point closest to 305 mOsm/kg solvent was assumed to be their isotonic osmolality. Thus, for the Zhao *et al.* data points, an isotonic osmolality of 302 mOsm/kg solvent was used in this thesis, with a corresponding isotonic volume of  $74.42 \pm 3.640$  fL.

Since the data from each source had a different isotonic osmolality, and therefore isotonic volume, each data set was divided by its own isotonic values before analyzing, ensuring that all data had a relative volume ( $V/V_o$ ) equal to 1 when the inverse relative osmolality ( $\pi/\pi_o$ ) was equal to 1. For lack of more specific information, it was assumed that the isotonic concentration of hemoglobin was 7.3 millimolal for all data sets [9; 28], and this resulted in a slightly different value for the isotonic concentration of ideal solute for each data set (see Table 5.2 for the values).

Combining the osmotic equilibrium data from our study and the literature, the osmotically-inactive fraction was determined by linear regression using the methods described previously (Chapter 2). The

results are plotted on graphs where the ordinate values are the relative equilibrium cell volume measurements ( $V/V_o$ ) and the abscissa values are either (i) the inverse relative osmolality ( $\pi_o/\pi$ ) for equation (5.1), or (ii) the inverse relative solute molality ( $m_o/m$ ) for equation (5.8). The slope is equal to  $[1-b]$  for equation (5.1) or  $[1-b^*]$  for equation (5.8). The intercept is equal to  $b$  for equation (5.1) or  $b^*$  for equation (5.8). The 95 % confidence intervals for the slope and intercept were calculated using the method described previously (Chapter 2) for calculating confidence intervals for linear regression coefficients.

#### 5.4. Results

The osmotic equilibrium data for human erythrocytes were analyzed using (i) the Boyle-van't Hoff equation (equation (5.1)), (ii) the proposed non-ideal replacement equation for osmotic equilibrium (equation (5.8)) using the osmotic virial model of the cytoplasm (equation (3.13)) to determine  $m(\pi)$  or (iii) the proposed non-ideal replacement equation for osmotic equilibrium (equation (5.8)) using the ESR data for human erythrocytes best fit with the osmotic virial equation (equation (5.9)) to determine  $m(\pi)$ .

#### 5.4.1. Boyle-van't Hoff equation

The osmotic equilibrium measurements from our study and the literature [27; 37] for human erythrocytes are shown in Figure 5.2 as relative cell volume  $\left(\frac{V}{V_o}\right)$  versus inverse relative equilibrium osmolality  $\left(\frac{\pi_o}{\pi}\right)$ . These data were fit to equation (5.1), the Boyle-van't Hoff equation, and the osmotically-inactive fraction ( $b$ ) determined from the y-intercept was  $0.51 \pm 0.040$ . This value of the osmotically-inactive fraction is similar to other reported values for human erythrocytes which range from 0.41 to 0.48 [2; 18; 28].

#### 5.4.2. Non-ideal osmotic equilibrium equation, with osmotic virial model prediction.

The intracellular solute molality of human erythrocytes was calculated as a function of equilibrium osmolality using the osmotic virial model in equation (3.13) and the same osmotic equilibrium data shown in Figure 5.2 were re-plotted in Figure 5.3 as relative cell volume  $\left(\frac{V}{V_o}\right)$  versus inverse relative *intracellular solute molality*  $\left(\frac{m_o}{m}\right)$ . Since the number of intracellular solute molecules remains constant, each solute concentrates at the same rate. Thus, the total solute molality ratio is equal to the hemoglobin solute molality ratio (which is also equal to the ideal solute molality ratio, see equation (3.12)). Using the new non-ideal osmotic

equilibrium equation (equation (5.8)), the osmotically-inactive fraction ( $b^*$ ) determined from the y-intercept is  $0.38 \pm 0.054$ .

*5.4.3. Non-ideal osmotic equilibrium equation, with ESR data osmotic virial equation best fit.*

Figure 5.4 is the plot of the same osmotic equilibrium data as in Figures 5.2 and 5.3, but using equation (5.9) fit to the ESR data fit [5; 23] to determine  $m(\pi)$  of the cytoplasm. The relative cell volume was plotted versus relative inverse intracellular solute molality in Figure 5.4. The osmotically-inactive fraction ( $b^*$ ) determined from the y-intercept is  $0.41 \pm 0.040$ . The osmotically-inactive fraction,  $b^*$ , that results from the grouped solute fit agrees, within error, with the  $b^*$  resulting from the hemoglobin and ideal solute model.

Table 5.3 displays all the values of the inferred osmotically-inactive fraction. Comparing the values from the two methods of obtaining the osmotically-inactive fraction from the same equation (i.e. intercept, and one minus the slope) is a test of the self-consistency of the data. The maximum difference between the values from the intercept and slope is 0.03.

**5.5. Discussion**

Although the osmotic equilibrium data appeared to be linear when plotted on a Boyle-van't Hoff plot, Figure 5.5 shows that non-linearity did

occur at very hypertonic solutions (i.e. small values of  $\pi_o/\pi$ ). Furthermore, the extrapolation to the y-axis on the Boyle-van't Hoff plot gave erroneously large values for the osmotically-inactive fraction. Compared to an analysis of the same data with the Boyle-van't Hoff equation (equation (5.1)) (yielding osmotically inactive fractions of 0.49 - 0.51), the new non-ideal osmotic equilibrium equation (equation (5.8)) resulted in osmotically-inactive fraction of human erythrocytes 20 % lower (0.35 - 0.41) and closer to the results of dry volume obtained from desiccation experiments (0.27 - 0.30) [2; 27].

ESR measures the water volume of the cell, independent of the total cell volume. Isotopically determining cell water mass is another approach to measure cell water independent of total cell volume (or mass). Both of these methods should result in an osmotically-inactive fraction of zero, since they are not measuring the cell solids. However, using the Boyle-van't Hoff equation (equation (5.1)), the authors of those studies [5; 23; 32] determined osmotically-inactive fractions in the range of 0.07 - 0.24, which could be interpreted as a measure of the non-ideality of the cytoplasm (i.e. the non-ideality in  $\pi(m)$ ). These values are in the same range as the difference between the ideal  $b$  (0.49 - 0.51) and the non-ideal  $b^*$  (0.35 - 0.41) that was obtained here (see Figure 5.5).

The cytoplasm of human erythrocytes does not behave as an ideal, dilute solution, particularly when cells are shrunken in very hypertonic solutions. The Boyle-van't Hoff equation commonly used to describe

cellular osmotic equilibrium is not thermodynamically correct for non-ideal, non-dilute solutions (even though osmolality appears in the equation). The non-ideal osmotic equilibrium equation presented in this chapter (equation (5.8)) describes the cytoplasm without making ideal, dilute solution assumptions and should be used to replace the Boyle-van't Hoff equation when determining an accurate value of the osmotically-inactive fraction is of importance.

To use the replacement equation, the typical osmotic equilibrium measurements are still used (equilibrium cell volume as function of osmolality). A non-ideal equation of state may be used to obtain  $\pi(m)$  for cytoplasm, which is inverted to obtain  $m(\pi)$ . The non-ideal equation of state may be predicted from a model (for example, the multisolute OVE model for hemoglobin and an ideal solute presented in Chapter 3) or found from a fit of experimental measurements (for example, ESR data). The non-ideal osmotic equilibrium equation (equation (5.8)) can then be used to determine the osmotically-inactive fraction,  $b^*$  from the appropriate plot of osmotic equilibrium measurements (for example, Figure 5.3 or Figure 5.4). The non-ideal osmotic equilibrium equation is a simple equation that can be applied to the entire range of solutions, both ideal and non-ideal, that are encountered during the biopreservation process.

## 5.6. References

- [1] B.W. Colombe, and R.I. Macey, Effects of Calcium on Potassium and Water Transport in Human Erythrocyte-Ghosts. *Biochimica Et Biophysica Acta* 363 (1974) 226-239.
- [2] J.S. Cook, Nonsolvent Water in Human Erythrocytes. *Journal of General Physiology* 50 (1967) 1311-1325.
- [3] D.A.T. Dick, *Cell water*, Butterworths, Washington, 1966.
- [4] D.A.T. Dick, and L.M. Lowenstein, Osmotic Equilibria in Human Erythrocytes Studied by Immersion Refractometry. *Proceedings of the Royal Society of London, Series B* 149 (1958) 241-256.
- [5] J. Du, Doctorate, *Biophysical Study of Mammalian Sperm Utilizing Electron Paramagnetic Resonance*, Purdue University, (1995), pp. 122
- [6] J.Y. Du, J. Tao, F.W. Kleinhans, A.T. Peter, and J.K. Critser, Determination of Boar Spermatozoa Water Volume and Osmotic Response. *Theriogenology* 42 (1994) 1183-1191.
- [7] S.L. Ebertz, and L.E. McGann, Osmotic parameters of cells from a bioengineered human corneal equivalent and consequences for cryopreservation. *Cryobiology* 45 (2002) 109-117.
- [8] H.Y. Elmoazzen, PhD Thesis, *Osmotic transport in cryobiology*, Department of Laboratory Medicine and Pathology, University of Alberta, Edmonton, Alberta (2006), pp. 221

- [9] J.C. Freedman, and J.F. Hoffman, Ionic and osmotic equilibria of human red blood cells treated with nystatin. *J Gen Physiol* 74 (1979) 157-85.
- [10] D.Y. Gao, Q. Chang, C. Liu, K. Farris, K. Harvey, L.E. McGann, D. English, J. Jansen, and J.K. Critser, Fundamental cryobiology of human hematopoietic progenitor cells I: Osmotic characteristics and volume distribution. *Cryobiology* 36 (1998) 40-48.
- [11] C.M. Gary-Bobo, and A.K. Solomon, Properties of hemoglobin solutions in red cells. *J Gen Physiol* 52 (1968) 825-53.
- [12] J.A. Gilmore, L.E. McGann, E. Ashworth, J.P. Acker, J.P. Raath, M. Bush, and J.K. Critser, Fundamental cryobiology of selected African mammalian spermatozoa and its role in biodiversity preservation through the development of genome resource banking. *Animal Reproduction Science* 53 (1998) 277-297.
- [13] J.A. Gilmore, L.E. McGann, J. Liu, D.Y. Gao, A.T. Peter, F.W. Kleinhans, and J.K. Critser, Effect of Cryoprotectant Solutes on Water Permeability of Human Spermatozoa. *Biology of Reproduction* 53 (1995) 985-995.
- [14] S. Glasstone, and S. Glasstone, *Textbook of physical chemistry*, Van Nostrand Co., New York, 1946.
- [15] P. Heubusch, C.Y. Jung, and F.A. Green, The osmotic response of human erythrocytes and the membrane cytoskeleton. *J Cell Physiol* 122 (1985) 266-72.

- [16] C.J. Hunt, S.E. Armitage, and D.E. Pegg, Cryopreservation of umbilical cord blood: 1. Osmotically inactive volume, hydraulic conductivity and permeability of CD34(+) cells to dimethylsulphoxide. *Cryobiology* 46 (2003) 61-75.
- [17] R.L. Levin, E.G. Cravalho, and C.E. Huggins, Concentration Polarization Effect in a Multicomponent Electrolyte Solution - Human Erythrocyte. *Journal of Theoretical Biology* 71 (1978) 225-254.
- [18] S.W. Levin, R.L. Levin, and A.K. Solomon, Improved Stop-Flow Apparatus to Measure Permeability of Human Red-Cells and Ghosts. *Journal of Biochemical and Biophysical Methods* 3 (1980) 255-272.
- [19] C. Liu, C.T. Benson, D.Y. Gao, B.W. Haag, L.E. McGann, and J.K. Critser, Water Permeability and Its Activation-Energy for Individual Hamster Pancreatic-Islet Cells. *Cryobiology* 32 (1995) 493-502.
- [20] B. Lucke, and M. McCutcheon, The Living Cell as an Osmotic System and its Permeability to Water. *Physiological Reviews* 12 (1932) 68-139.
- [21] G.A. Mansoori, Kinetics of Water-Loss from Cells at Subzero Centigrade Temperatures. *Cryobiology* 12 (1975) 34-45.
- [22] H.A. Massaldi, G.V. Richieri, and H.C. Mel, Alternative interpretation for the osmotic response of human erythrocytes. *J Cell Physiol* 127 (1986) 448-50.

- [23] M.M. Moronne, R.J. Mehlhorn, M.P. Miller, L.C. Ackerson, and R.I. Macey, ESR measurement of time-dependent and equilibrium volumes in red cells. *J Membr Biol* 115 (1990) 31-40.
- [24] H.N. Morse, and J.C.W. Frazer, The osmotic pressure and freezing-points of solutions of cane-sugar. *American Chemical Journal* 34 (1905) 1-46.
- [25] P.S. Nobel, Boyle-Vant Hoff Relation. *Journal of Theoretical Biology* 23 (1969) 375-379.
- [26] R.R. Roepke, and E.J. Baldes, A Study of the Osmotic Properties of Erythrocytes. *Journal of Cellular Physiology and Comparative Physiology* 20 (1942) 71-93.
- [27] D. Savitz, V.W. Sidel, and A.K. Solomon, Osmotic Properties of Human Red Cells. *Journal of General Physiology* 48 (1964) 79-94.
- [28] A.K. Solomon, M.R. Toon, and J.A. Dix, Osmotic properties of human red cells. *J Membr Biol* 91 (1986) 259-73.
- [29] H. Tedeschi, and D.L. Harris, Some Observations on the Photometric Estimation of Mitochondrial Volume. *Biochimica Et Biophysica Acta* 28 (1958) 392-402.
- [30] J.H. van't Hoff, The Role of Osmotic Pressure in the Analogy Between Solutions and Gases. *Zeitschrift fur physikalische Chemie* 1 (1887) 481-508.
- [31] J.H. van't Hoff, The Role of Osmotic-Pressure in the Analogy between Solutions and Gases (Reprinted from *Zeitschrift Fur Physikalische*

- Chemie, Vol 1, Pg 481, 1887). *Journal of Membrane Science* 100 (1995) 39-44.
- [32] S.C. Wiest, and P.L. Steponkus, The osmometric behavior of human erythrocytes. *Cryobiology* 16 (1979) 101-4.
- [33] C.E. Willoughby, P. Mazur, A.T. Peter, and J.K. Critser, Osmotic tolerance limits and properties of murine spermatozoa. *Biol Reprod* 55 (1996) 715-27.
- [34] P. Wong, The behavior of the human erythrocyte as an imperfect osmometer: A hypothesis. *Journal of Theoretical Biology* 238 (2006) 167-171.
- [35] E.J. Woods, M.A.J. Zieger, J.R.T. Lakey, J. Liu, and J.K. Critser, Osmotic characteristics of isolated human and canine pancreatic islets. *Cryobiology* 35 (1997) 106-113.
- [36] T.T. Zhang, A. Isayeva, S.L. Adams, and D.M. Rawson, Studies on membrane permeability of zebrafish (*Danio rerio*) oocytes in the presence of different cryoprotectants. *Cryobiology* 50 (2005) 285-293.
- [37] G. Zhao, L.Q. He, H.F. Zhang, W.P. Ding, Z. Liu, D.W. Luo, and D.Y. Gao, Trapped water of human erythrocytes and its application in cryopreservation. *Biophysical Chemistry* 107 (2004) 189-195.

**Table 5.1.** Osmotic virial coefficients for the solutes of the cytoplasm of human erythrocytes treated as a grouped solute (equation (5.9)).

Solute	Osmotic virial coefficients		
	A	B	C
Cytoplasm of Human Erythrocyte as a Grouped Solute [5; 23]	1.03	-0.230	0.185

**Table 5.2.** Isotonic values for each data set.

Data source	Isotonic values		
	Osmolality (mOsm)	Hemoglobin concentration (millimolal)	Effective ideal solute concentration (millimolal)
Savitz et al. [27]	290	7.3	197
Zhao et al. [37]	302	7.3	206
S. Hakda measurements	305	7.3	208

**Table 5.3.** Values of osmotically-inactive fraction for erythrocytes obtained from the traditional Boyle-van't Hoff equation and from the non-ideal osmotic equilibrium equation.

	Traditional Boyle-van't Hoff (equation (5.1))	Non-ideal replacement (Hb + ideal) (equation (5.8))	Non-ideal replacement (Grouped solute fit) (equation (5.8))
<b>b</b> from intercept	0.51 ± 0.040	0.38 ± 0.054	0.41 ± 0.040
<b>b</b> from (1-slope)	0.49 ± 0.040	0.35 ± 0.058	0.40 ± 0.041

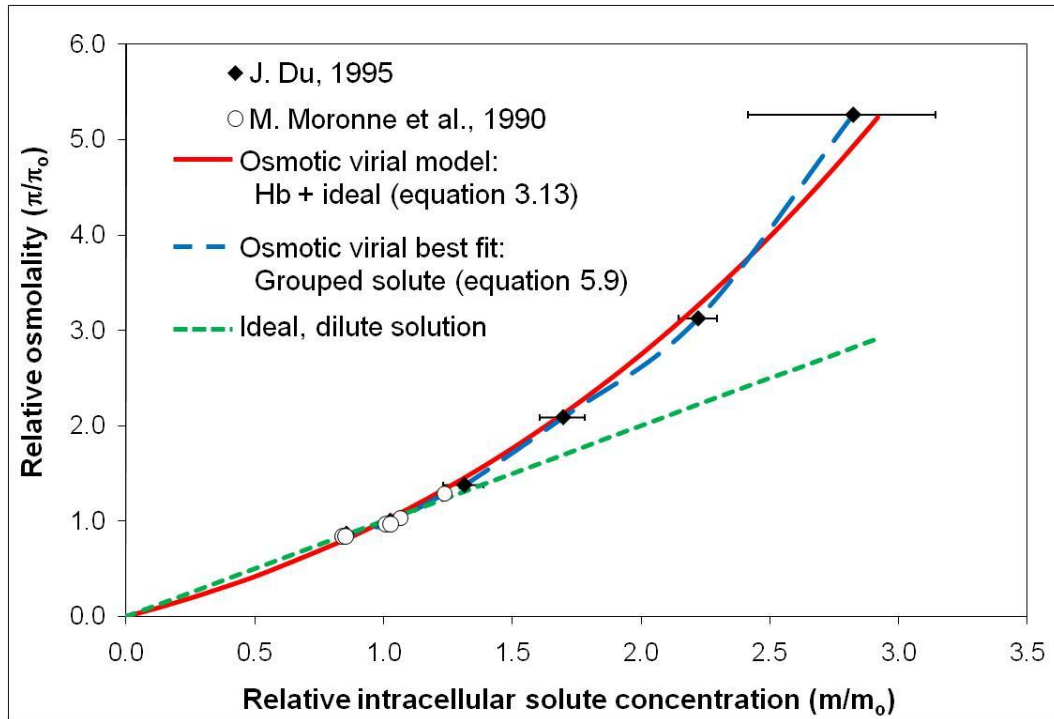


**Figure 5.1.** Relative osmolality as a function of relative intracellular molality for human erythrocytes. The closed diamonds are the ESR data from Du [5] and the open circles are the ESR data from Moronne *et al.* [23]. The red solid line is predicted using our multisolute OVE with hemoglobin and an ideal solute (equation (3.13), Chapter 3). The blue long-dashed line is the OVE best fit of the cytoplasm data, assuming all of the intracellular solutes are one grouped solute (equation (5.9)). The green short-dashed line is the prediction of the relative osmolality of the cytoplasm assuming an ideal, dilute solution.

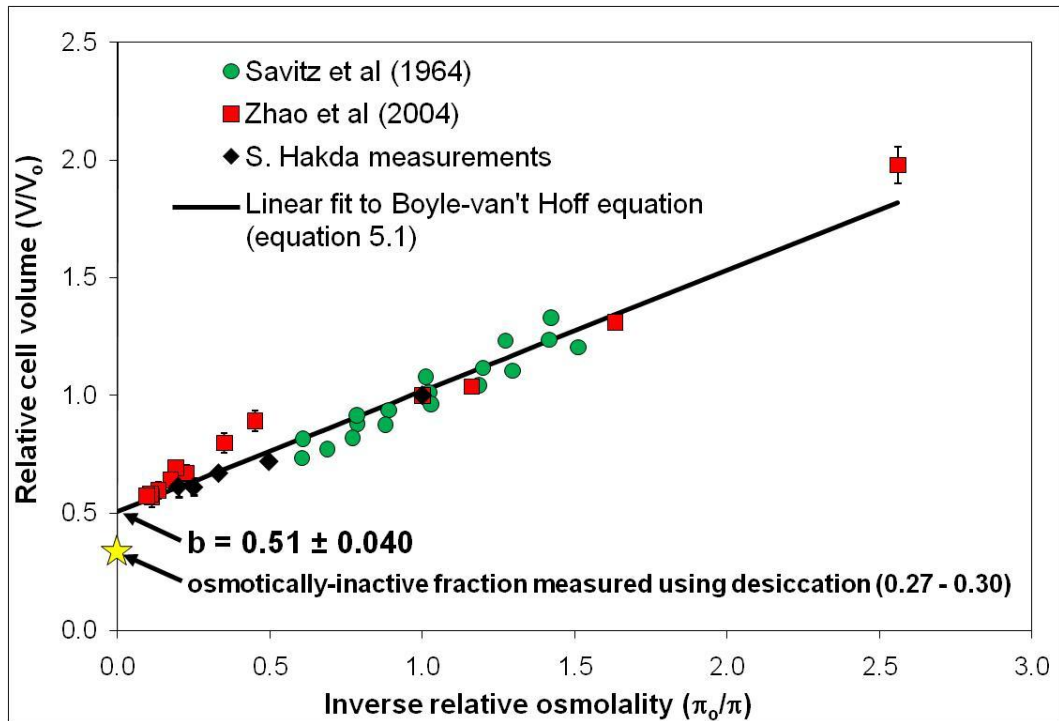


**Figure 5.2.** Boyle-van't Hoff plot for human erythrocytes in phosphate buffered saline solutions. The green circles are from Savitz *et al.* [27], the red squares are from Zhao *et al.* [37] and the black diamonds are the data points measured by S. Hakda. The solid line is the fit to equation (5.1) using linear regression. The star on the x-axis shows the osmotically-inactive fraction measured by desiccation experiments [2; 27].

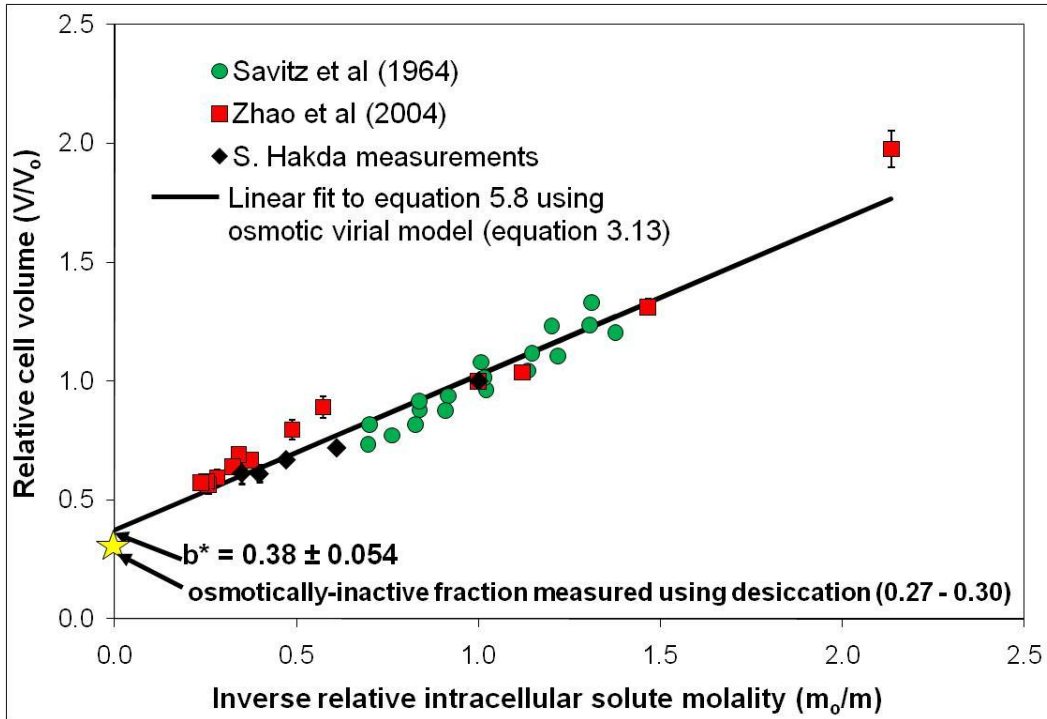


**Figure 5.3.** Non-ideal osmotic equilibrium plot for human erythrocytes in phosphate buffered saline solutions, using our osmotic virial equation model for hemoglobin and an ideal solute (equation (3.13)) to determine  $m(\pi)$ . The green circles are from Savitz *et al.* [27], the red squares are from Zhao *et al.* [37] and the black diamonds are the data points measured by S. Hakda. The solid line is the fit to equation (5.8) using linear regression. The star on the x-axis shows the osmotically-inactive fraction measured by desiccation experiments [2; 27].

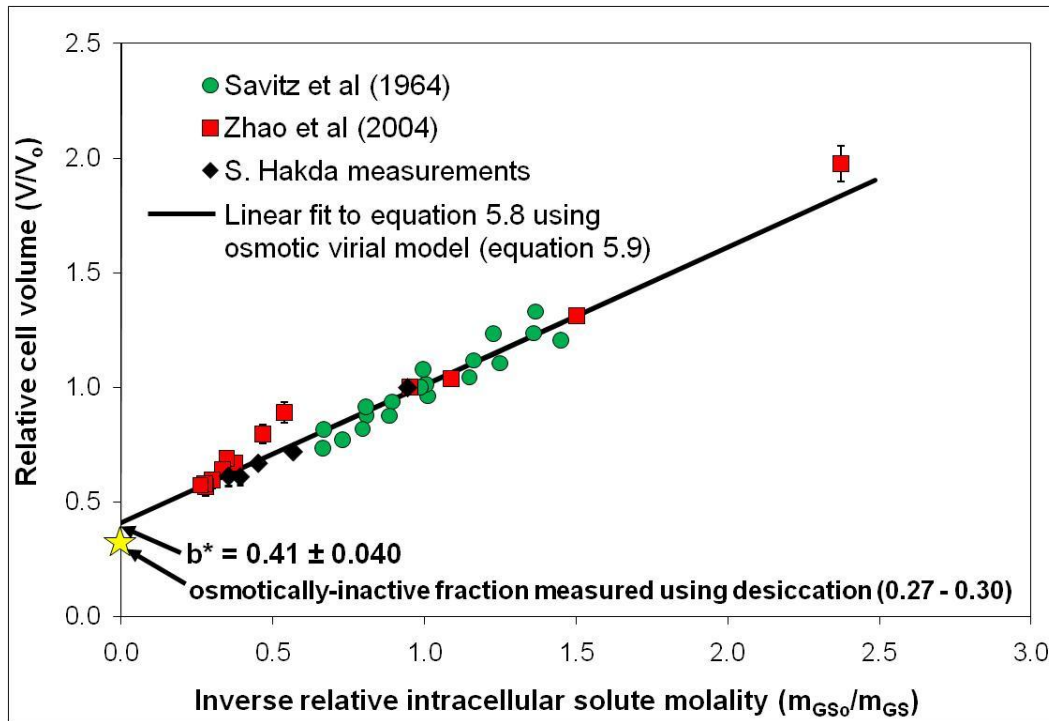


**Figure 5.4.** Non-ideal osmotic equilibrium plot for human erythrocytes in phosphate buffered saline solutions, fitting the ESR data to the osmotic virial equation for one “grouped solute” (equation (5.9)) to determine  $m(\pi)$ . The green circles are from Savitz *et al.* [27], the red squares are from Zhao *et al.* [37] and the black diamonds are the data points measured by S. Hakda. The solid line is the fit to equation (5.8) using linear regression. The star on the x-axis shows the osmotically-inactive fraction measured by desiccation experiments [2; 27].

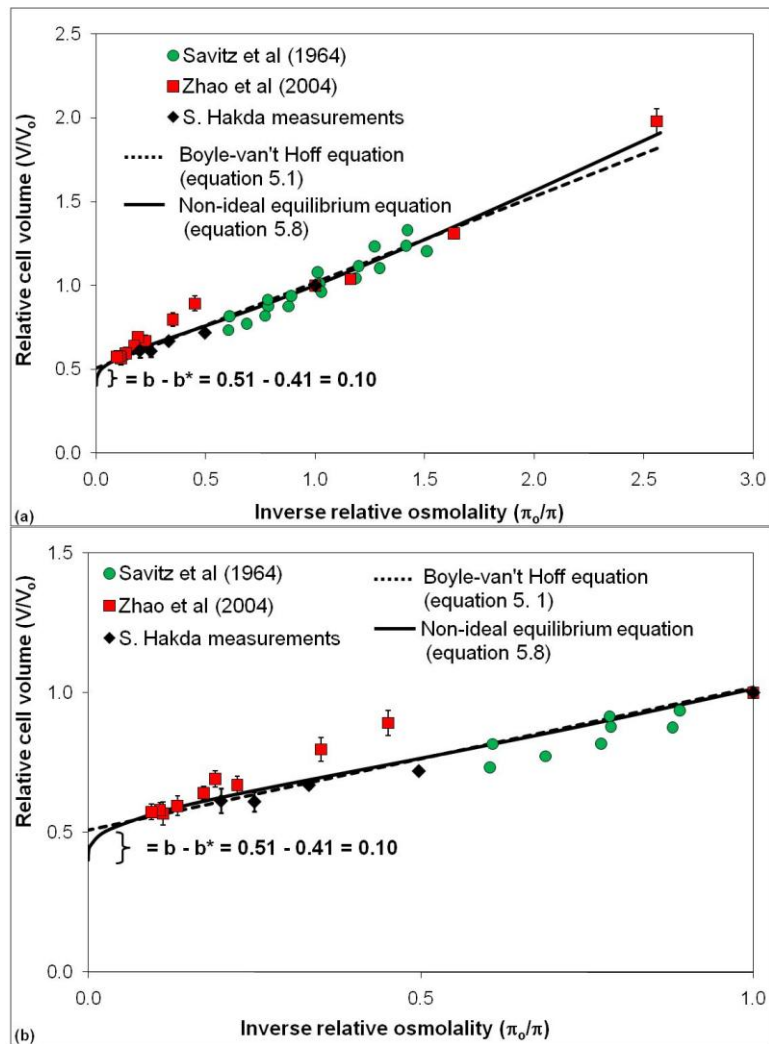


**Figure 5.5.** Osmotic equilibrium plot for human erythrocytes in phosphate buffered saline solutions (a) over the entire osmolality range and (b) over the initial osmolality range. The solid line is the Boyle-van't Hoff equation (equation (5.1)). The dashed line is the non-ideal osmotic equilibrium equation (equation (5.8)) using the fit to the ESR data to determine  $m(\pi)$ . The difference between the osmotically-inactive fraction from the Boyle van't Hoff ( $b = 0.51$ ) and the osmotically-inactive fraction from the non-ideal osmotic equilibrium equation ( $b^* = 0.41$ ) is a measure of the non-ideality of the cytoplasm.

## **Chapter 6 - Effect of supercooling and cell volume on intracellular ice formation.**

### **6.1. Introduction**

In this chapter, the effects of intracellular supercooling and cell volume on the occurrence of intracellular ice formation (IIF) were investigated using experimental measurements and mathematical modelling. Modelling, in addition to being used to design cryopreservation protocols, has been frequently used to interpret experimental data in order to gain additional insight into the conditions which lead to cellular damage [1; 29; 35; 43]. Modelling allows investigation into the relative importance of various parameters, such as intracellular supercooling and cell volume, on cellular responses to cryopreservation without the need to perform multiple experiments.

As mentioned in section 1.6, the conditions which lead to the nucleation of intracellular ice are not well understood. Thus, relationships between calculated parameters and the incidence of IIF are often investigated in order to elucidate possible mechanisms of IIF. However, in order to correctly identify relationships between calculated parameters, such as intracellular supercooling, with experimental outcomes, such as IIF, the models used to calculate the parameters of interest need to be accurate.

### *6.1.1. Current understanding of IIF in cryobiology*

IIF has been linked to cell death for cells in suspension [2; 3; 21; 28; 31; 32]. However, the exact mechanism of injury from the intracellular ice is unknown. Many mechanisms have been proposed [5; 14; 25; 36], but they have not been clearly corroborated with experimental evidence. Most evidence shows that the site of the IIF damage is the plasma membrane [3; 4; 29; 30].

There is evidence that the temperature at which IIF occurs is influenced by the presence of extracellular ice [18; 30; 42]. It is believed that the interaction between extracellular ice and the cell plays an important role in nucleating intracellular ice. There are three main theories of how extracellular ice nucleates intracellular ice: (i) the pore theory [1; 30]; (ii) the membrane failure hypothesis [5; 13; 36]; and (iii) the surface-catalyzed nucleation of intracellular ice [51]. However, none of the theories of the mechanism of IIF can explain the experimental observations of IIF for all cell types.

An overview of the range of mathematical models of IIF which have been proposed in an effort to further the understanding of the mechanism of IIF and predict its occurrence in various cell types was provided in section 1.6. In all of the mathematical models and many of the experimental observations of IIF, intracellular supercooling, cell volume, and extracellular nucleation temperature have been shown to be key

parameters which affect the nucleation of intracellular ice [8; 10; 13; 22; 29; 38; 39; 40; 51; 54].

#### *6.1.2. The role of intracellular supercooling in IIF*

In order to accurately investigate the effect of intracellular supercooling on IIF in the presence of extracellular ice, accurate calculations of the degree of supercooling in the intracellular solution combined with experimental measurements of IIF under a range of conditions are needed. Many measurements of the incidence of IIF have been performed as a function of constant cooling rate, both in the presence and absence of CPA [10; 11; 13; 18; 38; 40; 41; 51; 53]. The decrease in extracellular temperature with time results in an increase in the intracellular supercooling with time. The inclusion of permeating CPAs adds additional complexity since permeating CPAs cause a depression in the freezing point of the intracellular solution. The freezing point depression is a nonlinear function that is dependent on the intracellular composition of all solutes. Thus, the concentration of all intracellular solutes, including the CPA, must be taken into account when determining the intracellular supercooling at the time of IIF. In addition, when extracellular ice is nucleated, the cell will respond osmotically due to osmolality and concentration gradients between the intra- and extracellular solutions, thus changing the intracellular solution composition. Thus, the intracellular supercooling is increasing with time due to the decreasing

temperature, but also decreasing due to the increase in intracellular osmolality with osmotic dehydration and the transport of CPAs into the intracellular solution.

Others have performed isothermal (i.e. constant temperature) IIF experiments in order to determine the intracellular ice nucleation temperature, both in the presence and absence of CPAs [2; 3; 18; 35; 38; 39; 53]. These experiments eliminate the complexity of changing intracellular supercooling with temperature, but the decrease in intracellular supercooling due to osmotic dehydration and transport of CPA into the intracellular solution must be taken into account.

The degree of intracellular supercooling at the time of IIF can be determined from a non-ideal water and CPA transport model paired with an accurate model to predict the intracellular solution osmolality as a function of intracellular solute concentration. Alternatively, measurements of the cell volume at the time of IIF can be coupled with a non-ideal osmotic equilibrium equation.

Knowledge of the relationship between the intracellular supercooling and IIF may enable more accurate predictions of the incidence IIF and could lead to increased understanding of the mechanism of IIF in the presence of extracellular ice.

### *6.1.3. The role of cell volume and extracellular ice nucleation temperature in IIF*

Due to the stochastic nature of nucleation, the probability of a homogeneous nucleation event is a function of the sample volume [15]. For homogeneous nucleation, the predicted number of ice nuclei within a cell is dependent on the nucleation rate and the cell volume [22]. For heterogeneous nucleation, the probability of a nucleation event is proportional to the surface area of the nucleating agent [15]. It has been proposed that the heterogeneous nucleation of intracellular ice occurs via the surface of the plasma membrane acting as the nucleating site [51]. Thus, the probability of a nucleation event would depend on the surface area of the cell, which would be increased for larger cells. Determining the mechanism of ice nucleation (i.e. homogenous versus heterogeneous) is outside the scope of this study, but, assuming that the number of heterogeneous nucleation sites scales with the cell size, the probability of intracellular ice formation by either mechanism of nucleation would be increased for larger cells.

In addition to the effect of cell volume on the predicted probability of a nucleation event, for spherical cells, the larger cells have a smaller surface area to volume ratio which decreases the rate of water movement across the cell membrane. Thus, as the extracellular osmolality increases due to the formation of extracellular ice, larger cells cannot osmotically dehydrate

as fast as smaller cells in order to maintain equilibrium with the extracellular solution and are thus more likely to have IIF.

Decreasing extracellular ice nucleation temperature has been shown to increase the predicted probability and experimentally observed incidence of IIF [10; 18; 35; 53; 54]. However, the lower nucleation temperature is usually accompanied by an increase in the amount of intracellular supercooling at the time of extracellular ice nucleation; thus, de-coupling the effects of these two variables is difficult.

The relative importance of the cell volume and the extracellular ice nucleation temperature on the incidence of IIF as a function of intracellular supercooling could be investigated by osmotically dehydrating the cells before nucleating extracellular ice. The exposure to hypertonic solutions of non-permeating solutes changes the intracellular osmolality, which decreases the temperature at which a given degree of intracellular supercooling is generated. By exposing the cells to hypertonic solutions, the relative effect of decreased cell volume, which would be expected to decrease the probability of IIF, and decreased extracellular nucleation temperature, which would be expected to increase the probability of IIF, on the incidence of IIF can be investigated.

#### 6.1.4. *Limitations of current IIF models*

The models used to predict IIF have enabled major advances in the design of cryopreservation protocols [22; 27; 50]. However, improvements could be made in the equations used to describe the intra- and extracellular solutions in order to enable more accurate predictions and relationships between variables. In models used to predict the incidence of IIF and in calculations of the degree of intracellular supercooling at the time of experimentally observed IIF, the cytoplasm was typically treated as an ideal, dilute solution [8; 13; 22; 23; 29; 38; 39; 40; 51; 52; 53; 54], which becomes increasingly erroneous as the cells become more concentrated due to osmotic dehydration. The Boyle-van't Hoff equation, which contains an ideal, dilute solution assumption, is often used to calculate the intracellular osmolality at a measured volume [13; 38; 39; 40]. The osmolality of a solution in equilibrium with ice at -30 °C is 18.1 osmoles/kg solvent. This is 60 times greater than the isotonic osmolality of cells (0.3 osmoles/kg solvent) and also significantly greater than the osmolality range typically used to determine if the Boyle-van't Hoff equation adequately describes the cellular osmotic equilibrium [17; 19; 26; 46; 56]. In addition, the linear conversion between the freezing point and osmolality is often used to determine the osmolality of the extracellular solution at a given temperature [13; 38; 39; 40]. It was demonstrated in Chapter 2 that the linear conversion gives increasingly large errors in the calculation of the osmolality as the temperature is

decreased. The nonlinear conversion (equation (1.2)) should be used to more accurately determine the solution osmolality.

The OVE presented in Chapters 2 through 4 is a simple, easy to apply solution thermodynamic model that allows accurate predictions of the osmolality (and thus supercooling) of complicated multisolute solutions, such as the cytoplasm of a cell. The non-ideal osmotic equilibrium equation presented in Chapter 5, combined with the multisolute OVE, provides accurate predictions of the composition of the intracellular solution as it becomes increasingly non-ideal due to osmotic dehydration. The multisolute OVE and the non-ideal osmotic equilibrium equation can be used to create a more realistic model of the cytoplasm which captures the solution non-ideality at higher solute concentrations.

#### *6.1.5. Objective*

The objective of this chapter was to investigate the link between the calculated intracellular supercooling, the measured cell volume, and the experimentally observed occurrence of IIF in the presence of extracellular ice for human umbilical vein endothelial cells (HUVECs) in suspension. Using a cryomicroscope, HUVECs were cooled to temperatures which gave specific degrees of intracellular supercooling, extracellular ice was nucleated and the incidence of IIF was measured.

The cryomicroscope is an advantageous experimental system for IIF studies, since it allows visualization of the cells as they are subjected to sub-zero temperatures and extracellular ice nucleation. Direct correlation between various parameters, such as IIF, cell volume, and post-thaw membrane integrity can be done on the cryomicroscope, which cannot be done using other experimental systems. In addition, the small sample volume used on a cryomicroscope allows for virtually instantaneous dissipation of the latent heat of fusion, keeping the cells at the desired sub-zero temperature with no rebound to the freezing point, as occurs with larger sample volumes. The cryomicroscope has been used for numerous IIF studies [1; 2; 8; 10; 12; 13; 18; 23; 27; 35; 38; 39; 40; 41; 53].

In order to investigate the relative importance of cell volume and extracellular ice nucleation temperature on IIF, experiments performed with cells at isotonic volume were contrasted with experiments performed with cells shrunken in a hypertonic solution of PBS. The extracellular ice was nucleated at a lower temperature in the hypertonic solutions versus the isotonic solutions for each degree of supercooling investigated.

To investigate the incidence of IIF within a population of cells with a distribution of cell volumes, the initial cell diameters of the cells in isotonic PBS and in hypertonic PBS were measured and correlated with the incidence of IIF for one of the calculated degrees of intracellular supercooling.

In order to further understand the effect of cell volume on the cellular response to extracellular ice at a given degree of intracellular supercooling, a mathematical model was used to calculate the cellular osmotic responses. The multisolute OVE, the non-ideal osmotic equilibrium equation, and the non-linear conversion between freezing point depression and osmolality (equation (1.2)) were coupled with equations for the water transport across cell membranes and the temperature dependence of the water transport.

The experimental measurements and the model were used together to gain further understanding of the role of cell volume, extracellular ice nucleation temperature, and intracellular supercooling on the incidence of IIF in HUVECs.

## *6.2. Materials and methods - experimental and theoretical*

### *6.2.1. HUVEC cell culture*

HUVEC cells (LONZA, Walkersville, MD, USA) were grown at 37 °C in 5 % CO<sub>2</sub> in endothelial cell growth medium (LONZA), which consists of a basal medium augmented with eight reagents referred to as SingleQuots<sup>®</sup>. The added reagents are growth factors, cytokines, and other supplements, specifically human epidermal growth factor, hydrocortisone, fetal bovine serum, vascular endothelial growth factor, human fibroblast growth factor-basic, insulin-like growth factor-I, ascorbic acid, and heparin. An antibiotic

(GA-1000: Gentamicin, Amphotericin-B) is sold with the SingleQuots<sup>®</sup>, but was not added to the culture medium. The final concentration of serum in the culture medium was 2 % (v/v). The cells were grown in 150 cm<sup>2</sup> tissue culture flasks (Corning, Lowell, MA, USA) following the LONZA guidelines for HUVEC culture and were maintained at less than 80 % confluency for subculturing (approximately 3.0x10<sup>5</sup> - 3.3x10<sup>5</sup> cells per cm<sup>2</sup>). For use in experiments, cells were allowed to grow to 4.0 x10<sup>5</sup> cells per cm<sup>2</sup>. Before an experiment the cells were trypsinized following the LONZA guidelines and counted on a Coulter<sup>®</sup> Z<sub>2</sub><sup>™</sup> particle counter (Beckman Coulter, Mississauga, ON, Canada) to determine the cell number.

#### 6.2.2. *Experimental solutions*

Following the centrifugation step of the trypsinization procedure, the supernatant was removed leaving approximately 200 µL of solution. A washing step was not included to remove the trypsin, as this increased the cell clumping and decreased the cell viability.

For the isotonic experiments, a small volume of the cell culture media (~ 200 to 300 µL, depending on the cell count and the volume of solution left above the cell pellet) was added to the cells so that the cell concentration was approximately 10 - 19x10<sup>6</sup> cells/mL. To achieve the desired cell concentration of >5x10<sup>6</sup> cells/mL for the cryomicroscope experiments, 100 µL of 1X phosphate buffered saline (PBS) was added to 100 µL of the cell suspension. The 1X PBS was made by diluting 10X PBS

(Invitrogen, Burlington, ON, Canada) with distilled water, using a 9 to 1 ratio on a volume basis. The pH of the 1X PBS is adjusted to 7 - 7.1 by adding small amounts of sodium hydroxide (Sigma, Mississauga, ON, Canada). The osmolality of the 1X PBS was 280 - 300 mOsm/kg solvent. The osmolalities of all solutions were measured using a  $\mu$ Osmette Micro Osmometer (Precision Systems, Natick, MA, USA). From the cell suspension diluted with 1X PBS, a 100  $\mu$ L aliquot was taken and mixed with a ten (10)  $\mu$ L aliquot of SYTO® 13 (Molecular Probes, Eugene, OR, USA) and ethidium bromide (EB) (Sigma) stain using a pipette. The SYTO® 13/EB stain was prepared using 80  $\mu$ L of 2.5 mM (millimole solute/L solution) EB stock solution and 20  $\mu$ L of 5 mM SYTO® 13 stock solution, mixed with 700  $\mu$ L of 1X PBS. Final concentrations were 0.25 mM EB and 0.125 mM SYTO® 13. SYTO® 13 is a live cell nucleic acid dye, which permeates the cell membrane of all cells and complexes with both RNA and DNA. When exposed to UV light, the SYTO® 13 fluoresces green. Ethidium bromide penetrates only cells with damaged membranes and forms a complex with nuclear DNA. Upon exposure to UV light, the EB fluoresces red. The dual fluorescence allows for visual differentiation of cells with intact and damaged membranes [55].

The final osmolality of the cell solution containing the stain was 320 - 350 mOsm/kg solvent. The cell suspension was kept in an ice/water bath for the duration of the experiment (i.e. maximum two hours).

For the hypertonic experiments, after centrifugation and removal of the supernatant, a small volume of the cell culture media was added to the cell suspension so that the cell concentration was approximately  $6 - 9 \times 10^6$  cells/mL. A 150  $\mu$ L aliquot of the cell suspension was mixed with a 15  $\mu$ L aliquot of SYTO® 13/EB stain using a pipette. The cell suspension was kept in an ice/water bath for the duration of the experiment (i.e. maximum two hours). For each experimental run, 10  $\mu$ L of 10X PBS was mixed with 50  $\mu$ L of the cell suspension solution (containing the SYTO® 13/EB stain) to achieve a final cell concentration of  $>5 \times 10^6$  cells/mL and a final osmolality of approximately 750 mOsm/kg solvent. The cells were exposed to the hypertonic solution for approximately 5 minutes before the start of the experimental run.

### *6.2.3. Cryomicroscopy experiments*

The incidence of IIF in HUVECs following extracellular ice nucleation was investigated using isothermal holding experiments on a cryomicroscope in phosphate buffered saline (PBS) solutions without CPAs. The cryomicroscope system consisted of a Linkam FDSC196 stage, TMS 94 temperature controller, and LNP93/2 liquid nitrogen pump (Linkam Scientific, United Kingdom) mounted on a Nikon Eclipse 80i microscope (Nikon, Mississauga, ON, Canada). The desired temperature was set using the Linksys 32 temperature control software (Linkam Scientific). The sample loading apparatus consisted of a 0.17 mm thick

quartz crucible which was held by a crucible carrier (see Figure 6.1). When the crucible carrier was inserted in the cryostage, the quartz crucible was positioned on a silver cooling/heating element that was accurately controlled by a platinum temperature sensor mounted within 0.5 mm of the surface of the silver block. The temperature was regulated by the temperature control unit, which controlled the amount of heat generated and amount of liquid nitrogen (LN<sub>2</sub>) pumped into the heating/cooling block. The accuracy of the temperature control was within 0.1 °C of the set temperature. Images were recorded using a Hamamatsu ORCA -ER camera (Hamamatsu, Hamamatsu City, Japan) and the NIS Elements Advanced Research software (Nikon). Figure 6.1 shows the entire cryomicroscope system. Prior to each experiment, the microscope alignment was configured to achieve even illumination (often referred to as Kohler illumination) across the entire field of view [37]. This ensured high-quality images were captured.

A 2 µL volume of the cell suspension was placed on the quartz crucible. The sample was covered with a 12 mm diameter glass coverslip and the crucible carrier inserted into the cryostage. Under the UV light, an image of the SYTO® 13/EB fluorescence was captured so that the pre-freeze membrane integrity of the sample could be assessed. Figure 6.2 is an example of a SYTO® 13/EB image used to determine the membrane integrity of a sample. The Hamamatsu ORCA-ER camera is a monochrome camera, so three pictures were taken (1 brightfield, 1 under

UV light with the FITC filter to capture the SYTO® 13 fluorescence, and 1 under UV light with the Cy3 filter to capture the EB fluorescence) and the NIS-Elements software overlays the three images to construct images as seen in Figure 6.2. The number of green and red cells were counted manually from the individual pictures of the SYTO® 13 fluorescence and EB fluorescence, respectively. This ensures that any cell showing even slight EB fluorescence was counted as membrane-damaged. The same field of view was used for the duration of the experimental run and only the cells with intact cell membranes pre-freeze were included in the subsequent IIF analysis. The microscope was switched to brightfield and the NIS Elements software set to capture an image every 500 msec and compile the images into a timelapse image file of the entire freezing and thawing process. The cryostage was cooled at 50 °C/min until the required experimental sub-zero temperature, corresponding to a specific degree of calculated intracellular supercooling, was reached. The expected osmolality of the isotonic solution was 300 mOsm/kg solvent, which gives a calculated freezing point depression of -0.6 °C. The expected osmolality of the hypertonic solution was 750 mOsm/kg solvent, which gives a calculated freezing point depression of -1.4 °C. The degrees of intracellular supercooling investigated were 2, 3, 4, 5, 7, and 10 °C. A metal probe cooled in LN<sub>2</sub> (Praxair, Edmonton, AB, Canada) was used to nucleate ice in the experimental sample by touching the edge of the coverslip. After extracellular ice formation, the temperature was held

constant for a minimum of two minutes, during which time the incidence of intracellular ice formation (IIF) was determined using the standard flashing technique [6; 8; 13; 35; 38; 39; 40; 41; 49; 53]. When intracellular ice forms, the cell darkens or 'flashes'. The flashing has been attributed to the formation of small intracellular ice crystals which scatter light. Figure 6.3 is a still image extracted from the timelapse images which shows the cells flashing. The number of cells that flashed was determined by watching the timelapse images and counting the cells which flash. The number of cells that flashed in specific time intervals (i.e. less than one second, between 1 second and 60 seconds, and greater than 60 seconds) following extracellular ice nucleation was also determined. Following the two-minute hold, the temperature of the cryostage was increased at 50 °C/min to 20 °C and held for two minutes. After thawing, the UV light was turned on and the post-thaw membrane integrity assessed using the SYTO® 13/EB stain. By using the same field of view for the entire run, each cell in the field of view was tracked from the pre-freeze membrane integrity picture, throughout the freezing and thawing process, to the post-thaw membrane integrity picture. For the cells that had intact membranes pre-freeze, the occurrence of IIF was correlated on a cell-specific basis with the post-thaw membrane integrity.

For this study one experimental run involved: (1) the pre-freeze membrane integrity assay; (2) the protocol described above for the measurement of the incidence of IIF; and (3) the post-thaw membrane

integrity assay. In one experimental run, the same field of view was used for the entire run and contained approximately 10 to 50 cells. For each degree of supercooling that was investigated, three experimental runs were conducted on one day and the results pooled so that the number of cells analyzed for each data point was at least 50 cells. This was repeated with cells from three different passages ( $n = 3$ ) and the average and standard deviation calculated for the results from the three days.

For the isotonic experiments, the cells for the three experimental runs at a specific degree of intracellular supercooling were taken from the same solution of cells in 1X PBS and SYTO® 13/EB stain. After the three runs at a specific degree of supercooling, a 100  $\mu\text{L}$  aliquot of the cells in 1X PBS was mixed with a new 10  $\mu\text{L}$  aliquot of SYTO® 13/EB stain for the experiments done at the next degree of supercooling. For the hypertonic experiments, after each experimental run on the cryomicroscope a new solution of 50  $\mu\text{L}$  of cells in SYTO® 13/EB stain was mixed with 10  $\mu\text{L}$  of 10X PBS. After the three experimental runs at a specific degree of intracellular supercooling a new solution consisting of 150  $\mu\text{L}$  of cells mixed with 15  $\mu\text{L}$  of SYTO® 13/EB stain was made.

The measured osmolalities for each experimental solution were used to calculate the amount of supercooling for each experimental run. The measured osmolalities for the isotonic experiments ranged from 320 - 350 mOsm/kg solvent, which gave freezing point depressions of 0.6 to 0.7  $^{\circ}\text{C}$ . The measured osmolalities for the hypertonic experiments ranged from

610 - 880 mOsm/kg solvent, which gave freezing point depressions of 1.1 to 1.6 °C. Since small volumes of solutions were used, the variability in solution osmolality could be explained by variations of a few microlitres of the components of the experimental solution (i.e. the cell suspension, the 10 X PBS, the of SYTO® 13/EB stain, etc). The variability in osmolality resulted in slight variations ( $\leq 0.4$  °C) between experimental runs in the amount of intracellular supercooling at the time of extracellular ice nucleation.

#### *6.2.4. Cell volume measurements*

The cell diameters of the cells exposed to 4 °C of intracellular supercooling (isotonic and hypertonic) at the time of extracellular ice nucleation were measured using the measurement tool in the NIS Elements AR software. The diameters of the cells before extracellular ice was nucleated (referred to as the initial diameter) were measured and, for the cells that flashed, the diameters were measured at the time of flashing (referred to as the final IIF diameter); for cells that did not flash, the diameters were measured at the time that the last cell flashed (referred to as the final non-IIF diameter). When the measurements of the final IIF diameter were made, the time of flashing following extracellular ice nucleation was also recorded for the cells exposed to 4 °C of intracellular supercooling.

#### 6.2.5. *Statistical Analysis*

The cell diameter data were analyzed using SPSS version 12.0 (Lead Technologies, Charlotte, NC, USA). Results are expressed as mean  $\pm$  standard deviation, unless otherwise specified. Multivariate analysis of variance (ANOVA) (including the Post-Hoc Scheffe test) was performed to compare the data from each of the three days to ensure that day to day variability was not statistically significant. P-values less than 0.05 were considered significant. It was found that the results from the first day of the hypertonic experiments were significantly different than the results from the second and third day ( $p=0.008$  and  $p=0.002$ , respectively). However, further statistical analysis showed that including the data from day 1 in subsequent comparisons did not affect the findings. Thus, the p-values reported are for the comparisons made with the data pooled from each of the three experiments.

The diameters of the cells that flashed (IIF cells) were compared to the diameters of the cells that did not flash (non-IIF cells) using one-way ANOVA to determine if the IIF cells had diameters significantly different from the non-IIF cells. Furthermore, one-way ANOVA was also used to compare the diameters of the cells in the isotonic solution to the diameters of the cells in the hypertonic solution.

### 6.2.6. Mathematical model - equations and specifications

The model used to predict the cellular osmotic response to extracellular ice nucleation included the Jacobs and Stewart water transport equation [20], an Arrhenius temperature dependence of  $L_p$ , a multisolute OVE model (Chapter 3) of the cytoplasm which consisted of a protein and an ideal solute, the non-linear conversion between freezing point depression and osmolality (equation (1.2)), and measured cellular osmotic parameters, including the non-ideal osmotically-inactive fraction,  $b^*$  [43]. The model was designed in the following manner and the values for all parameters used are listed in Table 6.1.

#### (i) Cell osmotic parameters and composition at isotonic osmolality

The volume of intracellular water,  $V_w$ , was given by equation (5.3):

$$V_w = V - V_b = V - b^* V_o \quad (5.3)$$

where  $V$  is the cell volume,  $V_b$  is the osmotically-inactive volume of the cell, and  $b^* = \frac{V_b}{V_o}$  is the osmotically-inactive fraction of the cell volume determined from the non-ideal osmotic equilibrium equation presented in Chapter 5. The subscript  $o$  refers to the isotonic condition.

Equation (5.3) was used to calculate the isotonic cell water volume ( $V_{w,o}$ ) from the isotonic volume of the cell ( $V_o$ ):

$$V_{w,o} = (1 - b^*)V_o \quad (6.1)$$

It was assumed that the osmotically-inactive volume of the cell remained constant ( $V_b = b^*V_o$ ) even as the cell osmotically dehydrates. Thus, the cell water volume can be calculated from the cell volume at anisotonic osmolalities by using equation (5.3).

The mass of intracellular water ( $M_w$ ) was calculated using:

$$M_w = \rho_w V_w \quad (6.2)$$

where  $\rho_w$  is the density of water and was assumed to be constant with temperature ( $1 \times 10^{-15}$  kg/ $\mu\text{m}^3$ ).

For the purposes of this model, the cytoplasm of the HUVECs was assumed to be made up of a protein and an ideal solute. A similar model, consisting of a protein and an electrolyte, has been used to model the cytoplasm of TF-1 cells [43]. The multisolute OVE was used to calculate the osmolality of the cytoplasm, using the same form as the model of the erythrocyte cytoplasm (Chapter 3):

$$\pi = \left( \frac{m_{I,o}}{m_{P,o}} \right) m_p + m_p + B_p m_p^2 + B_p m_p \left( \frac{m_{I,o}}{m_{P,o}} \right) m_p + C_p m_p^3 \quad (6.3)$$

where  $m_I$  is the molality of the ideal solute (mole/kg solvent),  $m_p$  is the molality of the intracellular protein (mole/kg solvent),  $B_p$  is the second

virial coefficient for the protein for use in molality ( $[\text{mole/kg solvent}]^{-1}$ ), and  $C_p$  is the third virial coefficient for the protein for use in molality ( $[\text{mole/kg solvent}]^{-2}$ ).

The isotonic concentration of intracellular proteins of HUVECs is not known. For erythrocytes, the concentration of hemoglobin is 7.3 millimole Hb/kg solvent [16; 46; 47]. Thus, the isotonic concentration of intracellular protein for the HUVECs was assumed to be 7.3 millimole protein/kg solvent. The osmotic virial coefficients of the intracellular protein were assumed to be those of hemoglobin (see Table 2.1), which is the only intracellular protein that has been characterized in this thesis work. It can be seen from Figure 2.5 that the solution thermodynamics of three proteins (hemoglobin, ovalbumin, and whey protein) are quite similar, so assuming that the intracellular proteins of a HUVEC will display similar behaviour is justified. The ideal solute concentration in the cytoplasm at isotonic osmolality was calculated in the same manner as was done in Chapter 3 for the erythrocyte cytoplasm, using an isotonic osmolality for the HUVEC of 300 mOsm/kg solvent [43], which gave an isotonic ideal solute molality of 205 millimole/kg solvent.

The number of moles of protein and ideal solute were calculated using the mass of intracellular water,  $M_w$ :

$$\begin{aligned} n_p &= m_p M_w \\ n_l &= m_l M_w \end{aligned} \tag{6.4}$$

where  $n_p$  and  $n_l$  are the number of moles of protein and ideal solute, respectively. For the circumstances that are being modelled, it was assumed that only water crosses the cell membrane. Thus, the numbers of moles of protein and ideal solute remained constant.

(ii) Extracellular ice nucleation

When extracellular ice is nucleated at a given temperature, the extracellular osmolality ( $\pi^e$ ) of the unfrozen solution in equilibrium with the ice is defined by the relationship between the freezing point depression and osmolality (equation (1.2)):

$$\pi = \frac{T_{FP}^o - T_{FP}}{\left[ W_1 / \left( s_1^{0L} - s_1^{0S} \right) \right] RT_{FP}} \quad (1.2)$$

It was assumed that the extracellular solution is in equilibrium with ice at all times, so the extracellular solution osmolality was calculated from equation (1.2). The increase in extracellular osmolality creates a difference between the intracellular and extracellular solutions, so there will be water efflux from the cell in order to increase the intracellular osmolality. The Jacobs and Stewart [20] water transport equation used to model the efflux of water is:

$$\frac{dV}{dt} = L_p A R T \rho_w (\pi^i - \pi^e) \quad (6.5)$$

where  $\frac{dV}{dt}$  is the change in cell water volume with time,  $L_p$  is the hydraulic conductivity of the cell membrane ( $\mu\text{m}^3/\mu\text{m}^2/\text{min}/\text{atm}$ ),  $A$  is the cell surface area ( $\mu\text{m}^2$ ),  $R$  is the universal gas constant ( $8.21 \times 10^{13} \mu\text{m}^3 \text{atm}/\text{mole K}$ ),  $T$  is the absolute temperature (K),  $\rho_w$  is the density of water ( $\text{kg}/\mu\text{m}^3$ ), and  $\pi$  is the osmolality (where superscripts  $i =$  intracellular and  $e =$  extracellular). Since only water moved across the cell membrane under these conditions, the rate of change of cell water volume also represented the rate of change of total cell volume. Note that the change in volume with time was negative when the osmolality of the extracellular solution was greater than the osmolality of the intracellular solution, indicating water efflux from the cell. The temperature dependence of  $L_p$  was described with the Arrhenius equation:

$$L_p(T) = L_p(T_{ref}) \exp\left(\frac{E_a}{R} \left(\frac{1}{T_{ref}} - \frac{1}{T}\right)\right) \quad (6.6)$$

where  $L_p(T)$  is the value of  $L_p$  at the temperature of interest ( $\mu\text{m}^3/\mu\text{m}^2/\text{min}/\text{atm}$ ),  $L_p(T_{ref})$  is the  $L_p$  at a reference temperature ( $\mu\text{m}^3/\mu\text{m}^2/\text{min}/\text{atm}$ ),  $T_{ref}$  is the reference temperature (K),  $E_a$  is the activation energy of  $L_p$  (J/mol),  $R$  is the universal gas constant ( $8.314 \text{ J}/\text{moleK}$ ), and  $T$  is the temperature of interest (K).

The change in cell water volume (and total cell volume) was calculated by numerically solving equation (6.5) using Euler's method [7] and choosing a time increment ( $\Delta t$ ) that was sufficiently small, meaning that reductions in the time increment did not change the results from the model. The cell water volume was calculated after each time increment:

$$V_w(t + \Delta t) = V_w(t) + [L_p ART \rho_1 (\pi_i - \pi_e)] \Delta t \quad (6.7)$$

Once the cell water volume was calculated, the mass of intracellular water at time ( $t + \Delta t$ ) was calculated from equation (6.2).

With water efflux, the intracellular solutes become more concentrated and the osmolality of the intracellular solution increases. The molalities of the intracellular solutes at time ( $t + \Delta t$ ), recalling that the number of moles of protein ( $n_p$ ) and the number of moles of the ideal solute ( $n_i$ ) remain constant, were calculated, from:

$$m_p(t + \Delta t) = \frac{n_p}{M_w(t + \Delta t)} \quad (6.8)$$

$$m_i(t + \Delta t) = \frac{n_i}{M_w(t + \Delta t)}$$

The osmolality of the intracellular solution was calculated at time ( $t + \Delta t$ ) using the molalities of the intracellular solutes at time ( $t + \Delta t$ ) in

equation (6.3). Calculations using the above equations were repeated until osmotic equilibrium ( $\pi^i = \pi^e$ ) was reached.

### 6.3. Results

#### 6.3.1. *Percentage of IIF and percentage of cells with damaged membrane post-thaw*

The percentage of cells with IIF in the presence of extracellular ice and the percentage of cells with damaged membranes post-thaw as a function of calculated intracellular supercooling in the isotonic PBS solutions are shown on Figure 6.4, which shows that the incidence of IIF increased with increasing intracellular supercooling. Also, the percentage of cells with damaged membranes post-thaw was similar to the percentage of cells with IIF for all degrees of intracellular supercooling. On a cell-specific basis, Table 6.2 shows that 85 % of the cells with IIF were membrane-damaged post-thaw, while 98 % of the cells without IIF had intact membranes post-thaw.

The percentage of cells with IIF and the percentage of cells with damaged membranes post-thaw as a function of supercooling in the hypertonic PBS solutions are shown on Figure 6.5. As with the isotonic experiments, the incidence of IIF increased with increasing supercooling. However, at a given degree of supercooling, a smaller percentage of cells in the hypertonic solutions had IIF as compared with the same degree of

supercooling in the isotonic solution. Similar to the isotonic experiments, the percentage of cells with damaged membranes post-thaw was similar to the number of IIF cells for each degree of supercooling. On a cell-specific basis, Table 6.3 shows that 82 % of the cells with IIF were membrane-damaged post-thaw, while 90 % of the cells without IIF had intact membranes post-thaw.

A comparison of the percentage of IIF cells in the isotonic and hypertonic solutions is shown on Figure 6.6. The lines connecting the data points are sigmoidal best fit lines of the form:

$$\%IIF = a + \frac{b}{1 + [\exp(SC - c)]} \quad (6.9)$$

where  $a$ ,  $b$ , and  $c$  are fitting parameters and  $SC$  is the calculated amount of intracellular supercooling ( $^{\circ}C$ ). The fitting parameters were obtained by minimizing the sum of squared errors (SSE) between the predicted values of % IIF from equation (6.9) and the measured values of % IIF. The equation for the SSE can be found in Chapter 2 (equation (2.11)).

Figure 6.6 shows that the incidence of IIF was higher in the isotonic solution than in the hypertonic solution for a given degree of intracellular supercooling. A common measure to summarize the IIF behaviour of cells is the temperature at which 50 % of cells experience IIF [18; 35; 39; 51; 53]. In this study, the amount of intracellular supercooling required for 50

percent IIF (% IIF) was calculated from Figure 6.6 for both the isotonic and hypertonic experiments. For the isotonic, experiments, 50 % IIF was predicted to occur at 3.9 °C of supercooling (which corresponds to an extracellular ice nucleation temperature of -4.5 °C). For the hypertonic experiments, 50 % IIF was predicted to occur at 7.5 °C of supercooling (corresponding to an extracellular ice nucleation temperature of -8.9 °C).

### *6.3.2. Effect of cell volume on IIF*

The incidence of IIF was lower in the hypertonic solutions for all degrees of intracellular supercooling. The only physical variables which were different between the two sets of experiments are the extracellular ice nucleation temperature and the volumes of the cells. The lower extracellular ice nucleation temperature in the hypertonic solutions was expected to increase the incidence of IIF at a given degree of intracellular supercooling; however, the incidence of IIF in the hypertonic solutions was decreased at a given degree of supercooling. This indicated that the cell volume was playing a role in the decreased incidence of IIF in the hypertonic solutions. In order to examine this further, the diameters of the cells with IIF and the diameters of the cells without IIF were measured for a given amount of supercooling in both the isotonic and hypertonic experiments. For the 4 °C of intracellular supercooling experiments, the cell diameter before extracellular ice was nucleated (referred to as the initial diameter) for IIF and non-IIF cells were measured. For the IIF cells,

the cell diameter at the time of IIF (referred to as the final IIF diameter) was also measured. For the non-IIF cells, the cell diameters at the time the last cell flashed were measured (referred to as final non-IIF diameter). The results are listed in Table 6.4 as the average cell diameter  $\pm$  the standard deviation. In order to determine if there is a statistically significant difference between the cell diameters, one-way ANOVA was performed ( $\alpha < 0.05$  level of significance). For the isotonic experiments, there was a significant difference ( $p < 0.001$ ) between the initial diameters of the IIF and non-IIF cells, with the IIF cells being significantly larger. This difference was also seen in the hypertonic experiments, with the IIF cells again being significantly larger ( $p < 0.001$ ).

The initial diameters (i.e. diameter before extracellular ice nucleation) and final diameters (i.e. diameter at the time of flashing) of the IIF cells in the isotonic and hypertonic solutions were not significantly different ( $p=0.05$  and  $p=0.112$ , respectively). Thus, even though the cells in the hypertonic solution were shrunken due to osmotic dehydration, there were larger cells in the population with a volume that was not significantly different than the cells in the isotonic solution. These larger cells were more likely to have IIF. Since there was a small number of the cells in the hypertonic solution with volumes that were not significantly different than the volume of the cells in the isotonic solution, the incidence of IIF was reduced in the hypertonic solution.

The initial diameters and the final diameters of the non-IIF cells in the isotonic and hypertonic solutions were significantly different ( $p < 0.001$ ), which was expected since the cells in the hypertonic solution were shrunken due to the efflux of water.

It should also be noted that there was a difference between the diameter of the IIF cells before extracellular ice nucleation (initial diameter) and the diameter of the IIF cells at the time of flashing (final IIF diameter), indicating that the cells osmotically dehydrated in the presence of extracellular ice before IIF occurred. Since the osmolality of the intracellular solution increased as the cell shrinks, the actual amount of intracellular supercooling in the cells at the time of IIF was less than the amount at the instant of extracellular ice nucleation. The results shown on Figures 6.4 to 6.6 show the incidence of IIF as a function of the initial intracellular supercooling (i.e. at the time of extracellular ice nucleation) and did not take into account the decrease in intracellular supercooling due to osmotic dehydration.

### *6.3.3. Mathematical modelling to investigate effect of cell volume*

To investigate the impact of cell volume on the cellular osmotic response to extracellular ice nucleation, the mathematical model outlined in section 6.2.6 was used to calculate the cell volumes and degree of intracellular supercooling for hypothetical HUVECs of two different volumes. The calculations were done assuming an isotonic cell volume of

1115  $\mu\text{m}^3$  (approximately 75 % of the measured isotonic volume (1486  $\mu\text{m}^3$ ) for HUVECs [43] and an isotonic cell volume of 2230  $\mu\text{m}^3$ , while keeping all other cellular osmotic parameters equal. The assumed cell volumes were chosen to represent cells at the smaller and larger ends of the cell population. The extracellular ice nucleation temperatures investigated corresponded to the 4 degrees of intracellular supercooling experimental conditions (extracellular ice nucleation at -4.6 °C and -5.4 °C). The calculated cell volume as a function of time curves following extracellular ice nucleation are shown in Figure 6.7. In order to express the graphs on a similar scale, the volumes were expressed as relative cell volume (cell volume divided by the isotonic cell volume). At the time of extracellular ice nucleation, the cells in the hypertonic solution were already shrunken, so they had a relative cell volume of approximately 0.75; whereas the cells in the isotonic solution had a relative cell volume of 1.0.

The cell water volume, relative cell water volume (cell water volume/cell water volume at time of extracellular ice nucleation), and intracellular supercooling were also calculated. During the 4 °C supercooling experiments, all of the cells with IIF nucleated within 37 seconds of extracellular ice nucleation (see Figure 6.8). Thus, the calculated values of cell water volume, relative cell water volume, and intracellular supercooling are shown for the first 60 seconds following extracellular ice nucleation (Figures 6.9 - 6.11).

## 6.4. Discussion

### 6.4.1. *Comparison between this study and previous studies*

Experimental measurements of the incidence of IIF as a function of intracellular supercooling were done in this study at isothermal sub-zero temperatures and without CPAs. The relative importance of the effects of cell volume and extracellular nucleation temperature at a given degree of intracellular supercooling were investigated by suspending the cells in PBS solutions of differing osmolality (either  $\pi = 320 - 350$  mOsm/kg solvent or  $\pi = 610 - 880$  mOsm/kg solvent). Many other measurements of the incidence of IIF have been done for a range of cell types in various conditions [10; 11; 13; 18; 35; 38; 39; 40; 41; 51; 53]. In most of the previous studies, the incidence of IIF was correlated with extracellular ice nucleation temperature, not intracellular supercooling. The results from this study agree with the previous studies which show increasing IIF with increasing intracellular supercooling, which, in solutions with the same osmolality, occurs as the extracellular ice nucleation temperature decreases [10; 35; 41; 53; 54]. It should be noted that direct comparison between this study and previous studies on the relationship between IIF and degrees of intracellular supercooling is difficult due to the fact that in previous studies, the correlation of the incidence of IIF with intracellular supercooling is usually complicated by multiple factors, including: (i) changing temperature, (ii) permeating CPAs, and (iii) ideal, dilute solution assumptions used to calculate the degree of supercooling. The high

correlation between the incidence of IIF and post-thaw membrane damage shown in this study is similar to previous correlations for cells in suspension [2; 3]. The results from this study also agree with the previous hypothesis that the incidence of IIF decreases with decreased cell volume [29]. This study investigated the effect of cell volume on the incidence of IIF both for a population of cells in isotonic and hypertonic solutions for various degrees of intracellular supercooling and also on a cell-specific basis for cells in isotonic and hypertonic solutions for one specific degree of intracellular supercooling.

*6.4.2. Effect of cell volume on incidence of IIF for population of cells in isotonic and hypertonic solutions*

From the measurements of IIF made for the population of cells in the isotonic and hypertonic solutions, the experimental results indicated that, at the conditions studied, the cell volume played a more significant role in the incidence of IIF than the extracellular ice nucleation temperature. At a given degree of intracellular supercooling, a smaller percentage of cells had IIF in the hypertonic PBS solutions as compared to cells in isotonic PBS, even though the extracellular ice nucleation temperature in the hypertonic PBS solutions was 0.8 °C lower than in the isotonic PBS.

*6.4.3. Effect of cell volume on incidence of IIF on a cell-specific basis for cells in isotonic and hypertonic solutions*

From the cell-specific correlations between the incidence of IIF and cell volume for the 4 °C supercooling experiments in the isotonic and hypertonic experiments, it was concluded that the cells which have a larger diameter before extracellular ice nucleation in both the isotonic and hypertonic solutions had IIF, while the smaller cells did not. This corresponds with the prediction that the probability of a nucleation event increases with cell volume.

Comparing the diameters of the cells with IIF in the isotonic and hypertonic solutions demonstrated that IIF cell diameters in the two solutions were not significantly different, even though the cells in the hypertonic solution were shrunken due to efflux of water. This suggests that there may be a critical cell volume for IIF at a specified degree of supercooling, regardless of the extracellular ice nucleation temperature. Since the population of cells in the hypertonic solution were shrunken due to the efflux of water, there were fewer cells in the hypertonic solutions with the larger volume which leads to IIF. Thus, the percentage of IIF cells in the hypertonic solution was less than in the isotonic solution. Additional cell volume measurements for other degrees of intracellular supercooling would need to be done in order to verify the hypothesis of a critical volume for IIF at a given degree of intracellular supercooling. These results

confirmed that cells with a smaller diameter before extracellular ice nucleation have a decreased probability of IIF.

The measured diameters of the IIF cells at the time of IIF indicated that the cells shrink in response to the increased extracellular osmolality due to extracellular ice nucleation before IIF occurs. Thus, the amount of intracellular supercooling was reduced at the time of IIF as compared to the instant that extracellular ice was nucleated.

#### *6.4.4. Results from model and interpretation of experimental results*

From the calculated cellular osmotic responses it was demonstrated that the larger cells do not osmotically dehydrate in the presence of extracellular ice as quickly as the smaller cells. The calculated intracellular supercooling of the larger cells was greater at any given time than that of the smaller cells. The model demonstrated, that in addition to the effect of volume on nucleation which is expected from the stochastic nature of nucleation, the predicted cellular osmotic responses of the larger cells to extracellular ice nucleation resulted in a higher probability of IIF as compared to smaller cells.

#### *6.4.5. Assumption in the model of intracellular solution of HUVECs*

The cytoplasm of the HUVECs was modelled as an aqueous solution of protein and an ideal solute, with an isotonic protein concentration of 7.3

millimole/kg solvent. The assumed protein concentration was greater than the assumed protein concentrations used by Ross-Rodriguez (3.65 millimole protein/kg solvent) [43] and by de Freitas *et al.* (4 millimole protein/kg solvent) [9] in simulations of TF-1 cells and islets, respectively. However, subsequent to these thesis studies, a measurement of the solution thermodynamics of the HUVEC cytoplasm was made [43]. In Appendix D, the comparison between the protein and ideal model used in this thesis and the measured solution properties is shown. The comparison shows that the protein + ideal solute model works well for capturing the non-ideality of the cytoplasm.

#### *6.4.6. Translation of results into cryopreservation applications*

The knowledge that smaller cells can withstand more supercooling before experiencing IIF could be used to design novel cryopreservation protocols. The cells could be osmotically dehydrated before cooling using non-permeating CPAs and then rapidly cooled without the probability of IIF. This idea has been previously used by other researchers [24; 33; 48] and this study reinforces the applicability of such an approach for cells in suspension. In fact, from this study it appears that the addition of supplementary non-permeating CPAs would not be necessary and hypertonic solutions of PBS would enable the avoidance of IIF. In addition, nucleating extracellular ice in the sample at a high sub-zero temperature and allowing the cells to equilibrate with the extracellular ice before

subsequent cooling to lower temperatures may confer protection from IIF at the lower temperatures. The cells osmotically dehydrate during the equilibration and would thus be able to withstand more supercooling. The concept of using isothermal holding steps to dehydrate cells as part of a cryopreservation protocol has been proposed for human hepatocytes [18] and is one of the principles used in the design of two-step cooling protocols [34; 44; 45].

## 6.5. References

- [1] J.P. Acker, J.A.W. Elliott, and L.E. McGann, Intercellular ice propagation: Experimental evidence for ice growth through membrane pores. *Biophysical Journal* 81 (2001) 1389-1397.
- [2] J.P. Acker, and L.E. McGann, Cell-cell contact affects membrane integrity after intracellular freezing. *Cryobiology* 40 (2000) 54-63.
- [3] J.P. Acker, and L.E. McGann, Membrane damage occurs during the formation of intracellular ice. *Cryo-Letters* 22 (2001) 241-254.
- [4] J.P. Acker, and L.E. McGann, Innocuous intracellular ice improves survival of frozen cells. *Cell Transplantation* 11 (2002) 563-571.
- [5] E. Asahina, Frost Injury in Living Cells. *Nature* 196 (1962) 445-446.
- [6] R. Chambers, and H.P. Hale, The formation of ice in protoplasm. *Proceedings of the Royal Society of London Series B-Containing Papers of a Biological Character* 110 (1932) 336-352.
- [7] S.C. Chapra, and R.P. Canale, *Numerical methods for engineers : with programming and software applications*, WCB/McGraw-Hill, Boston, 1998.
- [8] R.C. de Freitas, and K.R. Diller, Intracellular ice formation in three-dimensional tissues: Pancreatic islets. *Cell Preservation Technology* 2 (2004) 19-28.

- [9] R.C. de Freitas, K.R. Diller, J.R.T. Lakey, and R.V. Rajotte, Osmotic Behavior and Transport Properties of Human Islets in a Dimethyl Sulfoxide Solution. *Cryobiology* 35 (1997) 230-239.
- [10] K.R. Diller, Intracellular freezing: effect of extracellular supercooling. *Cryobiology* 12 (1975) 480-5.
- [11] K.R. Diller, Intracellular freezing of glycerolized red-cells. *Cryobiology* 16 (1979) 125-131.
- [12] K.R. Diller, and E.G. Cravalho, A cryomicroscope for the study of freezing and thawing processes in biological cells. *Cryobiology* 7 (1970) 191-9.
- [13] M.F. Dowgert, and P.L. Steponkus, Effect of Cold-Acclimation on Intracellular Ice Formation in Isolated Protoplasts. *Plant Physiology* 72 (1983) 978-988.
- [14] J. Farrant, and G.J. Morris, Thermal Shock and Dilution Shock as Causes of Freezing Injury. *Cryobiology* 10 (1973) 134-140.
- [15] N.H. Fletcher, The chemical physics of ice, Cambridge U.P., London, 1970.
- [16] J.C. Freedman, and J.F. Hoffman, Ionic and osmotic equilibria of human red blood cells treated with nystatin. *J Gen Physiol* 74 (1979) 157-85.
- [17] D.Y. Gao, Q. Chang, C. Liu, K. Farris, K. Harvey, L.E. McGann, D. English, J. Jansen, and J.K. Critser, *Fundamental cryobiology of*

human hematopoietic progenitor cells I: Osmotic characteristics and volume distribution. *Cryobiology* 36 (1998) 40-48.

[18] C.L. Harris, M. Toner, A. Hubel, E.G. Cravalho, M.L. Yarmush, and R.G. Tompkins, Cryopreservation of isolated hepatocytes: Intracellular ice formation under various chemical and physical conditions. *Cryobiology* 28 (1991) 436-444.

[19] C.J. Hunt, S.E. Armitage, and D.E. Pegg, Cryopreservation of umbilical cord blood: 1. Osmotically inactive volume, hydraulic conductivity and permeability of CD34(+) cells to dimethyl, sulphoxide. *Cryobiology* 46 (2003) 61-75.

[20] M.H. Jacobs, and D.R. Stewart, A simple method for the quantitative measurement of cell permeability. *Journal of Cellular and Comparative Physiology* 1 (1932) 71-82.

[21] J.O.M. Karlsson, E.G. Cravalho, and M. Toner, Intracellular Ice Formation - Causes and Consequences. *Cryo-Letters* 14 (1993) 323-336.

[22] J.O.M. Karlsson, E.G. Cravalho, and M. Toner, A Model of Diffusion-Limited Ice Growth inside Biological Cells during Freezing. *Journal of Applied Physics* 75 (1994) 4442-4445.

[23] J.O.M. Karlsson, A. Eroglu, T.L. Toth, E.G. Cravalho, and M. Toner, Fertilization and development of mouse oocytes cryopreserved

using a theoretically optimized protocol. *Human Reproduction* 11 (1996) 1296-1305.

- [24] C.T. Knorpp, W.R. Merchant, P.W. Gikas, H.H. Spencer, and N.W. Thompson, Hydroxyethyl starch - Extracellular cryoprotective agent for erythrocytes. *Science* 157 (1967) 1312-&.
- [25] J. Levitt, Sulfhydryl-disulphide hypothesis of frost injury and resistance in plants. *Journal of Theoretical Biology* 3 (1962) 355-&.
- [26] C. Liu, C.T. Benson, D.Y. Gao, B.W. Haag, L.E. McGann, and J.K. Critser, Water Permeability and Its Activation-Energy for Individual Hamster Pancreatic-Islet Cells. *Cryobiology* 32 (1995) 493-502.
- [27] J. Liu, E.J. Woods, Y. Agca, E.S. Critser, and J.K. Critser, *Cryobiology of rat embryos II: A theoretical model for the development of interrupted slow freezing procedures.* *Biology of Reproduction* 63 (2000) 1303-1312.
- [28] P. Mazur, Physical Factors Implicated in the Death of Micro-Organisms at Subzero Temperatures. *Annals of the New York Academy of Sciences* 85 (1960) 610-629.
- [29] P. Mazur, Kinetics of Water Loss from Cells at Subzero Temperatures and the Likelihood of Intracellular Freezing. *J Gen Physiol* 47 (1963) 347-69.

- [30] P. Mazur, Role of Cell Membranes in Freezing of Yeast and Other Single Cells. *Annals of the New York Academy of Sciences* 125 (1965) 658-&.
- [31] P. Mazur, The role of intracellular freezing in the death of cells cooled at supraoptimal rates. *Cryobiology* 14 (1977) 251-72.
- [32] P. Mazur, Freezing of living cells: mechanisms and implications. *Am J Physiol* 247 (1984) C125-42.
- [33] L.E. McGann, Differing actions of penetrating and nonpenetrating cryoprotective agents. *Cryobiology* 15 (1978) 382-390.
- [34] L.E. McGann, and J. Farrant, Survival of tissue culture cells frozen by a two-step procedure to -196 degrees C. I. Holding temperature and time. *Cryobiology* 13 (1976) 261-8.
- [35] K. Muldrew, and L.E. McGann, Mechanisms of Intracellular Ice Formation. *Biophysical Journal* 57 (1990) 525-532.
- [36] K. Muldrew, and L.E. McGann, The Osmotic Rupture Hypothesis of Intracellular Freezing-Injury. *Biophysical Journal* 66 (1994) 532-541.
- [37] Microscope Alignment for Köhler Illumination, M. Parry-Hill, R.T. Sutter, and M.W. Davidson.(accessed on August 30, 2009)
- [38] R.E. Pitt, M. Chandrasekaran, and J.E. Parks, Performance of a kinetic model for intracellular ice formation based on the extent of supercooling. *Cryobiology* 29 (1992) 359-373.

- [39] R.E. Pitt, S.P. Myers, T.-T. Lin, and P.L. Steponkus, Subfreezing volumetric behavior and stochastic modeling of intracellular ice formation in *Drosophila melanogaster* embryos. *Cryobiology* 28 (1991) 72-86.
- [40] R.E. Pitt, and P.L. Steponkus, Quantitative analysis of the probability of intracellular ice formation during freezing of isolated protoplasts. *Cryobiology* 26 (1989) 44-63.
- [41] W.F. Rall, P. Mazur, and J.J. McGrath, Depression of the ice-nucleation temperature of rapidly cooled mouse embryos by glycerol and dimethyl sulfoxide. *Biophysical Journal* 41 (1983) 1-12.
- [42] D.H. Rasmussen, M.N. Macaulay, and A.P. Mackenzie, Supercooling and nucleation of ice in single cells. *Cryobiology* 12 (1975) 328-339.
- [43] L.U. Ross-Rodriguez, Cellular osmotic properties and cellular responses to cooling, Department of Laboratory Medicine and Pathology, University of Alberta, Edmonton, Alberta (2009), pp. 219
- [44] L.U. Ross-Rodriguez, J.A.W. Elliott, and L.E. McGann, Characterization of cryobiological responses in TF-1 cells using interrupted freezing procedures. *Cryobiology* (Accepted) (2009).
- [45] L.U. Ross-Rodriguez, J.A.W. Elliott, and L.E. McGann, Investigating cryoinjury using simulations and experiments: 1. TF-1 cells during

the two-step freezing (rapid cooling interrupted with a hold time) procedure. *Cryobiology* (Submitted) (2009).

[46] D. Savitz, V.W. Sidel, and A.K. Solomon, Osmotic Properties of Human Red Cells. *Journal of General Physiology* 48 (1964) 79-94.

[47] A.K. Solomon, M.R. Toon, and J.A. Dix, Osmotic properties of human red cells. *J Membr Biol* 91 (1986) 259-73.

[48] A. Sputtek, G. Singbartl, R. Langer, W. Schleinzner, H.A. Henrich, and P. Kuhl, Cryopreservation of red-blood-cells with the nonpenetrating cryoprotectant hydroxyethyl starch. *Cryo-Letters* 16 (1995) 283-288.

[49] P.L. Steponkus, and M.F. Dowgert, Gas bubble formation during intracellular ice formation. *Cryo-Letters* 2 (1981) 42-47.

[50] M.R. Tijssen, H. Woelders, A. de Vries-van Rossen, C.E. van der Schoot, C. Voermans, and J.M. Lagerberg, Improved postthaw viability and in vitro functionality of peripheral blood hematopoietic progenitor cells after cryopreservation with a theoretically optimized freezing curve. *Transfusion* 48 (2008) 893-901.

[51] M. Toner, E.G. Cravalho, and M. Karel, Thermodynamics and kinetics of intracellular ice formation during freezing of biological cells. *Journal of Applied Physics* 67 (1990) 1582-1593.

[52] M. Toner, E.G. Cravalho, and M. Karel, Cellular-Response of Mouse Oocytes to Freezing Stress - Prediction of Intracellular Ice

Formation. *Journal of Biomechanical Engineering-Transactions of the Asme* 115 (1993) 169-174.

[53] M. Toner, R.G. Tompkins, E.G. Cravalho, and M.L. Yarmush, Transport phenomena during freezing of isolated hepatocytes. *AIChE Journal* 38 (1992) 1512-1522.

[54] W.M. Toscano, E.G. Cravalho, O.M. Silveiras, and C.E. Huggins, Thermodynamics of Intracellular Ice Nucleation in Freezing of Erythrocytes. *Journal of Heat Transfer-Transactions of the Asme* 97 (1975) 326-332.

[55] H.Y. Yang, J. Acker, A. Chen, and L. McGann, In situ assessment of cell viability. *Cell Transplantation* 7 (1998) 443-451.

[56] G. Zhao, L.Q. He, H.F. Zhang, W.P. Ding, Z. Liu, D.W. Luo, and D.Y. Gao, Trapped water of human erythrocytes and its application in cryopreservation. *Biophysical Chemistry* 107 (2004) 189-195.

**Table 6.1.** Parameters used in the mathematical modelling of HUVECs.

<b>Cellular osmotic parameters</b>		
<b>Parameter</b>	<b>Value</b>	<b>Source/Notes</b>
osmotically-inactive fraction, $b^*$	0.524	[43]
Membrane hydraulic conductivity, $L_p$ at $T_{ref} = 20\text{ }^\circ\text{C}$	$0.147\ \mu\text{m}^3/\mu\text{m}^2/\text{min}/\text{atm}$	[43]
Activation energy of $L_p$ , $E_a$	$5.61 \times 10^4\ \text{J/mol}$	[43] (converted from kcal/mol)
Isotonic cell volume, $V_o$	$1115\ \mu\text{m}^3$ or $2230\ \mu\text{m}^3$	Assumed values; ~ 75 % and 150 % of the measured isotonic volume of HUVECs [43]
<b>Intracellular solution parameters</b>		
Isotonic concentration of protein	0.0073 mole/kg solvent	
Isotonic concentration of ideal solute	0.205 mole kg/solvent	Calculated from equation (6.3)
Second osmotic virial coefficient for protein, $B_p$	$49.3\ (\text{mole}/\text{kg solvent})^{-1}$	Chapter 2
Third osmotic virial coefficient for protein, $C_p$	$3.07 \times 10^3\ (\text{mole}/\text{kg solvent})^{-2}$	Chapter 2
<b>Solvent properties</b>		
Density of water, $\rho_1$	$1 \times 10^{-15}\ \text{kg}/\mu\text{m}^3$	Neglected temperature dependence of density
Molecular weight of water, $W_1$	$1.802 \times 10^{-2}\ \text{kg}/\text{mole}$	
Difference in molar entropy of water in liquid state and solid state $\left( \overline{s}_1^{0L} - \overline{s}_1^{0S} \right)$	$22.00\ \text{J}/\text{mole K}$	
Freezing point of pure water, $T_{FP}^o$	$273.15\ \text{K}$	

**Table 6.2.** Percentage of cells with intact and damaged membranes for cells undergoing IIF and cells not undergoing IIF in isotonic solutions.

<b>IIF cells</b>		<b>non-IIF cells</b>	
Intact membrane	Damaged membrane	Intact membrane	Damaged membrane
<b>15 %</b> (204/1361)	<b>85 %</b> (1157/1361)	<b>98 %</b> (846/859)	<b>2 %</b> (13/859)

**Table 6.3.** Percentage of cells with intact and damaged membranes for cells undergoing IIF and cells not undergoing IIF in hypertonic solutions.

<b>IIF cells</b>		<b>non-IIF cells</b>	
Intact membrane	Damaged membrane	Intact membrane	Damaged membrane
<b>18 %</b> (106/573)	<b>82 %</b> (467/573)	<b>90 %</b> (1178/1311)	<b>10 %</b> (133/1311)

**Table 6.4.** Cell diameters (average  $\pm$  standard deviation) for cells undergoing IIF and cells not undergoing IIF for isotonic and hypertonic experiments.

	<b>Isotonic</b>		<b>Hypertonic</b>	
	<b>IIF cells</b>	<b>Non-IIF cells</b>	<b>IIF cells</b>	<b>Non-IIF cells</b>
<b>Initial (<math>\mu\text{m}</math>)</b>	18.6 $\pm$ 5.6	16.4 $\pm$ 3.6	16.7 $\pm$ 5.8	13.2 $\pm$ 3.6
<b>Final (<math>\mu\text{m}</math>)</b>	17.7 $\pm$ 5.6	13.3 $\pm$ 3.8	16.2 $\pm$ 5.8	10.8 $\pm$ 3.3

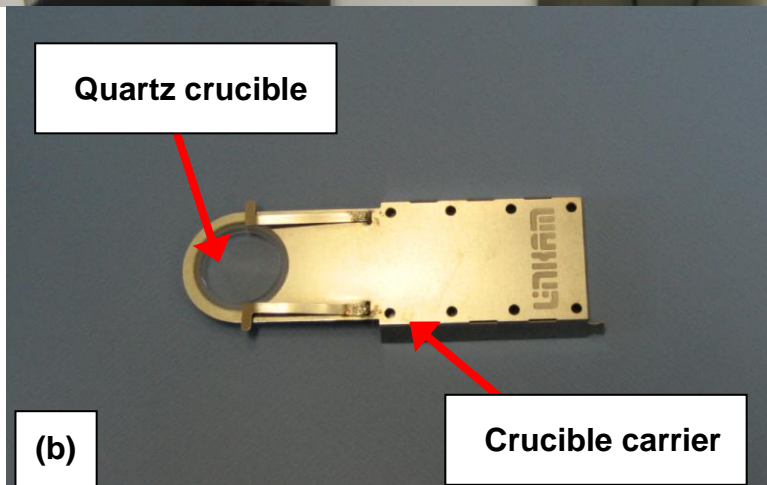


**Figure 6.1.** (a) Picture of entire cryomicroscope system, and (b) close-up of crucible carrier and quartz crucible for samples.

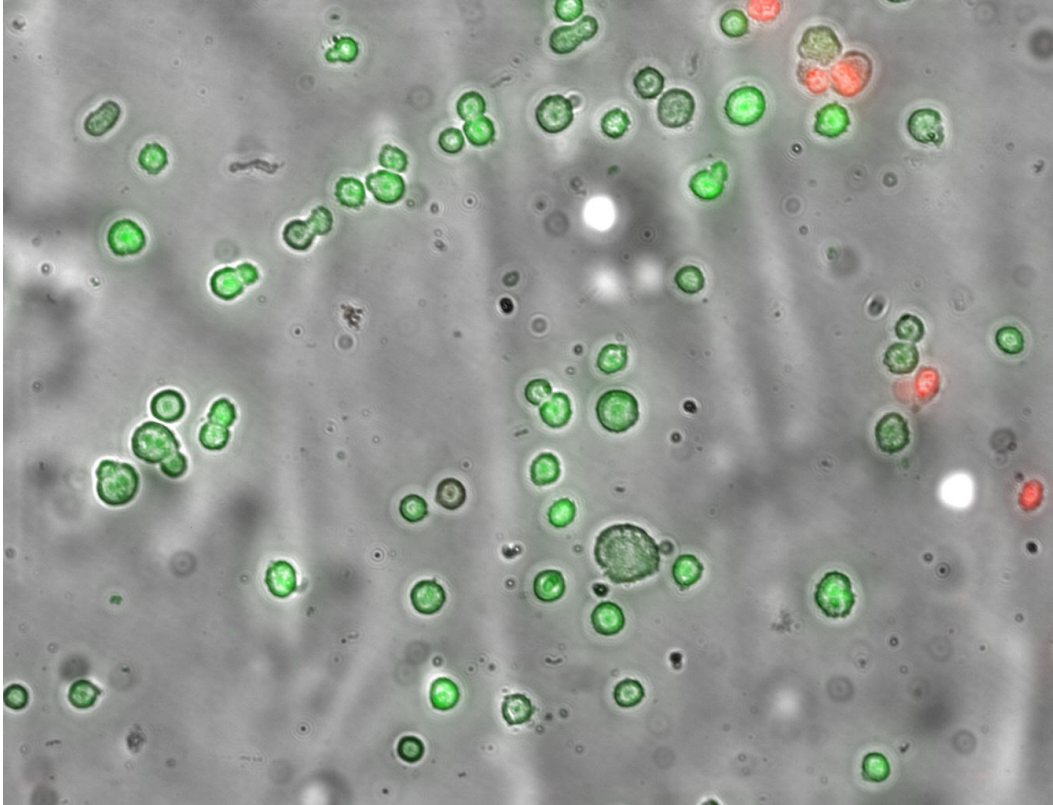


**Figure 6.2.** Image of SYTO® 13 (green)/EB (red) fluorescence used for membrane integrity assay. Green cells have intact membranes and red cells have damaged membranes.

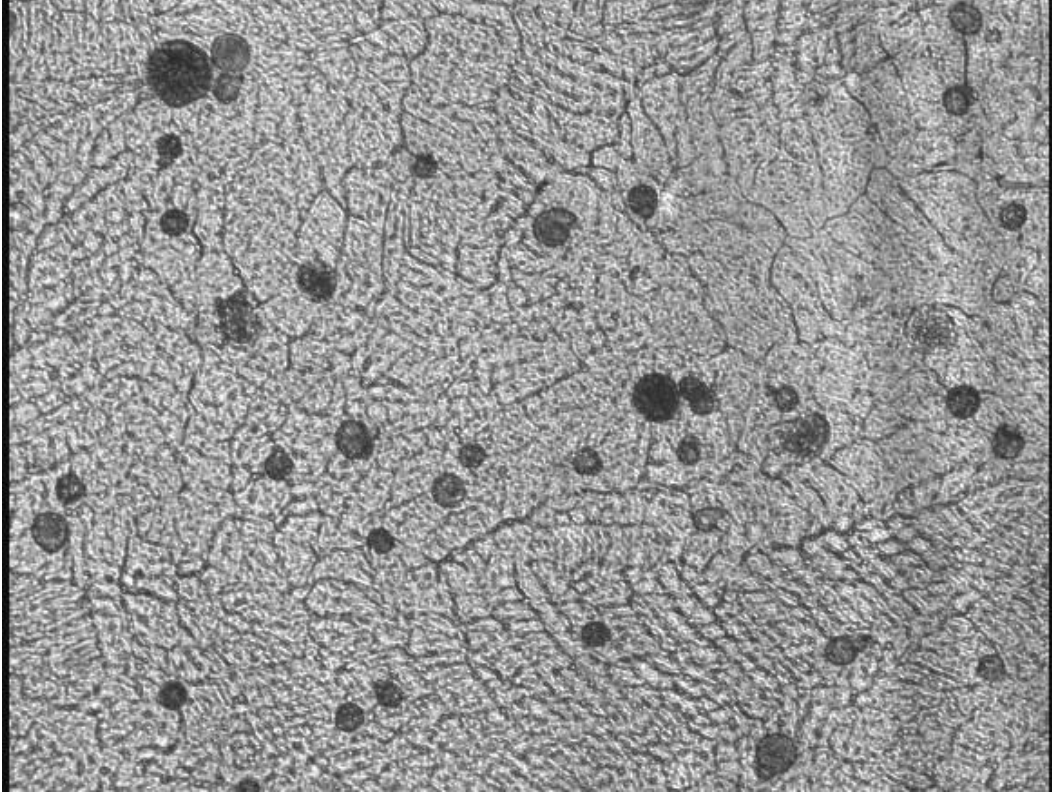


**Figure 6.3.** Image of cells flashing due to intracellular ice formation. This image is from the cells in isotonic PBS with 10 degrees of intracellular supercooling at the time of extracellular ice nucleation ( $T_{\text{nuc}} = -10.6 \text{ }^{\circ}\text{C}$ ), approximately 7 seconds after extracellular ice was nucleated.

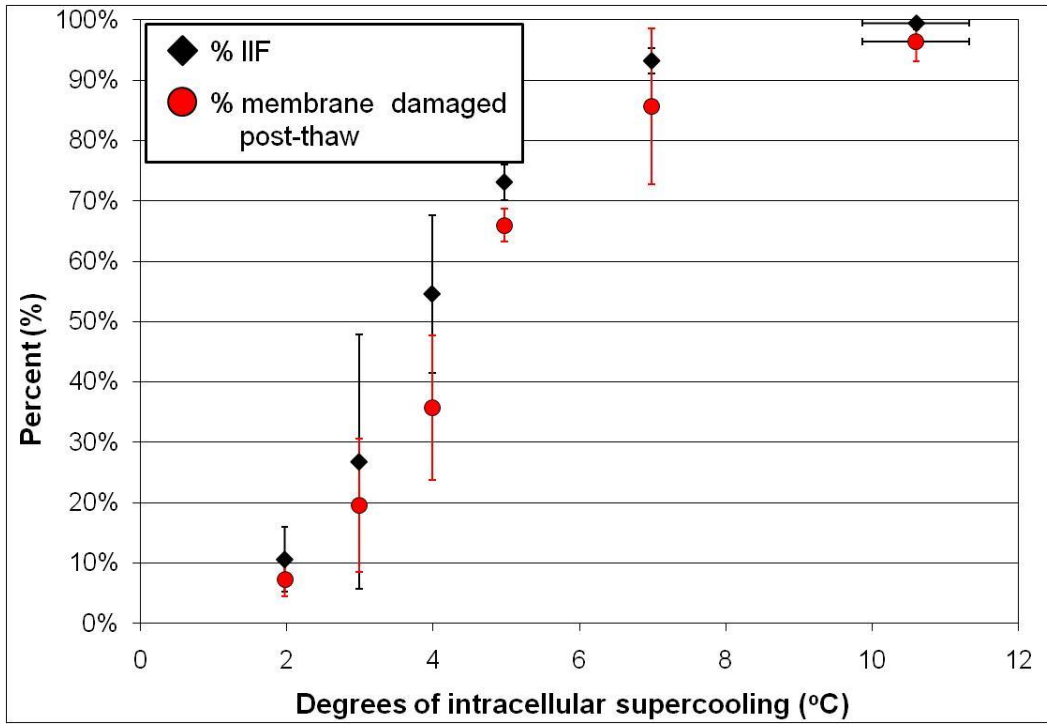


**Figure 6.4.** Percentage of cells with IIF (closed diamonds) and percent cells membrane damaged post-thaw (red circles) for isotonic experiments.

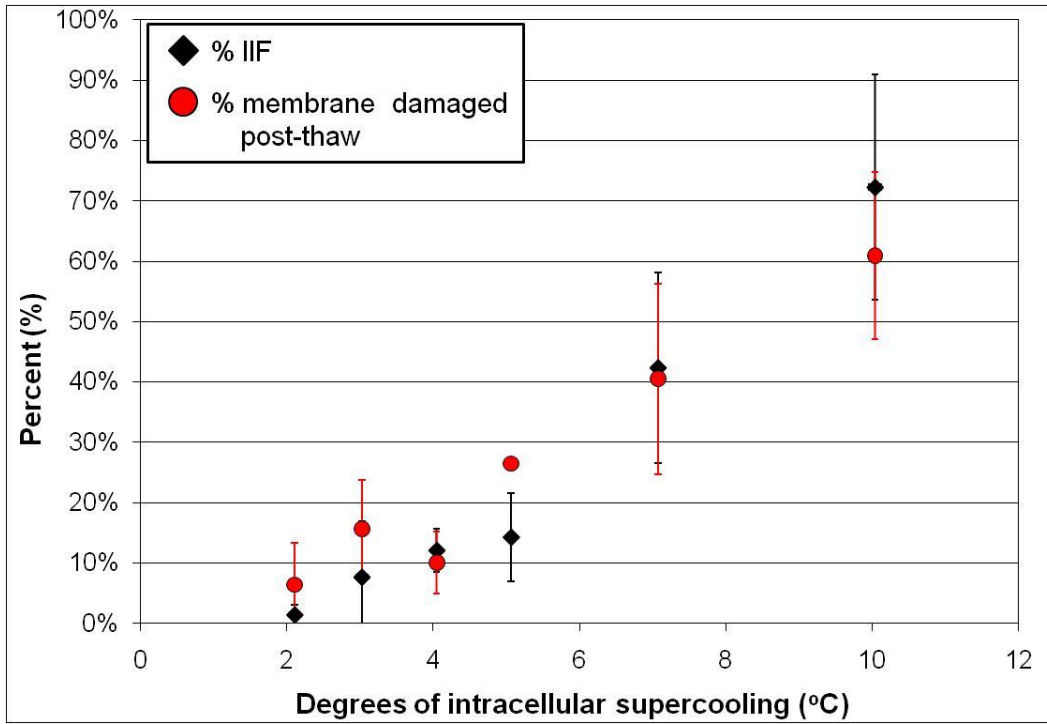


**Figure 6.5.** Percentage of cells with IIF (closed diamonds) and percent cells membrane damaged post-thaw (red circles) for hypertonic experiments.

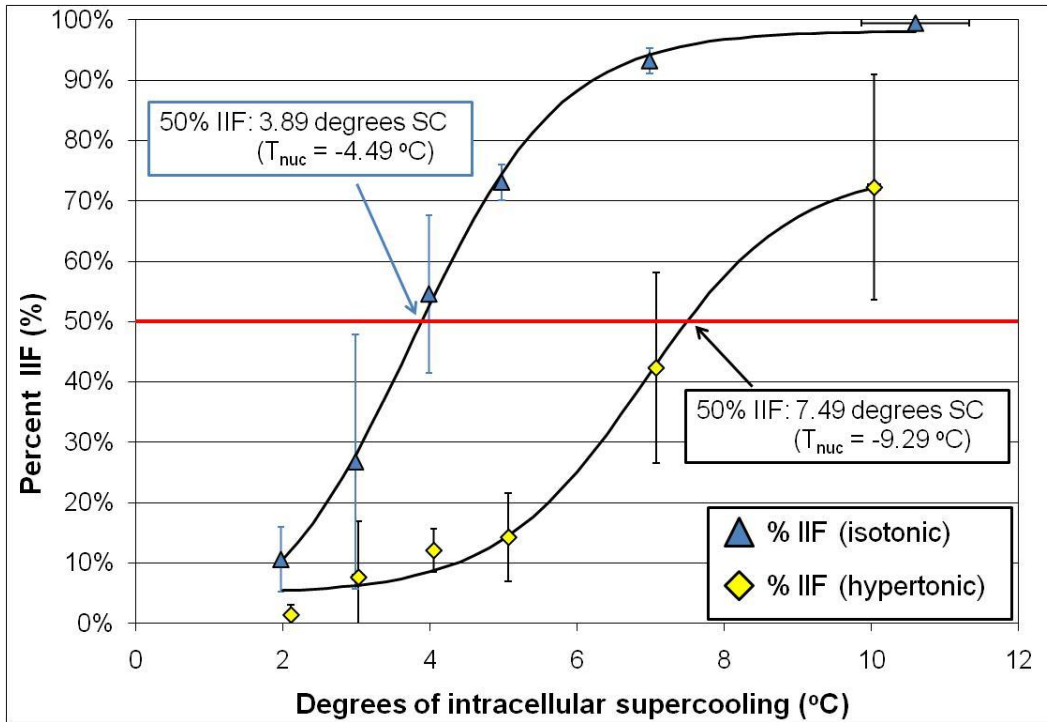


**Figure 6.6.** Percentage of cells with IIF for isotonic (blue triangles) and hypertonic (yellow diamonds) experiments. The solid lines through the data points are sigmoidal best fit lines. The equations from the best fit lines were used to calculate the amount of intracellular supercooling required for 50 % IIF.

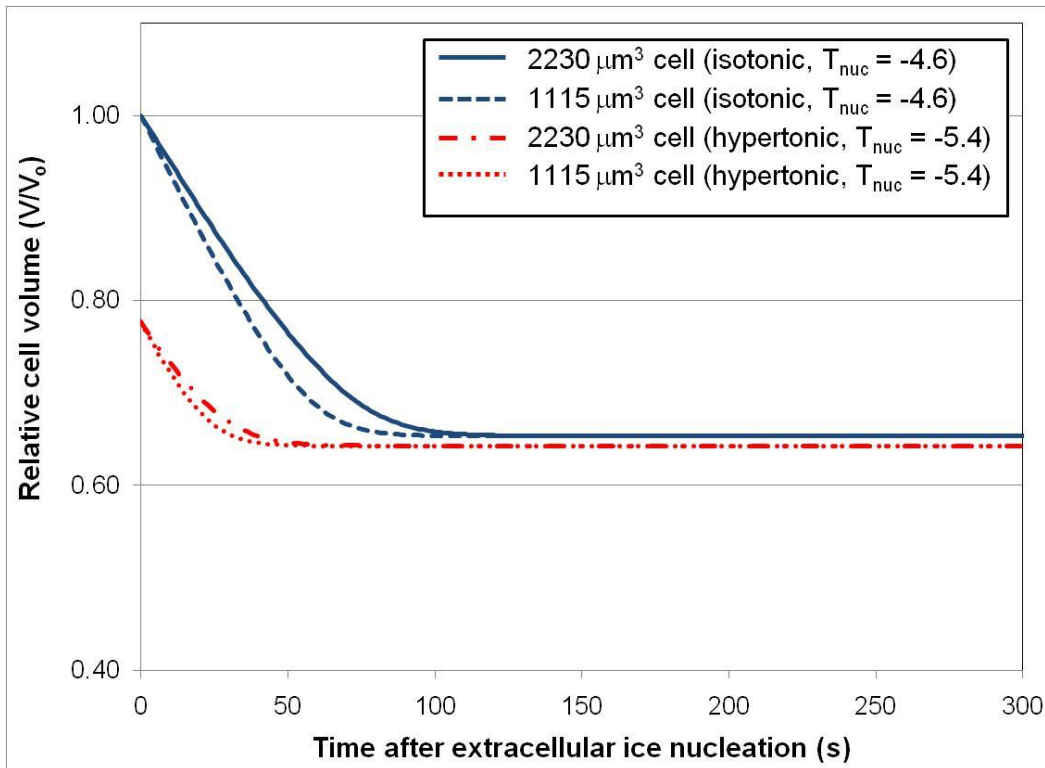


**Figure 6.7.** Calculated relative cell volume (volume / isotonic volume) as a function of time for cells in isotonic solution ( $\pi = 300$  mOsm/kg solvent) with extracellular ice nucleated at  $-4.6$  °C (4 degrees of intracellular supercooling) and cells in hypertonic solution ( $\pi = 750$  mOsm/kg solvent) with extracellular ice nucleated at  $-5.4$  °C (4 degrees of intracellular supercooling).

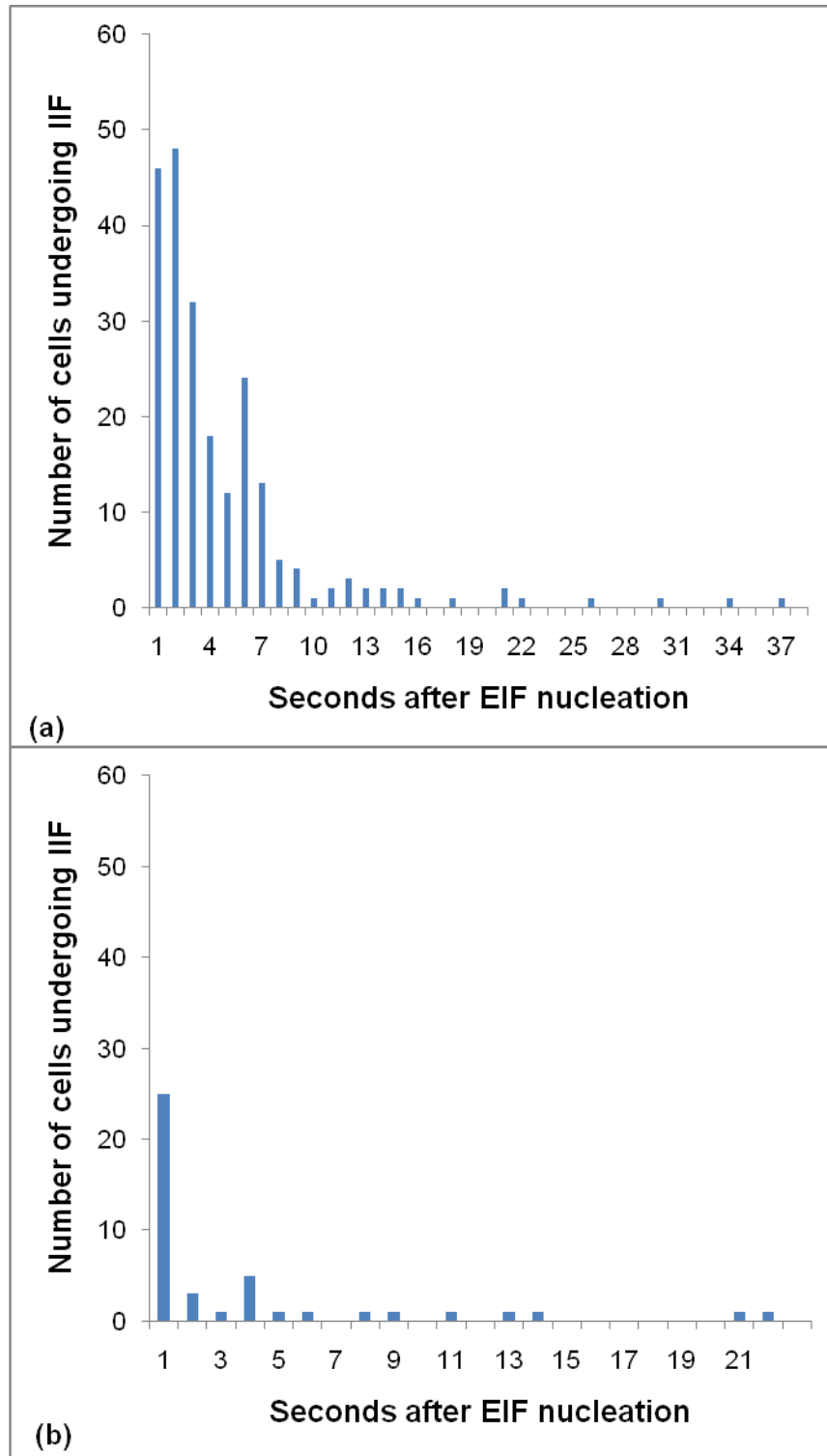


**Figure 6.8.** Histogram of number of cell undergoing IIF as a function of time following extracellular ice nucleation for (a) isotonic experiments and (b) hypertonic experiments.

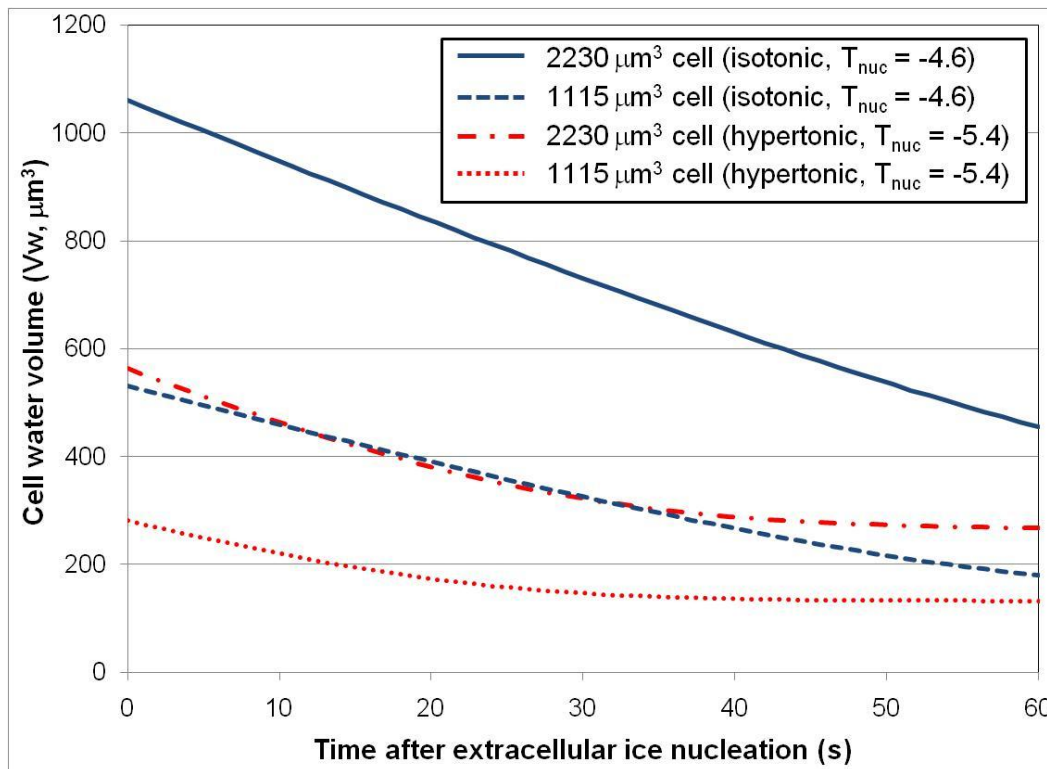


**Figure 6.9.** Calculated cell water volumes for 2230  $\mu\text{m}^3$  cells and 1115  $\mu\text{m}^3$  cells in isotonic ( $\pi = 300$  mOsm/kg solvent) and hypertonic solutions ( $\pi = 750$  mOsm/kg solvent).

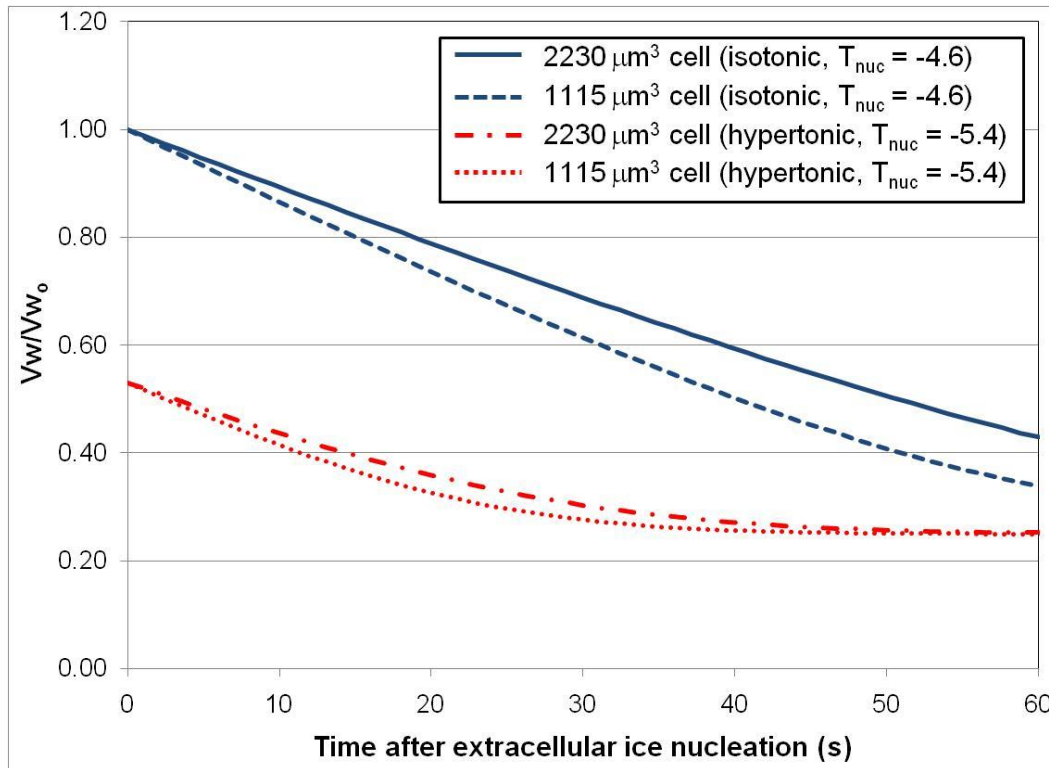


**Figure 6.10.** Calculated relative cell water volumes (cell water volume/isotonic cell water volume) for 2230  $\mu\text{m}^3$  cells and 1115  $\mu\text{m}^3$  cells in isotonic ( $\pi = 300$  mOsm/kg solvent) and hypertonic solutions ( $\pi = 750$  mOsm/kg solvent).

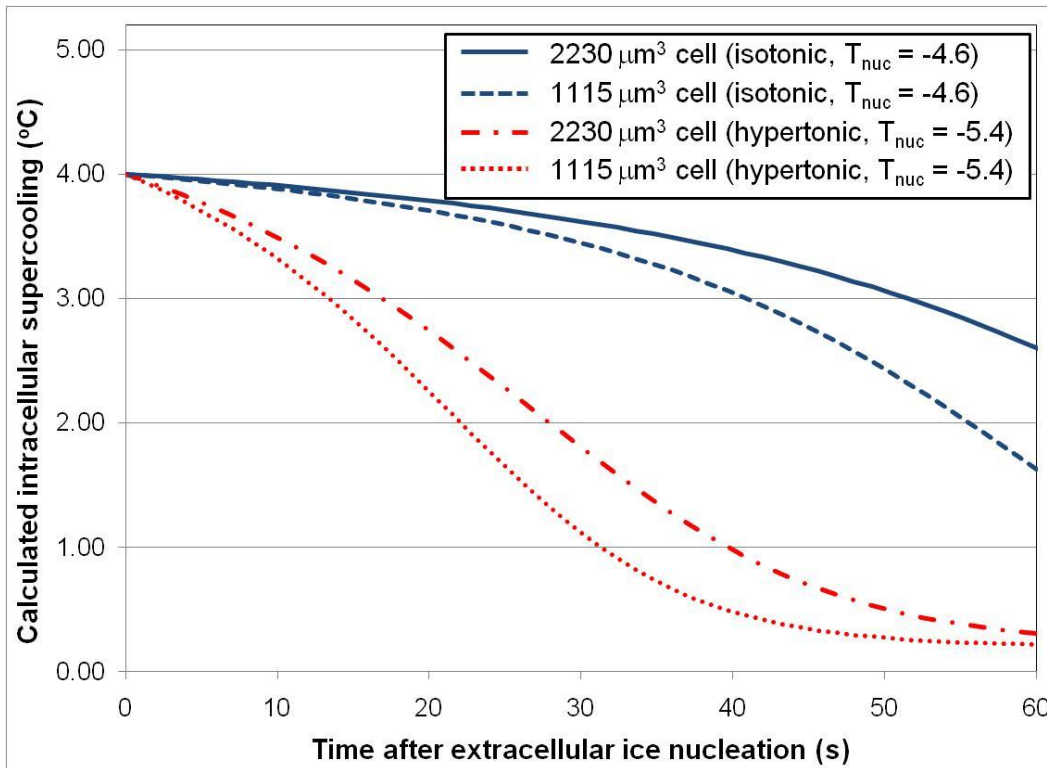


**Figure 6.11.** Calculated intracellular supercooling for 2230  $\mu\text{m}^3$  cells and 1115  $\mu\text{m}^3$  cells in isotonic ( $\pi = 300$  mOsm/kg solvent) and hypertonic solutions ( $\pi = 750$  mOsm/kg solvent).

## **Chapter 7 - Overall Discussion and General Conclusions**

### **7.1. Summary of thesis**

Increasingly complex obstacles are arising in the search for successful cryopreservation of a range of cells, tissues and organs. These challenges include: (i) designing complicated, multisolute CPA solutions in order to achieve successful low-temperature storage of cells and tissues; (ii) reducing or eliminating CPAs from the cryopreservation of cells in order to minimize toxicity-related damage and adverse patient reactions; and (iii) developing nonlinear cooling profiles to maximize efficacy of cryopreservation protocols for specific cell types. The traditional approach of empirical testing of protocols to find an optimum is time- and resource-consuming and new approaches to cryopreservation are needed, particularly to address the preservation of engineered cells and tissues that are being developed for a wide range of clinical applications.

One of the most rapidly growing areas of cryopreservation research is the use of mathematical modelling to interpret and understand experimental results; ascertain relationships between various parameters; and design novel cryopreservation protocols. However, there are significant limitations in the equations that are commonly used in cryobiological modelling. The equations used to describe the solution thermodynamics of the intra- and extra-cellular solutions either contain simplifying assumptions regarding the solute interactions or require fitting

of experimental data. Thus, they are very limited in the solutions to which they can be applied.

This thesis addressed the limitations in two key equations that are used in cryobiology: the equation to describe the osmolality as a function of concentration of complicated multisolute solutions and the equation for the osmotic equilibrium of cells. Experimental measurements were paired with a model developed using the improved equations in order to gain additional insight into the IIF behaviour of cells.

This thesis demonstrated that the multisolute osmotic virial equation (OVE) accurately predicts the osmolality as a function of concentration of a variety of types of non-ideal multisolute solutions, including aqueous solutions containing two CPAs, a protein and an ideal solute, two proteins, a CPA and an electrolyte, and a macromolecule and an electrolyte. This multisolute OVE, with novel mixing rules derived from thermodynamic first principles, requires only single-solute data to make predictions of multisolute data. In this work, the single-solute osmotic virial coefficients, for use with solute concentration in molality and mole fraction, were determined for a wide range of solutes, including electrolytes, CPAs, alcohols, sugars, and macromolecules. The single-solute coefficients can be used to determine the efficacy of different solutes as potential CPAs based on their thermodynamic freezing point depression (or osmolality) as a function of concentration. Most importantly, the single-solute coefficients can be used in the multisolute OVE to predict the osmolality as a function

of concentration for multisolute solutions. This equation represents the first solution thermodynamic model for cryobiological solutions which does not contain overly simplifying assumptions regarding solute interactions or require fitting of multisolute data.

The accuracy of the OVE for solutions containing electrolytes was compared to a more complicated electrolyte solution theory, the Pitzer-Debye-Huckel equation. The single-solute OVE was shown to fit the solution data of aqueous NaCl solutions as well as the Pitzer-Debye-Huckel equation. In addition, for solutions containing a CPA + NaCl in water, the predictions from the multisolute OVE were as accurate using the OVE to capture the behaviour of the multisolute solution as those using the Pitzer-Debye-Huckel equation (to capture the behaviour of the NaCl in the multisolute solution) combined with the multisolute OVE (to capture the behaviour of the CPA and solute interactions in the multisolute solution). The OVE is a much simpler approach than the Pitzer-Debye-Huckel equation, requiring only two fitting parameters to capture the NaCl solution behaviour versus the six empirical parameters and multiple functions required in the Pitzer-Debye-Huckel equation.

The form of the multisolute OVE that has been shown to be accurate in this thesis has already been incorporated by other researchers in the field of cryopreservation for a variety of applications [1; 4; 8; 10; 11] and cited as an accurate and simple method to model cryopreservation solutions [5]. In addition to being used to develop a non-ideal osmotic

equilibrium equation in this thesis, the proposed form of the multisolute OVE has been used in (i) the development of non-ideal, non-dilute transport equations for cellular systems [4], (ii) modelling CPA and water transport in articular cartilage [1; 8], and (iii) investigating cryo-injury and developing optimal protocols for a hematopoietic stem cell line (TF-1 cells) [10; 11]. The use of the multisolute OVE has been proposed in future studies of anhydrous preservation of cellular systems [2].

A new non-ideal osmotic equilibrium equation was derived in this thesis which is thermodynamically correct for ideal and non-ideal solutions. Combining the non-ideal osmotic equilibrium equation with the multisolute OVE, the inferred osmotically-inactive fraction of human erythrocytes was brought into closer agreement with the measured values of the dry volume of the cell. Improved predictions of the osmotically-inactive fraction of the cell allow for more accurate calculations of the amount of water in the intracellular solution. This in turn leads to more accurate predictions of intracellular supercooling and intracellular solute composition.

This thesis also combined experimental measurements of IIF as a function of calculated intracellular supercooling with the improved equations to study the interactions between intracellular supercooling, extracellular ice nucleation temperature, and cell volume on the incidence of IIF. The experimental results from this study indicate that, at the conditions studied, the cell volume played a more significant role in the

occurrence of IIF than the extracellular ice nucleation temperature. At a given degree of intracellular supercooling, the incidence of IIF was lower for cells in hypertonic solutions as compared to cells in isotonic solutions, even though the extracellular ice nucleation temperature in the hypertonic solutions was lower than in the isotonic solution for the same amount of intracellular supercooling.

Furthermore, correlating cell volume measurements with the incidence of IIF on a cell-specific basis in the two different osmolality solutions showed that there may be a critical cell volume for IIF at a specified level of supercooling, regardless of the extracellular ice nucleation temperature. A comparison of the cell diameters between the cells with IIF in the two solutions, both before extracellular ice nucleation and at the time of flashing, demonstrated that the diameters in the two solutions were not significantly different, even though the cells had osmotically dehydrated in the hypertonic solution. IIF still occurred in cells that retained a larger volume in the hypertonic solution. Since there were fewer cells that retained the critical volume in the population of cells in the hypertonic solution, the incidence of IIF in the hypertonic solution was lower than in the isotonic solution.

From the stochastic nature of ice nucleation it is expected that a larger volume will result in a higher likelihood of a homogeneous nucleation event. However, the larger cell volume also influences the cellular osmotic response on ice nucleation in the extracellular solution, leading to

conditions more favourable for IIF. A mathematical model was developed using the improved equations from this thesis to further investigate the role of cell volume on cellular osmotic responses. The results from the mathematical model indicated that the larger cells have more intracellular water and, when the extracellular osmolality increases due to extracellular ice formation, the larger cells lose water less rapidly than the smaller cells. This is due to their smaller surface area to volume ratio, although the cells are assumed to have the same hydraulic conductivity. This resulted in the intracellular solution of the larger cells remaining more supercooled than that of the smaller cells, which resulted in a higher probability of IIF. Thus, the results from the mathematical model indicated that, in addition to the effect of volume on nucleation which is understood from the stochastic nature of nucleation, the cellular osmotic responses of the larger cells to extracellular ice nucleation result in conditions which are more favourable to IIF as compared to smaller cells.

The knowledge that cells with smaller volumes can withstand more supercooling before IIF could be used to design novel cryopreservation protocols. These novel protocols could include the pre-freeze exposure to non-permeating hypertonic solutions or nucleating extracellular ice at a high subzero temperature, to allow some dehydration of the cells before rapid cooling without IIF. The use of exclusively non-permeating CPAs has been used by other researchers [6; 7; 12]. This study reinforces the applicability of such an approach for cells in suspension and also indicates

that any hypertonic solution, or the use of extracellular ice formation to create a hypertonic solution, confers protection to the cell, even in the absence of conventional CPAs.

## 7.2. Limitations of this study

There are several limitations inherit in this study that should be discussed and their implications understood. Certain assumptions were made in the derivation of the multisolute OVE which cannot be expected to be valid for all solutions. The form of the multisolute OVE in this thesis is consistent with regular solution theory, with the additional assumption of a semi-dilute solution [3; 4]. However, even with these assumptions, the OVE has been shown to be relatively accurate for very non-ideal aqueous solutions, including solutions of two proteins in water and solutions containing an electrolyte plus another solute in water.

None of the multisolute solutions investigated in this thesis contained two solutes that both had third osmotic virial coefficients, so the cubic mixing rule presented in Chapter 3 has not been tested in these studies. In addition, the applicability of the multisolute OVE to aqueous solutions containing more than two solutes has not been experimentally verified. It is expected that the multisolute OVE will provide more accurate predictions for both of these types of solutions than the other solutions theories that do not require fitting of multisolute data. This thesis has laid

the groundwork for additional studies on the applicability of the multisolute OVE for increasingly complex solutions.

The non-ideal osmotic equilibrium equation presented in Chapter 5 is limited by the lack of knowledge of the osmolality as a function of concentration ( $\pi(m)$ ) for the intracellular solutions of cells other than erythrocytes. There are very few measurements of the solution properties of the cytoplasm for living, nucleated cells. However, a novel method has been reported for measuring the solution properties of living cells and the solution properties for several cell types published [9]. The non-ideal osmotic equilibrium equation should be applied to additional cell types and verified using an independent measure of the osmotically-inactive fraction (i.e. the measured dry volume). In addition, new experimental methods should be developed that can accurately measure the equilibrium cell volume of the cells at very high osmolalities, where the non-ideality in the osmotic equilibrium would be more apparent.

The other proposed explanations for the deviation between the predicted and measured values of the osmotically-inactive fraction of erythrocyte may have been developed at least partly to describe observations that were actually due to ideal, dilute solution assumptions in the osmotic equilibrium equation. Using the non-ideal osmotic equilibrium equation developed in this thesis and incorporating the hypotheses which account for the additional complexity of the erythrocyte (i.e. the involvement of the cytoskeleton in the osmotic response) may result in

even closer agreement between the inferred osmotically-inactive fraction and the measured dry volume.

The incidence of IIF was measured for cells equilibrated in an isotonic solution and a hypertonic solution to investigate the relative importance of cell volume and extracellular ice nucleation temperature as a function of intracellular supercooling. Cell diameter measurements were performed only for cells with 4 °C of intracellular supercooling at the time of extracellular ice nucleation in the solutions with two different osmolalities. The results from the cell diameter measurements warrant further detailed investigation.

Although the mathematical model used to further investigate the role of cell volume on cellular osmotic responses to extracellular ice nucleation was not compared against other cryobiological models, the individual equations within the model had been previously shown in the thesis to be improvements over the other equations commonly used in cryobiology. This mathematical model does not predict for the incidence of IIF - it is a cellular osmotic model. Correlating the results from this model to cryobiological outcomes requires knowledge of the level of intracellular supercooling and cell volume that are required for IIF within a specific cell type. This is another area that warrants further detailed investigation.

### 7.3. Implications of this thesis

The multisolute solution theory investigated in this thesis is the first non-ideal solution theory for cryobiological solutions which has been derived from thermodynamic principles and can be applied to multisolute solutions without the need to fit multisolute data. Already this work has been cited seven times in the 30 months since its publication and the equation has been applied to various areas of cryobiology research, including in tissue systems.

The non-ideal osmotic equilibrium equation represents a method to more accurately determine the true osmotically-inactive fraction of cells. The ideal, dilute Boyle-van't Hoff relationship is commonly used in cryobiology, as the osmotically-inactive fraction is an important cellular parameter. The osmotically-inactive fraction of a cell determines how much water is available to act as a solvent for intracellular solutes, which, in turn, determines the cellular osmotic responses. The non-ideal osmotic equilibrium equation proposed in this thesis was recently used in a study which proposed a novel method to measure the intracellular solution behaviour of various cell types [9]. The non-ideal osmotic equilibrium equation predicts a lower osmotically-inactive fraction for several cell types, compared to the predictions from the Boyle-van't Hoff equation. Furthermore, the fit of the non-ideal osmotic equilibrium equation to the data was improved as compared to the fit of the Boyle-van't Hoff for those cell types. These improvements in the predictions of the osmotically-

inactive fraction will have far-reaching effects in interpreting and understanding cellular responses during cryopreservation.

The mechanism of IIF is still not understood and ascertaining the relationship between IIF and other variables, such as intracellular supercooling and cell volume, is important in developing protocols which avoid IIF. Experimental measurements of the incidence of IIF as a function of intracellular supercooling for a specific cell type under a range of conditions allows correlation of IIF with important parameters (including cell volume and post-thaw membrane integrity). The combination of experimental measurements with improved modelling provides a compelling platform for better understanding of the role of cell volume and intracellular supercooling in IIF. Using improved mathematical models to interpret experimental results gives additional insights into important relationships between variables and may contribute to the successful design of protocols.

#### 7.4. General conclusions and recommendations

As the use of mathematical modelling becomes even more prevalent in cryobiology, the challenge is to develop equations that use the information that is available, while still capturing the complicated behaviour of biological systems as accurately as possible. The equations proposed in this thesis provide significant improvements over the equations that are currently being utilized in cryobiology.

The multisolute OVE proposed herein has already been incorporated by other cryobiology researchers for a variety of applications [1; 2; 4; 5; 8; 10; 11]. In the absence of multisolute data of the solutions of interest, it is the only solution theory that does not assume ideal, dilute solution behaviour or ignore the interactions between the different types of solutes in solution. Thus, it should be used in cryobiological models to improve predictions of cellular osmotic responses, intra- and extra-cellular supercooling, and intra- and extracellular solution compositions.

As measurements of the solution properties of the cytoplasm for more cell types are performed and published, the non-ideal osmotic equilibrium equation should also be incorporated into cryobiological modelling. Improved predictions of the osmotically-inactive fraction will make cellular osmotic models more accurate.

The combination of mathematical modelling and experimental measurements demonstrated in this thesis is a valuable approach to gaining additional insight from experimental observations and understanding relationships between key parameters. The correlation of experimental observations of IIF with accurate calculations of intracellular supercooling may contribute to more accurate predictions of the effect of intracellular supercooling on IIF.

Equations that capture the complexity of the biological solutions over a range of concentration and temperatures may contribute to the design novel cryopreservation protocols. For example, Woelders and Chaveiro

recently proposed a novel design criteria for developing protocols which avoid IIF and solution effects injury, which involves cooling the cells as fast as possible, while remaining below a constant level of supercooling [13]. Woelders and Chaveiro assumed a supercooling tolerance of 2 °C and also used ideal, dilute solution assumptions in the design of the protocols. The work from this thesis should be used to develop more accurate constant supercooling protocols, without ideal, dilute solution assumptions.

The conclusions from this thesis have the potential for significant impact on the field of cryobiology, by improving the models used to predict cellular responses to cryopreservation and further elucidating the link between critical cryopreservation parameters, such as IIF, intracellular supercooling, and cell volume. These improvements will improve understanding and aid in the design of novel CPA cocktails and innovative cryopreservation protocols.

## 7.5. References

- [1] A. Abazari, J.A.W. Elliott, G.K. Law, L.E. McGann, and N.M. Jomha, A Biomechanical Triphasic Approach to the Transport of Nondilute Solutions in Articular Cartilage. *Biophysical Journal* (Accepted) (2009).
- [2] G.D. Elliott, N. Chakraborty, and D. Biswas, Anhydrous Preservation of Mammalian Cells: Cumulative Osmotic Stress Analysis. *Biopreservation and Biobanking* 6 (2008) 7.
- [3] J.A.W. Elliott, R.C. Prickett, H.Y. Elmoazzen, K.R. Porter, and L.E. McGann, A multi-solute osmotic virial equation for solutions of interest in biology. *Journal of Physical Chemistry B* 111 (2007) 1775-1785.
- [4] H.Y. Elmoazzen, PhD Thesis, Osmotic transport in cryobiology, Dept. of Laboratory Medicine and Pathology, University of Alberta, Edmonton, Alberta (2006), pp. 221
- [5] G.M. Fahy, Theoretical considerations for oocyte cryopreservation by freezing. *Reproductive Biomedicine Online* 14 (2007) 709-714.
- [6] C.T. Knorpp, W.R. Merchant, P.W. Gikas, H.H. Spencer, and N.W. Thompson, Hydroxyethyl starch - Extracellular cryoprotective agent for erythrocytes. *Science* 157 (1967) 1312-&.
- [7] L.E. McGann, Differing actions of penetrating and nonpenetrating cryoprotective agents. *Cryobiology* 15 (1978) 382-390.

- [8] I.N. Mukherjee, Y. Li, Y.C. Song, R.C. Long, and A. Sambanis, Cryoprotectant transport through articular cartilage for long-term storage: experimental and modeling studies. *Osteoarthritis and Cartilage* 16 (2008) 1379-1386.
- [9] L.U. Ross-Rodriguez, Cellular osmotic properties and cellular responses to cooling, Department of Laboratory Medicine and Pathology, University of Alberta, Edmonton, Alberta (2009), pp. 219
- [10] L.U. Ross-Rodriguez, J.A.W. Elliott, and L.E. McGann, Investigating cryoinjury using simulations and experiments: 1. TF-1 cells during the two-step freezing (rapid cooling interrupted with a hold time) procedure. *Cryobiology* (Submitted) (2009).
- [11] L.U. Ross-Rodriguez, J.A.W. Elliott, and L.E. McGann, Investigating cryoinjury using simulations and experiments: 2. TF-1 cells during the graded freezing (interrupted slow cooling without hold time) procedure. *Cryobiology* (Submitted) (2009).
- [12] A. Sputtek, G. Singbartl, R. Langer, W. Schleinzner, H.A. Henrich, and P. Kuhn, Cryopreservation of red-blood-cells with the nonpenetrating cryoprotectant hydroxyethyl starch. *Cryo-Letters* 16 (1995) 283-288.
- [13] H. Woelders, and A. Chaveiro, Theoretical prediction of 'optimal' freezing programmes. *Cryobiology* 49 (2004) 258-271.

**Appendix A: Relationship between freezing point depression  
and osmolality**

***Pure component equations***

The Gibbs-Duhem relation for a pure component is [36]:

$$SdT - VdP + nd\mu = 0 \quad (\text{A1})$$

where  $S$  is entropy,  $T$  is temperature,  $V$  is volume,  $P$  is pressure,  $n$  is the number of moles, and  $\mu$  is the chemical potential of the pure component.

The pressure and temperature dependence of the chemical potential are needed. To find the pressure dependence of the chemical potential, the temperature is set to be constant so that equation (A1) gives:

$$\begin{aligned} -VdP + nd\mu &= 0 \\ d\mu &= \frac{V}{n} dP \end{aligned} \quad (\text{A2})$$

where  $V/n = \nu$ , the molar volume. Assuming that the substance is incompressible ( $\nu = \text{constant}$ ) equation (A2) can be integrated to give:

$$\mu(T, P) = \mu(T, P_{ref}) + \nu(P - P_{ref}) \quad (\text{A3})$$

To determine the temperature dependence, set the pressure to be constant so that equation (A1) gives:

$$\begin{aligned} SdT + nd\mu &= 0 \\ d\mu &= \frac{-S}{n} dT \end{aligned} \quad (\text{A4})$$

where  $S/n=s$ , the molar entropy. Assuming that the molar entropy,  $s$ , does not depend on temperature, equation (A4) can be integrated to give:

$$\mu(T, P) = \mu(T_{ref}, P) + s(T_{ref} - T) \quad (A5)$$

Substituting equation (A3), evaluated at  $T_{ref}$ , for  $\mu(T_{ref}, P)$  in equation (A5) gives:

$$\mu(T, P) = \mu(T_{ref}, P_{ref}) + \nu(P - P_{ref}) + s(T_{ref} - T) \quad (A6)$$

Realizing that the above derivation was for a pure component, equation (A6) can be written for the pure solvent, water, denoted with subscript 1, in a multicomponent solution.

$$\mu_1^o(T, P) = \mu_1^o(T_{ref}, P_{ref}) + \bar{\nu}_1^o(P - P_{ref}) + \bar{s}_1^o(T_{ref} - T) \quad (A7)$$

where  $\bar{\nu}_1^o$  is the partial molar volume of water and  $\bar{s}_1^o$  is the partial molar entropy of water. The superscript  $o$  refers to the pure component.

### **Multicomponent equations**

For a multicomponent solution of solvent (subscript 1) and solute (subscript 2):

$$\mu_1(T, P, x_2) = \mu_1^o(T, P) - \bar{\nu}_1^o \Pi \quad (A8)$$

where  $x_2$  is the mole fraction of the solute and  $\Pi$  is the osmotic pressure.

Substituting equation (A7) into (A8) gives:

$$\mu_1(T, P, x_2) = \mu_1^o(T_{ref}, P_{ref}) + \overline{v}_1^o(P - P_{ref}) + \overline{s}_1^o(T_{ref} - T) - \overline{v}_1^o \Pi \quad (\text{A9})$$

At equilibrium (i.e. the freezing point), assuming that curvature effects can be neglected:

$$T^L = T^S = T_{FP} \quad (\text{A10})$$

$$P^L = P^S = P^R \quad (\text{A11})$$

$$\mu_1^L = \mu_1^S \quad (\text{A12})$$

where  $T^L$  is the temperature of the liquid,  $T^S$  is the temperature of the solid and  $T_{FP}$  is the freezing point temperature,  $P^L$  is the pressure of the liquid,  $P^S$  is the pressure of the solid,  $P^R$  is the pressure at which the freezing process is occurring,  $\mu_1^L$  is the chemical potential of the water in the liquid solution, and  $\mu_1^S$  is the chemical potential of the pure water in the solid ice.

Substituting equation (A9) into the equilibrium equation (A12) gives:

$$\begin{aligned} \mu_1^{oL}(T_{ref}, P_{ref}) + \overline{v}_1^{oL}(P^L - P_{ref}) + \overline{s}_1^{oL}(T_{ref} - T^L) - \overline{v}_1^{oL} \Pi = \\ \mu_1^{oS}(T_{ref}, P_{ref}) + \overline{v}_1^{oS}(P^S - P_{ref}) + \overline{s}_1^{oS}(T_{ref} - T^S) \end{aligned} \quad (\text{A13})$$

Since the freezing process is occurring at constant pressure, set the reference pressure to be  $P^R$  and the reference temperature to be the freezing point of the pure solvent,  $T_{FP}^o$ . Using this reference point and the other two equilibrium conditions, equations (A10) and (A11), gives:

$$\overline{s_1^{o^L}}(T_{FP}^o - T_{FP}) - \overline{v_1^{o^L}}\Pi = \overline{s_1^{o^S}}(T_{FP}^o - T_{FP}) \quad (\text{A14})$$

Rearranging and substituting  $\Pi = RT\rho_1\pi$  (where  $T = T_{FP}$  in this case)

into equation (A14) gives:

$$\Delta T_{FP} = T_{FP}^o - T_{FP} = \left[ \frac{\overline{v_1^{o^L}}}{\overline{s_1^{o^L}} - \overline{s_1^{o^S}}} \right] RT_{FP}\rho_1\pi = \left[ \frac{W_1}{\overline{s_1^{o^L}} - \overline{s_1^{o^S}}} \right] RT_{FP}\pi \quad (\text{A15})$$

## Appendix B: Concentration unit conversions

### Single-solute solutions:

#### (i) Mole fraction to molality

For a binary solution, containing a solvent (subscript 1) and a solute (subscript 2) and assuming 100 moles total of solution, the mole fraction of the solute,  $x_2$ , is:

$$x_2 = \frac{n_2}{n_1 + n_2} \quad (\text{B1})$$

$$n_1 + n_2 = 100 \quad (\text{B2})$$

where  $x_2$  = mole fraction of solute (moles solute/total moles),  $n_1$  = number of moles of solvent and  $n_2$  = number of moles of solute. Combining (B1) and (B2):

$$n_2 = x_2 \times 100 \quad (\text{B3})$$

$$n_1 = 100 - (x_2 \times 100) \quad (\text{B4})$$

The mass of the solvent,  $M_1$  (g), is:

$$M_1 = n_1 W_1 \quad (\text{B5})$$

where  $W_1$  is the molecular weight of the solvent (g/mole).

The molality of the solute,  $m_2$ , is:

$$m_2 = \frac{n_2}{M_1 \times \frac{1 \text{ kg}}{1000 \text{ g}}} \quad (\text{B6})$$

where  $m_2$  has units of moles of solute per kilogram of solvent.

(ii) Mass fraction to molality

For a binary solution containing 100 g of solution total, the mass fraction of the solute,  $X_2$ , is:

$$X_2 = \frac{M_2}{M_1 + M_2} \quad (\text{B7})$$

$$M_1 + M_2 = 100 \quad (\text{B8})$$

where  $X_2$  = mass fraction of solute (g solute/g total),  $M_1$  = mass of solvent and  $M_2$  = mass of solute. Combining (B7) and (B8):

$$M_2 = X_2 \times 100 \quad (\text{B8})$$

$$M_1 = 100 - (X_2 \times 100) \quad (\text{B9})$$

The number of moles of solute,  $n_2$ , is:

$$n_2 = \frac{M_2}{W_2} \quad (\text{B10})$$

where  $W_2$  is the molecular weight of the solute (g/mole).

$$m_2 = \frac{n_2}{M_1 \times \frac{1 \text{ kg}}{1000 \text{ g}}} \quad (\text{B11})$$

(iii) Mass fraction to mole fraction

Using  $M_1$  from equation (B9) and  $M_2$  from equation (B8):

$$n_1 = \frac{M_1}{W_1} \quad (\text{B12})$$

$$n_2 = \frac{M_2}{W_2} \quad (\text{B13})$$

Combining equation (B12) with (B13), the mole fraction of the solute,  $x_2$ , is:

$$x_2 = \frac{n_2}{n_1 + n_2} \quad (\text{B13})$$

(iv) Mass per volume solvent to molality

For a binary solution with concentration expressed as grams of solute per 100 mL of solvent ( $c_2$ ), the molality ( $m_2$ ) of the solution is:

$$m_2 = \left[ \left( \frac{c_2}{W_2} \right) \div \rho_1 \right] \times 1000 \frac{g}{kg} \quad (\text{B14})$$

where  $\rho_1$  is the density of water (g/mL).

**Multisolute solutions:**

(i) Total solute mass fraction to molality, mole fraction, and mass fraction:

Consider a ternary solution, containing a solvent (subscript 1) and two solutes (subscripts 2 and 3). For a given mass ratio (R-value) of the first solute (subscript 2) to the second solute (subscript 3), and a known solute mass fraction,  $X_T$ . The mass of water is:

$$M_1 = 100 - (X_T \times 100) \quad (\text{B15})$$

where 
$$X_T = \frac{M_2 + M_3}{M_1 + M_2 + M_3} = \frac{M_2 + M_3}{100}$$

$M_1$ ,  $M_2$ ,  $M_3$  being the mass (g) of solvent, first solute, and second solute, respectively.

The R-value is defined as:

$$R = \frac{M_2}{M_3} \tag{B16}$$

Equation (B16) can be used to express either of the solute masses as a function of the other solute mass and the R-value.

The total solute mass is:

$$M_T = M_2 + M_3 = (X_T \times 100) \tag{B17}$$

Using equation (B16) to express the mass of the first solute as a function of the mass of the second solute and the R-value:

$$M_2 = R \times M_3 \tag{B18}$$

Equations (B17) and (B18) can be combined to give the mass of the second solute:

$$M_3 = \frac{X_T \times 100}{R + 1} \tag{B19}$$

Once all of the masses are known, the moles of each solute can be determined:

$$\begin{aligned}n_1 &= \frac{M_1}{W_1} \\n_2 &= \frac{M_2}{W_2} \\n_3 &= \frac{M_3}{W_3}\end{aligned}\tag{B20}$$

where M is the mass (g) and W is the molecular weight (g/mol).

Each solute concentration can then be expressed as the mass fraction, mole fraction, or molality.

$$\text{Mass fraction: } X_2 = \frac{M_2}{M_1 + M_2 + M_3} = \frac{M_2}{100}\tag{B21}$$

$$X_3 = \frac{M_3}{M_1 + M_2 + M_3} = \frac{M_3}{100}$$

$$\text{Mole fraction: } x_2 = \frac{n_2}{n_1 + n_2 + n_3}\tag{B22}$$

$$x_3 = \frac{n_3}{n_1 + n_2 + n_3}$$

$$\text{Molality: } m_2 = \frac{n_2}{M_1 \times \frac{1 \text{ kg}}{1000 \text{ g}}}\tag{B23}$$

$$m_3 = \frac{n_3}{M_1 \times \frac{1 \text{ kg}}{1000 \text{ g}}}$$

### Appendix C: The van't Hoff relation

The van't Hoff relation [29,30] is:

$$\Pi \bar{V} = RT \quad (C1)$$

where  $\Pi$  is osmotic pressure (Pa),  $\bar{V}$  is volume per mole (L/mole), R is the universal gas constant ( $8.314 \times 10^{-3}$  L Pa/mole K), and T is temperature (K).

This can then be written as

$$\Pi V = nRT \quad (C2)$$

or

$$\Pi = \frac{n}{V} RT \quad (C3)$$

where V is volume in litres and n is the number of moles of solute.

Converting osmotic pressure to osmolarity, using

$$\Pi = \pi^* RT \quad (C4)$$

where  $\pi^*$  is osmolarity (osmoles/L solution), gives for (C3)

$$\pi^* RT = \frac{n}{V} RT \quad (C5)$$

van't Hoff states that this equation is valid when the volume of the solute molecules is negligible compared to the volume of the solution [29,30] so V can be assumed to be the volume of the water.

Multiplying both sides of the equation by the inverse of the density of water ( $1/\rho_w$ ):

$$\left(\pi^* RT\right) \frac{1}{\rho_w} = \left(\frac{n}{V} RT\right) \frac{1}{\rho_w} \quad (\text{C6})$$

Canceling RT from both sides of equation (C6) and realizing  $\pi^* \frac{1}{\rho_w}$  is equal to osmolality ( $\pi$ ) (when the volume of solution can be approximated as the volume of solvent) and  $\frac{n}{V} \frac{1}{\rho_w}$  is equal to molality gives

$$\pi = m \quad (\text{C7})$$

Thus, equation (C7) is equivalent to the van't Hoff relation (equation C1) and is only applicable to ideal, dilute solutions. This is stated by van't Hoff [29,30] and other sources that show the derivation of the van't Hoff equation [14]. It is the use of the van't Hoff relation in the Boyle-van't Hoff equation that makes the Boyle-van't Hoff equation only applicable to ideal, dilute solutions.

**Appendix D: Comparison between protein + ideal model and  
measured solution properties of the HUVEC cytoplasm**

In a recent study, the solution properties of the HUVEC cytoplasm were measured [1]. Using osmotic equilibrium data, the second osmotic virial coefficient,  $B_{\text{HUVEC}}$ , was measured for all of the intracellular solutes as one 'grouped solute' (similar to the approach used in Chapter 5 for the human erythrocytes). The measured  $B_{\text{HUVEC}}$  from that study was 2.437 (mole/kg solvent)<sup>-1</sup>. Using that measured value, a comparison to the protein plus ideal solute model used in Chapter 6 was made (Figure D.1). Figure D.1 shows that the proposed protein + ideal solute model of the cytoplasm agrees very well with the measured solution properties of the HUVEC cytoplasm. In addition, Figure D.1 shows that the ideal, dilute solution model does not agree well with the measured solution properties of the cytoplasm.

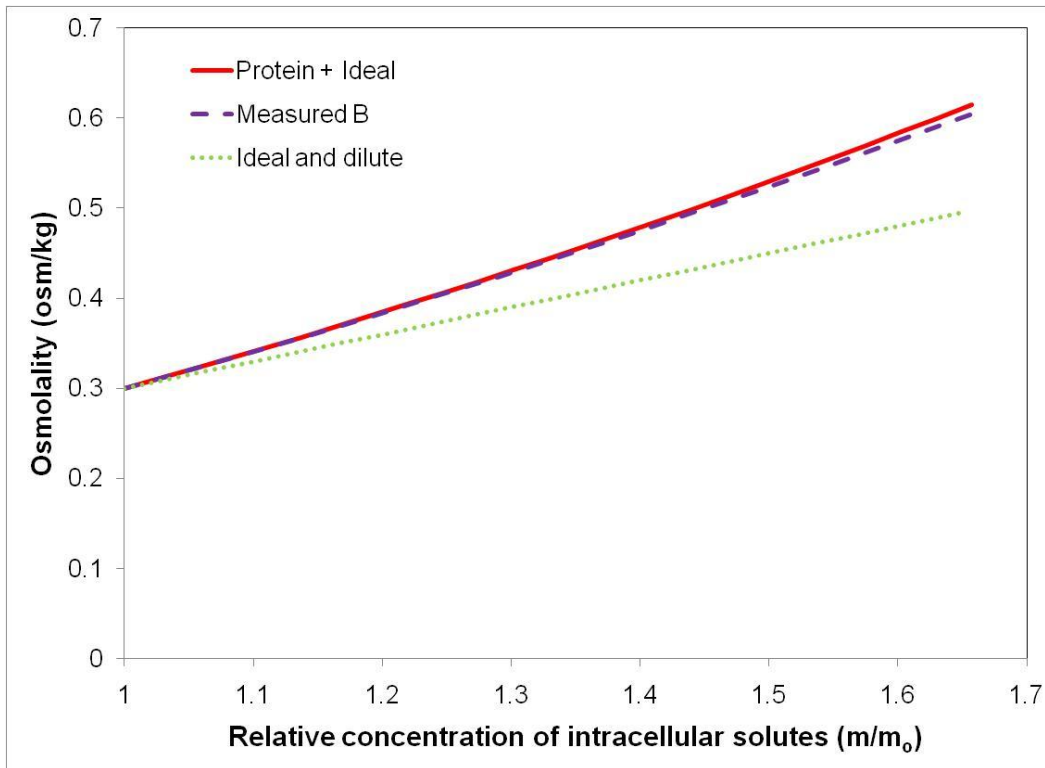


**Figure D.1.** The calculated osmolality as a function of the relative intracellular solute concentration. The solid red line is the predicted osmolality using the protein + ideal model from Chapter 6. The purple long-dashed line is the predicted osmolality using the measured  $B_{\text{HUVEC}}$  value from the literature [1] (where  $\pi = m_{\text{HUVEC}} + B_{\text{HUVEC}}m_{\text{HUVEC}}^2$ ). The green short-dashed line is the predicted osmolality from the ideal, dilute solution model ( $\pi = m$ ).

## References

- [1] L.U. Ross-Rodriguez, Cellular osmotic properties and cellular responses to cooling, Department of Laboratory Medicine and Pathology, University of Alberta, Edmonton, Alberta (2009), pp. 219